DNA methylation as a potential epigenetic driver of morphological development in *Candida albicans*

Dissertation

for the award of the degree

"Doctor rerum naturalium" (Dr.rer.nat.)

of the Georg-August-Universität Göttingen

within the doctoral program “Biology”

of the Georg-August University School of Science (GAUSS)

submitted by

Pia Simone Sternisek

born in

Frankfurt am Main, Germany

Göttingen, 2021

Supervisor:

Dr. rer. nat. Oliver Bader (Main Supervisor)
(Institute for Medical Microbiology and Virology, University Medical Center Göttingen)

Members of the Thesis Committee:

Prof. Dr. med. Uwe Groß
(Institute for Medical Microbiology and Virology, University Medical Center Göttingen)

Prof. Dr. sc. nat. Gerhard Braus
(Institute for Microbiology and Genetics, Department of Molecular Microbiology and Genetics, Georg August University Göttingen)

Dr. rer. nat. Oliver Bader
(Institute for Medical Microbiology and Virology, University Medical Center Göttingen)

Members of the Examination Board:

Prof. Dr. med. Uwe Groß (1st Reviewer)
(Institute for Medical Microbiology and Virology, University Medical Center Göttingen)

Prof. Dr. sc. nat. Gerhard Braus (2nd Reviewer)
(Institute for Microbiology and Genetics, Department of Molecular Microbiology and Genetics, Georg August University Göttingen)

Further Members of the Examination Board:

Dr. rer. nat. Oliver Bader
(Institute for Medical Microbiology and Virology, University Medical Center Göttingen)

Prof. Dr. rer. nat. Carsten Lüder
(Institute for Medical Microbiology and Virology, University Medical Center Göttingen)

Prof. Dr. rer. nat. Stefan Scholten
(Institute for Agricultural Sciences, Division of Crop Plant Genetics, Georg August University Göttingen)

Prof. Dr. rer. nat. Rolf Daniel
(Institute for Microbiology and Genetics, Department of Genomic and Applied Microbiology, Georg August University Göttingen)

Date of oral examination: 8th December 2021

If you think of your DNA as an immense piano keybord and our genes as keys
– each key symbolizing a segment of DNA responsible for a particular note, or trait,
and all the keys combining to make us who we are –
then epigenetic processes determine when and how each key can be struck,
changing the tune being played.

- Peter Miller, National Geographic -

TABLE OF CONTENT

ACKNOWLEDGEMENTS

Writing a doctoral thesis is not possible without the help of various people who contributed to the project, to which I want to express my deepest thanks.

First, I want to express my appreciation to my supervisor Dr. Oliver Bader. Thank you so much for giving me the opportunity to work on this topic, especially as I know it is very important to you. Thanks for your trust, your patience, your guidance and your helpful advices. You were always there, when I needed your support and always had an open ear for any occurring problem. As for every project, also for us not everything went straight and we had to deal with some hurdles in between, but in the end we always found a way together and it was real fun working on this project. Also many thanks for our fruitful discussions on the project - I learned a lot from your scientific creativity! And also for the good and funny times we shared besides research! You have been an excellent supervisor all along the way! Thank you!

I also would like to express my deepest thanks to my supervisor Prof. Dr. med. Uwe Groß. Thank you for giving me the opportunity to work on this project, for your guidance and supervision during this time, constructive questions and advices, and for the opportunity to participate in interesting conferences, seminars and training courses on the topic.

Also, many thanks to my supervisor Prof. Dr. Gerhard Braus. Thank you for your guidance in the progress reports, the interesting discussions, your suggestions, and critical questions to help to bring this project forward.

Further, I want to thank Prof. Dr. med. Michael Weig and Dr. med. Christine Noll, who gave me the opportunity to work in their labs, thank you for your support.

Many thanks also to our collaborators: Prof. Dr. Toni Gabaldón and Ester Saus (IRB, Barcelona, Spain) for whole genome bisulfite sequencing of our clinical isolates and providing data on lncRNAs; Prof. Dr. Julian Naglik, Dr. Jonathan Richardson and Antzela Zavou (King's College, London, Great Britain) for cell damage capacity analysis, *ECE1* gene expression analysis and providing strains; Prof. Dr. Ilse Jacobsen, Prof. Dr. Bernhard Hube, Sarah Vielreicher, Wibke Krüger, and Osama Elshafee (Hans-Knöll-Institut, Jena, Germany) for providing strains and isolates from their experiments; Dr. Gabriela Salinas, Fabian Ludewig, and Susanne Luthin (NIG, Göttingen, Germany) for RNA sequencing. Many thanks also to Dr. Nicolas Cerveau (Geobiology, Georg-August-Universität, Göttingen, Germany) for helpful discussions on experimental setup and support with our first steps in NGS data analysis. A very special thanks also to Prof. Dr. Stefan Scholten (Institute for Agricultural Sciences, Georg-August-Universität Göttingen, Germany) for sharing his great knowledge on epigenetics and for our interesting meetings and helpful discussions on our WGBS and RNAseq analysis results. Further, also many thanks to Dr.

Florian Wegwitz, who contributed with his knowledge on transcriptomic data analysis and interpretation.
Also, I would like to acknowledge the team of the Freiburg Galaxy Team for their great workshop on using Galaxy for WGBS and RNAseq analysis and providing extra storage capacity on their servers for my extended data analysis, as well as ecSeq Bioinformatics GmbH for their great workshop on WGBS data analysis.
My warmest thanks also to my colleagues of the Institute for Medical Microbiology and Virology in Göttingen. Thanks to my awesome labmates Agnieszka Goretzki, Sabine Ceramella, Nina Gerkens, and Yvonne Laukat. Without your help I could not have managed my extensive experiments. Further I would like to thank especially Emilia Gomez (thank you amazing Emi for this great time we had together, I missed you a lot, when you went back to Spain), Sabrina Minatelli (thank you for everything, we had so much fun together), Julian Schwanbeck (many, many thanks for your help with Python, funny experimental constructions, scientific discussions and long evenings on the institutes balcony), as well as Annika Dreyer (for sharing these good times) and Ines Oehmig my supernice office collegue. Further many thanks to my former colleagues Anastasia Dieckmann, Matthias Emele, Roswitha Nast, Daniela Wetzel, Noémie Thieffenat, Friederike Tillkorn, Kathrin Gunka, Felix Joppe, Marcel te Vruigt, and to my students Abdelmalek Ahlees, Lena Krause and Philipp Stegen, it was a lot of fun working with all of you.
Also, many thanks to the other PI's, Prof. Dr. Carsten Lüder, Dr. Wolfgang Bohne, and Dr. Raimond Lugert, who always were very helpful, as well as the staff of our institute, Maik, Ruth, Marco, Frank and Frau Althaus.

A special thanks to my close friends, Susanne Krejcek (thank you for your help with the correction reading and the mental support), Franziska van der Meer (thank you for the time we had!), Alice Wegmann, Karoline Assig, and Mandy Skunde. You all were always there for me, cheering me up and supporting me. You were and are very important to me.

Finally, I would like to thank my parents Ingrid and Harald and my brother Thorsten, as well as my aunt and uncle H. and U. Hanisch, who always trusted in me and supported me where they could. Also, a special thanks to the family of my husband (A. und M. Tietjen, E. Günther, Dr. P. Becker, B., P., F., and E. Schmeling), who always were interested in my studies and also encouraged me a lot.

The dearest thanks goes to my husband Ole! I don't know, how I could have managed this time without you. I am so thankful for your patience, your support and your love.

PUBLICATIONS

Mühlhausen, S., Schmitt, H. D., Plessmann, U., Mienkus, P., Sternisek, P., Perl, T., Weig, M., Urlaub, H., Bader, O., Kollmar, M. (2021). Proteogenomics analysis of CUG codon translation in the human pathogen *Candida albicans.* BMC Biol. [under revision]
https://doi.org/10.1101/2020.06.03.131292

ABSTRACTS

Sternisek, P. S., Cerveaux, N., Groß, U., Bader, O. "Epigenetic control of filamentation in the human pathogenic fungus *Candida albicans*". 17th International PhD Student Symposium "Horizons in Molecular Biology", 14th – 17th September 2020.

TALKS

Sternisek, P. S., Cerveaux, N., Groß, U., Bader, O. "DNA methylation as a potential epigenetic driver of morphological development in *Candida albicans*". Statusworkshop DGHM-Fachgruppe Eukaryontische Krankheitserreger, Berlin, Germany, 22nd - 23rd November 2018.

LIST OF TABLES

LIST OF FIGURES

LIST OF ABREVIATIONS

ATCC®	American type cell culture
5-Aza	5-Azacytidine
bp	Base pairs
BP	Biological process
°C	Degree Celsius
CBS	Centraalbureau voor Schimmelkultures
CC	Cellular component
CGD	Candida genome database
α-CHCA	α-cyano-4-hydroxycinnamic acid
cm	Centimeter
ddH_2O	Bidistilled water
DE	Differentially expressed
DGE	Differential gene expression
DNA	Deoxyribonucleic acid
DNMTase	DNA methyltransferase
dNTP	Deoxynucleosidtriphosphate
e.g.	*exempli gratia* (for example)
et al.	*et alii* (and others)
EDTA	Ethylendiaminetetraacetic acid
Eucast	European Committee on Antimicrobial Susceptibility Testing
F/fwd.	Forward
FG	Filamentous growth
g	Gramm
GC	Guanine/cytosine
GO	Gene ontology
h	Hour
HG	Hyphal growth
IC	Invasive candidiasis
IL	Interleukine
kb	kilobases
l	Liter
lncRNA	long non-coding RNA
log2FC	log2 fold change
mbp	Megabase pairs
5mC	5-methyl cytosine
MF	Molecular function
mg	Milligramm
mg/ml	Milligramm per milliliter
min	Minutes
ml	Milliliter
mm	Millimeter
mM	Millimolar

mRNA	Messenger ribonucleic acid
MS	Mass spectrometry
µg	Microgramm
µg/µl	Microgramm per microliter
µl	Microliter
µm	Micrometer
µM	Micromolar
nm	Nanometer
OD	Optical density
o.n.	Over night
ORF	Open reading frame
PBS	Phosphate buffered saline
PCA	Principal component analysis
PCR	Polymerase chain reaction
PE	Paired end
pH	Preponderance of hydrogen ions
pmol	Picomol
R/rev	Reverse
RFP	Red fluorescent protein
RIN	RNA integrity number
RNA	Ribonucleic acid
rDNA	Ribosomal deoxynucleic acid
RNAseq	Ribonucleic acid sequencing
rpm	Revolutions per minute
RT	Room temperature
SAB agar	Sabouraud agar
SE	Single end
sec	Second
sp./spp.	species (singular/plural)
TAE	Tris acetate EDTA
TF	Transcription factor
TOF	Time of flight
tRNA	Transfer ribonucleic acid
Taq.	*Thermus aquaticus*
UMG	Universitätsmedizin Göttingen
V	Volt
v/v	Volume per volume
w/v	Weight per volume
WGD	whole genome duplication
WGBS	Whole genome bisulfite sequencing
WT	Wild type

ABSTRACT

Candida albicans is a commensal yeast in the mammalian gut, but also has retained its virulence potential while co-evolving in mammalian species. As a perfectly adapted opportunist colonizing mucosal surfaces, it is also the most frequently observed human fungal pathogen. Additionally to superficial infections of skin, nails, and mucosal surfaces, it can also invade and disseminate via the bloodstream into the organs, causing life-threatening infections. Changing its morphology in response to environmental cues is a crucial characteristic and central part of its virulence. Previous studies indicated the presence of varying levels of the epigenetic modification 5-methylcytosine in the DNA of *C. albicans*. The apparent differential distribution of 5mC between yeast- and hyphae-form states brings up the question of its potential involvement in gene regulation.

Here, we looked at DNA methylation in different genomic features in *C. albicans* using WGBS at single-base resolution. Our results confirmed a very low global methylation content of ~0.08 – 0.11% distributed over the whole genome, in CG as well as CHG and CHH contexts.

We observed characteristic patterns of methylation: in protein coding sequences methylation levels were higher in the 5' and 3' adjacent regions and dropped in between. Regions encoding lncRNA or transposable elements showed higher levels of methylation. This shows that DNA methylation is not random in *C. albicans*, but occurs in meaningful patterns, indicating a different function of DNA methylation in different genomic features.

Treatment of *C. albicans* with the demethylating agent 5-Azacytidine resulted in the de-repression of hyphae related genes already in the yeast stage. 5-Azacytidine also induced hyphae formation in previously morphologically attenuated clinical isolates, together indicating an involvement of DNA methylation in mechanisms of hyphae repression.

Screening *C. albicans* clinical isolates from different clinical specimen types on hyphae inducing medium suggested a correlation between sample origin (primary sterile vs. coinhabitated body sites) and morphological attenuation. Partial conversion of attenuated to non-attenuated strains by 5-Aza treatment increased tissue invasion. Likewise, attenuation of SC5314 after gut passage could be partially restored again by 5-Aza treatment.

Taken together our results strongly suggest a direct connection of DNA methylation and the repression of morphological development of *C. albicans*, which might be the key to its high adaptation potential to host environments.

1 INTRODUCTION

1.1 Epidemiology of *Candida* spp.

Several species of the fungal genus *Candida* are part of the normal human microbial flora, colonizing the human skin as well as the gastrointestinal, oropharyngeal, and reproductive tract, where they usually do not cause severe symptoms. They are found as commensalists in around 50 – 70% of healthy humans (reviewed in Pappas *et al.*, 2018). Several studies showed the dominance of *Candida* species amongst fungi in the feces in healthy patients, especially *Candida albicans* (Hallen-Adams and Suhr, 2017). Nevertheless, worldwide *Candida* spp. are the predominant cause for opportunistic mycoses (reviewed in Pfaller and Diekema, 2007).

Currently, 15 *Candida* spp. are known to cause infections in humans, of which *C. albicans*, *C. glabrata*, *C. parapsilosis*, *C. tropicalis*, and *C. krusei* are the most prevalent in Europe and in the US (Tortorano *et al.*, 2006; Yapar, 2014). These infections (Candidiasis) can be mild and superficial, affecting the oesophagus, oropharynx, or reproductive organs. However, they can present with severe disease expression, caused by invasive growth of the fungus (IC, 'invasive Candidiases'), which can result in bloodstream and disseminated infections, including candidemia, endocarditis, central nervous system infections, and potentially can lead to live-threatening systemic infections, sepsis or even death.

Several studies of the last decades identify *C. albicans* as the most prevalent of all *Candida* species. For example, the ARTEMIS surveillance program showed, that *C. albicans* accounted for 61 – 73% of all IC infections between 1997 and 2003 (Meis *et al.*, 2000; Hazen *et al.*, 2003; Ostrosky-Zeichner *et al.*, 2003; Pfaller and Diekema, 2007) within the study group. Interestingly, this study also showed a declining incidence in *C. albicans* and a concomitant increase of non-*albicans Candida* infections during the supervised time.

A European ECMM survey (1997 – 1999) produced similar results, concluding that *C. albicans* infections ranged between 50 - 70% of all cases, followed by *C. glabrata* and *C. parapsilosis*. This distribution was found to be dependent on the underlying pathology, and patient age (Tortorano *et al.*, 2006). In general, *C. glabrata* is found more often in elderly patients and *C. parapsilosis* in premature neonates (Malani *et al.*, 2011; Dotis *et al.*, 2012; Wojak *et al.*, 2021). Most recent studies support this trend and show, that *C. albicans* is still the most prevalent *Candida* species globally. Geographical variations exist concerning non-*albicans Candida* spp.,

with mostly *C. glabrata* and second-most *C. parapsilosis* infections (reviewed in Pappas *et al.*, 2018; Koehler *et al.*, 2019). A rather worrying development is the newly globally emerging species *C. auris*, as a cause of nosocomial outbreaks with rapid spread and high mortality rates of up to 59% (Chowdhary, Sharma and Meis, 2017; Lockhart *et al.*, 2017).

Specific factors promote the transition from commensalism to opportunism, like an impaired immune system (e.g., as a result of diabetes mellitus, patients with AIDS, immunosuppressive therapies, infections with other microbes or even through stress situations), a disturbed microbial flora as consequence of antibiotic treatment, or changes in the host environment (e.g. a change in pH or the presence of nutrients) (Nobile and Johnson, 2015). Additionally, some commensal bacteria of the gut promote the release of defensive components from the gut mucosa, which is an important protective factor for disease prevention (Fan *et al.*, 2015). Consequently, an impaired microbial flora can lead to fungal overgrowth. Further, damage of the skin or the gastrointestinal barrier caused for example by surgeries or catheters, or after chemotherapeutic or corticosteroid treatment, can enable the fungus to grow invasively, especially if the immune system is weakened anyway due to an underlying disease (Pappas *et al.*, 2018).

Most *Candida* spp. are capable of complex biofilm formation, which had been shown for example for mucosal infections (Dongari-Bagtzoglou *et al.*, 2009). Further, they can form biofilms on several synthetic materials. Thus, medical devices like dentures, catheters, and prosthetic implants represent a further risk factor for *Candida* infections (Kojic and Darouiche, 2004; D'enfert and Janbon, 2016).

The most common form of IC with more than 50% is the bloodstream infection, which is fatal for 15 – 20% of patients (Mccarty and Pappas, 2015). Timing of an appropriate therapy has been shown to be a crucial factor to improve the outcome of an invasive *Candida* infection.

Additionally to fast and reliable identification techniques, like MALDI-TOF MS (Bader *et al.*, 2011; Bernhard *et al.*, 2014), T2*Candida* Magnetic Resonance (Zervou *et al.*, 2017), or specific PCR assays, the choice of the right antifungal therapy is pivotal. Commonly used therapeutic antifungals include echinocandin, fluconazole, amphotericin B, and voriconazole, with the first two serving as a typical therapy option for *C. albicans*, sometimes also combined (Pappas *et al.*, 2018). Nevertheless, similar to the emerging resistances to antibiotics in bacteria, resistances against antifungals are an increasing problem in therapy of mycoses. Therefore, drug susceptibility testing of the respective isolate referring to the EUCAST or CLSI guidelines,

allows for determination of the best antifungal therapy. Resistance against more than one antifungal drug is still rare, but multidrug resistances have emerged in *Candida* species and only a very limited number of antifungals of different drug classes are available. Especially the further development of *C. auris* infections and resistances has to be observed carefully, as the case numbers of this organism are very alarming with 93% of resistances against fluconazole, and 41% of resistances against two antifungal classes (Lockhart *et al.*, 2017). In contrast to bacteria, resistance mechanisms in *Candida* are not exchanged by horizontal gene transfer between two cells, but can occur intrinsically in the patient or by horizontal transmission of strains between patients (Arendrup and Patterson, 2017).

Currently used drugs to treat *C. albicans* infections target enzymes that are required by the fungus to build and maintain its cell wall: i.e., β-D-glucan synthase (echinocandin), and lanosterol 14 α-demethylase (fluconazole).

Increasing drug resistances in *Candida* species generally requires novel strategies in drug development. Therefore, advances for the identification of new drug targets are essential.

1.2 *C. albicans'* diverse morphology and its underlying genetic mechanisms

A very remarkable characteristic of *C. albicans* is its diversity of cell morphology. Each morphology plays a distinct role in the challenging environment of the human host during persistence, commensal growth, dissemination, and virulence, as well as in sexual reproduction. The different cell morphologies known so far are yeast-form cells, hyphae, pseudohyphae, chlamydospores, opaque-form cells, GUT-form cells, and grey cells (reviewed in Noble, Gianetti and Witchley, 2017). The best described morphologies are yeast and hyphal cells (Figure 1, A-B). Yeast cells are of ovoid shape, 3 – 8 µm in size, and reproduce by budding: spindle pole bodies separate the chromosomes into the two developing cells across the septin band until mother and daughter cell are parted by a septum. During this process, yeast cells show polarized growth, which is determined by a polarisome located at the tip of the growing bud. After cytokinesis the cells separate (reviewed in Berman, 2006; Whiteway and Bachewich, 2007). The initially formed septin ring (budding point) remains visible after cell separation (Figure 1, A). In yeast cells, polarity is restricted to the first part of the cell cycle and alternates with isotropic growth. Reproduction is similar for pseudohyphae, with the difference that the polarisome is active for a longer time. Additionally, they have a longer G2

growth phase. Altogether, this leads to elongated buds. In contrast to yeasts, pseudohyphae do not split up after cytokinesis and form filaments with constrictions (Figure 1, C). Hyphae on the other hand exhibit constant apical growth, characterized by a polarisome and a Spitzenkörper at the hyphal tip. The latter induces germ tube evagination from the yeast cell and the polarisome supports elongated growth of the tube. Nuclei are divided across the pre-septum, which is then transferred to a closed septum (reviewed in Lew and Reed, 1995; Berman, 2006; Whiteway and Bachewich, 2007). Hyphae are characterised by germ tube growth without constrictions and in contrast to pseudohyphae the septation is not directly located at the transition from mother to daughter cell, but takes place further inward in the hyphal tube, which can be visualized by chitin staining with Blankophore P (Figure 1, B).

Chlamydospores are assumed to be a kind of resting cell type that typically forms under suboptimal conditions, i.e., low levels of oxygen, nutrition, or light, and low temperatures. They originate from terminal cells (suspensor cells) of mycelia, which can be either hyphae or pseudohyphae. Nuclear division takes place in the suspensor cell and one nucleus is then transferred to the newly formed chlamydospore. This cell type is bigger than a normal blastospore, with a thick cell wall (Figure 1, D) (reviewed in Whiteway and Bachewich, 2007).

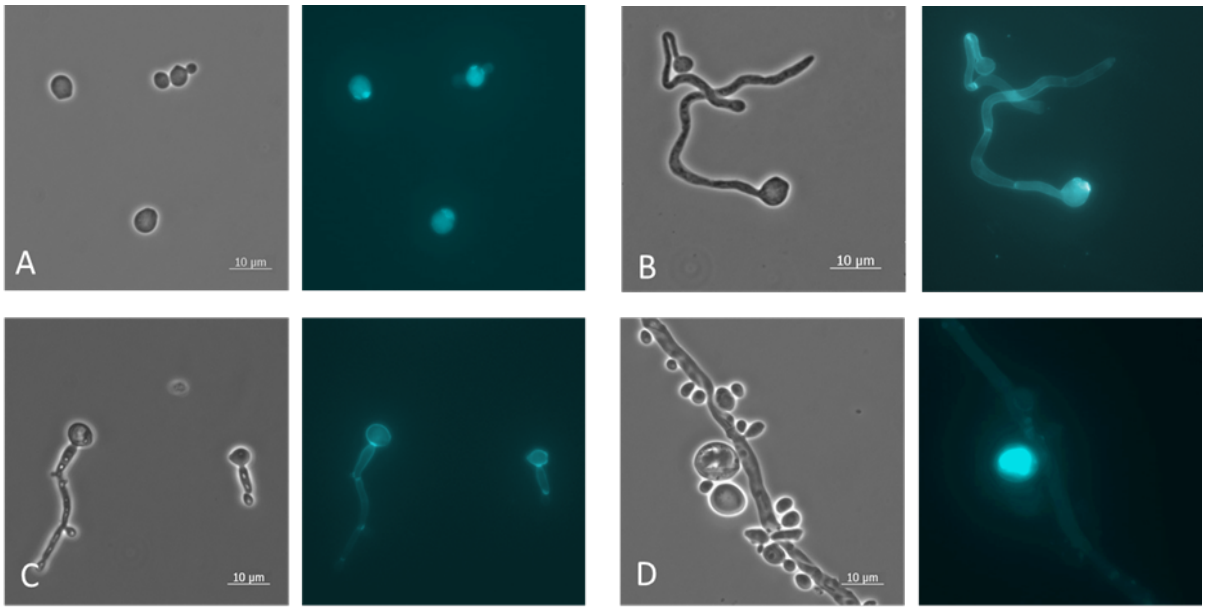

Figure 1: Different morphological states of *C. albicans*. (A) Yeast, (B) hyphae, (C) pseudohyphae, and (D) chlamydospore. Chitin staining with Blankophore P. Scalebar 10 µm.

The opaque morphology represents a specific mating-competent yeast-like cell type, which is characterized by a ~3 times larger cell size, a more elongated shape, more pronounced

vacuoles, and spots on the cell surface which are visible through electron-microscopy (Anderson, Mihalik and Soll, 1990). Mating involves the Mating Type Like locus (*MTL*), which resembles the *MAT* locus in *Saccharomyces cerevisiae*. *C. albicans* cells normally are heterozygous and have both, an **a** and α *MTL* locus. During this state the cells are unable to mate. Through the loss of one allele, which is assumed to happen epigenetically, the cells become homozygous for one allele. These homozygous **a** or α cells undergo a morphological switch from white to opaque phenotype. Subsequently, pheromone sensing is possible between opaque cells of the opposite mating type and leads to sexual filament production and mating (described in more detail in section 1.3) (Tsong *et al.*, 2003).

Other yeast-type morphologies are 'grey' cells. These cells can originate from both, 'normal' white (a/α) cells and opaque (a/α) cells (which are not capable of mating). These two cell types can also switch from one to the other state. Grey cells are characterized by a smaller size than the original cells, as well as ellipsoid shape without spots on their cell surface. Like for heterozygous opaque (**a**/α) cells, their function remains unknown (Xie *et al.*, 2013; Tao *et al.*, 2014).

The GUT (gastrointestinally induced transition) cell type had been isolated from a mammalian host. This GUT phenotype is characterized by elongated cells and darker, flattened colonies on agar medium compared to the normal white colonies. In a mammalian gastrointestinal experiment these cells were more fit as compared to the white and opaque phenotype, suggesting a strong adaptation of this cell type to the commensal lifestyle. Further, under laboratory conditions as well as in a bloodstream infection animal model, these cells grew more slowly than white and opaque cells. These findings support the hypothesis, that GUT cells are specialized to the commensal lifestyle in the mammalian gut (Pande, Chen and Noble, 2013).

The ability of *C. albicans* to switch its morphology is considered a key factor for the virulence of this opportunistic fungus (Gow, Brown and Odds, 2002). Morphogenic change takes place as a response to environmental cues, such as changes in temperature, pH, nutrients, oxygen/CO_2, host defence mechanisms, presence of other microbiota, attachment to surfaces, and many more, making it a perfectly adapted opportunistic species. The yeast form and two distinct filamentous forms – hyphae and pseudohyphae – enable this pathogen to spread inside the human body. Especially the transition from yeast to hyphal morphology seems to play an important role in its virulent life cycle. Additionally, pseudohyphae have also

been observed to penetrate the agar like hyphae. Thus, a specific role during infection has been proposed for them as well (Sudbery, Gow and Berman, 2004). Mutants defective in hyphal growth are avirulent in a mouse model (Lo *et al.*, 1997), whereas preformed hyphal inocula locked in the hyphal stage were virulent in a disseminated model and fatal for all animals (Cleary *et al.*, 2016). Nevertheless, yeast cells play an important role for dissemination via the bloodstream, as they adhere better to endothelial cell walls under flowing conditions than hyphae or pseudohyphae (Grubb *et al.*, 2009). Further, infected tissues or biofilms harbour yeast as well as both filamentous forms, emphasizing the importance of the different morphologies during infection (reviewed in Noble, Gianetti and Witchley, 2017).

Moreover, also during commensalism both morphologies play important roles, as yeasts as well as hyphae had been found in the digestive tract in the murine model. The yeast morphology was predominant in the gut and in the small intestine (~60% and ~80% respectively), whereas the hyphal morphology was predominant in the ceca and large intestine (both ~60%) (Witchley *et al.*, 2019).

Hyphal development is regulated by positive as well as negative signalling pathways and there are several extrinsic signals leading to the switch of a yeast cell to a hyphal cell (Figure 2). One example for an important factor is the environmental pH: acidic pH represses the transition from yeast to hyphal growth, whereas neutral to alkaline pH promotes hyphal growth (Fonzi *et al.*, 1998; Davis, 2003; Biswas, Van Dijck and Datta, 2007). The Rim101 pathway senses specifically alkaline pH by two possible receptors, Dfg16 and Rim21, which initiate a proteolytic signalling cascade leading to activation of the central transcription factors Efg1 and Ume6. Other pathways include, but are not limited to, the protein kinase A (PKA) pathway or the MAPK pathway. These signalling pathways are triggered by various cues, such as high CO_2 levels, bacterial peptidoglycan, amino acids, matrix embedded growth, osmotic stress, and can be negatively regulated by farnesol (Stoldt *et al.*, 1997; Braun and Johnson, 2000; Davis, Wilson and Mitchell, 2000; El Barkani *et al.*, 2000; Davis, 2003; Davis-Hanna *et al.*, 2008; Leberer *et al.*, 2008; Xu *et al.*, 2008; Sudbery, 2011; Noble, Gianetti and Witchley, 2017).

Hyphae-specific genes are also negatively regulated, for example by the transcriptional corepressor Tup1, which is targeted by specific DNA-binding proteins (Nrg1 and Rfg1) to the promotors of hyphae-specific genes (Braun and Johnson, 1997; Khalaf and Zitomer, 2001; Murad *et al.*, 2001). Additionally, a link between farnesol and Tup1 has been found, as farnesol treatment resulted in higher *TUP1* expression as well as protein levels (Kebaara *et al.*, 2008).

A further transcriptional repressor of hyphae-inducing genes is the RPG-box binding factor Rbf1 (Aoki *et al.*, 1998).

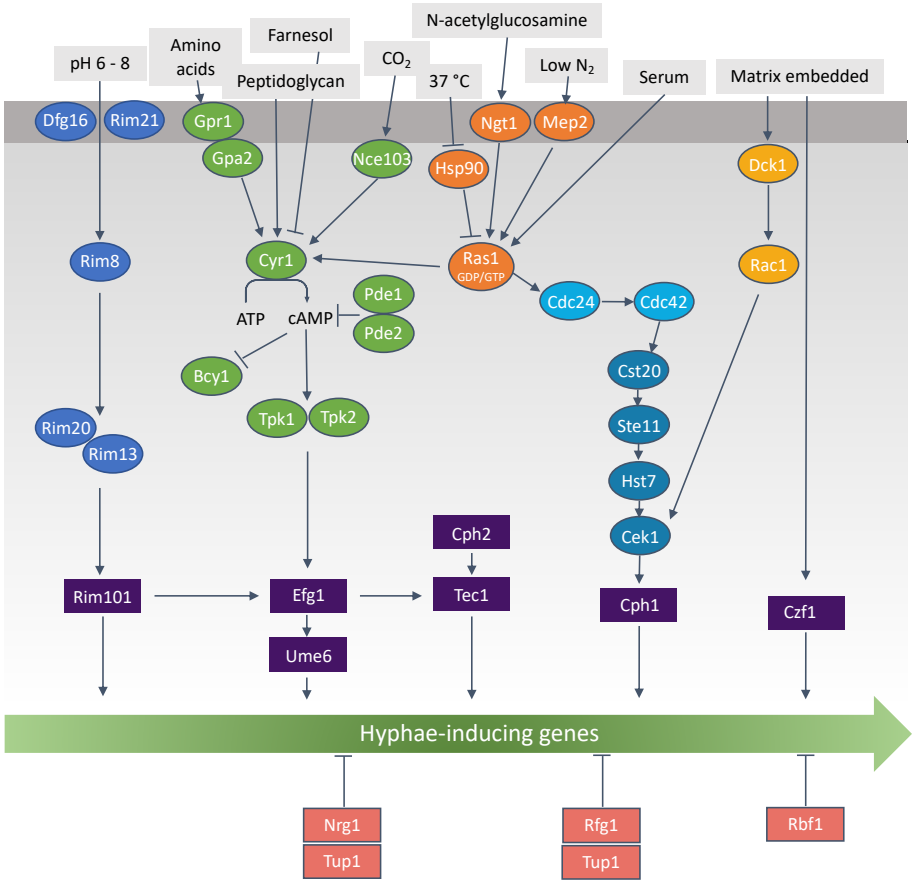

Figure 2: Hyphae related signalling pathways. Different environmental triggers activate specific signalling cascades, which finally activate transcription factors directly acting on hyphal genes. For simplicity not all known interactions are depicted (adapted from Noble, Gianetti and Witchley, 2017).

The different signal transduction pathways result in the transcription of genes that are typically expressed during hyphal development, e.g. the fungal peptide toxin *ECE1* (coding for Candidalysin), the cell wall adhesin *ALS3* (agglutinin-like sequence protein, adhesin), the cell wall proteins *RBT1* and *HWP1* (hyphal wall protein, adhesin), or the secreted aspartyl protease (SAP) family proteins (*Sap4*, *Sap5*, and *Sap6*, tissue degradation) (reviewed in Sudbery, 2011). Several studies have examined the most upregulated genes in hyphae inducing conditions. Martin *et al.* (2013) analysed the transcriptome of three differently induced hyphal cultures (pH shift, serum, and GlcNAc) in the early and later phase after infection and modelled a core filamentation response network from their data. Their result showed a network of eight genes, including the known hyphae-inducing genes *ALS3*, *ECE1*, *HWP1*, and *RBT1*, plus *IHD1* (a GPI-anchored protein), *HGT2* (putative MFS glucose transporter), *DCK1* (required for

embedded filamentous growth), and *orf19.2457* (unknown function). Further differentially expressed genes were *UME6* (important for hyphal elongation), *PHR1* (encodes putative glycosidases, typical in alkaline pH), *EED1*, (regulator of hyphal elongation), and *NRG1* (a regulator of hyphae-inducing genes) (Martin *et al.*, 2013).

ECE1 gained importance when its function as a precursor for fungal peptide toxin Candidalysin was discovered. This toxin represents the first fungal cytolytic toxin. After cell adhesion and invasion Ece1 is secreted at the hyphal tip in eight separated proteins. One of them - Candidalysin - attacks the host cell and permeabilizes it, enabling cell invasion (Moyes *et al.*, 2016).

The interaction of all these different genes promotes essential properties for the fungus' virulence, as many of them represent virulence factors, playing important roles in adhesion and invasion processes.

C. albicans represents the most diverse species of the *Candida* clade. The most closely related species *C. dubliniensis* and *C. tropicalis* are able to form true hyphae as well, but in more limited conditions and with lower filamentation rates compared to *C. albicans* (Stokes *et al.*, 2007; Lackey *et al.*, 2013). Most other *Candida* species only form yeast and pseudohyphae. The ability to switch between different morphologies has been linked to the virulence of many species (Sharma *et al.*, 2019). The newly emerging pathogen *C. auris* is closely related to *C. lusitaniae* (Muñoz *et al.*, 2018). Interestingly, *C. auris* is the only species of the haploid clade which forms true hyphae, though only after passage through a mammalian host (Yue *et al.*, 2018).

1.3 General genetic characteristics of *C. albicans*

Candida spp. are part of the kingdom of fungi, the division of Ascomycota, the subphylum Saccharomycotina, and the order Saccharomycetales. Within this order they have been assigned to a monophyletic group together with the *Saccharomyces* spp. (Figure 5), which was verified by rDNA divergence analysis (Kurtzman and Robnett, 2013). Within the *Candida* clade, haploid (e.g., *C. lusitaniae*, *C. guillermondii*) as well as diploid species (e.g., *C. parapsilos*is, *C. tropicalis*, *C. dubliniensis*) are represented and divided into two subclades.

In addition to the mitochondrial genome (ChrM), *C. albicans* contains a diploid set of eight chromosomes (Chr1 – 7 and ChrR). According to the Candida Genome Database (CGD,

September 2021) its genome has a total size of 15.47 Mb (one of the largest within *Candida* spp., Butler *et al.*, 2009) with a GC content of only 33.6%. Currently 6218 protein coding open reading frames (ORFs) are annotated, of which only 1764 (28.37%) are considered to be verified, and 152 ORFs (2.44%) are indicated as 'dubious'. The mean coding length is 1439 bp. Only 215 ORFs contain at least one intron of a total of 224 introns present in the whole genome (Braun *et al.*, 2005).

Candida species belonging to the haploid subclade like *C. lusitaniae* are known to have a complete sexual cycle (Young, Lorenz and Heitman, 2000), whereas diploid strains like *C. albicans* and *C. parapsilosis* were initially thought to be asexual. In fact, *Candida* spp. show a large sexual diversity. Even though *C. albicans* is not able to undergo meiosis, it is able to mate in a parasexual cycle: diploid cells merge, generating a tetraploid product. This tetraploid cell can grow stably or return to diploidy in stressful conditions by 'concerted chromosome loss' and subsequent mitosis instead of meiosis (Tzung *et al.*, 2001; Bennett and Johnson, 2003; Noble and Johnson, 2007; Forche *et al.*, 2008). This mating process can occur between species with different (**a** and α) or the same mating type (heterothallic and homothallic, respectively), whereas homothallic mating has only been observed with mating type **a** (Alby, Schaefer and Bennett, 2009). Interestingly, the conserved 'meiosis-specific' factors *SPO11* and *REC8* control depolyploidization and promote inter-homolog recombination, enabling genetic variation and diversity in the progeny (Anderson *et al.*, 2019).

Through multi locus sequence typing (MLST, based on DNA sequences of distinct housekeeping genes) isolates can be divided into 17 clades with multiple clonal clusters. Five of those constitute the major clades to which the most isolates can be assigned to. Nevertheless, when comparing mutations at individual sequence loci with phylogenetic MLST analysis, discrepancies can be observed, suggesting spontaneous recombination events may lead to new allelic variants (Odds *et al.*, 2007).

Local mutations and large-scale rearrangements are indicators for a highly dynamic genomic landscape in *C. albicans* (Wang, Bennett and Anderson, 2018). In some cases, these chromosome alterations seem to occur in response to environmental cues, as it had been shown for example for chromosome 5: growth on sorbose induces loss of one copy of chromosome 5, as this chromosome contains a negative regulator of *SOU1*, which is required for sorbose uptake (Greenberg *et al.*, 2005). For chromosome 5, also the reversible formation of an isochromosome has been described, which is composed of its two left arms where genes

involved in azole drug resistance are encoded (Selmecki, Forche and Berman, 2006). Additionally, spontaneous chromosome alterations occur at a frequency of 1.4% of cases, accompanied by abnormal colony shape (Rustchenko-Bulgac, Sherman and Hicks, 1990). Genomic variation can be found as polymorphisms, copy number variations, loss of heterozygosity (LOH), subtelomeric hypervariations, chromosomal inversions, and whole or partial aneuploidies.

All these findings show the plasticity of the *C. albicans* genome, which can lead to changes in phenotype, correlating with altered virulence/commensalism, or susceptibility.

1.4 Epigenetic regulation in eukaryotes

Epigenetic regulation is a mechanism by which information affecting the transcriptome are inherited, without modifying the DNA nucleotide sequence. In complex eukaryotic organisms epigenetic modifications are controlled intrinsically and play a role in developmental processes, enabling the differentiation of distinct cell types. Further, also environmental influences can alter the so-called epigenome.

Epigenetic regulation involves reversible modifications of the DNA or highly conserved DNA-associated proteins, the histones. Histones are responsible for condensation and regulation of DNA, which is packed in units of ~146 bp around a histone octamer. It is composed of the core histones H2A, H2B, H3, and H4. (Richmond *et al.*, 1984; Luger *et al.*, 1997). This so-called nucleosome core particle is connected to a linker histone (H1), which stabilizes the nucleosome. Further, by binding to the linker-DNA, it contributes to the formation of a higher-order chromatin structure, resembling “beads-on-a-string” (reviewed by Harshman *et al.*, 2013). Specific histone variants have been shown to mark regulatory regions and active promotors (Jin *et al.*, 2009), but can also be involved in the transformation of transcriptionally active to silent chromatin (reviewed in Kouzarides, 2007).

Each histone has an amino-terminal domain, lying on the outside of the histone. These lysine-rich domains are targets for acetylation. As for example shown for H4, acetylation reduces the affinity of the respective histone to DNA (Hongs *et al.*, 1993). In consequence DNA is wrapped less tightly around the histone octamer and nucleosomes are consequently packed less efficiently in arrays (Norton *et al.*, 1989; Bauer *et al.*, 1994). Thus, histone acetylation leads to an extensive change in accessibility of DNA, generally resulting in higher transcription rates in

acetylated regions, by higher transcription factor and RNA polymerase binding rates, in turn correlating with less 5mC DNA methylation (Lee *et al.*, 1993; Vettese-Dadey *et al.*, 1996; Tse *et al.*, 1998). Histone acetylation is a highly dynamic process, regulated by histone acetyltransferases (HATs) and histone deacetylase (HDACs) (reviewed by Bannister and Kouzarides, 2011). Also, in *C. albicans* the chromatin structure is important for gene expression, as chromatin alterations contribute to yeast-hyphal transition. These interactions can be mediated by known transcription factors, like Efg1 or Ssn6 (Lu *et al.*, 2008, 2011; Lee *et al.*, 2015).

And also the methylation state of nucleosomal histones is tightly correlated with transcriptional activity (Jenuwein and Allis, 2001) and can occur on the side chains of lysins and arginines (reviewed by Bannister and Kouzarides, 2011). In all eukaryotes methylation of histone 3 at lysine 4 and lysine 9 (H3K4 and H3K9) belong to the most conserved modifications, correlating with gene activation and silencing. Up to three methyl groups can bind to a lysine, with different functions for the respective methylation state (Du *et al.*, 2015). In mammalian and yeast systems H3 Lys 9 methylation for example could be associated to transcriptionally repressed heterochromatin (Bannister *et al.*, 2001; Nakayama *et al.*, 2001). Like shown for acetylation, also methylation is a reversible process, which is conducted by specific histone demethylases (reviewed by Bannister and Kouzarides, 2011).

The third possible histone modification is phosphorylation, which is highly dynamic. Phosphorylation can be found on serines, threonines and tyrosines in the N-terminal histone tails. This modification is controlled by kinases and phosphatases. The negative charge of the phosphor modification influences the chromatin state (Bannister and Kouzarides, 2011).

Further structures involved in chromatin assembly are specific complexes, like the histone chaperone complex HIR (Duc *et al.*, 2015). For *C. albicans* it could be shown, that HIR is a crucial modulator of hyphal development. The subunit Hir1 is especially important in the early phase of hyphal development for keeping up sensitivity to morphogenetic stimuli (Jenull *et al.*, 2017).

1.4.1 The process of 5mC DNA methylation is different across the phylogenetic tree

In many eukaryotes the chromatin state is also influenced by methylation of the cytosines in the DNA (Rountree and Selker, 2010). The interaction between nucleosomes and DNA methylation is not fully understood yet. Some studies suggest that DNA methyltransferase (DNMT) activity can be reduced by nucleosomes, leading to DNA methylation outside of nucleosome cores. On the other hand, it was shown that DNA methylation was enriched within nucleosome core DNA, or that methylated DNA has effects on the positioning of the nucleosomes (reviewed in Huff and Zilberman, 2014).

In most eukaryotic organisms, DNA methylation and demethylation are on one side very dynamic processes and transient and on the other hand they can be stably inherited (reviewed in Gómez-Díaz *et al.*, 2012). However, in some species it seems to be absent, e.g., in the subphylum *Saccharomycotina* including *Saccharomyces cerevisiae*, or *Shizosaccharomyces pombe, Cryptomycota*, *Microsporidia* and *Cryptosporidium parvum*. Alternatively it may also only occur in traces in these species (Capuano *et al.*, 2014; Hu *et al.*, 2015; Bewick *et al.*, 2019). Several different types of DNA methylation had been discovered: 5-methylcytosine (5mC), N4-methylcytosine (4mC), and N6-methyladenine (6mA). 6mA and 4mC methylation are thought to be mostly restricted to prokaryotes, whereas 5mC methylation is predominant in eukaryotic DNA (reviewed in Hernando-Herraez *et al.*, 2015).

To establish DNA methylation, a methyl group from the cofactor S-Adenosyl-L methionine (SAM) is enzymatically transferred to the 5’ position of cytosine (Figure 3) (Chen *et al.*, 1991).

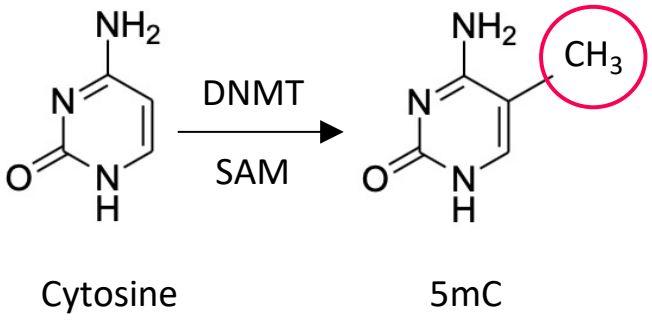

Figure 3: Methylation of Cytosine. Cytosine is methylated by a DNA methyltransferase (DNMT) at the 5th carbon position. S-adenosylmethionine (SAM) serves as methyl-group donor.

Enzymes establishing DNA methylation on previously unmethylated sequences are called *de novo* DNA methyltransferases. In hemimethylated palindromic sequence contexts like CpG or CHG these patterns are recognized and copied to the unmethylated DNA strand by maintenance DNA methyltransferases. This usually happens after replication, when one DNA strand is newly synthesized and palindromic methylation patterns are maintained (Valinluck and Sowers, 2007). Contrary to the long-standing assumption, that the fate of hemimethylated CpG residues is to become fully methylated or unmethylated, the hemimethylated state can be inherited over several cell cycles and maintained as a stable epigenetic state as well (Xu and Corces, 2018). The mechanisms of 5mC establishment at specific sequence sites still are only partially understood. But there is evidence for involvement of pairing of repetitive sequences, histone tail modifications, and small RNA pathways (Dhayalan *et al.*, 2010; Matzke and Mosher, 2014; Gladyshev and Kleckner, 2017). Further, transcription factor binding to possible target sequences seems to prevent potential DNA methylation and support hypomethylation of differentially methylated regions (DMRs) (Domcke *et al.*, 2015; Zhu, Wang and Qian, 2016).

In vertebrates, methylation is maintained by a Dnmt1 methyltransferase and, depending on the species, differing numbers of *de novo* methyltransferases from the Dnmt3 family (Okano *et al.*, 1999). Further, mammalian genomes also encode for the stimulatory cofactor DNMT3L, which lacks important catalytic motifs. This cofactor enables methylation in the germline (Bourc'his *et al.*, 2001). Other vertebrate species, who do not have the cofactor DNMT3L, seem to substitute its absence by a higher number of different *Dnmt3* genes, e.g. *Danio rerio* (zebrafish), which has six different Dnmt3 methyltransferases (Goll and Halpern, 2011). Dnmt3 interacts with H3K36me3 to enable *de novo* methylation (Dhayalan *et al.*, 2010). In insects with DNA methylation (some have lost DNA methylation, Bewick et al., 2016), one or more maintenance methyltransferases of the Dnmt1 family are encoded, as well as at least one *de novo* methyltransferase of the Dnmt3 family, resembling the vertebrate Dnmt3 (Bewick *et al.*, 2017). Interestingly, in some insects only one type of Dnmt can be found, suggesting that enzymes of the respective Dnmt family may have developed the capacity to perform both, *de novo* and maintenance DNA methylation (Schmitz, Lewis and Goll, 2019).

Plants also code for DNA methyltransferases responsible for maintaining DNA methylation. These enzymes are orthologs to Dnmt1 and are named MET1. *De novo* methyltransferases, which are similar to Dnmt3 of animals, can only be detected in early land plants. Instead, most

plants encode DRM2 methyltransferases, which contain rearranged domains responsible for methyltransferase activity. These enzymes are related to Dnmt3 and responsible for *de novo* methylation (Cao and Jacobsen, 2002). Further, chromomethylases (CMT3) are responsible for maintaining CpNpG methylation in retrotransposon sequences (Lindroth *et al.*, 2001). Interestingly, in the case of CMTs it was described, how they are recruited to sequences by H3K9me2 methylation and that the CMT-dependant methylation subsequently recruits enzymes, mediating H3K9 methylation to these sequences, resulting in a long-term feedback-loop of non-CpG and H3K9 methylation (Jackson *et al.*, 2002; Schmitz, Lewis and Goll, 2019). Furthermore, a mechanism different from the classical enzymatic DNA methylation had been described in plants: the RNA-directed DNA methylation. Here, a correlation between antisense RNAs and transcriptional and post-transcriptional gene silencing could be observed (Wassenegger, 2000).

1.4.1.1 The process of 5mC DNA methylation in different fungal clades

In fungi, four classes of DNA methyltransferases have been identified, divided into two monophyletic clades: on one hand DNMT5 and on the other hand DNMT1, DIM-2, and RID (RIP defective). The *de novo* MTase DNMT3 is not present in any of the investigated fungal species (Bewick *et al.*, 2019). A phylogenetic analysis by the same group suggested, that a maintenance- and *de novo*-like 5mC MTase occurred in the ancestor of all eukaryotes. Further, they observed that the tRNA methylating MTase Dnmt2 is structurally related to Dnmt5. Gene duplication and loss events of 5mC MTases during fungal evolution led to very diverse combinations of MTases genotypes, which can be found all over the fungal clades. In general, ascomycetes encode more homologs of DIM-2 and RID, resulting in a non-CG methylation preference, whereas basidiomycetes encode more homologs of DNMT1 and DNMT5, showing a CG methylation preference. But the respective other DNMTases can be found in the other clades as well (Bewick *et al.*, 2019; Nai *et al.*, 2021). Fungal Dnmt1 orthologs show substantial homology to plant Dnmt1 (MET1). Dnmt5 had been identified as a very specific maintenance CpG methyltransferase (Huff and Zilberman, 2014), which was found as sole DNMTase in *Cryptococcus neoformans* (Catania *et al.*, 2017). Here, it serves as a maintenance DNMTase, which specifically methylates hemimethylated double strands and in a CG context. In general, Dnmt5-containing eukaryotes (verified for fungi, chlorophyte algae, and stromatopiles) show

clustered methylation, which is specifically found in nucleosome linkers and does not provide *de novo* activity (Huff and Zilberman, 2014; Dumesic *et al.*, 2020). The dim-2 MTase shows limited homology to Dnmt1/MET1 maintenance DNMTs and is specific to fungi (Bewick *et al.*, 2019; Möller *et al.*, 2021). In *Neurospora crassa* Dim-2 mediates *de novo* DNA methylation under the direction of histone H3 methyltransferase Dim-5 (Kouzminova and Selker, 2001; Tamaru and Selker, 2001, 2003). Also RID MTases developed specifically in fungi (Bewick *et al.*, 2019). RID is associated to repeat induced point mutation (RIP, described in detail below), which was primarily discovered in *N. crassa*. RID methylates genome regions that had been targeted by RIP to protect genes from mutation and maintain their function (Selker *et al.*, 1987; Aramayo and Selker, 2013). In another genus belonging to Ascomycota, *Ascobolus,* Masc1 represents a *de novo* DNA methyltransferase. Masc1 has homologies to the catalytic domains of classical eukaryotic 5mC DNMTases, but is lacking a regulatory N-terminal domain. Methylation with Masc1 is involved in 'methylation induced premeiotically' (MIP), and thus important as genome defence mechanism. Further, it is crucial in sexual reproduction (Malagnac *et al.*, 1997). Also, in some *Aspergillus* species a DNA methyltransferase and DNA methylation could be determined. In *A. nidulans* DmtA is required for early sexual development and viable ascospores, but does not result in DNA methylation (Lee *et al.*, 2008). DmtA in *A. flavus* contributed to asexual development, aflatoxin biosynthesis, sclerotical development, and virulence. However, only a low DNA methylation level could be detected (Yang *et al.*, 2016). Homologues of RID have further been shown to be relevant in the sexual reproduction of *A. immersus* and A. *nidulans* (Lee *et al.*, 2008).

1.4.2 Removal of 5mC DNA methylation

DNA *de*methylation can happen passively during cell division without keeping up present methylations, or actively by demethylating enzymes (TETs). In animals, one to three TET enzymes can be present. These enzymes oxidize 5mC to 5hmC, 5fC, and finally 5caC in DNA (Figure 4) (Kriaucionis and Heintz, 2009; Iyer *et al.*, 2009; Tahiliani *et al.*, 2009; Ito *et al.*, 2011). TET genes are also present in basidiomycota and have been shown to be associated to a specific class of transposable elements. Also certain Ascomycota carry these TET genes, such as *S. pombe*, who carries an inactive version of this gene (reviewed by Iyer *et al.*, 2014).

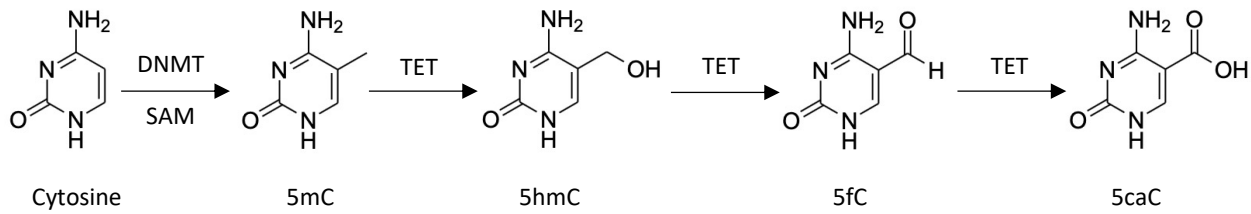

Figure 4: Cytosine modifications and their catalysation process. Cytosine is methylated by a DNA methyltransferase (DNMT). The demethylation process can happen enzymatically by a DNA demethylase. This was shown for many eukaryotes to happen by the TET demethylase, which oxidizes 5mC in several steps until 5caC. In the last step 5caC is converted to cytosine.

Nevertheless, a possible function of 5hmC, besides only being a degradation product of 5mC, has also been discussed, as it had been associated to transcription, splicing and other processes (Wang *et al.*, 2008; Shi *et al.*, 2017).

1.4.3 Genome-wide patterns of DNA-methylation

In many organisms DNA methylation regulates gene expression and is also a genome defence mechanism by suppressing the activity of transposable elements (Zemach *et al.*, 2010), enforcing long-term transcriptional repression. Further, in mammals DNA methylation is involved in embryonic development (Li, Bestor and Jaenisch, 1992; Okano *et al.*, 1999), X-chromosome inactivation, allele-specific silencing in genomic imprinting (Li, Beard and Jaenisch, 1993; Paulsen and Ferguson-Smith, 2001). Consequently, defects associated with DNA methylation can be responsible for a lot of human diseases (Robertson, 2005). This had been shown for example for specific tumour suppressor genes, where hypermethylation can lead to silencing and result in cancerogenesis (Jones and Laird, 1999).

DNA methylation can occur symmetrically in CpG or CHG context, where both DNA strands are methylated, or in CHH context (asymmetrical methylation) (H = A, C, or T). These modifications can occur *de novo* or conservatively during DNA replication, leading to inheritance of the epigenetic memory in the progeny.

Looking at the different eukaryotic phyla of animals, plants, or fungi, it becomes apparent that genomes are epigenetically modified in different ways in diverse organisms. In humans 60% – 80% of the genome are methylated (Smith and Meissner, 2013). In most animals, methylation occurs symmetrically on both DNA strands in a CpG context (Su, Han and Zhao, 2011). In human, DNA methylation can occur also in other contexts (non-CpG), of which the biologic

function is still unclear (Laurent *et al.*, 2010; Fuso, 2018). In insects, DNA methylation is not present in all species. When present, then only at levels below 15%. Further, methylation is enriched in exons of expressed genes, especially in housekeeping genes (Hunt *et al.*, 2013; Bewick *et al.*, 2017). In higher plants methylation can occur in both symmetric sequence contexts (CpG and CHG), as well as in the asymmetric CHH context. In fungi, several species show predominant CpG methylation, especially in the basidiomycete clade, but in most of these species CHG, and CHH methylation is also present, even though often on a lower level. Within the Ascomycota clade most species with DNA methylation show a balanced level of CpG, CHG and CHH methylation (Bewick *et al.*, 2019).

Patterns of DNA methylation are very different between species. The mammalian genome is globally methylated, with only CpG islands being free of methylation. These are often located at the 5' end of genes (Bird, 2002; Rabinowicz *et al.*, 2003; Eckhardt *et al.*, 2006).

Plants in general all show 5mC methylation (Schmitz, Lewis and Goll, 2019). Some in the form of 'mosaic methylation', heavily methylated domains interspersed with non-methylated domains, for example in *Arabidopsis thaliana*. Here, this specific pattern is due to gene-body methylation similar to patterns seen in invertebrates (Bewick and Schmitz, 2017), and is *not* associated to gene silencing (Zhang *et al.*, 2006). Some plants show levels of up to 50% methylation (Montero *et al.*, 1992). In *Zea mays* this seems to be due to high numbers of transposable elements (SanMiguel *et al.*, 1996; Palmer *et al.*, 2003), which are specifically targeted. Methylation of transposable elements leads to silencing of these regions (Lisch, 2009) and a decrease of 5mC methylation correlates with increased expression of TEs and unusual expression of some genes (Schmitz, Lewis and Goll, 2019).

In fungi (for phylogenetic relations see Figure 5), there is only little taxonomical knowledge about DNA methylation, as DNA methylation seems to be completely absent in many fungal species. This was shown for example for the model organisms *S. cerevisiae*, *S. pombe,* and *A. nidulans*. The highest levels of 5mC can be detected in basidiomycetes. Other than animal and plant species, gene-body methylation is absent in most fungal genomes and is instead localized primarily in repeat sequences (Bewick *et al.*, 2019). As in other species, this is assumed to be a genome defence mechanism in fungi.

This is also the case for *Neurospora crassa*, where transposable elements are specifically and highly methylated, forming also a pattern of 'mosaic methylation' throughout the genome (Selker *et al.*, 2003; Suzuki and Bird, 2008). Further, most of the methylated cytosines in the

N. crassa genome are associated with a specific process called 'repeat induced point mutation' (RIP). This mechanism targets duplicated sequences in the genome and leads to GC to AT mutations (Selker and Garrett, 1988; Cambareri *et al.*, 1989; Grayburn and Selker, 1989). RIP mutation can also affect gene coding sites, which then are methylated at the remaining cytosines to keep these genes active, as the RIP mechanism can result in gene damage of both alleles (Selker, Fritz and Singer, 1993; Singer, Marcotte and Selker, 1995). Interestingly, in *N. crassa* methylation in the proximal promotor regions does not inhibit the transcription itself significantly, but it inhibits transcriptional elongation (Rountree and Selker, 1997). The authors of this study also concluded from their experiments, that DNA methylation could affect the distribution of RNA polymerases along a methylated gene, for example by preventing binding of a specific TF for elongation. In most fungal species, 5mC is observed in all dinucleotide contexts (Su, Han and Zhao, 2011; Bewick *et al.*, 2019).

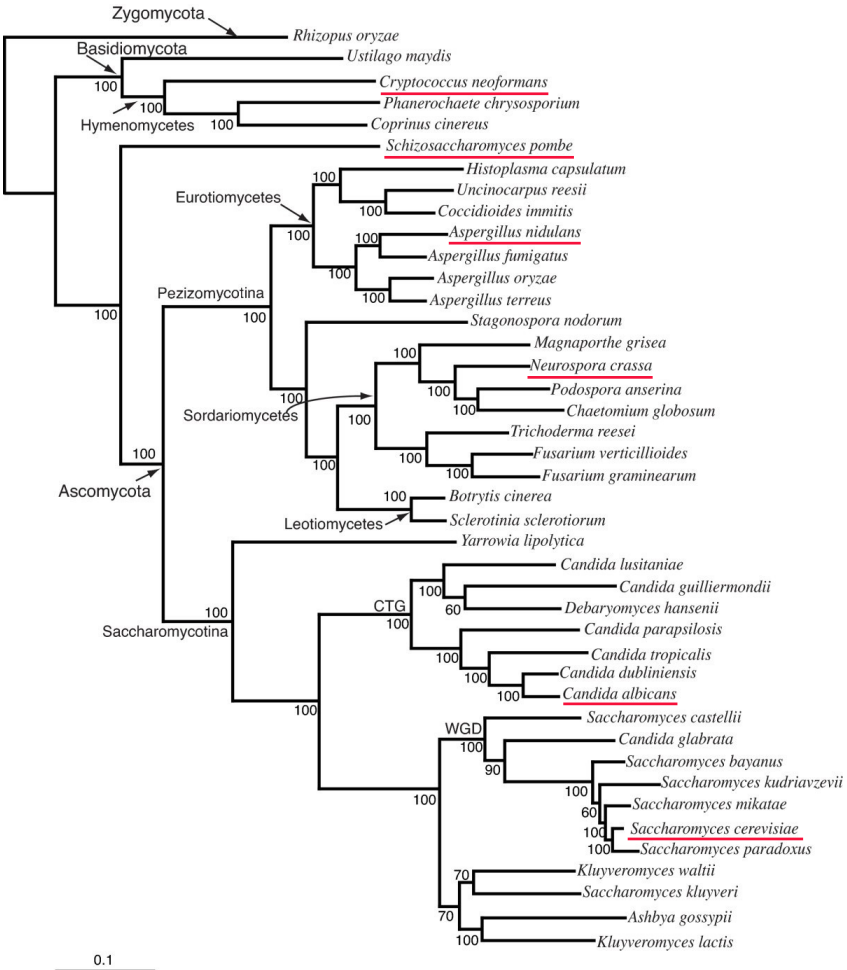

Figure 5: Fungal phylogeny. Phylogenetic categorization of the Candida clade and specifically *Candida albicans* into the Saccharomycotina clade. *Candida* and *Saccharomyces* spp. form one monophyletic group (multigene phylogeny, modified from Fitzpatrick et al., 2006). Details on DNA methylation of red underlined species are specifically discussed in the text.

Traditionally, DNA methylation had been seen as a silencing mechanism for DNA expression, but recent studies draw a much more complex picture. In mammals, cell-type specific methylation correlates with gene-body methylation of highly conserved sequences, whereas the smaller proportion is found in 5' CpG island promotors (Ching *et al.*, 2005; Eckhardt *et al.*, 2006; Illingworth *et al.*, 2008). Interestingly, tissue-specific gene-body methylation can reduce, or even enhance transcription elongation efficiency (Flanagan and Wild, 2007; Ball *et al.*, 2009). In human cells it was shown, that the predominantly methylated CpG islands are found in inter- and intragenic regions, and in promotor sites. In all three locations overlaps with RNA markers of transcription initiation were observed. This correlates with the observation that transcription commonly initiates within and between genes. Further, unmethylated CpG islands significantly overlapped with presence of trimethylated histone H3K4, which is often enriched at promotors (Carninci *et al.*, 2006; Kimura *et al.*, 2006; Maunakea *et al.*, 2010).

The relation between DNA methylation and gene expression can be positive as well as negative, depending on genetic variations as well as correlation with TF abundance (Kulis *et al.*, 2012; Gutierrez-Arcelus *et al.*, 2013).

In some eukaryotes active gene-bodies are specifically targeted and a parabolic relationship between gene-body methylation and transcriptional level has been shown: moderately expressed genes were more likely to be methylated, whereas genes expressed at either the lowest or the highest level were usually less methylated (Flores *et al.*, 2012).

1.4.4 What is known about DNA methylation and its epigenetic regulation in *C. albicans?*

The first study on DNA methylation in *C. albicans* was conducted by Russel *et al*. in 1987, who found a different amount of methylated cytosines in yeast compared to mycelial cultures by mass spectrometry. Yeast cultures contained between 0.11% - 0.097% 5mC on molar bases, and in the yeast-mycelial cultures between 0.045% - 0.053% were detected (Russell *et al.*, 1987), suggesting approximately double the methylation in yeast cells as compared to mycelial cultures.

Shortly after, it was shown that pre-treatment with 5-Azacytidine (5-Aza) [10 mM] – a known DNA demethylating agent – can accelerate and synchronize germ tube formation in *C. albicans* cells, upon induction of mycelial growth (Sabouraud's glucose broth + serum, 37°C). No effect could be seen in yeast cells growing in non-mycelial inducing medium (SGB, 27°C). This data suggested a modulation of gene activity together with phenotypic modification by DNA demethylation (Pancaldi *et al.*, 1988).

A first molecular study on 5mC methylation in *C. albicans* was performed with methyl-CpG affinity chromatography of fractionated DNA and subsequent PCR of bisulfite treated DNA (Mishra, Baum and Carbon, 2011). This way, the authors investigated 0.2% (55 regions) of the genome of *C. albicans* reference strain SC5314. 5mC DNA methylation was found in symmetric as well as in asymmetric contexts, with a preference for methylation of CpA (43.3%) and CpT (24.6%) contexts. Further, DNA methylation was localized mainly in gene bodies, and repeat sequences as well as multigene families mostly free of methylation. A part of the genes subject to methylation could be assigned to dimorphic transition between yeast and hyphal forms, white opaque switch, and iron metabolism. Further, this study gave a first hint for a relation between DNA methylation and the suppression of genes linked to yeast to hyphae transition. This relation was specifically shown for *PBI2*, which is necessary for proteolysis during sporulation: hyphal cells were largely free of methylation, whereas yeast cells showed a methylated cytosine at variable positions in this gene locus. Interestingly, mostly only one 5mC could be detected per sequenced clone in this 383 bp long gene. Further, they were able to remove methylation by 5-Aza [100 µM] treatment, which resulted in a repression of transcription for this gene, as shown by Northern blot analysis.

The opposite was the case for *RBT5*, an iron-dosage dependent gene repressed as well by serum and alkaline pH, a high iron dose depleted DNA methylation and the transcriptional product. Here removal of methylation by 5-Aza treatment did not restore transcription (Mishra, Baum and Carbon, 2011).

In another study focusing on the evolutionary changes of the mitochondrial *C. albicans* genome, the impact of environmental conditions specifically on the mitochondrial genome methylation was analysed using WGBS (Bartelli, Bruno and Briones, 2018). Surprisingly, the findings of this group differed substantially from previous findings on DNA methylation levels, as they found a mean methylation level of 99% in the mitochondrial DNA of strain SC5314 and

strain L757. After growing the strains under hypoxia for 12 weeks, in both strains' mean mitochondrial methylation levels were reduced to around 60%. As the methylation state of mitochondrial DNA is subject to debates questioning the presence of methylation in mitochondria in general (Formighieri *et al.*, 2008; Mechta *et al.*, 2017; Fan *et al.*, 2019), and mitochondrial DNA is even used as unmethylated control for bisulfite conversion experiments to detect bisulfite conversion rates (Bewick *et al.*, 2019), this result is difficult to interpret.

Bewick *et al*. looked at multiple fungal species from diverse phyla using WGBS as well, including *C. albicans*. This study detects CpG, CHG, and CHH methylation levels at only a very low level of <0.5% in the whole genome as well as in intergenic regions, exons, and introns (Bewick *et al.*, 2019). For *N. crassa* they found a methylation level of around 2.0%, comparable to the previously reported result of 1.5% (Russell *et al.*, 1987), showing the reproducibility of this result.

Taken together, there is only little known on DNA methylation and its effects on cellular processes in *C. albicans*. On one side the global genomic methylation landscape is completely unknown, i.e., promotor methylation patterns or methylation of genes encoding for specific features like RNAs or TEs. On the other hand, the relation between methylation and gene expression still is not clear and needs more study

1.5 The methylation inhibiting effect of 5-Azacytidine

5-Aza is a well-known, irreversibly binding DNA methyltransferase inhibitor, that was primarily discovered as a cytostatic agent for cancer patients (Šorm *et al.*, 1964). As a cytidine analogue 5-Aza is incorporated into DNA and RNA and leads to inhibition of DNA, RNA, and protein biosynthesis (reviewed in Christman, 2002). Further, a DNA methylation inhibiting effect could be shown in the human cell line (Jones and Taylor, 1980).

In several cancer diseases, a hypermethylation of promotors of cancer- related genes and specifically genes relevant for tumour suppression (tumour suppressor genes) often leads to the development of carcinogenesis by gene silencing. This is also the case for the tumour suppressor gene TCF21, a transcription factor which is epigenetically inactivated in a variety of human cancers. Accordingly, 5-Azacytidine is used as therapeutic agent especially for treatment of myelodysplastic syndrome (MDS) and non-M3 acute myeloid leukaemia (AML)

(Gu *et al.*, 2019). It is the only disease modifying drug and can decrease the rate of and prolong the time to a potential leukemic transformation (Raj, 2006).

The demethylating effect of 5- Aza is based on the fact, that azanucleosides are cytidine analogues and as such incorporated into replicating DNA during mitosis instead of cytosine. But 80% – 90 % of 5-Aza are incorporated into RNA in vivo, because ribonucleotide reductase limits the conversion of 5-Azacytidine to 5-Aza 2'deoxycytidine. Once incorporated into the DNA, potential DNA methyltransferases initiate the methylation reaction, and a covalent bond is formed. This bond is normally released by beta-elimination through the carbon-5 atom after the transfer of the methyl group, but this release reaction is blocked with azacytosine, as carbon-5 is substituted by nitrogen in 5-Aza (Figure 6). In consequence the methyltransferase function is also blocked (reviewed in Stresemann and Lyko, 2008). This leads to a loss of DNA methylation during replication. Further, the drug induces proteasome activity, targeting the blocked enzyme and leading to its degradation (Ghoshal *et al.*, 2005). *In vitro* studies show, that undermethylation by 5-Aza correlates with activation of previously inactive genes and transposable elements (Chiu and Blau, 1985; Pancaldi *et al.*, 1988; Ohtani *et al.*, 2020).

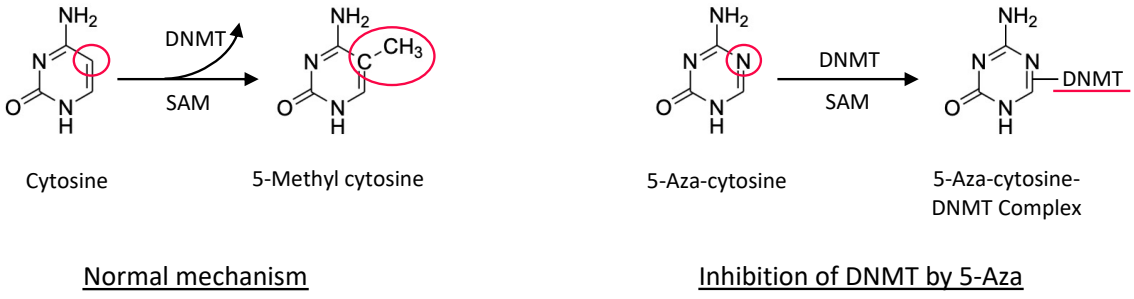

Figure 6: Mechanism of methylation inhibition by 5-Azacytidine. During the normal methylation mechanism, the carbon-5 atom of cytosine is methylated by a DNA methyltransferase (DNMT), which afterwards is released from DNA. S-adenosylmethionine (SAM) serves as methyl-group donor. If cytosine is replaced by 5-Azacytidine, the covalent bond between the DNMTase and 5-Aza-cytosine cannot be released anymore as the 5th carbon atom is replaced by a nitrogen. A methyl group transfer from SAM to the DNA cannot take place (adapted from Huang et al., 2011).

1.6 Aims of the study

The virulence potential of *C. albicans* is based on its ability to perfectly adapt to its environment, accompanied by a brought phenotypic plasticity. DNA methylation at cytosines as an epigenetic modification has been shown to be a crucial regulator of gene expression in other organisms and presence of 5mC in *C. albicans* had been indicated by a few previous studies. Still, the role of DNA methylation and its underlying mechanisms are only poorly understood.

Based on the available few hints in the literature that DNA methylation could be connected to morphogenesis, the goal of this thesis was to analyse 5mC DNA methylation in *C. albicans* more deeply and put it into context of morphogenesis. In contrast to previous studies relying either on context-free quantification or reduced subsets of the genome only, the intention was to perform a more global analysis of DNA methylation in the genome of *C. albicans* by whole genome bisulfite sequencing. This technique is seen as the current gold-standard of DNA methylation analysis. To this end, strategies for data analysis were to be established, that would allow analysis at single-base resolution for *C. albicans*.

It was of special interest, if DNA methylation was found just randomly across the whole genome or in specific patterns, depending on the features targeted (e.g., protein coding vs. RNA-encoding features). Further, the question was, if specific regions of the genome (i.e., subtelomeric regions, the mitochondrial genome, or hyphae-relevant gene sets) were preferentially targeted by 5mC.

The effect of DNA methylation on the morphology of *C. albicans* was of particular interest. As a potential DNMTase in *C. albicans* is still unknown and thus no target for genetic approaches was available, the demethylating agent 5-Azacytidine ought to be used instead. The underlying hypothesis was, that random demethylation in the genome could activate specific gene sets and thereby induce morphological changes. Whole genome transcriptomic analysis by RNA sequencing should reveal how the demethylating effect of 5-Azacytidine affects gene expression in yeast and hyphae inducing environments.

2 MATERIALS AND METHODS

2.1 Materials

2.1.1 Chemicals and disposables

Materials and disposables for general use were purchased from Carl Roth GmbH (Karlsruhe, Germany), Eppendorf AG (Hamburg, Germany), Merck KGaA (Darmstadt, Germany), Sarstedt AG & Co. KG (Nümbrecht, Germany), Sartorius AG (Göttingen, Germany), Sigma-Aldrich Chemie GmbH (Steinheim, Germany), or Thermo Fisher Scientific GmbH (Schwerte, Germany). Deviant manufacturers are specified in Table 1.

Table 1: Chemicals and disposables

Chemicals and materials	Manufacturer
Agar agar	Carl Roth GmbH
Agarose	Carl Roth GmbH
5-Azacytidine	Sigma Aldrich Chemie GmbH
α-cyano-4-Hydroxycinnamic acid ($C_{10}H_7NO_3$), HCCA	Sigma-Aldrich Chemie GmbH
Acetonitrile LC – MS Chromasolv ®	Sigma-Aldrich Chemie GmbH
Alanine	Carl Roth GmbH
Ammonium sulfate $(NH_4)_2SO_4$	Sigma-Aldrich Chemie GmbH
Ampicillin	Sigma-Aldrich Chemie GmbH
Arginine	Carl Roth GmbH
Bacto ™ Peptone	BD, Becton Dickinson and Company, Le-Pont de-Claix, France
Bacto ™ Yeast Extract	BD, Becton Dickinson and Company, Le-Pont de-Claix, France
Biotin	Carl Roth GmbH
Blankophor P	Prechel GmbH, Schwetzingen, Germany
Calcium chloride ($CaCl_2$)	Sigma-Aldrich Chemie GmbH
Chloroform 99% p.a.	Carl Roth GmbH
Copper(II) sulfate pentahydrate ($CuSO_4$ * $5H_2O$)	Sigma-Aldrich Chemie GmbH

Chemicals and materials	Manufacturer
D + Glucose Monohydrate	Carl Roth GmbH
Dimethyl sulfoxide (C_2H_6OS)	Sigma-Aldrich Chemie GmbH
Di-potassium hydrogen phosphate (K_2HPO_4)	Sigma-Aldrich Chemie GmbH
DNA Gel Loading Dye 6X	Thermo Fisher Scientific
DNA Ladder	Thermo Fisher Scientific
Ethanol 99.8 % p.a	Carl Roth GmbH
Ethylenediaminetetraacetic acid ($C_{10}H_{16}N_2O_8$)	Sigma-Aldrich Chemie GmbH
Filter tops (screwable), 0.2 µm	Corning Inc., Corning, NY, USA
Formic acid Rotipuran ® 98 % (CH_2O_2)	Carl Roth GmbH
GelRed ®, 10000X	Genaxxon Bioscience, Ulm, Germany
Glacial acetic acid (CH_3COOH)	Carl Roth GmbH
Glass beads, 0.5 mm	BioSpec Products, Carl Roth GmbH, Karlsruhe, Germany
Glass microscopic slide	Menzel, Thermo Fisher Scientific
Glass cover slip	Menzel, Thermo Fisher Scientific
Hydrochloric acid (HCl)	Carl Roth GmbH
Isoamylalkohol p.a.	Merck KGaA
Iron (III) chloride ($FeCl_3$)	Carl Roth GmbH
Isopropanol 99.8% p.a.	Carl Roth GmbH
Leucine	Carl Roth GmbH
Lysine	Carl Roth GmbH
Magnesium chloride ($MgCl_2$ * $6H_2O$)	Sigma-Aldrich Chemie GmbH
Magnesium sulfate heptahydrate ($MgSO_4$*$7H_2O$)	Sigma-Aldrich Chemie GmbH
Mast Cryobanks	Mast Diagnostica GmbH, Reinfeld, Germany
Methanol	Carl Roth GmbH
Methionine	Carl Roth GmbH
$MgCl_2$ 25 mM	Roche Pharma AG, Grenzach-Wyhlen, Germany
Midori Green Advance	Nippon Genetics Europe GmbH, Düren, Germany
Mowiol® 4-88	Polyscience Europe GmbH, Hierschber a.d. Bergstraße, Germany
MSP 96 polished steel BC targets	Bruker Daltonics, Bremen, Germany
Ornithine	Carl Roth GmbH

Chemicals and materials	Manufacturer
PCR grade nucleotide Mix (dATP, dCTP, dGTP, dTTP) [10 mM] each	Roche Pharma AG, Grenzach-Wyhlen, Germany
PCR reaction buffer + Mg (10X) 25 mM	Roche Pharma AG, Grenzach-Wyhlen, Germany
Phenol-Chloroform-Isoamylalkohol (25:24:1), pH 8.5	Carl Roth GmbH
Phenylalanine	Carl Roth GmbH
Potassium chloride (KCl)	Sigma-Aldrich Chemie GmbH
Potassium hydrogen phosphate ($KHPO_4$)	Sigma-Aldrich Chemie GmbH
Proline	Carl Roth GmbH
RNAse A [5µg/µl]	Lucigen Corporation, Middleton, WI, USA
RNAse I [10U/µl]	Thermo Fischer Scientific GmbH
RNAse T1 [1000U/µl]	Lucigen Corporation, Middleton, WI, USA
Sabouraud´s agar	Merck KGaA
Sabouraud´s agar plates with or without gentamicin and chloramphenicol	Oxoid GmbH, Wesel, Germany
Serological pipettes	Labsolute, Th. Geyer GmbH & Co. KG, Renningen, Germany
Sodium chloride (NaCl)	Sigma-Aldrich Chemie GmbH
Sodium dodecyl sulfate (SDS)	Merck KGaA
Sodium hydrogen phosphate (Na_2HPO_4)	Merck KGaA
Sodium hydroxide (NaOH)	Sigma-Aldrich Chemie GmbH
Square petri dish (120 x 120)	Greiner Bio-One, Kremsmünster Österreich
Syringe	Terumo, Tokio, Japan
Taq DNA polymerase, 5 U/µl	Hoffmann-La Roche, Basel, Switzerland
Threonine	Carl Roth GmbH
Tris	Carl Roth GmbH
Tri-fluoro acetic acid (TFA)	Carl Roth GmbH
Trizol	Ambion Inc., Austin, Texas, USA
X-Gal	Thermo Fisher Scientific
Zinc sulfate solution ($ZnSO_4$)	Sigma-Aldrich Chemie GmbH

Table 2: Media composition

Medium	Components
LB-Amp agar	0.5% (w/v) tryptone, 1% (w/v) yeast extract, 0.5% (w/v) NaCl, 1.35 % (w/v) agar, dissolved in ddH_2O; 0.01% (w/v) Ampicillin (added after autoclaving at maximum 50°C medium temperature)
Lee's medium (Lee, Buckley and Campbell, 1975)	1) 0.696% (w/v) arginine solution (1ml/l); 2) 0.001% (w/v) biotin solution (1ml/l); 3) trace metal solution I: 20.3% (w/v) $MgCl_2$, 14.7% (w/v) $CaCl_2*2H_2O$ (1ml/l); 4) trace metal solution II: 0.006% (w/v) $ZnSO_4$, 0.027% (w/v) $FeCl_3$, 0.00625% (w/v) $CuSO_4$ (1ml/l); 5) 50% (w/v) glucose solution (25ml/l); 6) 0.05% (w/v) alanine, 0.13% (w/v) leucine, 0.1% (w/v) lysine, 0.01% (w/v) methionine, 0.00714% (w/v) ornithine, 0.05% (w/v) phenylalanine, 0.05% (w/v) proline, 0.05% (w/v) threonine; 7) 0.5% (w/v) $(NH_4)_2SO_4$, 0.02% (w/v) $MgSO_4*7H_2O$, 0.25% (w/v) K_2HPO_4 (anhydrous), 0.5% (w/v) NaCl, pH 4.5 or 6.5 with HCl
Sabouraud agar (SAB)	6.5% (w/v) Sabouraud agar dissolved in ddH_2O (pH = 5.6 ± 0.2)
Spider agar	1 % (w/v) nutrient broth, 1 % (w/v) mannitol, 0.2 % (w/v) K_2PO_4, 1.35 % (w/v) agar, dissolved in ddH_2O

For one litre of Lee's medium the 1) arginine stock solution, 2) biotin stock solution, 3) trace metal stock solution I, 4) trace metal stock solution II, 5) the glucose stock solution, and 6) a 10x amino acids stock solution were prepared in ddH_2O and filter sterilized. Then, all other components (7) were dissolved in ddH_2O, 100 ml of the 10x amino acid solution were added, and the volume filled up to 900 ml with ddH_2O. The pH was set to 4.5 or 6.5 with HCl and NaOH, for induction of yeast or hyphal growth, respectively. The volume was filled up to 971 ml with ddH_2O. Afterwards, the main solution was filter-sterilized and 25 ml glucose solution, and 1 ml each of arginine solution, biotin solution, and trace metal solutions I and II were added to a final volume of 1000 ml. When Lee's medium was supplemented with 5-Azacytidine, that was dissolved directly in an appropriate amount of Lee's medium and filter sterilized, before adding to the medium.

LB medium was used as selective medium after cloning and therefore supplemented with Ampicillin. Ampicillin stock solutions were prepared with ddH_2O and filter sterilized.

Agar containing media were autoclaved at 121°C for 15 min (LB medium 20 min) for sterilization. In case of Ampicillin supplementation, the medium was cooled to 50°C before

ampicillin was added under sterile conditions. The medium was mixed thoroughly and poured into petri dishes.

Filter sterilization of supplements was done with 0.2 µm filters.

Table 3: Solutions

Solution	Components
Lysis buffer (for genomic DNA isolation)	100 mM Tris-HCl (pH = 8), 50 mM EDTA, 1% (w/v) sodium dodecyl sulfate (SDS); filter-sterilized
Matrix (for MALDI-TOF)	1% (w/v) HCCA in 50% (v/v) acetonitrile and 2.5% (v/v) TFA acid
PBS 10x	0.8% (w/v) NaCl, 0.02% (w/v) KCl, 0.14% (w/v) Na_2HPO_4, 0.24% (w/v) $KHPO_4$ in a final volume of 1 liter (pH = 7.4)
Saline solution	0.9% (w/v) NaCl in ddH_2O
TAE 50x (for gel electrophoresis)	24.2% (w/v) Tris base, 5.71% (v/v) glacial acetic acid, 1.86% (w/v) EDTA; working solution 1x
TE buffer, pH 8.5 (+RNAse)	0.12% (w/v) Tris base, 0.03% (w/v) EDTA, pH 8.5 (+ 0.02% (w/v) RNAse A; added after autoclaving)
Tris-HCl, pH 8.5	0.061% (w/v) Tris, pH 8.5

PBS, saline solution, TE buffer, and Tris-HCl solution were autoclaved for 20 min at 121°C.

Table 4: Commercial kits

Kit	Manufacturer
5-mC DNA ELISA Kit	ZymoResearch Europe GmbH, Freiburg, Germany
EZ DNA Methylation-Lightning Kit	ZymoResearch Europe GmbH, Freiburg, Germany
Invitrogen TOPO TA Cloning® Kit with pCR 2.1 TOPO	Thermo Fisher Scientific GmbH, Darmstadt, Germany
Master Pure™ Yeast DNA Purification Kit	Lucigen Corporation, Middleton, WI, USA
Nucleospin® Gel and PCR Clean-up Kit	Macherey&Nagel, Düren, Germany

2.1.2 Instruments

Table 5: Instruments

Instrument	Model and manufacturer
Centrifuge for falcon tubes	Megafuge 16R, Heraeus, Hanau, Germany
Electrophoresis power supply	EPS – 301, Amersham Pharmacia Biotech, Amersham, UK
FastPrep® machine	Thermo Savant, FP120 cell homogenizer, Qbiogene Inc., Carlsbad, CA, USA
Gel imaging system	Chemidoc, Gel Doc XR+, Biorad, Hercules, CA, USA
Incubator for agar plates	Function Line, Heraeus, Hanau, Germany
Inverse light microscope, incl. AxioCam MRm, Fluorescence Lamp HBO100/HAL100 Lens 100x/1.3 Oil Ph3 Plan-Neofluar Software Axiovision 4.8.2 SP3	Axiovert 200M, Zeiss, Oberkochen, Germany
Inverse light microscope, Objective 40x/0.60 Plan Fluor ELWD	Eclipse TE2000-S, Nikon Corporation, Tokio, Japan
Magnetic stirrer	RCT basic, IKA Werke, Staufen, Germany
MALDI Biotyper	Autoflex III smartbeam and microflex LT, Bruker Daltonics, Bremen, Germany
Microcentrifuge	5417R, Eppendorf, Hamburg, Germany
Microplate reader	Epoch2, BioTek Instruments, Winooski, VT, USA
MilliQ water filter machine	Arium pro F, Sartorius AG
NanoDrop Spectrophotometer	NanoDrop 2000c, PeqLab, Erlangen, Germany
PCR Cycler	T3 Thermocycler, Biometra, Göttingen, Germany
PH meter	766 Calimatic, Knick KG, Berlin, Germany
Precision scale (0.0001g)	ENTRIS 64-1S, Analytical balance, Sartorius AG
Shaker for liquid cultures	SM-30, Edmund Bühler GmbH, Bodelshausen, Germany
Spectrophotometer	Ultraspec 1000, Pharmacia Biotech, Amersham, UK
Scale	BL 310, Sartorius AG
Thermoblock	Thermomixer C, Eppendorf, Hamburg, Germany
Vortex	Genius 3, IKA-Werke, Staufen, Germany
Waterbath	1092, GFL, Burgwedel, Germany

2.1.3 Synthetic oligonucleotides

Synthetic oligonucleotides for polymerase chain reaction (PCR) and sequencing were purchased from Sigma-Aldrich (Steinheim, Germany). Stock solutions were prepared with sterile ddH_2O to a concentration of 100 µM.

Table 6: Oligonucleotides

Name	Sequence
F3-C1_00050C	5‘-AAGTTAGATATTATTGAGTTAGTTTAA
R3-C1_00050C	5‘-CAAACCCCCTCTTTATTTTTATTTACAC
M13F	5’-TGTAAAACGACGGCCAGT
M13R	5’-CAGGAAACAGCTATGACC
RFP-fwd	5’-GCAAGCAAGCTTATTCAGAA
RFP-rev	5’-CCAGTTGAATGTCTACCTTC
F_ACC1	5’-GCAAGAGAAATTTTAATTCAATG
R_ACC1	5’-TTCATCAACATCATCCAAGTG
F_AAT1a	5’-ACTCAAGCTAGATTTTTGGC
R_AAT1a	5’-CAGCAACATGATTAGCCC
F_MPIb	5’-ACCAGAAATGGCCATTGC
R_MPIb	5’-GCAGCCATGCATTCAATTAT
F_SYA1	5’-AGAAGAATTGTTGCTGTTACTG
R_SYA1	5’-GTTACCTTTACCACCAGCTTT
F_ADP1	5’-GAGCCAAGTATGAATGATTTG
R_ADP1	5’-TTGATCAACAAACCCGATAAT
F_VPS13	5’-TCGTTGAGAGATATTCGACTT
R_VPS13	5’-ACGGATGGATCTCCAGTCC
F_ZWF1b	5’-GTTTCATTTGATCCTGAAGC
R_ZWF1b	5’-GCCATTGATAAGTACCTGGAT

2.1.4 Clinical isolates

All *C. albicans* clinical isolates used in this study were obtained from the diagnostic unit of the Department for Medical Microbiology of the University Medical Center Göttingen (UMG) and are specified in detail in the appendix (Supplementary Table 1). All collected isolates were placed as cryo stocks into the strain collection of our laboratory (PEU collection). Clinical isolates used for 5-Aza experiment, whole genome bisulfite sequencing (WGBS), and cell damage assay are listed below (Table 7).

Table 7: *C. albicans* clinical isolates used in 5-Aza experiment, WGBS, and cell damage assay

Internal No.	Collection No.	Source of isolation
03	PEU3692	Tracheal secretion (respiratory)
10	PEU3782	Bronchial lavage (respiratory)
21	PEU3784	Urine
23	PEU3694	Urine
30	PEU3786	Stool
33	PEU3696	Stool
36	PEU3788	Punctate abdomen (invasive)
37	PEU3698	Intraoperative abdominal swab (invasive)
44	PEU3700	Blood culture aerob
46	PEU3790	Blood culture aerob
49	PEU3792	Blood culture aerob
58	PEU3794	Swab throat (oral)
60	PEU3796	Swab tonsil (oral)

Further isolates, other than *C. albicans*, were taken from the PEU collection of clinical isolates or from the reference strain collection (section 2.1.5).

Table 8: Clinical isolates of diverse fungal species

Collection No.	Clinical isolate	Source of isolation
PEU2699	*Aspergillus flavus*	Swab ear
PEU3819	*Candida auris*	unknown
PEU2541	*Candida glabrata*	Blood culture
PEU3585	*Candida parapsilosis*	Punctate knee
PEU2579	*Candida tropicalis*	Intravenous catheter
PEU2756	*Cryptococcus diffluens*	unknown
PEU3509	*Saccharomyces cerevisiae*	Sputum

2.1.5 Reference strains

Table 9: *C. albicans* reference strains

Clinical isolate	Further details	Collection	Reference
SC5314	Wildtype, ATCC® MYA-2876™, clinical human specimen, unknown	American Type Culture Collection, ATCC®, Manassas, USA	(Maestrone and Semar, 1968); W. Fonzi, Georgetown University
SC5314-*RFP*	SC5314 derivate, *ADH1*/*adh1*::(*RFP*-Ca*SAT1*) (M2396)		Osama Elshafee, 2017, Jena, Germany
DSM11225	ATCC 90028, NCCLS 11, CBS8837 clinical human specimen, blood, USA, Iowa	German Collection of Microorganisms and Cell Cultures, DSMZ, Leibniz Institute, Braunschweig, Germany	A. F. Schmalreck - ATCC, M. Pfaller - NCCLS
DSM11949	ATCC 76615, Y01.09	German Collection of Microorganisms and Cell Cultures, DSMZ, Leibniz Institute, Braunschweig, Germany	A. F. Schmalreck, Pfizer Co.; Y01.09
BWP17	SC5314 derivate *Ura3Δ*::*imm434/ura3Δ*::*imm434 his1*::*hisG/his1*::*hisG arg4*::*hisG/arg4*::*hisG*		Wilson, Davis and Mitchell, 1999
529L	Clinical human specimen, oral isolate		Rahman *et al.*, 2007

Table 10: Further reference strains of other fungal species

Clinical isolate	Further details	Collection	Reference
Af293	*Aspergillus fumigatus*, clinical human specimen, lung biopsy, NCPF 7367 CBS 101355	National Collection of Pathogenic Fungi, Bristol, UK; Centraal Bureau voor Schimmelcultures (CBS), Baarn, NL	Pain *et al.*, 2004
CBS 10085	*Cryptococcus neoformans*, WM148; VNI, AFLP1, clinical human specimen, cerebrospinal fluid	Centraal Bureau voor Schimmelcultures (CBS), Baarn, NL	Meyer *et al.*, 2003

2.2 Methods

2.2.1 Isolation of *Candida albicans* during routine diagnostics

Clinical isolates of *C. albicans* used in our study were collected from different clinical specimen types in the diagnostic unit of the Institute for Medical Microbiology and Virology, University Medical Center Göttingen (UMG). Categories collected were respiratory, oral, urine, stool, invasive, and blood culture samples. Depending on the clinical specimen type, samples were plated on different selective media, like blood agar, chocolate agar (incubated in 5% CO_2 atmosphere), Sabouraud GC agar or grown in blood culture flasks (BacT Alert aerobic/anaerobic) in case of blood samples. All samples were incubated at 37°C until growth could be observed and then analysed by MALDI-TOF MS with the YOTL database (Bernhard *et al.*, 2014).

2.2.2 Cultivation of *C. albicans* isolates and reference strains and strain maintenance

All *C. albicans* clinical isolates obtained from the diagnostic unit, were streaked on Sabouraud agar plates for separation and incubated at 30°C over night. To ensure purity of the cultures, a single colony was picked and subcultured on Sabouraud agar. The subcultures' species was confirmed using MALDI-TOF MS again, and then used for further analysis.

Reference strains of *C. albicans* were thawed from the laboratory culture collection, plated onto Sabouraud agar plates and incubated at 30°C. To verify their purity, their species were confirmed by MALDI-TOF MS as well.

Before using isolates or reference strains for any experiments, they were subcultured three times, to let them reach a normal fitness. For long-term storage, all samples were frozen in cryotubes at -80°C.

2.2.3 Identification of strains by MALDI-TOF MS

MALDI-TOF MS was used to identify the species of all clinical strains and to verify the identity and purity of strains from our strain collection. In principle, a sample is put on a target plate and embedded in a crystalline matrix containing HCCA. A pulsed laser leads to desorption of the analyte molecules together with the matrix and their vaporization, whilst ions are transferred from the matrix to the analyte. The resulting ionized analyte is accelerated by an electric field in the vacuum and time of flight (TOF) of the different molecules is measured by a detector. By time-of-flight-measurement masses of different molecules can be determined directly, which results in a mass spectrum for each sample. As each specie has its individual spectrum of proteins, the resulting spectrum can then be evaluated with a spectra database of known species.

For our samples we used the yeast-on-target-lysis (YOTL) protocol (Bernhard *et al.*, 2014). In detail, a fresh colony was smeared onto a MALDI steel target spot with a toothpick. Cell lysis was achieved by adding 1 µl of 70% formic acid. After drying, 1 µl of matrix solution was added. If samples could not be analysed by this short protocol the manufacturers extraction protocol was used. Here, first a 1 µl inoculation loop full of cells from a pure culture was suspended in 300 µl ddH_2O. 900 µl of absolute ethanol were added to the cell suspension and mixed well. The suspension was centrifuged at 12000 rpm for 2 min. The supernatant was discarded, and the pellet dried for 10 – 15 min at 37°C until the pellet was just dry. Depending on the size of the pellet between 25 to 50 µl 70% formic acid were added to the pellet, mixed by pipetting, and kept at RT for 10 min. An equal amount of MS-grade acetonitrile was added, mixed again, and kept for 5 min at RT. The sample was centrifuged at 12000 rpm for 2 min and 1 µl of the supernatant containing the cell proteins was spotted on the target. After drying, 1 µl of matrix was added. Each sample was spotted twice. Spectra were analyzed by MALDI-TOF MS. During

measurement, the standard acquisition mode was used. A cut-off score of ≥ 2.00 identified results as valid.

2.2.4 Sample preparation for microscopy

To visualize the different cell morphologies of *C. albicans* from liquid culture, cells were prepared and stained with Blancophor P. This fluorescent optical brightening agent is typically used in the medical diagnostic for the staining of fungal mycelia, as it stains especially chitin. Material from 1 ml of liquid culture was pelleted at 12000 rpm for 5 min. The supernatant was discarded, and cells were stained with 100 µl Blankophore P [0.1%] for 15 min at RT. Afterwards, cells were washed with 100 µl 1x PBS and fixed with 50 µl of 100% methanol for 5 min. Then, cells were washed twice with 1x PBS, and finally resuspended in 100 µl 1x PBS. 5 µl of the sample were spread by pipetting onto a glass microscopy slide. When the sample was just dry, a coverslip with Mowiol was pipetted on the sample and kept for drying until the next day.
Samples were observed by microscopy at a total magnification of 1000x with immersion oil in brightfield as well as with fluorescence (DAPI filter, 409 nm).

2.2.5 Genomic DNA extraction I

DNA extraction for analysis of DNA methylation by Bisulfite Sequencing and WGBS was carried out in two steps: first, a kit was used (MasterPure^{TM} Yeast DNA Purification Kit, lucigen), based on chemical lysis of the fungal cell wall, to extract high molecular weight DNA. A 10 µl inoculation loop full of cell material from a fresh Sabouraud agar plate was suspended in 300 µl lysis solution. Cells were mixed well by vortexing and incubated for 15 min at 65°C to enable lysis. Then, samples were put on ice for 5 min, before adding 150 µl of MPC Protein Precipitation Reagent and vortex mixing for 10 sec. The resulting cellular debris was pelleted by centrifugation in a microcentrifuge for 10 min at 12000 rpm. The supernatant was transferred to a clean tube, 500 µl of pure isopropanol were added, and mixed thoroughly by inverting several times. Afterwards, the precipitated DNA was pelleted by centrifugation for 10 min at 12000 rpm. The supernatant was removed, and the DNA pellet washed with 500 µl

70% ethanol. After drying the pellet for 10 min at 37°C in a thermo block, it was dissolved in 35 µl of TE buffer pH 8.5 with 1 µl RNAse A (5 µg/µl) and 1 µl RNAse I (2.5 U/µl) + T1 (25 U/µl) for 30 – 60 min at 37°C for RNA digestion. Subsequently, phenol-chloroform-precipitation was used to remove RNAses to obtain a pure DNA solution. For this purpose, the volume of the sample was filled up to 200 µl with TE buffer pH 8.5. An equal volume of phenol-chloroform-isoamyl alcohol was added and mixed well by inverting the tube several times. For separation of the two phases, the sample was centrifuged for 5 min at 12000 rpm and the upper hydrophil phase was transferred into a fresh tube. To remove potential residues of phenol, an equal volume of chlorophorm-isoamyl alcohol (24:1) was added. Again, the tube was mixed well by inversion and then centrifuged for 5 min at 12000 rpm. The upper phase was transferred to a fresh tube and 900 µl of 100% ethanol were added. The sample was mixed carefully by inversion and then frozen for 1h at -20°C (or 15 min at -80°C) to support precipitation. After inverting the tube again for several times, the sample was centrifuged for 15 min at 12000 rpm and 4°C. The supernatant was discarded, and the pellet was dried for 10 min at 37°C, before dissolving in 30 µl Tris-HCl pH 8.5 for 1h at 37°C, or overnight at 4°C.

Quality of the genomic DNA was confirmed in a 1% agarose gel. The DNA should be highly molecular and not degraded. For all gels, agarose was dissolved in 40 ml 1x TAE and 3 µl Midori Green were added. The electrophorese was run at 130 volts for 40 min. Genomic DNA was stained additionally with GelRed for 10 min after running, to make potential remaining RNA visible. In case of remaining RNA, RNAse digestion and phenol-chloroform-precipitation were repeated with the above-mentioned conditions.

2.2.6 Genomic DNA extraction II

For standard PCR and 5mC DNA methylation analysis by ELISA the classical phenol-chloroform-precipitation of DNA with chemical plus mechanical lysis of cells with glass beads was used. As DNA is fragmented in this process, it is not suitable for Next Generation Sequencing techniques.

A 10 µl inoculation loop full of fresh cell material was suspended in 200 µl lysis buffer in a 2 ml screw cap tube. 0.5 mm glass beads (an approximate double volume to the pellet) were added, as well as 200 µl of phenol-chloroform-isoamyl alcohol. Additionally to the chemical lysis by the buffer, cells were mechanically disrupted in a FastPrep machine, running two

cycles at 4.5 m/sec for 20 sec. In between, samples were put on ice. 200 µl of TE buffer pH 8.5 were added and phase separation was achieved again by centrifugation for 10 min at 12000 rpm. The upper phase was transferred to a new tube and an equal volume of chlorophorm-isoamyl alcohol (24:1) was added. The sample was mixed well by inversion and phases separated again by centrifugation for 5 min at 12000 rpm. The upper phase was transferred into a fresh tube and 1 ml of 100% ethanol were added for precipitation of DNA. This part was conducted like described already under 2.2.5. The pellet was dissolved in 30 µl TE buffer + RNAse A. For removal of RNAse A, phenol-chloroform precipitation was repeated and conducted again as described under 2.2.5.

2.2.7 DNA Sanger sequencing

PCR products were purified using the Nucleospin Gel and PCR clean-up Kit (Macherey&Nagel, Düren, Germany). Sequencing was performed by Microsynth Seqlab (Göttingen, Germany) applying Sanger technology. In general, 18 ng per 100 bp of purified PCR product were sent in a volume of 12 µl. Additionally, 3 µl of the specific primer, were added to a final concentration of 4 µM. Provided sequences were analysed with geneious.

2.2.8 5mC DNA methylation analysis by Bisulfite Sequencing

<u>Culture conditions for Bisulfite Sequencing</u>

A *C. albicans* colony was taken from a fresh Sabouraud agar plate and 50 ml of Lee's medium were inoculated. To induce pure yeast growth, the medium had been adjusted to pH 4.5 and the culture was incubated at 30°C. The culture was shaken at 170 rpm overnight. OD_{600} was measured the next morning, cells were centrifuged at 5000 rpm for 10 min and resuspended in fresh medium. Subsequently, 100 ml Lee's pH 4.5 were inoculated to an OD_{600} of 0.5. This culture was then grown again at 30°C until the exponential phase was reached at an OD_{600} of around 1.5 – 2.5. Several 1 ml samples of this yeast culture were taken for methylation analysis, spun down at 12000 rpm, the supernatant discarded, and the tubes with the cell pellets shock frozen in liquid nitrogen before storing at -80°C. The yeast culture was then washed again with fresh medium (centrifugation at 5000 rpm for 10 min and resuspension in

fresh medium) and used to inoculate the hyphal culture in Lee's 6.5 to an OD_{600} of 0.5 and grown at 37°C and 170 rpm. The culture was grown over 6 h (Figure 7).

Hyphal development was followed by microscopy, taking samples each 30 min. Germination was visible at approximately 2 h after hyphae induction. Samples for methylation analysis were taken at 0 min, 15 min, 1 h, 2 h, 4 h, and 6 h post induction, with the goal to test for changes in the methylation pattern during the morphological transition. For each timepoint several 1 ml samples were taken, spun down at 12000 rpm, the tubes with the cell pellets were shock frozen in liquid nitrogen and samples stored at -80°C.

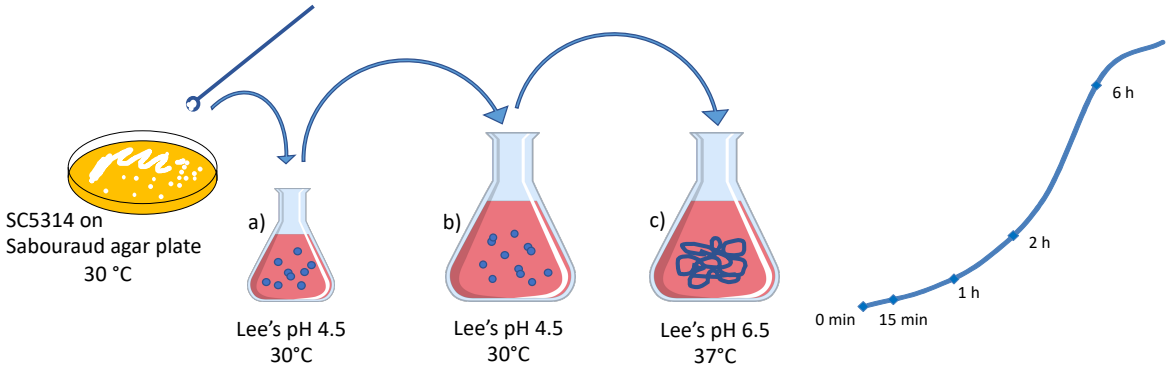

Figure 7: Sample collection for bisulfite sequencing. C. albicans SC5314 was inoculated in Lee's liquid medium in yeast inducing conditions. A yeast overnight culture (a) was used for inoculation of a fresh yeast culture (b). This culture was grown until the exponential phase. Samples were collected from this culture, and it was used for inoculation of a hyphae-inducting culture (c). Samples of the developing hyphal culture were collected at the timepoints indicated.

Bisulfite reaction and sequencing

Bisulfite conversion of genomic DNA (for extraction method see 2.2.5) was conducted with the EZ DNA Methylation-Lightning™ Kit (Zymo Research). The conversion process consists of three steps, during which non-methylated cytosines are chemically modified and converted to uracil (Figure 8), whereas methylated cytosines remain unchanged. Mapping of the sequenced fragments to the original reference DNA, reveals methylated cytosines.

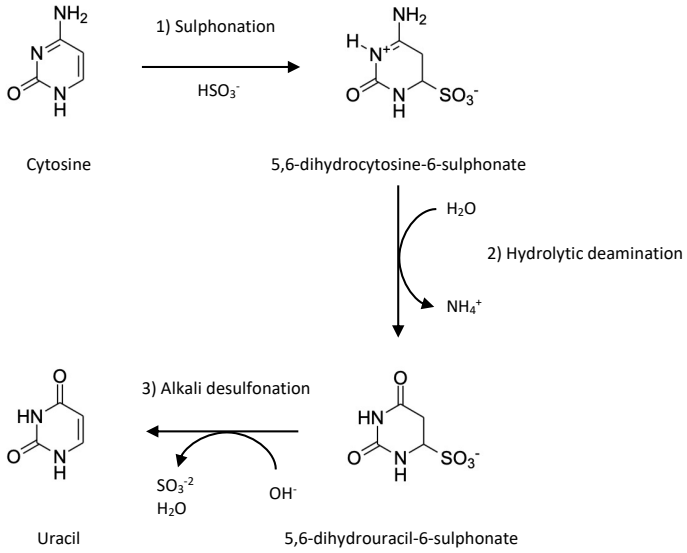

Figure 8: Bisulfite Conversion of unmethylated cytosines. Lightning Conversion Reagent from the ZymoResearch Kit modifies unmethylated cytosines by sulphonation (1) and hydrolytic deamination (2), resulting in 5,6-dihydrouracil-6-sulphonate, which is then converted to uracil by alkali desulphonation (3) with Desulphonation Buffer (ZymoResearch) in a later step.

Following the kit protocol, 500 ng of input DNA were used for each sample. The volume was filled up to 20 µl with ddH_2O and 130 µl of Lightning Conversion Reagent were added to the samples. Afterwards, samples were put in a thermal cycler, heated to 98°C for 8 min to denature DNA, incubated at 54°C for 1h to enable the first two steps of the bisulfite conversion reaction (Figure 8), and cooled down to 4°C until further treatment. Further steps were conducted as described in the protocol. Before DNA elution, the column was dried for 10 min at 37°C and elution of DNA was accomplished with 20 µl of prewarmed M-Elution Buffer. To control the bisulfite conversion efficiency, a human unmethylated control (Human HCT116 DKO Non-Methylated DNA, Zymo Research) was run in parallel.

The concentration of each sample was measured in a NanoDrop spectrophotometer in the RNA mode, as bisulfite converted DNA is single stranded.

Subsequently, polymerase chain reaction of bisulfite converted DNA was realized with specific primers, fitting to the bisulfite converted DNA sequence of the region of interest. PCR reactions contained 20 - 40 ng bisulfite converted genomic DNA, 12.5 µl 2x Zymo-Taq™ PreMix (containing 1 U of a “hot start” Taq DNA polymerase, 1.75 mM $MgCl_2$, 0.25 mM of each dNTP), each 0.6 mM forward and reverse primer, 2.25 mM additional $MgCl_2$, and DNAse/RNAse-free H_2O for a final volume of 25 µl. The PCR conditions consisted of a 10 min

initial denaturation and polymerization step at 95°C, followed by 38 cycles of 30 sec at 95°C for denaturation, 40 sec at 52°C (C1_00050C primers) for annealing and 45 sec at 72°C for elongation, and a subsequent elongation step of 7 min at 72°C.

Quality of PCR fragments was analyzed by gel electrophoresis using a 1% agarose gel. PCR products were cleaned with a PCR clean-up kit following the manufacturer's protocol and DNA was eluted with 30 µl prewarmed DNAse/RNAse-free H_2O.

Thereafter, PCR products were cloned in chemically competent *E. coli* Top10 cells with a TOPO TA cloning kit, following the manufacturer's instructions. Incubation time was 30 min for ligation reaction at RT and 30 min for transformation in *E. coli* TOP10 cells on ice. For each sample 50 µl and 80 µl cell culture were streaked onto two LB-Amp plates (ampicillin 100 µg/ml), readily prepared with X-Gal (40 mM, 40 µl / plate). X-Gal served as indicator for beta-galactosidase activity. Successful cloning leads to disruption of the *lacZ* gene, resulting in positive white and negative blue colonies.

After incubation overnight at 37°C, 20 white colonies of each sample were picked for colony PCR. For this purpose, a colony was dissolved in 10 µl H_2O and heated for 10 min at 95°C. For the PCR 2 µl of the suspension were added to 23 µl of Mastermix containing 12.5 µl 2x Zymo-Taq™ PreMix, 0.6 mM M13 forward and M13 reverse primer, and 2.25 mM additional $MgCl_2$. PCR conditions were a 10 min denaturation step, followed by 30 cycles of 30 sec denaturation at 95°C, 40 sec annealing at 55°C, 1 min elongation at 72°C, and 7 min final elongation at 72°C. Again, quality of the PCR was verified by gel electrophoresis, and subsequently PCR products were cleaned with a PCR clean-up kit. Elution was conducted with 30 µl of prewarmed DNAse/RNAse-free H_2O.

Sanger sequencing was performed at Microsynth SeqLab (Göttingen, Germany) and provided sequences were mapped to assembly 22 of the reference genome of *C. albicans* with the "Geneious" software. This way, bisulfite converted Cs could be distinguished from non-converted Cs. For sequence context analysis six bases in both directions of the methylated cytosine were documented. Sequence logos were constructed with WebLogo 3.7.4 (Crooks et al., 2004).

2.2.9 WGBS of SC5314 yeast vs. hyphal morphology - culture conditions and sampling

For the analysis of DNA methylation on the whole genome level we chose whole genome bisulfite sequencing (WGBS) as the major technique. WGBS allows genome wide DNA methylation observation on single-base resolution by combining bisulfite conversion of unmethylated cytosines and next generation sequencing (NGS). In our initial investigation on DNA methylation we compared the yeast morphology with the hyphal morphology of *C. albicans* in a single experiment without technical replicates. For this purpose, a yeast and a hyphal culture were inoculated the same way as explained in section 2.2.8 (Figure 7). A 1.5 ml sample of the yeast culture (b) was taken after reaching the exponential phase. The hyphal culture sample (c) was harvested 6h after hyphal induction. Samples were centrifuged at 12000 rpm for 10 min, and the supernatant was discarded. Subsequently, cells were shock frozen in liquid nitrogen and stored at -80°C for later processing.

Sample DNA was isolated as explained in 2.2.5. After a quality analysis on an 1% agarose gel, the DNA was sent for WGBS to GATC Biotech AG (nowadays Eurofins Genomics Europe Sequencing GmbH). Bisulfite conversion and library preparation were conducted by the provider. Samples were sequenced on a HiSeq4000 sequencer, generating 125 bp PE reads.

2.2.10 WGBS and RNAseq analysis of 5-Aza-treated and morphologically induced SC5314 - culture conditions and sampling

To gain a better understanding on how DNA methylation affects gene expression and possibly morphological transition in *C. albicans*, we conducted a more elaborate morphologic time-course experiment with 3 independent replicates, and in the presence or absence of 5-Azacytidine, which would give us insights in the differences of DNA methylation patterns between yeast and hyphal morphology. Further, the application of the known DNA methyltransferase inhibitor 5-Azacytidine could show us the effect of blocking DNA methylation on the transcriptome and on morphological development.

Here, the reference strain SC5314 was used. Samples were taken for whole genome bisulfite sequencing (WGBS), to analyse DNA methylation, as well as for mRNA sequencing (in the

following abbreviated as RNAseq), to investigate the effect of 5-Azacytidine on the transcriptome in yeast and hyphal morphology. Additionally, the combination of WGBS and RNAseq would allow us to analyse correlations between methylome and transcriptome of yeast and hyphal morphology (Figure 9).

The experimental setup was split up into two branches: a 5-Aza treated branch with yeast and hyphal culture and in parallel an untreated branch with the same cultures. The experiment was conducted in triplicates (e.g., PA1-1, PA1-2, and PA1-3), each handled by a different person. Induction of yeast and hyphal cultures were implemented by a specific temperature and pH impulse – 30°C and pH 4.5 for yeast growth, 37°C and pH 6.5 for hyphal growth. Two studies conducted with 5-Aza in *C. albicans* indicate a working concentration between 0.1 and 10 mM as effective. A phenotypic effect was visible with concentrations of 10 mM, but not with 1 mM (Pancaldi *et al.*, 1988). An effect on molecular bases was observed already at a concentration of 0.1 mM (Mishra, Baum and Carbon, 2011). For our experiment we accordingly decided to work with a concentration between 0.1 and 1 mM.

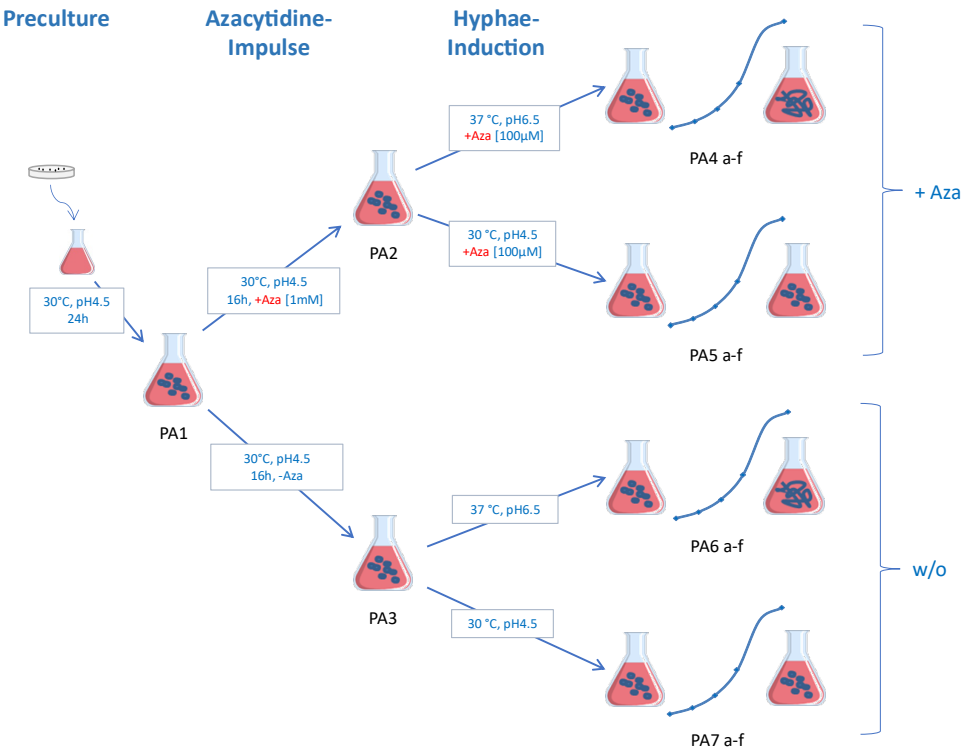

Figure 9: 5-Aza experiment setup. Each culture condition consisted of three replicates. The experiment was divided into two branches: the upper branch represents the 5-Aza treated part; the branch below represents the part without treatment. The original yeast culture (PA1) was split up into a treated culture (PA2) with 1mM 5-Azacytidine and an untreated culture (PA3), which were grown for 16 hours until the late exponential phase. These cultures served as bases for the morphology related experimental part: each culture was used to inoculate one hyphal culture (PA4 or PA6), as well as a further yeast culture (PA5 or PA7). Cultures PA4 and PA5 were further treated with 100 µM 5-Azacytidine. The transition from yeast to hyphal culture was achieved by changing pH and temperature from pH 4.5 and 30°C for yeast growth to pH 6.5 and 37°C for the induction of hyphal growth. During a 24-hour time-course experiment samples were taken at different timepoints after induction (a=0h, b=1h, c=2h, d=4h, e=6h, and f=24h).

The initial preculture (PA1) was inoculated with fresh SC5314 colonies from Sabouraud agar plates (previously incubated at 30°C). The colonies were resuspended in 4ml of Lee's medium pH 4.5 to a McFarland of 2.0. An Erlenmeyer flask with 1.2 l prewarmed Lee's medium set to pH 4.5 was inoculated with 4 ml of this suspension. Of each of the three replicates 100 µl were taken for the determination of colony forming units (CFU). For this purpose, a dilution of $1:10^4$ was plated on Sabouraud agar, incubated at 30°C, and counted after 24h. This first culture (PA1) was incubated for 24 hours at 30°C and 150 rpm. Low pH and temperature induced yeast growth.

After 24 hours the first samples for WGBS and RNAseq were taken from each flask in parallel. Therefore, of each culture three 50 ml falcons full of cell suspension were harvested. Suspensions were centrifuged at 5000 rpm for 5 min. The cells of two falcons were used for

WGBS and resuspended in 5ml Lee's pH 4.5 as a washing step. Then the suspension was aliquoted to 2 ml screw cap tubes. The samples were centrifuged again at 12000 rpm, the supernatant was discarded, and the eppis with the remaining cells were shock frozen in liquid nitrogen. Samples were kept at -80°C until DNA extraction.

The cells in the remaining falcon for RNAseq were also resuspended and washed in 5ml Lee's pH 4.5 and centrifuged again at 5000 rpm for 5 min. The supernatant was discarded, and cells were resuspended in 1 ml Trizol (a higher volume was used with increasing OD, always the double amount of the cell pellet). The Trizol suspension was aliquoted in two 2 ml screw cap tubes with glass beads. Cells were immediately disrupted in a FastPrep machine for 30 sec at a speed of 4.5, kept at RT for 5 min, and subsequently put on ice. Then the samples were frozen at -80°C until RNA extraction.

Besides the samples for WGBS and RNAseq, samples for microscopy were prepared (see section 2.2.4), and OD_{600} was measured each time when samples were taken. After sampling of culture PA1 this culture was used to inoculate the basic yeast cultures of the two branches: the 5-Aza treated culture PA2 [1mM] and the untreated culture PA3. A small growth inhibition by 5-Aza at the concentration of 1 mM was observed in long term cultures. As all cultures needed to start at the same OD at the next experimental step, cultures were inoculated to different ODs: PA2 was inoculated at an OD_{600} of 0.04 and PA3 at an OD_{600} of 0.02. Cells were washed once before inoculation with prewarmed medium. 5-Aza was prepared freshly, filter-sterilized, and added to prewarmed Lee's medium (pH 4.5) prior to inoculation. The final volume was 1 200 ml. The cultures were incubated again at 30°C and 150 rpm. After 16h samples for DNA extraction, RNA extraction, and microscopy were taken as described above and OD_{600} was measured.

In the next step a timecourse experiment was conducted, where yeast and hyphal morphology were induced for the 5-Aza-treated as well as for the untreated experimental arm. For the treated cultures PA4 and PA5, 5-Aza was prepared freshly as described above. The final concentration in the culture was set to 100 µM in a total amount of 1 200 ml Lee's medium. Hyphal growth was induced by a pH of 6.5 and incubation temperature of 37°C. Cultures PA2 and PA3 served as inoculum for the 5-Aza treated and for the untreated cultures, respectively. All cultures were inoculated to an OD_{600} of 0.8. Before inoculation, cells were washed with prewarmed Lee's pH 4.5 and resuspended in 5 ml of the appropriate medium (pH 4.5 for the

yeast culture and pH 6.5 for the hyphal culture). The cultures were incubated at 30°C or 37°C, - according to the induced morphology - at 150 rpm.

Samples were taken at the following timepoints: 0 min (a), 1 h (b), 2 h (c), 4 h (d), 6 h (e), and 24 h (f). At each timepoint OD_{600} was measured, and samples were taken for DNA extraction, RNA extraction, and microscopy as described above.

For WGBS analysis we focused more on the morphological aspect without 5-Aza treatment (samples PA3, PA6 and PA7) and investigated two timepoints after induction of the hyphal morphology (b = 1h and e = 6h), to allow analyses how fast DNA methylation could adapt to altered environmental conditions and if the methylation pattern changes over time. The following samples were taken for WGBS: PA3 (preculture yeast), PA6b (timecourse hyphae 1h), PA6e (timecourse hyphae 6h), PA7b (timecourse yeast 1h), and PA7e (timecourse yeast 6h) (Figure 10). Only two of the three replicates were sequenced, replicate 1 and replicate 3.

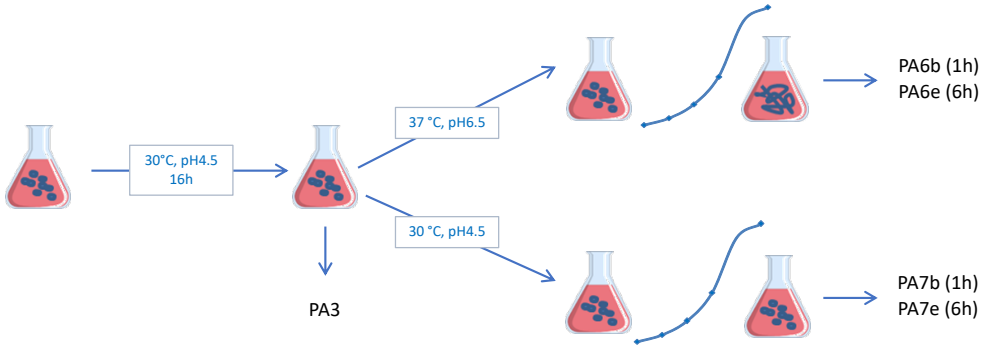

Figure 10: Samples for WGBS. PA3 = yeast preculture, PA6b = hyphal culture 1h, PA6e = hyphal culture 6h, PA7b = yeast culture 1h, PA7e = yeast culture 6h.

Samples for RNAseq were transferred to the "NGS-Serviceeinrichtung für Integrative Genomik" (NIG, formely "TAL", Transkriptomanalyselabor der UMG) of the University Medical Center Göttingen (UMG). There, RNA was further extracted, according to their standard protocol and quality was controlled in a fragment analyser.

By RNAseq we intended to see the effect of 5-Aza, implementing reduced DNA methylation, on gene transcription. Therefore, treated cultures had to be related to untreated cultures. We chose the timepoint 1h after hyphal induction (b), as transcriptional regulation is a biological process, that adapts immediately to changes in the environment – in our case higher temperature and pH. Further aspects for the choice of RNAseq samples were the quality of

the isolated RNA (RIN) at each timepoint. Also, for a later comparison of WGBS and RNAseq, samples from the same cultures and timepoint (samples PA3, PA6b and PA7b) would be necessary. This way, a comparison of methylome and transcriptome would be possible. Including all these aspects, the following samples were chosen for RNAseq analysis: PA2 (yeast preculture +5-Aza [1mM]), PA3 (yeast preculture w.o.), PA4b (hyphal culture 1h +5-Aza [100µM]), PA5b (yeast culture 1h +5-Aza [100µM]), PA6b (hyphal culture 1h w.o.), and PA7b (yeast culture 1h w.o.) (Figure 11). For each sample all three replicates were sequenced.

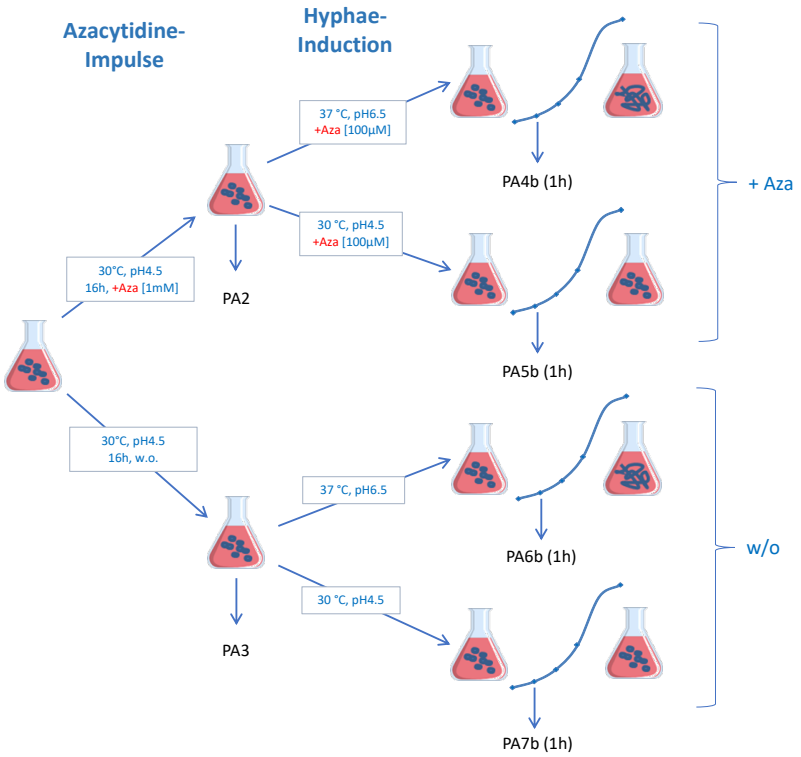

Figure 11: Samples for RNAseq. PA2 = yeast preculture +5-Aza [1mM], PA3 = yeast preculture w.o., PA4b = hyphal culture 1h +5-Aza[100µM], PA5b = yeast culture 1h +5-Aza [100µM], PA6b = hyphal culture 1h w.o., and PA7b = yeast culture 1h w.o.

2.2.11Clinical isolate collection

Fresh clinical isolates of *C. albicans* were collected from the diagnostic unit from our institute, which were swabs from different body locations, tissue samples or excretions.

In detail, these were respiratory samples (bronchial lavage, bronchial secretion, and tracheal secretion), oral samples (swab from oral mucosa, throat, and tongue), stool samples, urine samples (renal pelvis urine, midstream urine, and catheter urine), invasive samples

(intraoperative swabs from bile, abdomen, sternum, jaw, tissue from knee, backbone, and abdominal tissue, ascites punctures, bile punctures, and bile secretion), and blood samples. These samples can be grouped in two groups: 1. non-sterile environment (respiratory, oral, and stool) and 2. Primary sterile environment (urine, invasive, and blood).
Clinical isolates were subcultured and identified previous to usage in further experiments as described in 2.2.1 - 2.2.3.

2.2.11.1 Morphological screening of *C. albicans* clinical isolates on Spider medium

For morphological analysis of clinical isolates, they were spotted onto Spider medium. This medium is known for its hyphal growth inducing effect, which is based on beef extract peptides, including peptides found in human blood (Daniels *et al.*, 2013). The morphological screening of fresh clinical isolates on Spider medium served as a screening for attenuation. Attenuated isolates did not show any hyphal development, despite the hyphae inducing characteristics of Spider medium (see blue marked colonies in Figure 12).
After confirmation of species identity by MALDI-TOF MS, clinical samples were freshly grown on SAB agar plates at 30°C overnight. Cells were resuspended in saline solution to a McFarland of 2.0, and 3 µl of the cell suspension were pipetted onto Spider agar plates. The Spider agar plates were incubated at 37°C and sealed partially with parafilm to prevent drying. After 7 days the colony morphology was analysed by eye and colonies were classified into three categories: attenuated (no or very few hyphal growth, with just single very short and thin hyphae, colony smooth), intermediate (hyphae all around the side of the colony visible, but short, colony can be slightly wrinkled), and strong hyphal growth (meaning dense and strong growth of hyphae all around the colony, colony can be wrinkled) (Figure 12, A).
Further the colony surface areas were analysed with Fiji image software (version 2.0.0-rc-69/1.52p, ImageJ). The pictures of the plates, which were taken 7 days after inoculation, were converted into black and white images (Figure 12, B). A scale was set up with a ruler, which was always visible on each picture. This way the program was scaled to pixels per mm and the colony surface areas were measured by marking the white areas.

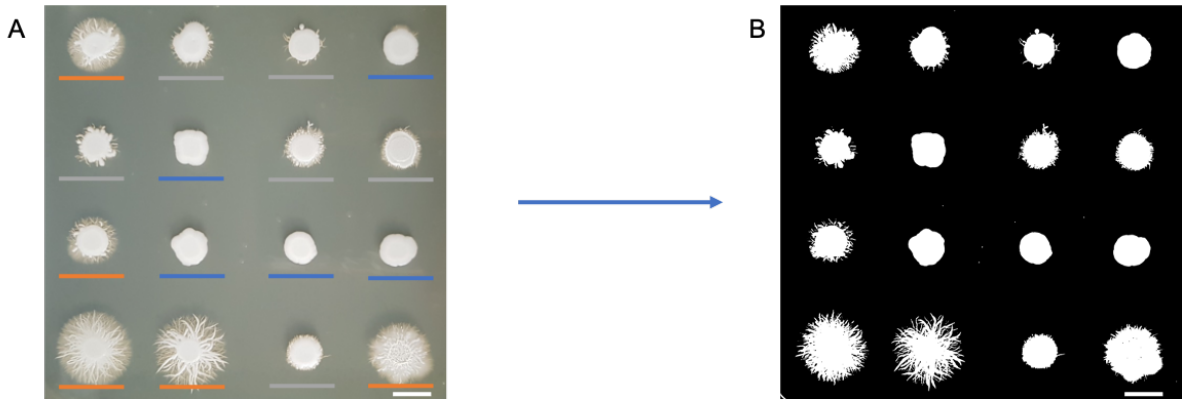

Figure 12: *C. albicans* clinical isolates on Spider medium. Samples originate from different clinical specimen types. Plates were incubated for 7 days at 37°C. (A) Colonies were classified by their morphology: orange = strong hyphal growth, grey = intermediate hyphal growth, and blue = no/low hyphal growth (attenuated). (B) Black and white version of image A. Colony surface areas were measured with Fiji image software (ImageJ). Scalebar 1 cm.

2.2.11.2 5-Azacytidine treatment and morphological screening

Reference strains of *C. albicans* were screened on Spider medium after 5-Aza treatment, to directly observe the potential impact of 5-Aza in *C. albicans* morphology.

Referring to the findings of Mishra and Pancaldi, who observed effects of 5-Aza in concentrations of 0.1 mM and 10 mM respectively (Pancaldi *et al.*, 1988; Mishra, Baum and Carbon, 2011), samples were incubated for 24 hours with a concentration of 1 mM or 5 mM, before spotting them on Spider medium. In a previous experiment a higher concentration of 10 mM had a slightly inhibitory effect on colony growth (data not shown).

One colony of each isolate was resuspended in 5 ml Lee's medium pH 4.5 containing 1mM (only SC5314) or 5 mM (SC53214, DSM 11225, DSM 11949, and 529L) 5-Azacytidine and incubated at 30°C and 150 rpm. In parallel, a culture without 5-Aza was inoculated for each strain as a control. By low pH and temperature, the cells were first induced to grow in yeast morphology. After 24 hours cells were transferred to a falcon tube, centrifuged for 10 min at 5000 rpm, and the supernatant was discarded. Cells were resuspended in 5 ml fresh Lee's medium pH 4.5. For 5-Aza treated samples this washing step was repeated. From each culture 2 ml saline solution were inoculated to a McFarland of 2.0. In our first analysis with 1 mM 5-Aza treatment of SC5314, 3 µl of a 10-fold serial dilution starting with a McFarland 2.0 suspension was spotted on Spider medium. In the later experiment with the four reference strains 3 µl of the suspension were directly spotted onto the medium. The plate was incubated

for 7 days at 37°C to support hyphal development. Over several days, progressive growth of the colonies was documented macroscopically and microscopically.

By treating selected attenuated clinical isolates with 5-Aza, we aimed to alter their 5mC DNA methylation pattern. If morphology and DNA methylation are connected in *C. albicans*, we would expect to observe a significant change in the morphology of these attenuated isolates after 5-Aza treatment.For this purpose, twelve attenuated and one hyper-filamenting clinical isolate were chosen, representing each clinical specimen type. Strain 529L and SC5314 were also included in the experiment.

Again, we incubated the cells for 24 h in Lee's medium pH 4.5 containing 5mM 5-Azacytidine and followed the same protocol as described above for the different reference strains. 3 µl of a McFarlan 2.0 suspension were spotted on Spider medium and the plate was incubated at 37 °C. On the 7th day of incubation pictures of the plates were taken for qualitative and quantitative analysis as described in the previous section (2.2.11.1).

Cell material for further WGBS analysis was collected from each colony (5-Aza treated and untreated) and was shockfrozen in 2 ml screwcap tubes in liquid nitrogen, before storing at -80°C. Further, material of each colony was frozen in cryobank tubes.

Afterwards the colonies were subcultured to see if the altered phenotype is stable. From each colony, material was taken and resuspended in saline solution to a McFarland of 2.0. Again, 3µl of each sample were spotted on a fresh Spider medium plate, which was incubated at 37°C. Pictures of the plates were taken after 7 days of incubation.

2.2.12Screening of SC5314-*RFP* isolates after gut passage and 5-Aza-treatment

Isolates of the SC5314 derivate SC5314-*RFP* (containing an integrated red fluorescent protein gene) were obtained from Prof. Ilse Jacobsen, Wibke Krüger and Sarah Vielreicher from the Hans-Knöll-Institute in Jena (Germany). The samples originated from a mouse feeding experiment. The animals were treated with different antibiotic therapies four days pre infection until dissection of the animals. The different groups we obtained were a) *C. albicans* colonization without antibiotic treatment, b) *C. albicans* colonization with Penicillin treatment, and c) *C. albicans* colonization with Penicillin/Doxycycline/Streptomycin treatment. The samples came from faeces seven days after treatment, faeces 14 days after

treatment, and colon and caecum content 14 days after treatment, which were already plated and grown on YPD plates containing Chloramphenicol.

In our lab the single colonies on the plates were numbered, picked, and spotted directly on Spider medium. Colony morphology was judged seven days after incubation at 37°C. Attenuated colonies (no or only few hyphae visible compared to the inoculum) were sequenced with primers targeting the integrated *RFP* gene and the neighbouring *ADH1*. Colonies without a positive PCR result were discarded.

As described in section 2.2.11.2, isolates were treated with 5-Aza [5 mM] and plated again on Spider medium. Changes in morphology compared to the untreated sample were documented five to seven days after spotting.

2.2.13 Analysis of cell damage capacity of 5-Aza treated and untreated Spider-screened isolates

Analysis of cell damage capacity was conducted by Prof Julian Naglik, Dr. Jonathan Richardson, and Antzela Zavou from King's College in London (Great Britain). Three groups of samples were sent for analysis: a) completely attenuated and strongly filamenting Spider-screened clinical isolates, b) untreated and 5-Aza treated clinical isolates (four attenuated, one filamenting, 529L, and SC5314) (samples were analysed by WGBS as well), and c) attenuated 5-Aza treated and untreated SC5314-*RFP*. Isolates from a) and b) were thawed from cryo stocks and the morphology was checked again on Spider medium before sending. Isolates from c) were taken from the original plate and subcultured on Sabouraud agar. Samples were sent as Sabouraud agar slants. Isolates were grown in YPD broth at 30°C and 180 rpm for 24 hours. Subsequently, growth morphology was observed microscopically. Oral epithelial cells (TR146) were infected with an MOI (multiplicity of infection) of 0.1 (for LDH also 0.01). The parameters investigated indicating cell damage were LDH (lactate dehydrogenase), G-CSF (granulocyte-colony stimulating factor), GM-CSF (granulocyte-macrophage colony stimulating factor), IL-6 (interleukine 6), IL-1 alpha (interleukine 1 alpha), and IL-1 beta (interleukine 1 beta). Statistical analysis of the single sample significance was performed with a one-way ANOVA and Tukey's multiple comparison test by the working group.

2.2.13.1 Analysis of *ECE1* expression in attenuated and reconstituted 5-Aza treated SC5314-*RFP* by qPCR

Analysis of *ECE1* expression capacity was conducted by Prof Julian Naglik, Dr. Jonathan Richardson, and Antzela Zavou from King's College in London (Great Britain). Two of the attenuated SC5314-*RFP* isolates (PEU3801 and PEU3804) and their respective 5-Aza treated sample with the reconstituted filamenting phenotype were analysed by qPCR for the expression of the invasion relevant gene *ECE1*. Actin as housekeeping gene served as internal control.

2.2.14RNAseq data analysis

The complete pipeline (Figure 13) for RNAseq data analysis was realized using Galaxy, an open-source web-based platform, providing the respective programs (Afgan *et al.*, 2018). Partially, the analysis was conducted with the Galaxy server of the GWDG - Gesellschaft für wissenschaftliche Datenverarbeitung mbH Göttingen (galaxy.gwdg.de) and partially with the European Galaxy server (usegalaxy.eu) from the Freiburg Galaxy Team. Reference genome, feature files, and GO files for computational analysis were all taken from the *Candida* Genome Database (candidagenome.org, assembly version A22-s07-m01-r112). The gene ontology file (go-basic.obo) for enrichment analysis was downloaded from geneontology.org/docs/download-ontology/.

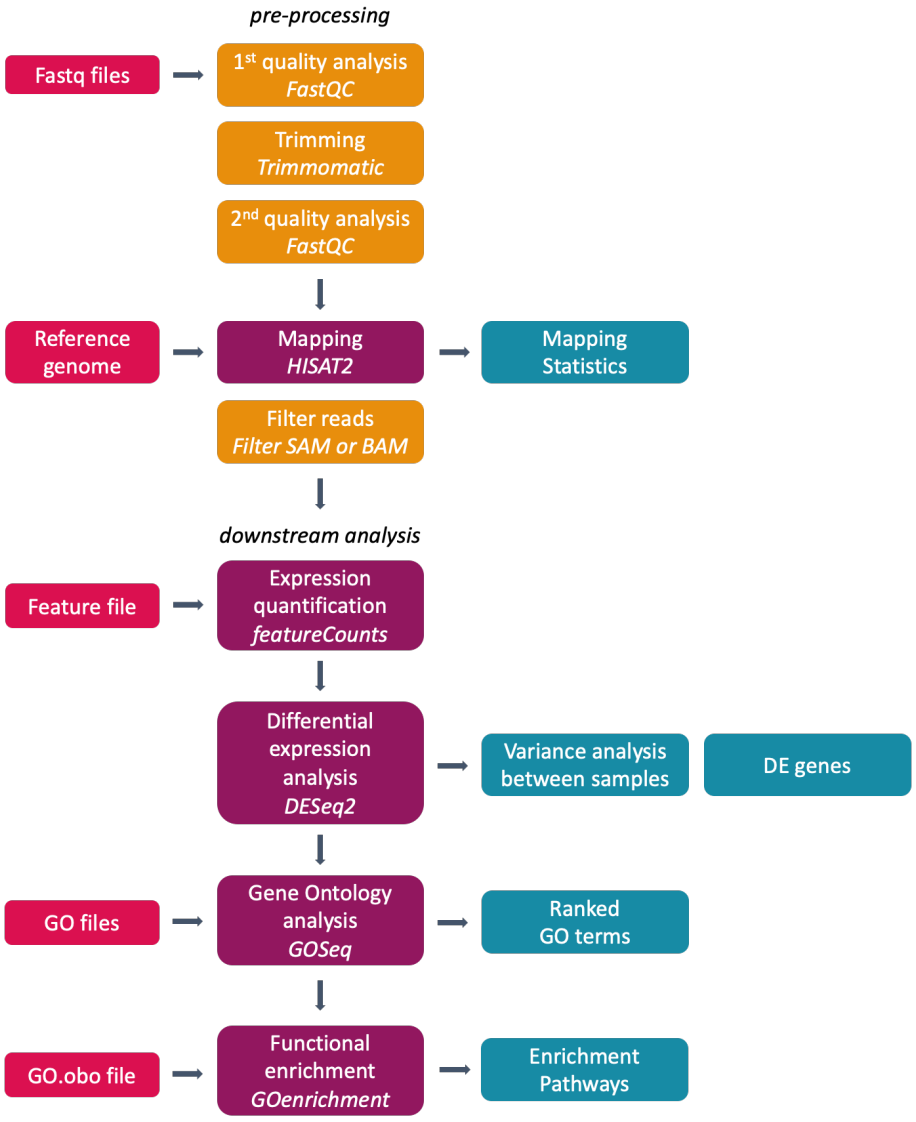

Figure 13: RNAseq analysis pipeline. Tools in italics. Pink = input files, orange = data processing/quality control steps, purple = central data calculation steps, petrol = output files.

RNAseq reads obtained from the NIG Göttingen were 50 bp single-end (SE). Quality analysis was performed with *FastQC* (version 0.72; Andrews, S. "FastQC A Quality tool for High Throughput Sequence Data", https://www.bioinformatics.babraham.ac.uk/projects/fastqc/). Reads were trimmed using *Trimmomatic* (version 0.38.0; Bolger, Lohse and Usadel, 2014), discarding all reads below 20 bp, below an average Phred score of 20, and trimming low quality bases from start and end of the reads. After a second quality analysis, reads were aligned to the *C. albicans* reference genome SC5314 using *HISAT2* (version 2.1.0+galaxy5) with default settings (Kim, Langmead and Salzberg, 2015). Non- and multi-mapped reads were discarded by applying *Filter SAM or BAM, output SAM or BAM* (version 1.1.2, based on

SAMtools toolkit (Li *et al.*, 2009)). In the next step, gene expression was quantified by counting reads per feature with *featureCounts* (version 1.6.3+galaxy2) with default settings (Liao, Smyth and Shi, 2014).

Table 11: Selected morphological relevant genes

Gene name	ID*	Position	Function
Expected as upregulated under hyphae inducing conditions			
HGT2	C1_02110C	434412 – 436049	Putative MFS glucose transporter, Spider biofilm induced
orf19.2457	C1_05920W	1236305 – 1238380	Protein of unknown function, Spider biofilm induced
UME6	C1_06280C	1314438 – 1316969	TF, controls transition to FG
CPH1	C1_07370C	1590522 – 1592492	TF, regulates galactose metabolism genes, filamentation on solid media, pheromone-stimulated biofilms, rat catheter biofilm repressed
RIM101	C1_14340C	3158465 – 3160450	TF, required for alkaline-induced HG
DCK1	C2_04050C	847533 – 853277	Regulated by Nrg1, required for embedded filamentous growth, (not upregulated in liquid cultures), Spider biofilm induced
TEC1	C3_04530C	949762 – 951993	TF, hyphal gene regulation, required for biofilm formation on distinct media
ECE1	C4_03470C	726514 – 727329	Candidalysin, hyphae-specific protein, farnesol-induced, Spider biofilm induced
RBT1	C4_03520C	745166 – 747331	Cell wall protein, serum, hyphal and alkaline induced
HWP1	C4_03570W	762835 – 764739	Hyphal cell wall protein, Spider biofilm induced
CZF1	C4_06820C	1518979 – 1520136	TF, HG regulator, Spider biofilm induced
IHD1	C6_03850C	838281 – 839459	GPI-anchored protein, hyphae-induced
FLO8	C6_04350C	959560 – 961938	TF, required for hyphal formation, regulates hyphal gene expression
HSP90	C7_02030W	439525 – 441648	Essential chaperone, temperature-induced morphogenesis, localizes to surface of hypha – not yeast cells
CYR1	C7_03070C	662700 – 667772	Adenylyl cyclase, involved in regulation of filamentation
ALS3	CR_07070C	1532277 – 1535744	Cell wall adhesin, endothelial invasion, induced in Spider biofilm
EFG1	CR_07890W	1723489 – 1725146	TF, hyphal growth, cell-wall gene regulation

Expected as downregulated under hyphae inducing conditions			
TUP1	C1_00060W	12163 – 13701	Represses FG
RPG1A	C1_12770W	2782398 – 2785190	Putative translation initiation factor, Spider biofilm repressed and upon phagocytosis
YWP1	C2_08590W	1746839 – 1748440	Yeast wall protein, Spider biofilm repressed
SSN6	C3_07020W	1607932 – 1611174	HG regulator, Repressed during HG (HG regulator)
RHD3	C4_04050C	867681 – 868295	Yeast-associated cell wall protein, Spider biofilm repressed
RBF1	C6_02840C	586391 – 587995	TF, mutation leads to accelerated induction of hyphal growth
NRG1	C7_04230W	918812 – 919744	TF, regulates hyphal gene induction genes, Spider biofilm repressed
RFG1	CR_02640W	600287 – 602089	Transcriptional repressor of filamentous growth and hyphal genes

*Last letter of ID corresponds to DNA strand (W= Watson strand = +strand; C= Crick strand = -strand). Information on genes extracted from CGD (candidagenome.org).

Then, differentially expressed features were determined by applying *DESeq2* (version 2.11.40.6+galaxy1), specifying 1. for treatment and 2. for induced morphology (Love, Huber and Anders, 2014). *DESeq2* normalizes raw counts for sequencing depth and library composition as median of ratios. Significantly differentially expressed genes were defined by a log2FC >1.1/<-1.1 (>214%/<46.7% of the previous condition) and a p-adjusted value of 0.01. Data was visualized using *Volcano Plot* (version 0.0.3) and *heatmap2* (version 3.0.1). Additionally, the log2FC was analysed for selected morphological relevant genes (Table 11). To determine biological processes to which differentially expressed genes can be assigned to (categories: biological process, cellular component, and molecular function), gene ontology analysis was carried out with *GOseq* (Young *et al.*, 2010). The Benjamini-Hochberg (1995) method was applied for multiple hypothesis test correction and a log2FC of >1.1/<-1.1 and P-adjusted value of 0.01 were used. P-values were calculated using the Wallenius method. Functional enrichment analysis was performed using *GOenrichment* (Galaxy version 2.0.1; Faria, Daniel (2017)), with a Benjamini-Hochberg multiple test correction and a p-value cut-off of 0.01.

2.2.15 WGBS data analysis

A major part of WGBS data analysis pipeline (Figure 14) was carried out using the Galaxy environment (galaxy.gwdg.de and usegalaxy.eu) and a small part by command line perl scripts (preparation of input datasets for some downstream tools). Reference genome, feature files, and positions of long terminal repeats and retrotransposons for computational analysis were taken from the *Candida* Genome Database (candidagenome.org, assembly version A22-s07-m01-r112). In *C. albicans* the ends of the chromosomes had been defined as 5kb telomeric + 15 kb subtelomeric (Dunn and Anderson, 2019). Nevertheless, as subtelomeric CDSs we investigated the first and last 50 kb of a chromosome, to cover the whole GC rich part. Positions of lncRNAs were provided by Prof. Toni Gabaldon (IRB, Barcelona, Spain). The 529L genome was downloaded from the NCBI GenBank (accession number ASHC00000000 (Cuomo *et al.*, 2019)).

Reads obtained from the different sequencing facilities were 125 bp paired-end (PE) (GATC biotech AG; Illumina Sequencing, bisulfite conversion rate >99.5%), 150 bp PE (Eurofins Genomics; Illumina Sequencing, bisulfite conversion rate >99.2 – 99.3%), and 100 bp PE (Prof. Toni Gabaldon, IRB, Barcelona, Spain; Illumina sequencing, bisulfite conversion rate >99.6%). Quality analysis of the reads was performed with *FastQC*. Subsequently, remaining Illumina adapter sequences were trimmed using *Cutadapt* (version 1.16.8) (Martin, 2011). Further, reads below 40 bp and with a Phred score below 20 were discarded. Additionally, methylation bias at the 5’ and 3’ positions of the reads was trimmed with *Trimmomatic* (1 – 3 bp, depending on the detected bias by *Methyldackel* after read mapping).

Subsequently, reads were mapped using *Bismark Mapper* with default settings (Bisulfite reads mapper version 0.22.1+galaxy4; Krueger and Andrews, 2011). Mapping was first carried out without the mitochondrial chromosome. All unmapped reads were written to an extra output file and subsequently mapped to the mitochondrial chromosome. As mitochondrial sequences are assumed to be not methylated (Formighieri *et al.*, 2008; Mechta *et al.*, 2017; Fan *et al.*, 2019), the mitochondrial mapping served as a control. Coverage was calculated using *BAM Coverage Plotter* (version 20201223+galaxy0). Dependencies in coverage and GC content were analysed by plotting against each other (1000 nt bins). Further, coverage of replicates or pairs of treated and untreated samples were checked for variances by plotting against each other. *Bismark Mapper* gives already a cytosine methylation report, which was documented for the mitochondrial and nuclear genome. PCR duplicates were removed with *Samtools*

RmDup (version 2.0.1). Reads were then filtered with *Filter SAM or BAM, output SAM or BAM*, keeping reads mapped in proper pairs and discarding unmapped and multi-mapped reads.

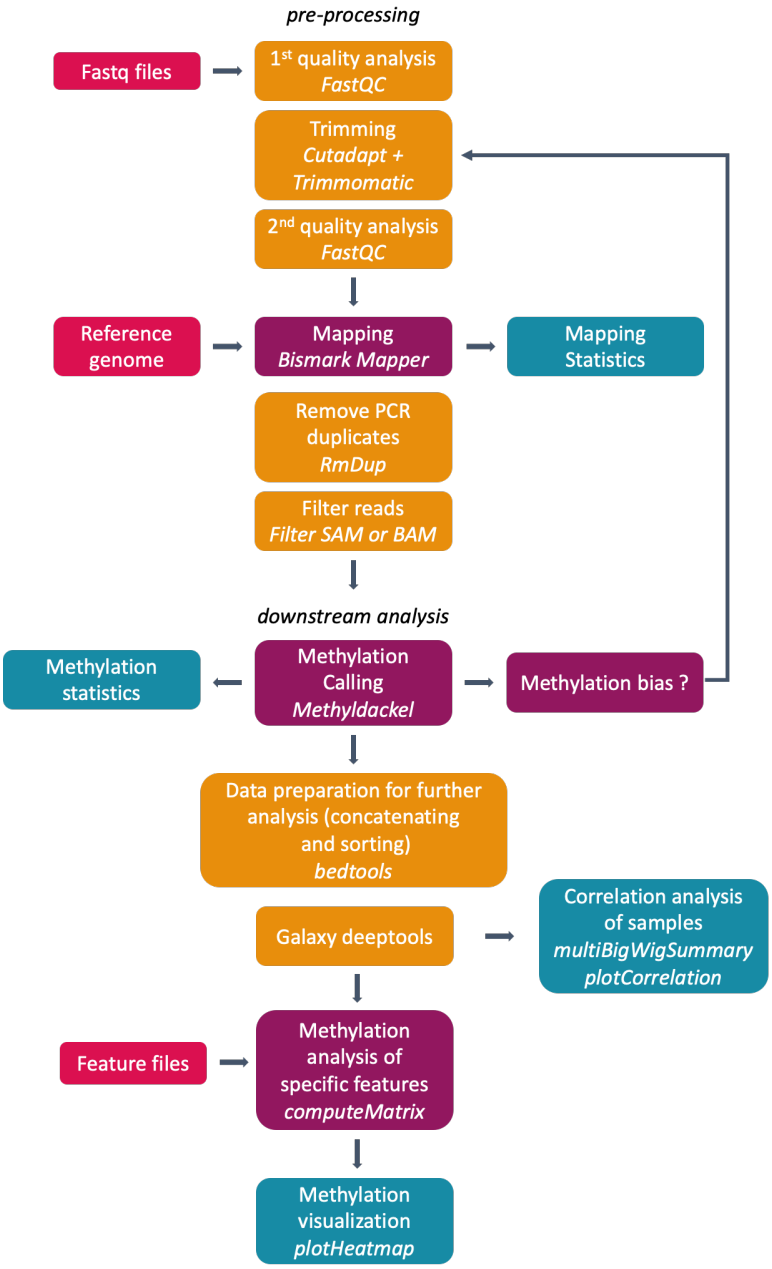

Figure 14: WGBS analysis pipeline. Tools in italics. Pink = input files, orange = data processing/quality control steps, purple = central data calculation steps, petrol = output files.

The tool *Methyldackel* was used in two ways: 1. to determine position-dependent methylation bias in a dataset and 2. to extract methylation metrics from the aligned and filtered reads (version 0.3.0.1; https://github.com/dpryan79/MethylDackel). For methylation calling a minimum per base depth of 10 reads was applied and methylation in CpG as well as in CHG

and CHH contexts was determined. The output files of the nuclear genome methylation sites were used to calculate the methylation levels in the three contexts, as the Bismark Mapper report only calculates one decimal position. Here, percentage was calculated by summing up methylated and unmethylated positions and calculating the percentage for the methylated positions for each context (CpG, CHG, and CHH) for the nuclear genome. For further analysis of methylation patterns throughout the whole genome, methylation position files of all three sequence contexts were then concatenated.

Downstream data analyses were performed with the toolset deepTools hosed on the Freiburg Galaxy server (Ramírez *et al.*, 2016). With *multiBigwigSummary* (version 3.3.2.0.0) correlation scores between samples were calculated with default settings and afterwards visualized using *plotCorrelation* with the Pearson correlation method (version 3.3.2.0.0). For visualization of methylation distribution in specific genomic features, the data was compressed using the *computeMatrix* tool (version 3.3.2.0.0). In general, methylation scores were averaged (calculated mean) over 25nt bins and the distance up- and downstream of the feature was set to 1000 bp. Depending on the feature analysed, an average feature length to which all regions were scaled, was set (CDS 1400 bp, mCDS 550, lncRNA 800 bp, tRNA 300 bp, transposable elements (TE) 2800 bp). Matrix data was visualized using *plotHeatmap* (version 3.3.2.0.1), including a summary plot with the calculated mean of methylation of all regions.

2.2.16 MLST analysis of clinical isolates

Multilocus sequence typing (MLST) analysis was performed for the following clinical isolates used for WGBS: PEU3692 (respiratory), PEU3694 (urine), PEU3696 (stool), PEU3698 (invasive), and PEU3700 (blood). Seven fragments of housekeeping genes were sequenced according to Bougnoux *et al.* (2003): *AAT1*a, *ACC1*, *ADP1*, *MPIb*, *SYA1*, *VPS13*, and *ZWF1b*.

For the PCR 2 µl of extracted DNA were added to 48 µl of Mastermix, containing 5 µl 10x buffer, 0.6 mM of the respective forward and reverse primer, 1 mM dNTPs, 1 mM additional $MgCl_2$ and 2.5 U Taq polymerase. PCR conditions for all primer pairs were a 5 min denaturation step at 95°C, followed by 35 cycles of 30 sec denaturation at 95°C, 1 min annealing at 58°C, 1 min elongation at 72°C, and 10 min final elongation at 72°C. Quality of the PCR products was verified by gel electrophoresis, and subsequently PCR products were cleaned with a PCR clean-up kit. PCR products were eluted with 30 µl of prewarmed DNAse/RNAse-free H_2O.

Sanger sequencing was performed as previously described (section 2.2.7). Provided sequences were checked in the *Candida albicans* MLST database (curated by M.-E. Bougnoux) of the PubMLST.org website (Jolley, Bray and Maiden, 2018).

2.2.17 ELISA immunoassay for 5mC DNA methylation analysis of diverse fungal species

To quantify the presence of DNA methylation in *C. albicans* by a further method, ELISA immunoassay was performed with the 5mC DNA ELISA Kit from Zymo Research. This assay is based on indirect detection: an anti-5-methylcytosine monoclonal antibody binds to 5mC of denatured, single-stranded DNA, attached to the well surface. In the next step a secondary antibody, labelled with horseradish peroxidase (HRP) binds to the 5mC specific antibody. A chromogenic substrate finally is added, and colour intensity indicates the quantity of 5mC in the sample.

The reference strains SC5314 and 529L (non-filamenting and filamenting on Spider medium without treatment) as well as several isolates of *C. albicans* used in the previous experiments (PEU3692, PEU3694, PEU3698, PEU3700) were analysed from 5-Aza treated and untreated samples. Additionally, the quantity of 5mC in DNA was investigated for further fungal species with known and unknown DNA methylation state: *C. auris*, *C. glabrata*, *C. parapsilosis*, *C. tropicalis*, *Cryptococcus neoformans*, *Cryptococcus diffluens*, *Saccharomyces cerevisiae*, *Aspergillus flavus*, and *Aspergillus fumigatus*. Further, the 5mC quantity was measured for strain SC5314-*RFP* and its attenuated derivate PEU3801 (5-Aza treated and untreated). The DNA of human THP1 monocytes (~3.6 - 4.1% 5mC) and *Lentinula edodes* (shiitake fungus) served as positive controls (Flores-Sierra *et al.*, 2016; DongLai *et al.*, 2018). As the detection limit of the kit is specified with ≥ 0.5% mC / 100 ng single stranded DNA, the maximum possible amount of 200 ng was used per sample. The assay was performed according to the manufacturer's protocol. Each sample was tested as duplicate. Absorbance at 405 nm was measured after 45 min in an ELISA plate reader. For later calculations a standard curve was assayed in parallel with 0%, 0.5%, 1.0%, 2.5%, 5.0%, 10.0%, and 25% 5mC. The 5mC concentration of the samples was calculated using a 4-parameter logistic equation (4PL).

3 RESULTS

3.1 Verification of 5mC DNA methylation in *C. albicans*

3.1.1 Bisulfite sequencing PCR reveals similar methylation sites in yeast and hyphal morphology

Initially, the traceability of DNA methylation in *C. albicans* was demonstrated by direct bisulfite sequencing, as this technique represents a simple and fast approach for the detection of 5-methylcytosine (5mC) at a specific gene locus. For this purpose, a region was chosen, which was previously described by Mishra *et al.* (2011) to be methylated. This region is ORF C1_00050C, an ORF of unknown function, located between *CTA2* (alias *CTA21*) and *TUP1* (Figure 15). Tup1 is known as a repressor of hyphal development (Braun and Johnson, 1997) and Cta2 as putative transcription factor, repressed by Efg1 (Doedt *et al.*, 2004), which is an important transcription factor for hyphal development (Stoldt *et al.*, 1997). The close proximity to *CTA2* and *TUP1*, both genes which are – or in case of *CTA2* seem to be - involved in morphological development, makes ORF C1_00050C a very interesting target for our analysis, as a functional correlation of the combined loci could be possible. The selected region was 360 bp in length.

A central question of this analysis is if yeast- and hyphal form cells show different patterns of methylation. For this purpose, samples were taken from a pure yeast culture and at several timepoints after hyphal induction. We used cloning-based bisulfite sequencing PCR, as direct bisulfite sequencing after bisulfite treatment leads to a poorer sequencing quality and overlapping peaks in partially methylated sites.

Isolated DNA was bisulfite converted, amplificated with bisulfite-specific primers and cloned into *E. coli* Top10 cells. Up to 20 clones were picked for a subsequent standard colony PCR, and the amplificated fragment was sent for sequencing with the standard M13 primers. Between 10 to 17 samples were analysed finally for each condition or timepoint.

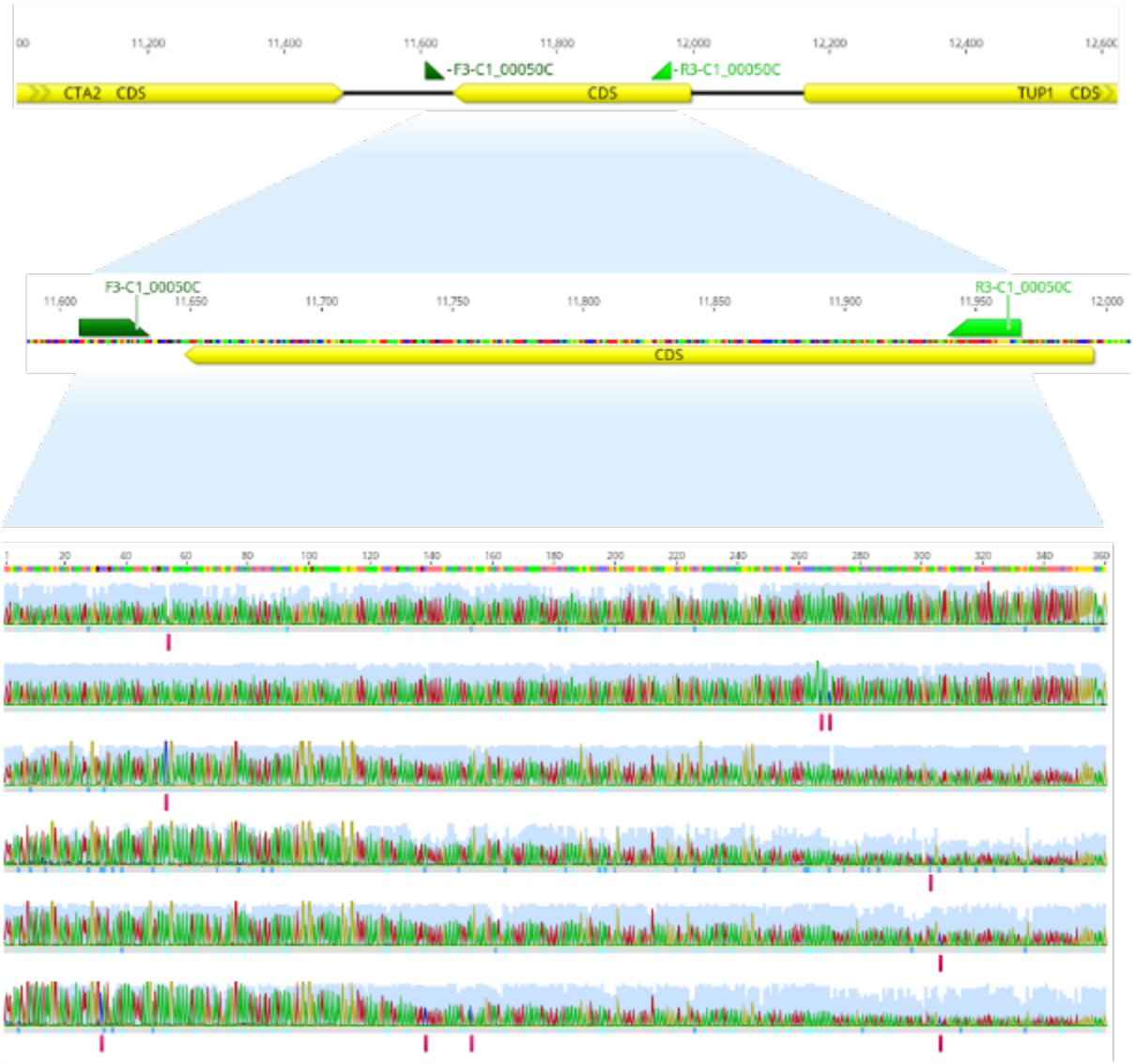

Figure 15: **Examples for DNA methylation in the genomic region C1_00050C.** C1_00050C is located between the genes CTA2 and TUP1. Primers F3/R3-C1_00050C are marked in green. The sequenced region is 360 bp long. Sequence analysis was performed with "geneious". The figure exemplarily illustrates methylated cytosines in the different sanger sequencing chromatograms (pink bars). Yellow boxes: protein coding ORFs. Green halfarrows: Amplification primers.

DNA methylation was not observed in all clones sequenced. In the yeast preculture and at the different timepoints after hyphal induction - 0 min, 15 min, 1 h, 2 h, and 6 h – at least one methylated C was observed in 41.7%, 46.7%, 50%, 50%, 45.5%, and 33.3% of the sequences (Figure 16, B), respectively. The number of methylated positions in each methylated sequence ranged between 1 and 4, but in most of the methylated sequences only one or two cytosines of 71 were methylated.

Some sequence regions showed repeated occurrence of methylation. We observed areas where methylation also reoccurred not only within one condition, but also between different

conditions (red frames in Figure 16, A). These areas had a range of up to 9 bp in 8 cases, and two areas ranging between 11 to 13 bp, supporting the idea that methylation of any cytosine within these areas could have the same function.

Regarding the transition from yeast to hyphal morphology 5mC methylation was shifting from the sides of the gene more to the centre: in the yeast culture, as well as 0 min after induction, until 1 h after induction, methylation occurred often around 30, 50, and 320 bp, which represent the outer part of the gene, whereas 2h and 6h after induction of the hyphal morphology these positions were not methylated anymore. Instead, here we saw more methylation around 80 and 270 bp, hence, the methylation seemed to have shifted more to the centre of the coding sequence. The stop codon is located at position 39-41 and very close by surrounded by multiple methylated Cs, which are only between 6 and 13 bp away (positions 28–33 and 51–54). Also, the methylation at position 318 and 324 is very close to the transcriptional start site, which is only 25 bp away.

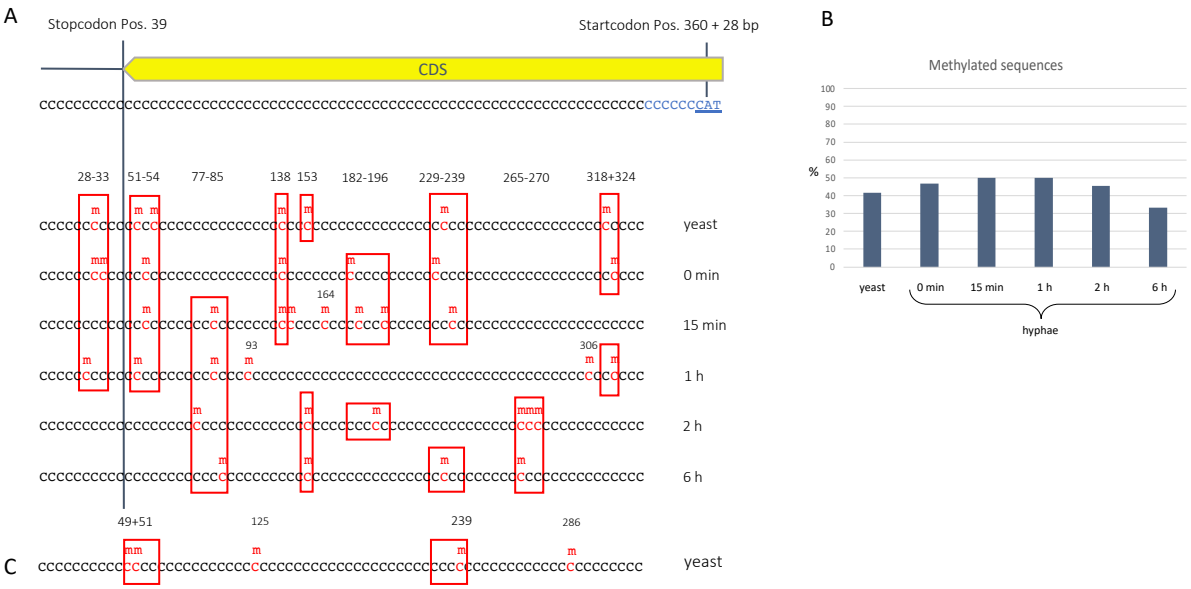

Figure 16: *C. albicans* SC5314 methylated cytosines in the genomic region C1_00050C. (A) 5mC DNA methylation in yeast-hyphae-transition. For each condition between 11 and 17 clones were picked and sequenced. Samples were obtained from a liquid preculture in yeast morphology, at the time of hyphal induction (0 min) and several timepoints after induction (15 min, 1 hour, 2 hours, and 6 hours). From the whole sequence only cytosines are listed. Blue bases lie outside of the amplificated fragment. Methylated cytosines are highlighted in red and marked with "m". Numbers indicate base position of methylated cytosines in the sequence. Red frames show concordant regions between the different conditions. (B) Proportion of methylated sequences at the different timepoints. (C) Replicating experiment; samples were obtained from a liquid yeast culture. 22 clones were picked and sequenced. Methylated cytosines are marked in red. Methylation positions that matched to the regions of methylation of our previous experiment are marked with a red frame.

In a replicating experiment[1], the same genomic region under the same conditions as the first yeast culture in sample group A described above was sequenced. This time, 22 sequences were analysed from which 27.3% showed methylation in the targeted sequence. Yet, three of the five methylated cytosine positions detected, were concordant to methylated regions found in the previous bisulfite sequencing experiment (Figure 16, B). According to our previous findings, these yeast cells showed methylation at similar loci like the yeast culture and at early timepoints after hyphal induction. Further, they were located mainly at the beginning and end of the coding sequence, a methylation pattern that was present only in yeast and early hyphal culture in our first experiment. Furthermore, none of the hyphal-specific methylation sites from the later timepoints (2 h and 6 h) after hyphal induction could be found in this sample.

Depiction of the relative frequency of bases close to methylated cytosines from both experiments showed different patterns for yeast and hyphal morphology (Figure 17, B and C).

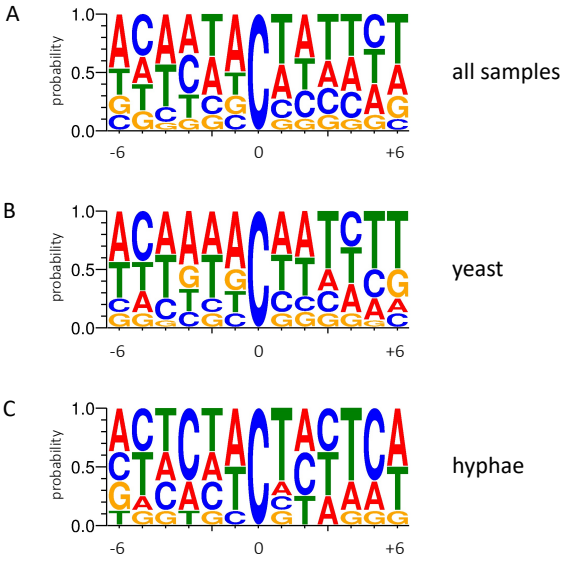

Figure 17: Context of 5mC methylation in ORF C1_00050C. Logos depict 6 bases each 5' and 3' of the methylated C. (A) Context of 5mC methylation in all samples sequenced – yeast and hyphal morphology, (B) 5mC methylation only in yeast samples (preculture and 0 min after induction), (C) 5mC methylation only in hyphae samples (2 and 6 h after hyphal induction).

The average AT content in this region was around 64%, which means a proportion of around 32% each for A or T, as well as around 18% each for G or C would present average values.

[1] conducted by Abdelmalek Ahlees.

Nevertheless, a dominance of adenine in the 5' region and a slightly more frequent ApCpT context, with a probability of around 50% for the preceding adenine and around 45% for the following thymine, was visible as an average of all samples analysed (Figure 17, A). At position -5, -3, and +5 cytosine with an occurrence of 25 – 30% seems to play a role in methylation context as well. Further a CpG context seems to play a minor role (around 10%) (Figure 17, A-C) in contrast to many other organisms.

Specific methylation patterns become more obvious when comparing yeast (Figure 17, B) and hyphal (Figure 17, C) morphology: the yeast form sequence is characterized by a strong presence of adenine around the methylated C (around 50% at positions -1 and -3), a dominant cytosine at position -5 and very dominant thymine at positions +3, +5, and +6 (each around 50%). The hyphal form sequence by contrast is dominated by cytosine at positions -5 (>30%), -3 (>60%), +3 (>30%), and +5 (>60%). Very strong as well, is the ApCpT context of the methylated C, with around 50% for adenine and 65% for thymine. Guanine in general seems to play a minor role adjacent to methylated Cs, at least at this locus.

3.1.2 Detection of 5mC DNA methylation in SC5314 yeast and hyphal morphology by WGBS

To gain a deeper understanding of DNA methylation and its effects in *Candida albicans*, we investigated the whole genome for 5mC DNA methylation by whole genome bisulfite sequencing (WGBS). As the methylation rate in *C. albicans* seems to be very low, a global approach with high coverage rates is important for a reliable analysis.

3.1.2.1 WGBS reveals distinct methylation patterns in SC5314 yeast and hyphal morphology – a one-to-one sample analysis

In a first approach we investigated only two samples with differing morphology, taken from a yeast and a hyphal liquid culture of reference strain SC5314. The hyphal culture was subcultured from the yeast culture and hyphal development was induced by changing pH and temperature. The culture was harvested after 6 hours of growth, when hyphae were already clearly visible in the microscope. Sequencing reads were 125 bp in length and paired end.

Reads were mapped to the reference genome of *C. albicans*. First, reads were mapped only to the nuclear genome, all unmapped reads were then mapped to the mitochondrial genome. Technical and quality parameters of the mapping are detailed in the appendix (Supplementary Table 2, Supplementary Figure 1).

Further, variance analysis for genome coverage and GC content did not show any remarkable discrepancies in our data (Supplementary Figure 2).

In general, we found a very low methylation content (overall proportion of methylated cytosines within entire genome) of ~0.5% for all sequence contexts, calculated by the mapping program (*Bismark Mapper*), which, however, only outputs data rounded to one decimal position. Methylation contents of the nuclear genome were therefore calculated more accurately to two decimal positions by using the output file of the methylation detection program *Methyldackel*. This calculation revealed small differences between samples and sequence contexts: the average DNA methylation in non-symmetric sequence contexts (CHH) was slightly higher than in classical palindromic contexts (CpG and CHG), in both morphologies (Table 12). Further, the methylation content appeared marginally lower in the yeast compared to the hyphal morphology.

Table 12: Content of methylation in different sequence contexts.

Sample ID	CpG (%)	CHG (%)	CHH (%)
Ca_yeast_nucl	0.49	0.49	0.52
Ca_hyphae_nucl	0.50	0.51	0.54

Methylation Calling of all methylated cytosines (CpG, CHG, and CHH contexts) and plotting of score distributions around different loci of interest confirmed further observation of our initial Sanger-based bisulfite sequencing experiment: first, the detected methylation level (score per region) was very low as well and ranged between 0.5% and 0.6%. Second, methylation patterns 5’ and 3’ of coding sequences (CDS) could be detected, regarding the overall mean methylation of the whole genome: While the CDSs themselves had a low level of methylation of around 0.5%, there was an increase in the 5’ and 3’ regions of the CDSs in the yeast as well as in the hyphal morphology (Figure 18, A). Further, there was no difference in the overall methylation pattern between yeast and hyphal morphology. The methylation level was slightly higher in the hyphal morphology, but only to a very small degree.

In subtelomeric coding sequences (here defined as the first and last 50000 bp of a chromosome) a moderately lower methylation level of around 0.46% was determined for both morphologies. A similar methylation pattern like shown for CDSs of the whole genome could be observed, even though a bit less distinct (Figure 18, B).

Long terminal repeats (LTRs) and retrotransposons (Figure 18, C) displayed an entirely different methylation pattern: taking 0.5% methylation as a baseline, there was a peak around 0.7% in the first third and a second peak in the second part of the sequences, which was the same in both, yeast and hyphal morphologies. A smaller peak was visible in the 5' region (0.6%), in the 3' region the pattern was not clear. The methylation level exceeded the level of most other features.

lncRNAs also showed a totally different methylation pattern as compared to the CDSs for both morphologies: 5' adjacent to the region of the lncRNA sequence an increase of methylation was present, which even increased more inside the feature region and dropped again at the end of the feature (Figure 18, D). Thus, the pattern of methylation between CDS and lncRNA seems to be different. The level of methylation was marginally higher in the hyphal than in the yeast sample.

The methylation pattern of tRNAs was again different between yeast and hyphal morphology, as a slight drop of methylation from 0.5% to 0.4% could be detected at the beginning and end of the tRNA sequence in the yeast sample. In the hyphal sample this drop was not as much incisive (Figure 18, E).

Methylation of the CDS of the mitochondrion (mCDS) and its adjacent regions was on one level of around 0.5% in the yeast sample, whereas an increase to over 0.7% could be observed in the hyphal sample in the 5' region (Figure 18, F).

In the heatmaps of CDSs and lncRNAs stronger methylation in the upper part of yeast and hyphal sample (indicated by red spots) revealed a concordance concerning the regions of methylation in both morphologies. Nevertheless, the part below with less methylation in the yeast (more yellow to green), is more interspersed with methylated regions in the hyphal morphology, also indicating regions that are differentially methylated between the two morphologies.

In a broad sum, no fundamental differences were visible between the two morphologies when regarding the methylation patterns of the different features.

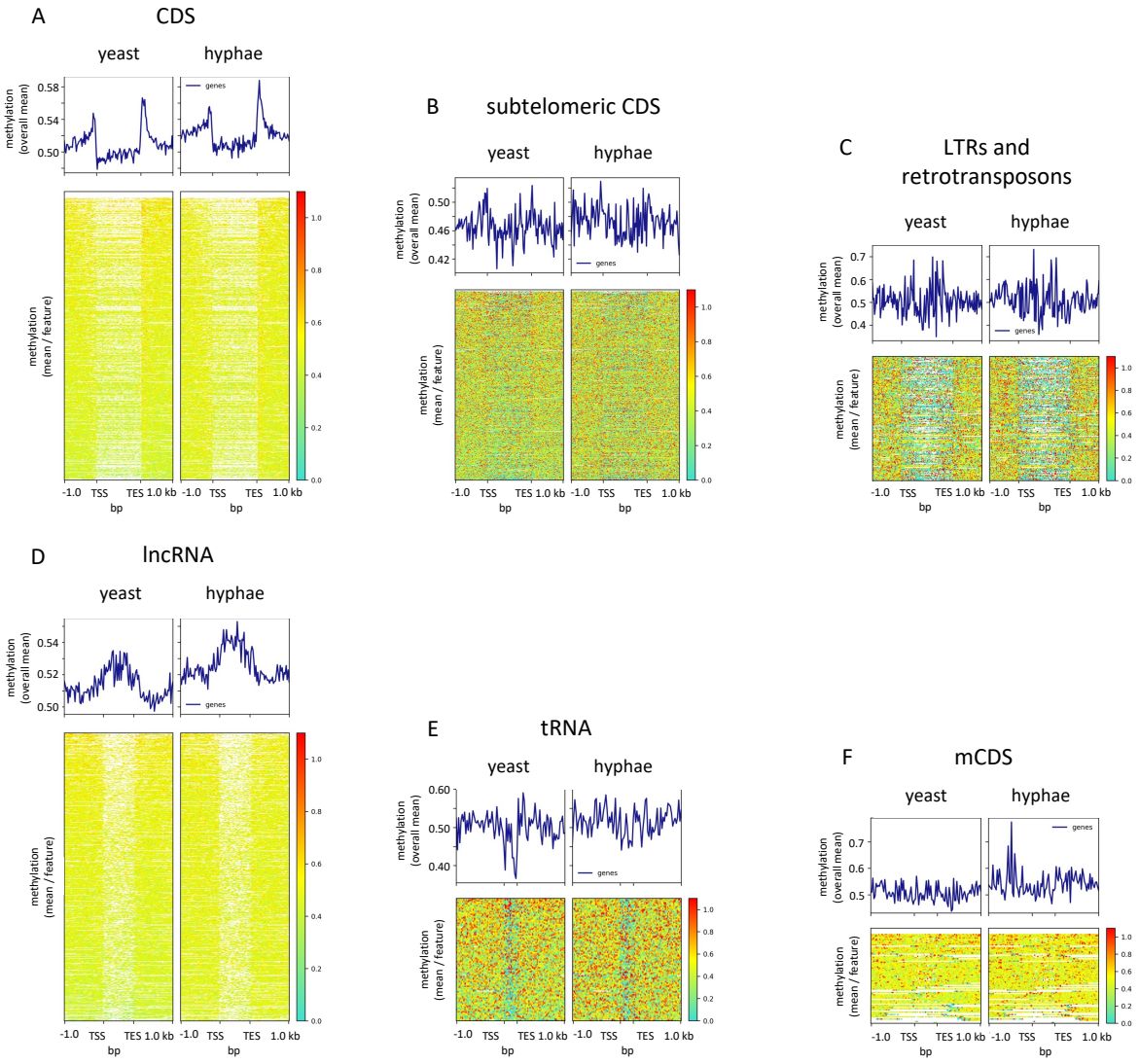

Figure 18: Mean 5mC DNA methylation levels of different feature sets and adjacent regions. All features (y-axis) are scaled to average length from transcriptional start side (TSS) to transcriptional end side (TES) (x-axis): coding sequences (CDS) of the nucleus 1400 bp (N=6599), LTRs and retrotransposons 1800 bp (N=177), lncRNAs 800 bp (N=7190), tRNAs 300 bp (N=126) and mitochondrial coding sequences (mCDS) 550 bp (N=32). Subtelomeric CDSs include the first and last 50000 bp of each chromosome (N=478). Adjacent regions are -/+ 1kb for all panels. Colour bars show scale for level of methylation in percent. Summary plots on top show mean of methylation of all features plotted. Bin size 25 bp. White: Missing data. Gene features on y-axis are ordered according to the yeast sample in descending order concerning mean methylation level, the same gene order was applied to the hyphal sample irrespectively to degree of methylation.

3.1.2.2 Reproducible methylation patterns by WGBS in SC5314 yeast and hyphal morphology

Having found meaningful patterns of methylation in the preliminary analysis, a similar experiment was then conducted with two replicates per condition and after different timepoints of induction of yeast and hyphal morphology. Again, samples from a liquid yeast culture of SC5314 were harvested, which was then used to inoculate a hyphal culture. In the present experiment, a fresh yeast culture was inoculated in parallel to the hyphal culture, to have yeast and hyphal culture in the same growth phase. From each culture samples were taken at 1h and 6h post inoculation (Figure 19), allowing for analysis of a possible change of the methylation pattern over time.

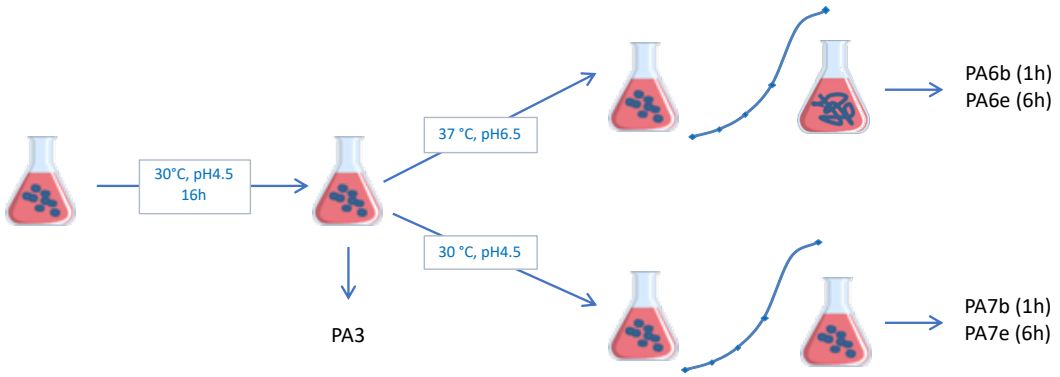

Figure 19: Experimental setup and culture conditions for WGBS. Yeast and hyphal morphology were induced by specific pH and temperature. Sample PA3 = yeast culture 16h after inoculation (p.i.), PA6b = hyphal culture 1h p.i., PA6e = hyphal culture 6h p.i., PA7b = yeast culture 1h p.i., and PA7e = yeast culture 6h p.i.

Technical and quality parameters of the mapping are documented in detail in the appendix (Supplementary Figure 3). Further, variance analysis for genome coverage and GC content again did not show any remarkable discrepancies in our data (Supplementary Figure 4).

The methylation content of the different samples ranged between 0.69% to 0.78% for the nuclear genome (Table 13). As shown in the previous experiment, a marginally higher methylation content rate for non-palindromic (CHH) methylation was observed in all nuclear genome samples compared to their corresponding palindromic samples (CpG and CHH), with an average difference of 0.04%.

Table 13: Content of methylation in different sequence contexts

Sample ID (replicate 1 and 2)	description	methylated CpG [%]	methylated CHG [%]	methylated CHH [%]
PA3-1_nucl	yeast 16h	0.75	0.74	0.78
PA3-3_nucl	yeast 16h	0.70	0.69	0.73
PA6b-1_nucl	hyphae 1h	0.75	0.74	0.78
PA6b-3_nucl	hyphae 1h	0.70	0.70	0.74
PA6e-1_nucl	hyphae 6h	0.72	0.72	0.76
PA6e-3_nucl	hyphae 6h	0.72	0.71	0.75
PA7b-1_nucl	yeast 1h	0.73	0.73	0.76
PA7b-3_nucl	yeast 1h	0.74	0.74	0.77
PA7e-1_nucl	yeast 6h	0.73	0.72	0.75
PA7e-3_nucl	yeast 6h	0.70	0.69	0.73

Methylation calling (CpG, CHG, and CHH) reproduced the different methylation patterns at different feature types, even though with a slightly higher methylation level baseline of around 0.7% to 0.75% (Figure 20). Correspondingly, a peak was visible in the 5' as well as in the 3' region adjacent to the CDS, but not in the CDS itself (Figure 20, A). Further, all other features show methylation patterns comparable to our first experiment. Also, increased methylation levels compared to CDSs were observed again for LTRs.

The replicates of all samples had slightly differing methylation baselines. However, in sum no differences between the global methylation patterns of yeast and hyphal morphologies could be found. Only one feature type, the tRNAs, had a different methylation pattern between the different conditions: the drop in methylation at the beginning and at the end of the feature was less pronounced in the 6h samples (yeast and hyphal), compared to the yeast preculture and the 1h samples (yeast and hyphal), however, a bit less in the 6h hyphal sample (Figure 20, E). In the mCDS the methylation pattern was not that clear and peaks were a bit stronger than

in the previous experiment. In some of the samples, methylation was a bit higher in the whole 5’ and 3’ region than in the mCDS (Figure 20, F).

Further, when comparing 1h and 6h samples of each morphology (PA6b vs PA6e and PA7b vs PA7e), the methylation pattern appeared a bit clearer with less diffuse peaks in between over time. Also, the descending order of the methylation pattern in the heatmap could be found in the other samples as well, to which the order of the regions from the first sample was applied. Thus, similar regions were stronger methylated in the different samples. Here again, this pattern became sharpened in the 6h samples compared to the 1h samples. This was most clearly visible in the CDSs and lncRNAs (Figure 20, A and D), as these features represent the greater part of the genome.

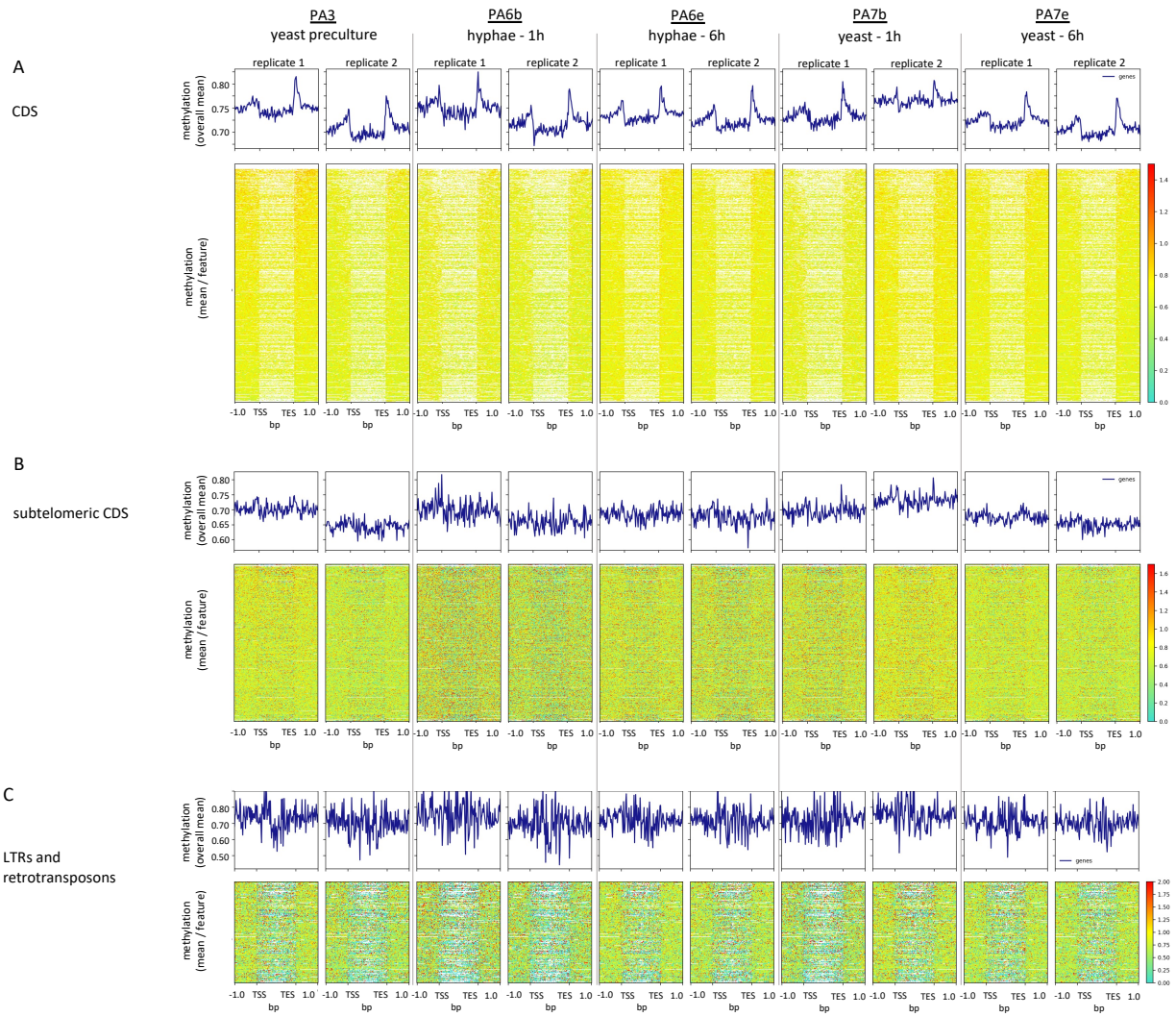

Figure 20: Mean 5mC DNA methylation levels of different features and adjacent regions. All features are scaled to average length from transcriptional start side (TSS) to transcriptional end side (TES): (A) coding sequences (CDS) of the nucleus 1400 bp (N=6599). (B) Subtelomeric CDSs include the first and last 50000 bp of each chromosome (N=478). (C) LTRs and retrotransposons 1800 bp (N=177). Adjacent regions are -/+ 1 kb. Colour bars show level of methylation in percent. Summary plots show mean of methylation of all features plotted. Bin size 25 bp. Missing data is white. The first replicate of the yeast preculture is always in descending order concerning mean methylation level, gene order was applied to the following samples.

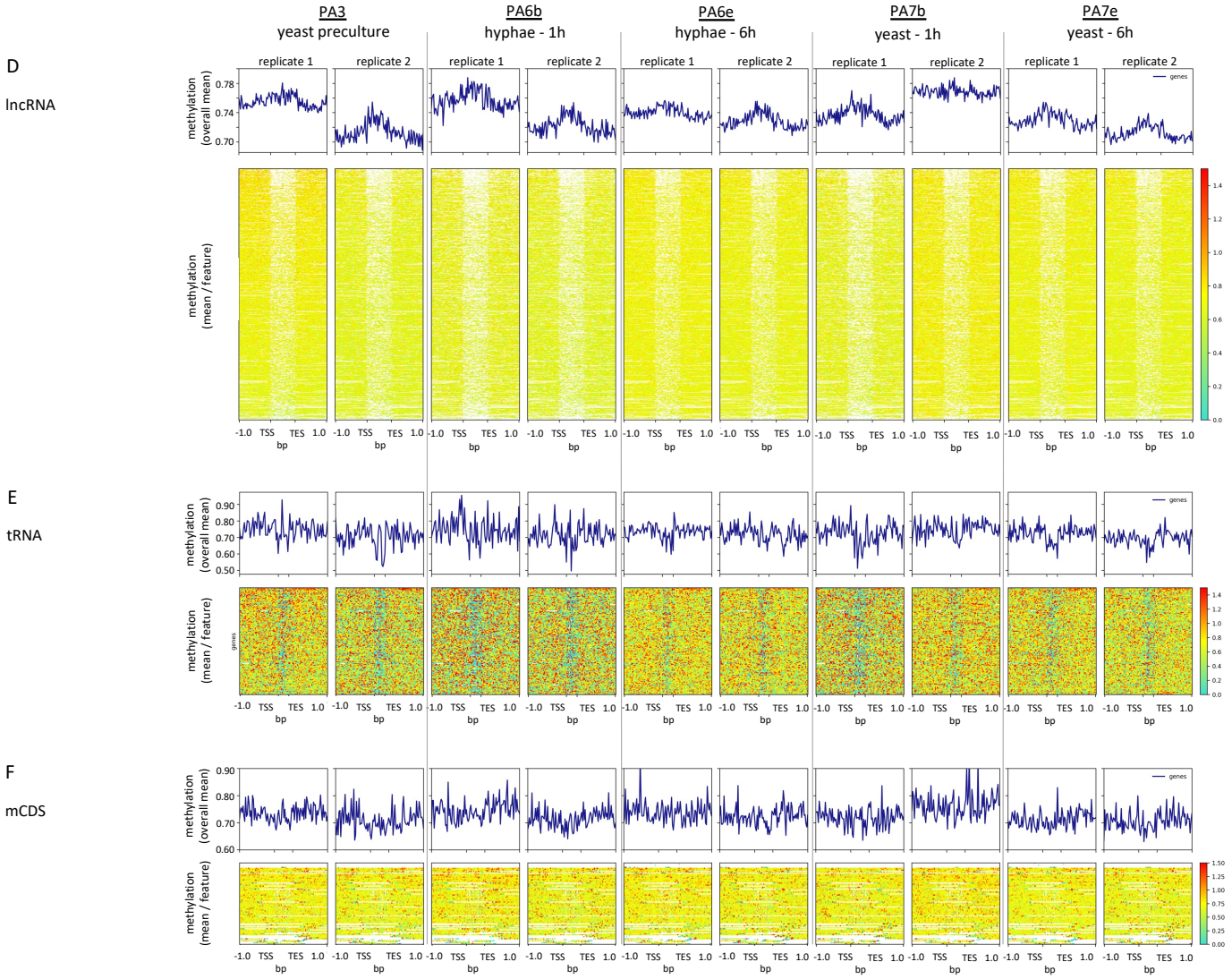

Continued from previous page:

Figure 20: (D) lncRNAs 800 bp (N=7190). (E) tRNAs 300 bp (N=126). (F) mitochondrial coding sequences (mCDS) 550 bp (N=32).

In a correlation analysis (Pearson correlation) using the average methylation scores of all samples (10000 nt bins), biological replicates of each sample clustered together (Figure 21), showing the similarities in their methylation pattern. Strikingly, all yeast samples of the late cultures (yeast pre-culture (16h) and yeast 6h after induction) clustered together. In contrast the yeast 1h culture was most distant to all other samples. As among yeast cultures, the 6h hyphal culture was even more similar to the 6h yeast culture than to its counterpart, the 1h hyphal culture. Further, both 1h cultures – yeast and hyphae – showed the highest variances within their replicates.

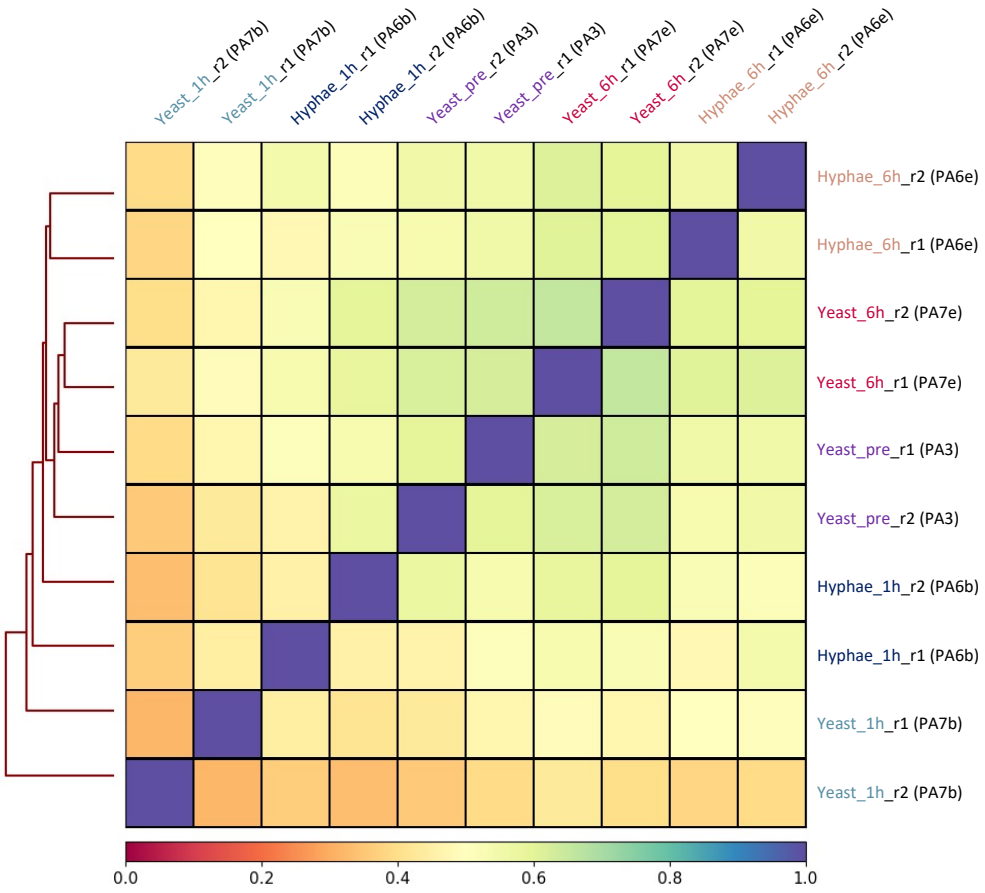

Figure 21: Correlation of methylation sites in different morphologies. Correlation coefficients (colour bar) were calculated with Pearson method on 10 kb bins of the genome.

3.2 Effect of the DNMTase inhibitor 5-Azacytidine on *C. albicans* SC5314

As described before, 5-Azacytidine is a known DNMTase inhibitor, that is also used as treatment for hypermethylation induced cancerogenesis in humans.

Based on the fact, that 5-Aza affects *C. albicans* morphologically in the way that it accelerates germ tube formation during hyphal induction (Pancaldi *et al.*, 1988), as well as it reduces DNA methylation in strain SC5314 (Mishra, Baum and Carbon, 2011), we wanted to investigate this phenomenon and use the demethylating characteristics of this drug to correlate specific DNA methylation patterns to morphological transition on one hand and to gene expression on the other hand. The hypothesis is, that the demethylating effect of 5-Aza could lead to a methylation pattern that promotes hyphae specific gene expression.

Samples for the analyses were taken from a complex experiment with reference strain SC5314 (2.2.10, Figure 9). They were harvested from yeast precultures with (PA2) and without (PA3) 5-Aza, and from their subcultures, where yeast and hyphal growth were induced by specific pH and temperature, and samples harvested at several timepoints. The whole experiment was set up in triplicates.

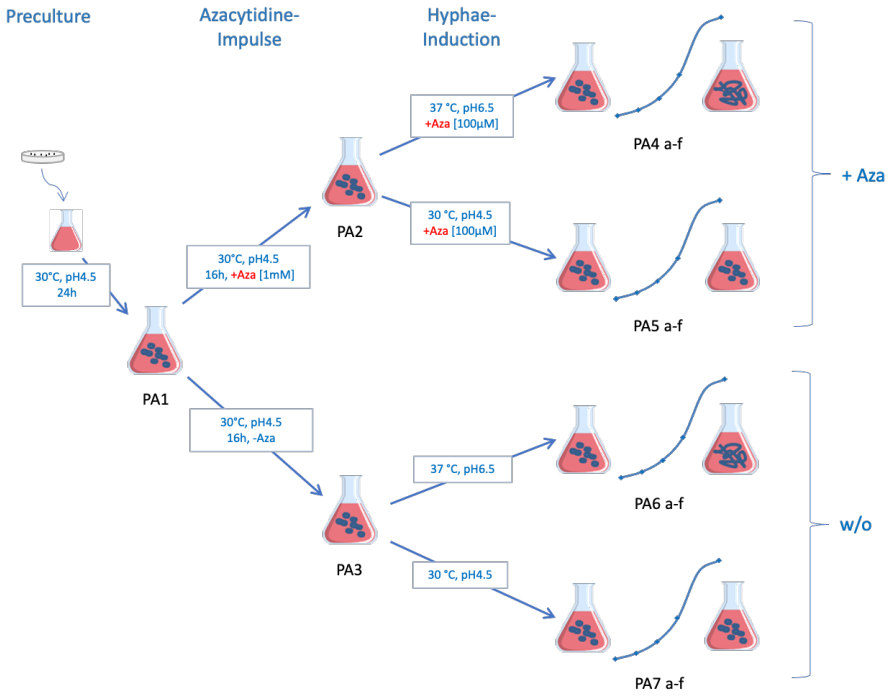

Figure 22: 5-Aza experiment setup. Part I – originating from culture PA2 – 5-Aza treated, part II – originating from culture PA3 – untreated. Both parts were run as parallel timecourse experiment, where yeast and hyphal growth were induced by specific pH and temperature. Samples were taken from the yeast precultures PA1, PA2, and PA3, as well as from several timepoints during the timecourse experiment, which were 0h (a), 1h (b), 2h (c), 4h (d), 6h (e), and 24h (f).

3.2.1 Effect of 5-Aza treatment on growth and morphology

During growth of the cultures OD_{600} was measured each time samples were harvested (Figure 23, A). In the yeast precultures no big difference in growth could be observed between treated and untreated samples. The same was observed for the cultures of the timecourse experiment. Treated and untreated culture of the same morphology showed the same OD over the whole time of the experiment. The only difference observed was the higher OD of the yeast cultures compared to hyphal cultures in the later phase of the experiment.

However, microscopic analysis of the cultures revealed a slight difference in the morphology between treated and untreated yeast culture 6h after inoculation (Figure 23, B): the treated yeast culture showed increased pseudohyphal growth compared to the untreated culture. Nevertheless, the untreated culture as well showed some elongated yeast cells, but only very few pseudohyphae. Further, cells in the 5-Aza treated samples seem to be a bit bigger in size than in the untreated samples. No morphological difference could be observed for the 5-Aza treated and untreated culture.

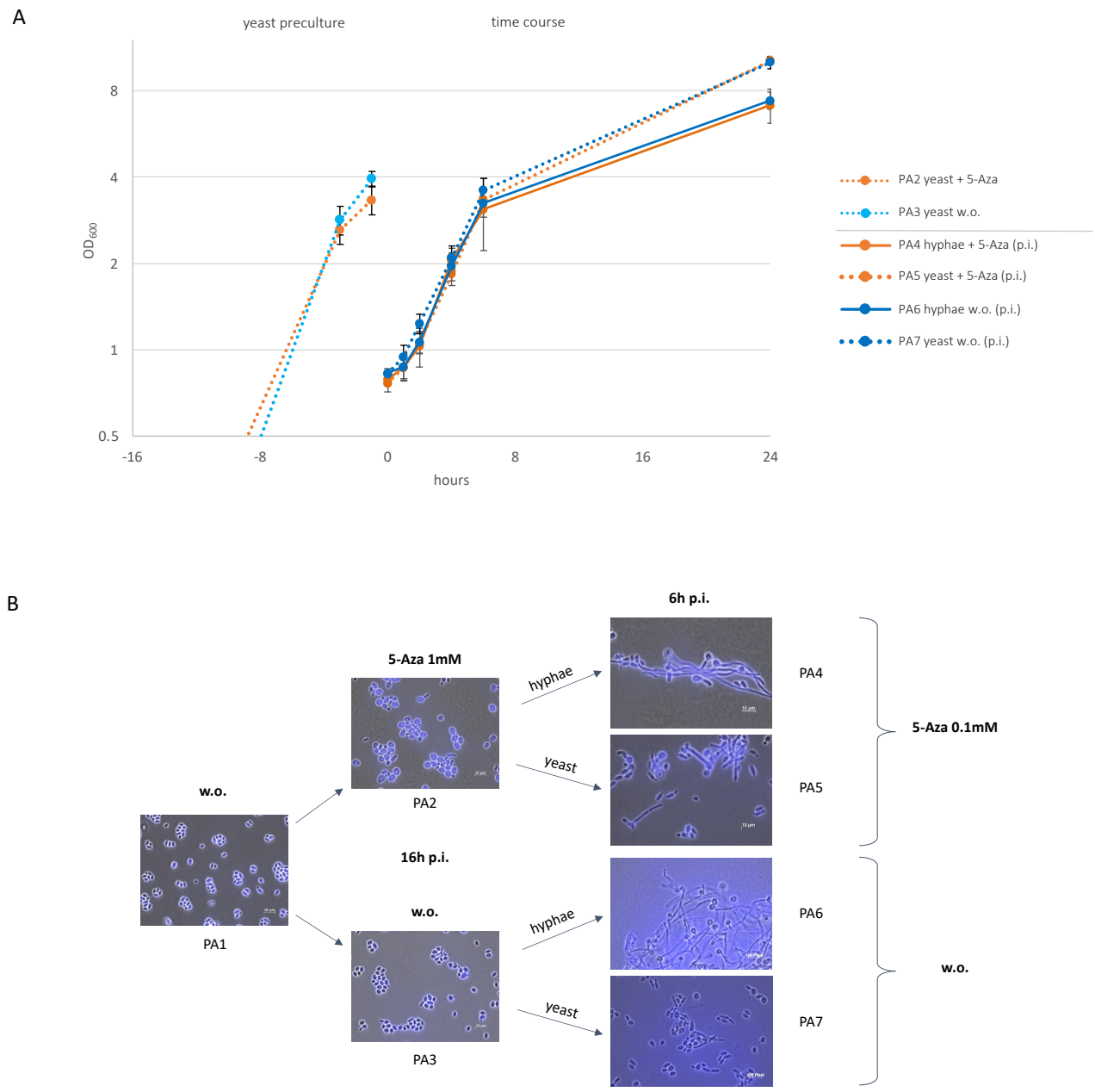

Figure 23: Cell growth and morphology under 5-Aza treatment. (A) Cell growth curves: OD_{600} was measured for the precultures PA2 and PA3 before inoculation of the timecourse experiment and at several time points after inoculation (0h, 1h, 2h, 4h, 6h, and 24h). Orange *time* points indicate cultures with 5-Aza treatment and blue *time* points indicate cultures without treatment. Dotted lines refer to yeast cultures, solid lines refer to hyphae cultures. *(B)* Exemplarily one sample of the cultures is shown for each condition. The pictures of the yeast preculture show the culture at the harvesting time point after 16h and cultures of the timecourse are shown 6h after inoculation. Total magnification 1000x, bright-field/fluorescence (DAPI filter) overlay, scalebar 10 µm.

3.2.2 5-Aza treatment relaxes transcriptional repression of hyphae-specific pathways under yeast-growth conditions

Transcriptional changes induced through treatment of *C. albicans* cells with the known DNA methyltransferase inhibitor 5-Aza were investigated by using whole mRNA sequencing under two different morphological triggers, temperature, and pH. (Figure 22). This was carried out under the assumption that 5-Aza treatment promoted higher expression levels for hyphae specific genes, following the idea that a loss of methylation (or any fundamental change of the methylation pattern) activated the affected genes (Russell *et al.*, 1987; Pancaldi *et al.*, 1988) - also in a non-hyphae-inducing environment.

Samples for RNAseq were taken from 5-Aza treated (PA2 = yeast culture + 5-Aza [1 mM]) and untreated (PA3 = yeast culture w.o.) preculture, as well as from the 1 h timepoints of the timecourse experiment (PA4b = hyphae culture + 5-Aza [100µM], PA5b = yeast culture + 5-Aza [100µM], PA6b = hyphae culture w.o., and PA7b = yeast culture w.o), of each of the triplicates (Figure 22).

Mapping to the reference genome revealed a good quality of the reads (>92% uniquely mapping reads for all samples and variance analysis revealed a good correlation of replicates for further downstream analysis (Appendix, section 6.3).

3.2.2.1 Differential gene expression through overnight 5-Aza treatment

Our first focus was on differential gene expression (DGE) between treated (PA2, 1mM 5-Aza) and untreated (PA3) yeast precultures (Figure 22). When globally looking at all protein coding genes which were significantly regulated (p adjusted value <0.01) and had a log2FC of >1.5 and <-1.5 in the treated culture as compared to the untreated culture, many more up- than downregulated genes could be observed (Figure 24, A and B). Additionally, the rate of differential regulation was higher in the upregulated (203 genes with an average log2FC of +2.21 and a maximum of +7.6), than in the downregulated genes (80 genes with an average log2FC of -1.83 and a minimum of -2.81).

The most strongly upregulated gene *C5_03770C* (a protein similar to formate dehydrogenase in *Candida boidinii,* enabling this fungus to use methanol oxidation as energy source and methanol as carbon source) showed a log2FC of +7.60 (correspondingly a 194-fold higher

transcription rate compared to the untreated sample), whereas the most downregulated gene *OPT4* (oligopeptide transporter 4) only had a log2FC of -2.81 (-7 fold).

Among upregulated genes, we observed a dominance of genes coding for enzymes with dehydrogenase activities, especially formate dehydrogenases (*C5_03770C* +7.60, *C2_10070W* +6.85, and *FDH1* +5.82), which oxidize formate to CO_2. Other upregulated genes included *DUT1* (*dUTP pyrophosphatase 1*, +4.20), which is usually decreased in the stationary phase yeast, *ICL1* (*isocitrate lyase 1*, +3.89), which is farnesol-regulated, and normally stationary phase enriched. Additionally, this important citric acid cycle enzyme is known to be relevant for the virulence of fungi (Dunn, Ramírez-Trujillo and Hernández-Lucas, 2009). Further, typical cell-cycle proteins were observed (*POL1* +3.67, *RFA2* +3.32, *MCD1* +3.28, and *IRR1* +3.25), several genes involved in DNA repair, like *C1_09670C* (+3.80), *MSH6* (+3.48), and *MPH1* (+2.97) and finally genes involved in hyphal development, like the adhesin-like protein *PGA6* and the dehydratase *CHA1*, which showed a strong upregulation with a log2FC of +3.56 and +3.13, respectively (Figure 24, C).

The top downregulated genes were *C4_03960W* (-2.76), a stationary phase protein of unknown function, *GPI14* (-2.64), involved in GPI anchor biosynthesis, *CRG1* (-2.64), a methyltransferase involved in sphingolipid homeostasis, which is interestingly also decreased in hyphae compared to yeast, the oligopeptide transporter protein *OPT3* (-2.49), and further proteins of diverse functions. Strikingly, the NADP-glutamate dehydrogenase *GDH3* (-2.27), which is hypha- and Efg1-repressed (the central hyphal gene TF) is also downregulated, suggesting a hyphae-supporting environment in the 5-Aza treated culture. Further, several Hap43-repressed genes are downregulated, including *OPT4* (-2.81), *CRG1* (-2.64), *OPT3* (-2.49), *RNR22* (-2.33), *OPT2* (-2.22), and *C6_02100W* (-2.02). Interestingly, also one normally Hap43-induced gene (*CR_04750W*, a protein of unknown function, -2.10), is downregulated. Additionally, some morphology related proteins, e.g., *CHA1* (similar to ser/thr dehydratase, repressed by Rim101, filament induced, -3.13), *GAP2* (regulated by Nrg1 and Tup1, -1.93), *URA1* (dihydroorotate dehydrogenase, regulated by yeast-hypha switch, -2.08), and *AMS1* (a putative alpha-mannosidase, transcript regulated by Nrg1, -1.92) were also downregulated in this condition (Figure 24, D, Supplementary Table 6).

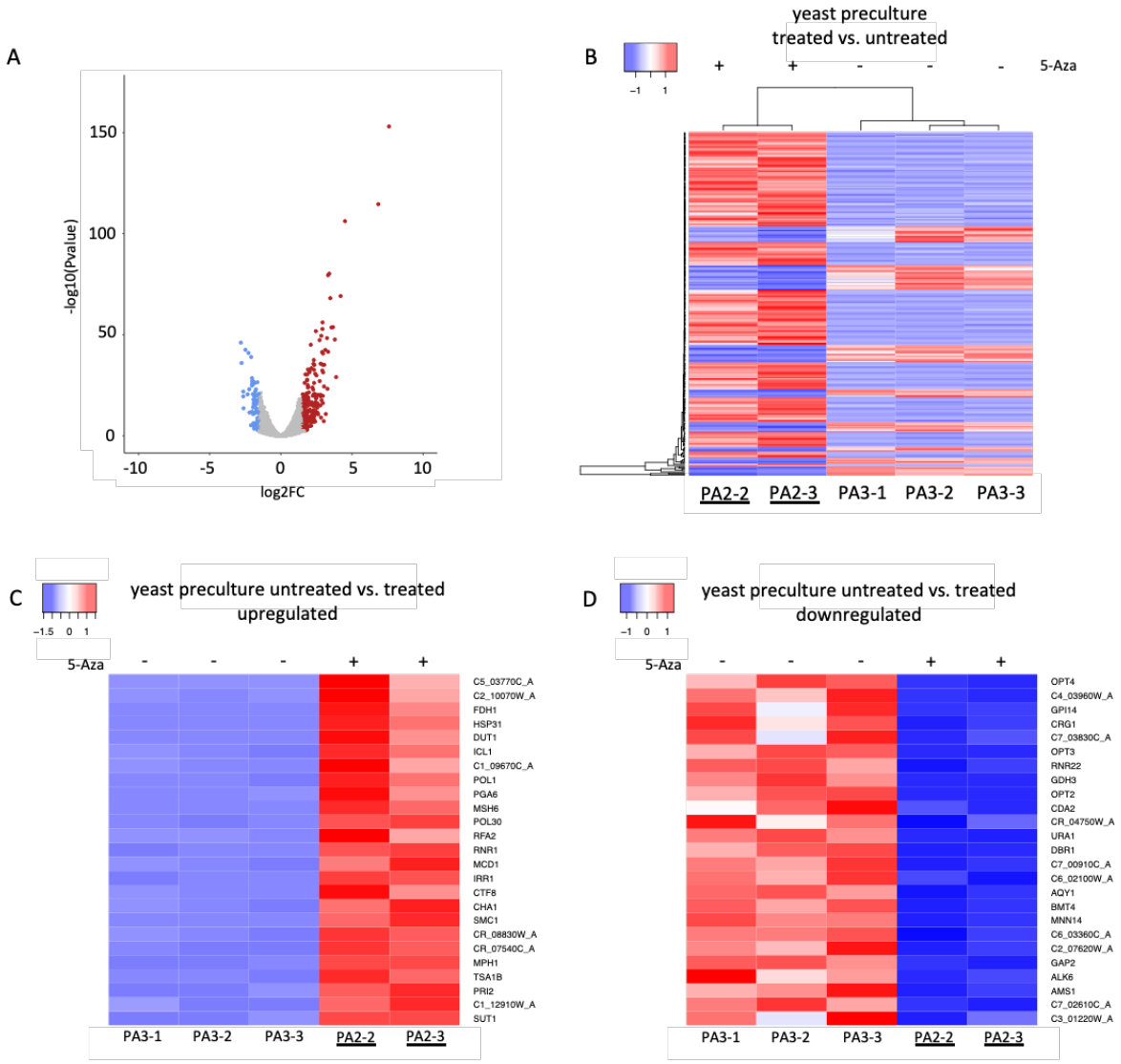

Figure 24: DE analysis of 5-Aza treated and untreated *C. albicans* yeast precultures (PA2 vs. PA3). (A) Volcano plot showing significantly up- and downregulated genes. Differentially expressed genes are coloured, with a threshold of >1.5 and <-1.5 for up- (red) and downregulated (blue) genes, respectively. (B) Heatmap of 281 significantly differentially regulated genes in the treated yeast preculture. (C) top 25 upregulated genes in 5-Aza treated (PA2) yeast precultures. (D) top 25 downregulated genes in 5-Aza treated yeast preculture. All analysis performed using thresholds for p adjusted value <0.01 and log2FC >1.5 for upregulated genes and <-1.5 for downregulated genes.

In total 202 genes were differentially upregulated (log2FC > 1.5), and 79 genes downregulated (<-1.5) in the treated yeast preculture as compared to the untreated one. Without a threshold of 1.5 for the log2FC, 826 genes were significantly upregulated, and 692 genes downregulated.

These results from the precultures indicate that 5-Aza treatment leads primary to an answer of the fungus to the DNA incorporation of the drug with a strong upregulation of oxidative stress and DNA damage response genes. As a secondary effect indeed an effect on morphology related genes was observed, as some hyphae promoting genes became significantly upregulated and hyphae suppressive genes downregulated.

3.2.2.2 Differential gene expression through hyphae-induction in the presence/absence of 5-Azacytidine

In the next step we analysed the 1h time points in comparison to their respective precultures, i.e., yeast and hyphal induction from a yeast preculture. For the 5-Aza-treated samples this also included a 10-fold lower initial concentration of the drug in both, the hyphal, as well as in the yeast culture.

More genes were differentially regulated (p adjusted <0.01 and log2FC >1.5 and <-1.5, referring to all following descriptions on top differentially up- and downregulated genes) after 1h of stimulus (Figure 26, A and B, Figure 27, A and B), as compared to the DGE between the precultures themselves, especially in the yeast culture. When only applying the p adjusted value of 0.01 (i.e., no log2FC threshold employed), the 5-Aza treated hyphal culture had 1337 genes differentially regulated, and the treated yeast culture 2102 genes (Figure 25). In contrast the untreated hyphal culture had 3201 genes differentially regulated, and the untreated yeast culture 4151 genes.

As the treated cultures originated already from a 5-Aza treated preculture with an even 10-fold higher concentration, where already 1518 genes had been observed as differentially regulated, we concluded a deregulation by demethylation to be already present in the preculture. Thus, hyphal induction would not lead to a differential regulation in that many genes as without a previous treatment.

Additionally, more genes were also stronger regulated in the untreated part (i.e., more genes with higher or lower log2FC) compared to the 5-Aza treated part. This was observed especially for the upregulated genes of the hyphal morphology.

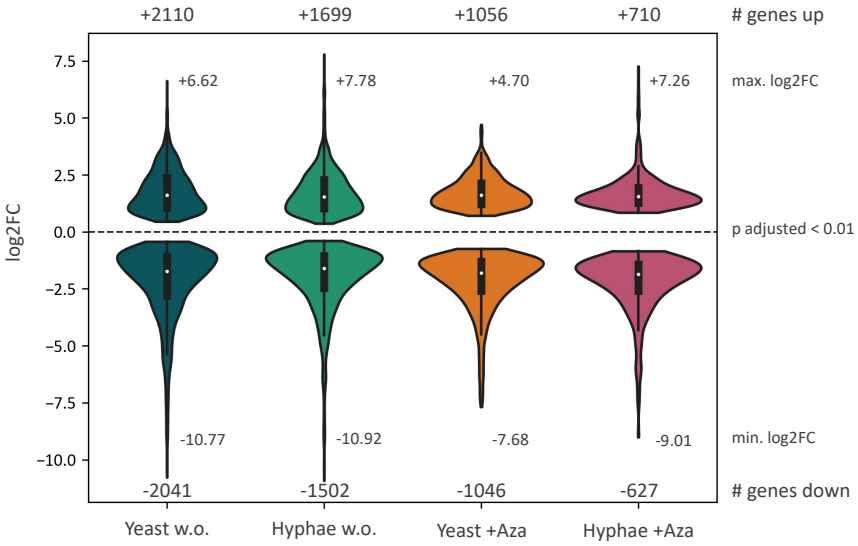

Figure 25: Differential gene regulation after subculturing of untreated and 5-Aza treated samples. Only genes with p adjusted value of <0.01 plotted. Plots were constructed independently for up- and downregulated genes. Number of up- and downregulated genes and maximum and minimum log2FC indicated above and below the respective plot.

After transition from yeast to hyphae (PA4) in the 5-Aza-treated arm (Figure 26, C-F) many expected hyphae-related genes were upregulated, like *UME6*, *GCV2*, *ECE1*, *HGT12*, *HWP1*, and *RBT1*. The most upregulated gene was *SOD5* (a superoxide dismutase, induced during hyphal growth; +6.9). The differentially top downregulated genes involved genes of drug response that previously had been upregulated in the treated yeast culture, reflecting the response to the 10-fold lower 5-Aza concentration. Other downregulated genes were morphology related, like *RBR1* (Supplementary Table 7). Interestingly, *RBR1* is needed for hyphal growth in acidic pH, a further indicator for hyphal growth in the 5-Aza treated yeast preculture.

Most strikingly, amongst the top upregulated genes of the treated yeast subculture (PA5, no hyphal induction), we also found typical hyphal growth-related genes, like *ECE1*, *RBT1*, and *HGT12*, and some other genes, which also were upregulated in the hyphal culture. Further, many ribosomal genes were downregulated, as well as also some morphology related genes like *RBT5* or *C2_08260W*, which are regulated by well-known TFs like Rim101 or Efg1, respectively, which promote hyphal growth (Supplementary Table 8).

In the untreated part of our experiment similar genes were upregulated for the transition from yeast preculture to hyphal culture (PA6), like in the treated part (Figure 27, C-F), amongst

those the classical hyphae promoting genes *RBT1*, *ECE1*, *UME6*, *HWP1*, and others. Downregulation in this context also involved quite some of the genes downregulated in the treated part, for example heatshock proteins, but in general genes with very diverse functions (Supplementary Table 9).

In the untreated yeast subculture (PA7) none of the classical hyphae promoting genes were present amongst the top upregulated genes. Downregulated genes involved again very diverse genes, similar to the corresponding untreated hyphal culture, involving some heatshock proteins, but also other, mostly metabolism related genes (Supplementary Table 10).

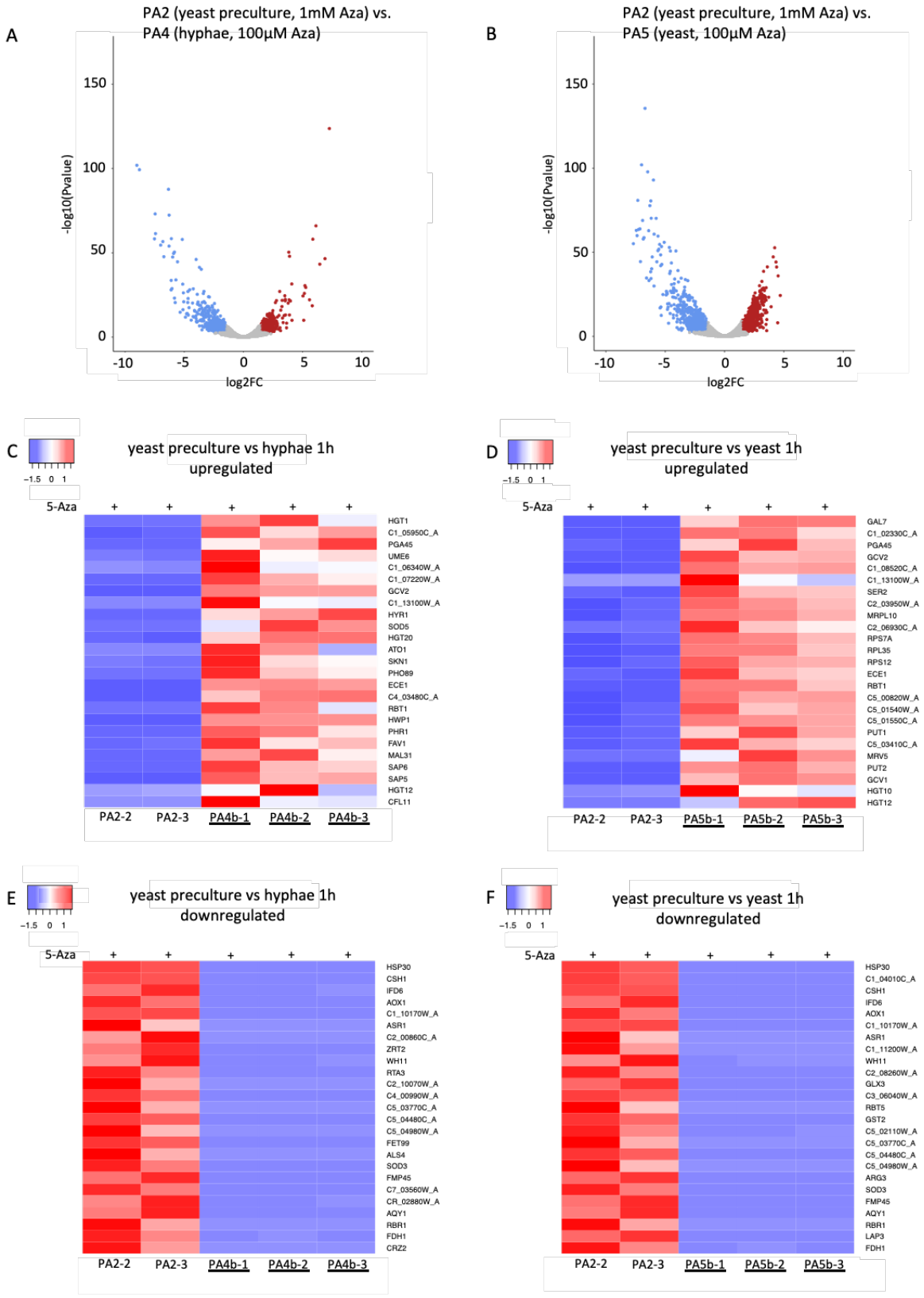

Figure 26: Differential expression analysis of 5-Aza treated *C. albicans* yeast preculture and their subcultures. (A)+(B) Genes plotted as volcano plot showing significantly up- and downregulated genes. Significant genes are coloured, with a threshold of 1.5 and -1.5 for up- (red) and downregulated (blue) genes, respectively and p adjusted value of <0.01. (C)+(D) Heatmap of top 25 significantly upregulated genes (p adjusted value <0.01, log2FC >1.5). (E)+(F) Heatmap of top 25 significantly downregulated genes (p adjusted value <0.01, log2FC <-1.5).

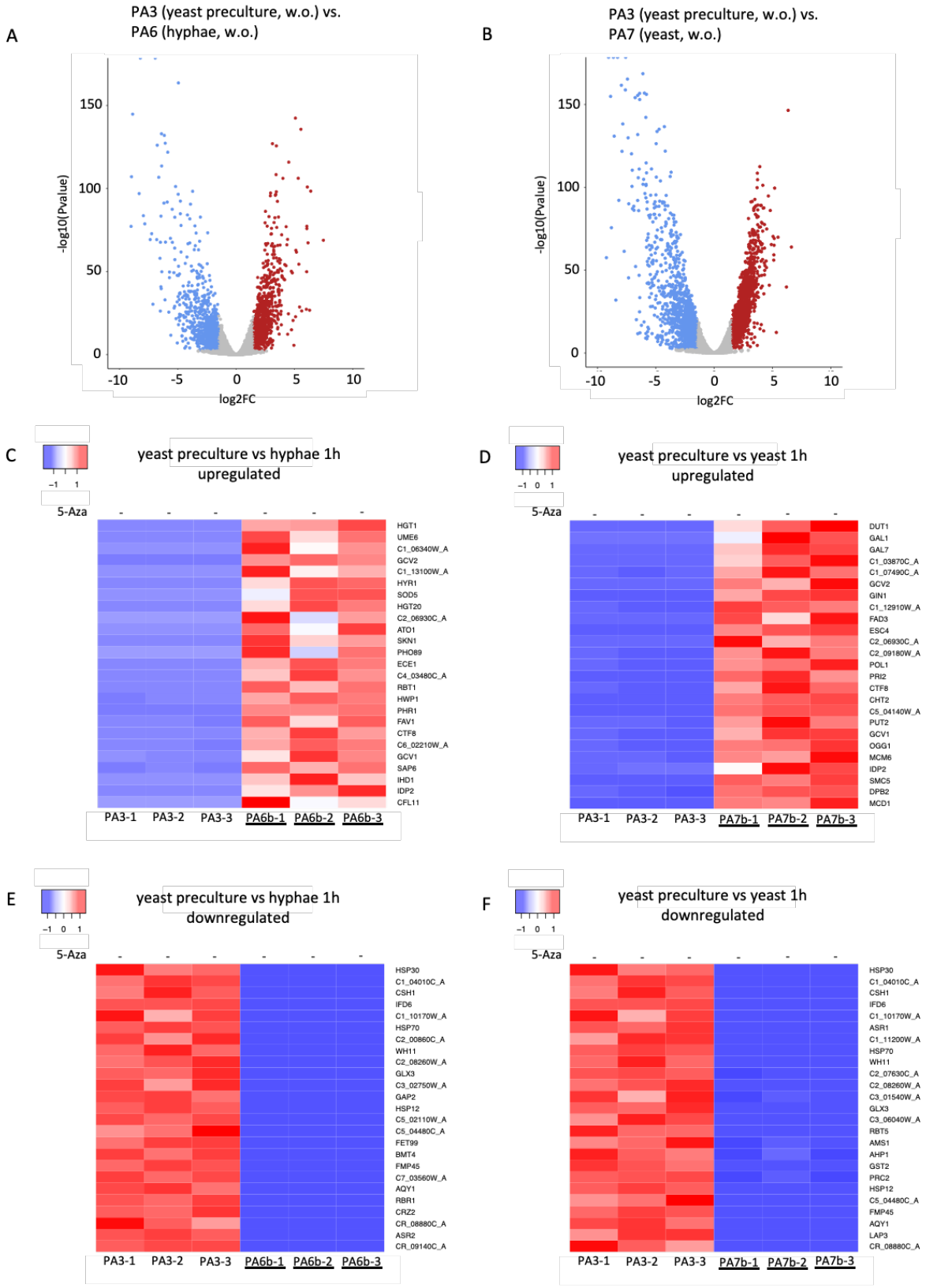

Figure 27: Differential expression analysis of untreated *C. albicans* yeast preculture and their subcultures. (A)+(B) Genes plotted as volcano plot showing significantly up- and downregulated genes. Significant genes are coloured, with a threshold of 1.5 and -1.5 for up- (red) and downregulated (blue) genes, respectively and p adjusted value of <0.01. (C)+(D) Heatmap of top 25 significantly upregulated genes (p adjusted value <0.01, log2FC >1.5). (E)+(F) Heatmap of top 25 significantly downregulated genes (p adjusted value <0.01, log2FC <-1.5).

3.2.2.3 Differential gene expression in untreated vs. 5-Aza-treated cells, within cultures of the same morphological stimulus

When comparing the 1h yeast cultures originating from 5-Aza-treated and untreated precultures directly (PA5 and PA7, Figure 28, B, D, and F) 40 genes were differentially upregulated (p adjusted <0.01, log2FC >1.5) and 9 genes differentially downregulated (log2FC<1.5) (Supplementary Table 12). Amongst the upregulated genes *ICL1* (isocitratelyase 1, which is usually increased in fungal virulence) was the most upregulated, like in all other treated samples. Again, some genes were upregulated, indicating a possible direct reaction to 5-Aza, like *AHP1* (alkyl hydroperoxide reductase) which belongs to the core stress response, or *OYE32* (coding for a NADP(H) oxidoreductase family protein), as well as further dehydrogenases. Two genes, *CIP1* and *HGT12*, strongly indicating hyphal growth, were differentially upregulated as well. Amongst the genes differentially downregulated we found two mitochondrial ribosomal proteins (*C1_12280C* and *IMG2*), and mainly proteins of unknown function (Supplementary Table 12).

In contrast, in the hyphae-induced cultures (PA4 and PA6, Figure 28, A, C, and E), only 3 genes were found differentially regulated in 5-Aza treated cultures. These were, *C2_01630W* (2-hydroxyacid dehydrogenase domain containing protein), *TNA1* (a putative nicotinic acid transporter) and again *ICL1*. No genes were found as differentially downregulated (Supplementary Table 11).

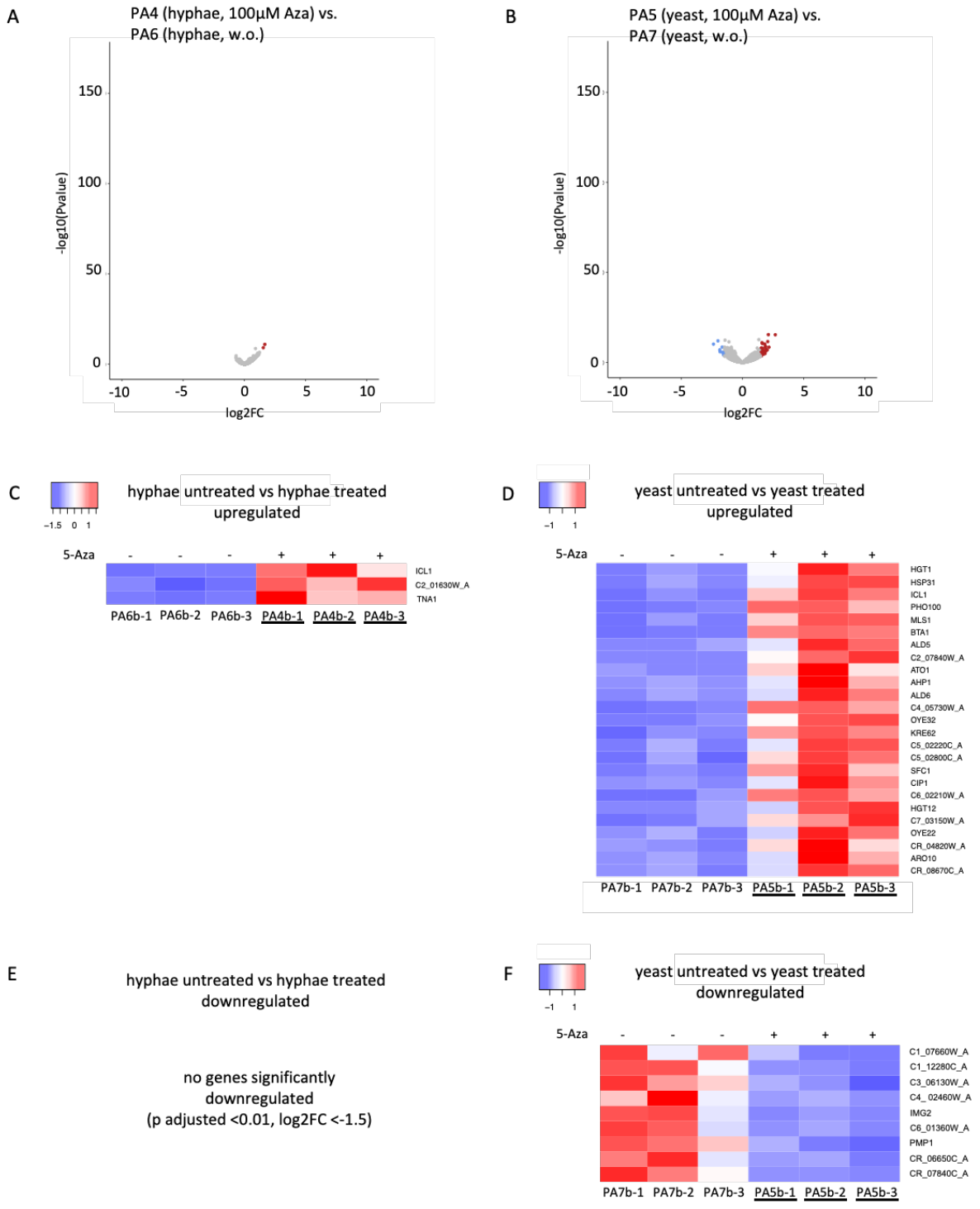

Figure 28: Differential expression analysis of 5-Aza treated *C. albicans* yeast and hyphal cultures and their corresponding untreated cultures. (A)+(B) Genes plotted as volcano plot showing significantly up- and downregulated genes. Significant genes are coloured, with a threshold of 1.5 and -1.5 for up- (red) and downregulated (blue) genes, respectively and p adjusted value of <0.01. (C)+(D) Heatmap of top 25 significantly upregulated genes (p adjusted value <0.01, log2FC >1.5). (E)+(F) Heatmap of top 25 significantly downregulated genes (p adjusted value <0.01, log2FC <-1.5).

3.2.3 Gene ontology analysis of 5-Aza-treated and untreated parallel cultures

To obtain a clear assignment of the differentially regulated pathways in the presence of 5-Azacytidine and without treatment to specific components and regulatory networks, GO analysis was performed. For this purpose, we compared treated and untreated yeast precultures (PA2 and PA3), treated and untreated 1h hyphal cultures (PA4 and PA6), and treated and untreated 1h yeast cultures (PA5 and PA7). The three sub-ontologies - biological process, molecular function, and cellular component - were analysed separately. We implied all significant genes (p adjusted <0.01) with a log2FC >1.1 and <-1.1 in this analysis.

Concerning differentially upregulated genes in the 5-Aza treated yeast precultures (PA2), in all three categories, noticeably, top GOs mainly corresponded to “DNA repair”, “DNA replication”, “chromosomal components”, and “mitosis” (Figure 29). Other interesting GOs not listed in the plots, but also significantly upregulated (overrepresented p value <0.01, Supplementary Table 13 - 15) referred to morphology, e.g., “filamentous growth” (10% of genes), “morphogenesis checkpoint” (75%), and “conidiophore development” (60%). Downregulated GOs also involved morphologically relevant terms, like “yeast form cell wall” and “hyphal cell wall”, but only 20% of the related hyphal cell wall genes were actually differentially downregulated in the treated yeast culture.

GO enrichment analysis (Supplementary Figure 13) revealed that the main triggered upregulated biological processes in the 5-Aza treated yeast precultures were “cell cycle process”, “response to stimulus”, “chromosome organization”, and “reproductive process”. As molecular functions “catalytic activity” and “small molecule binding processes” were enriched. As cellular components categories the “DNA polymerase complex” played the major role, but also many processes referred to the cellular anatomical entity.

In summary, treatment with 1mM 5-Aza in the yeast precultures predominantly activated processes involved in DNA repair, cell cycle, and various catalytic activities, but also indeed significantly affected some morphology related processes, or GO-entities.

Among differentially regulated genes in the 5-Aza treated 1h hyphal subcultures (PA4) we only found a few single genes upregulated, belonging to different metabolic processes, transmembrane transporters, and enzymes belonging to redox processes, as well as the “peroxisome” as a cellular component, and again isocitrate lyase activity (Figure 30 and Supplementary Table 16 - 18). No genes were significantly downregulated in this context. In

the GO enrichment analysis, the “peroxisome” was the only component found as enriched (Supplementary Figure 16), corresponding to our observation in the GO analysis that different metabolic processes were upregulated: oxidative catabolic processes of many compounds take place in the peroxisome. No enriched GOs could be found for significantly downregulated genes.

A similar result was obtained for the 5-Aza treated 1h yeast subculture (PA5) (Figure 31): “oxidation-reduction processes” were found to be upregulated, the “glyoxylate cycle” (to which also *ICL1* belongs to), many related processes and enzymes, as well as the “peroxisome”. Very interesting was the observation of our cellular component analysis, which showed quite some morphology related GOs differentially upregulated, namely “yeast form cell wall”, “hyphal cell wall”, “fungal-type cell wall”, and “cell surface” (Supplementary Table 19 - 21). Downregulation was found for single genes of the mitochondrion, “Golgi apparatus”, “nuclear telomere complex”, “ribonucleoprotein complex”, and several metabolism-related GO terms. Another intriguing observation was the downregulation of “mitochondrial tRNA methylation”.

The associated GO enrichment analysis clearly confirmed these observations (Supplementary Figure 15). As biological processes we saw enrichment of “catabolic processes” and “detoxification of hydrogen peroxide, monocarboxylic acid and cellular aldehyde metabolic processes”, and “carbon utilization”. The main molecular function observed was “peroxisome activity”. Enriched cellular components were “fungal-type cell wall”, “cellular surface”, “peroxisomal matrix”, and “extracellular region”. As well as for the hyphal samples, there were no enriched GOs for downregulated differentially expressed genes.

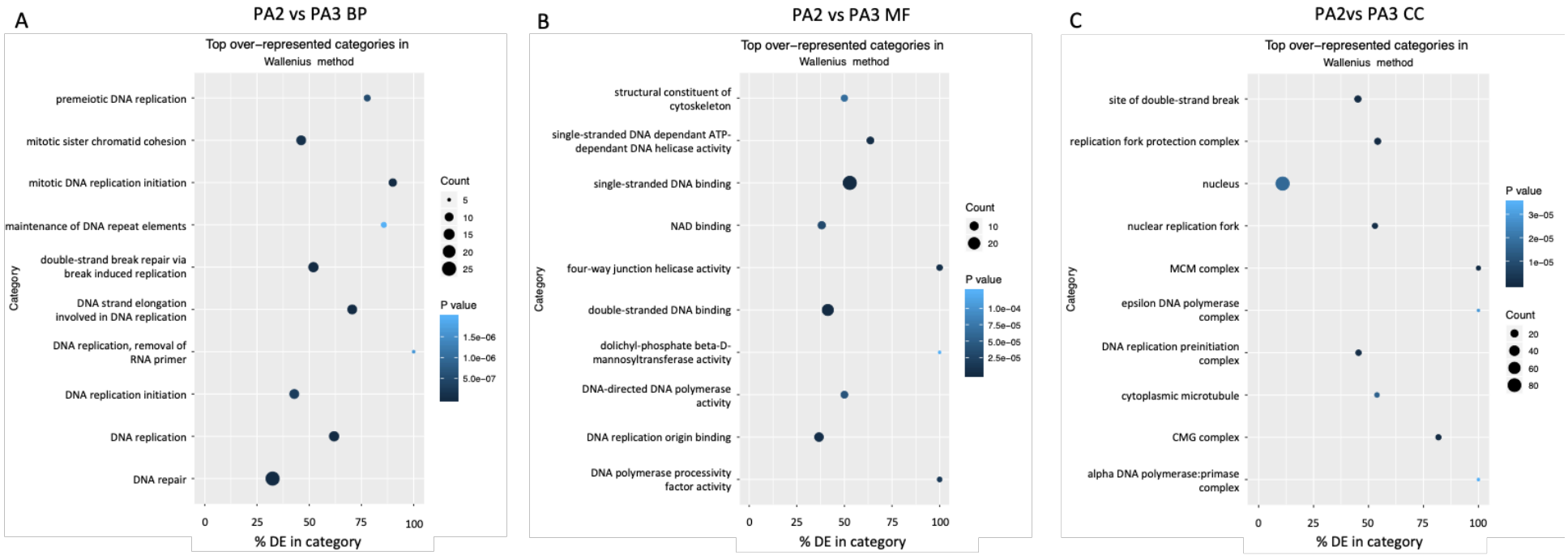

Figure 29: GO analysis with top GO terms of upregulated differentially expressed genes. GO terms of 5-Aza treated [1mM] (PA2) versus untreated (PA3) yeast precultures were analysed. (A) Biological process (BP). (B) Molecular function (MF). (C) Cellular component (CC). Analysis was conducted with goseq with the Wallenius method. All GOs listed with p adjusted value <0.01 and log2FC >1.1.

A

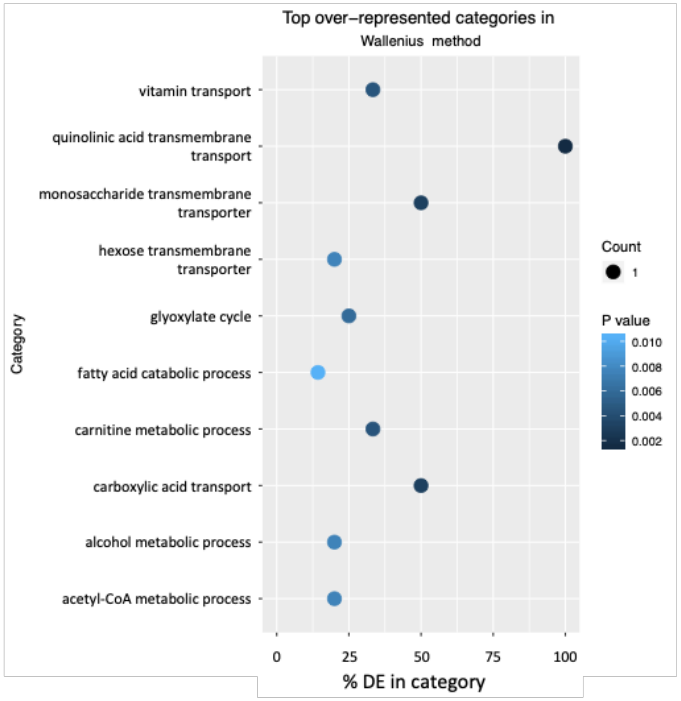

B

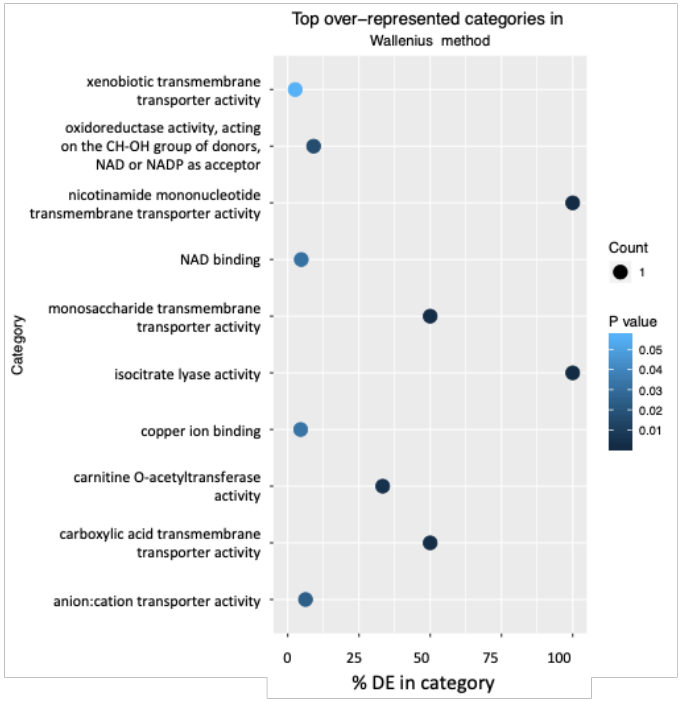

C

PA4 vs PA6 CC

Top over-represented categories

Category	% in category	Over represented p value
peroxisome	3.7	0.0028
peroxisomal matrix	9.1	0.017

Figure 30: GO analysis with top GO terms of upregulated differentially expressed genes. GO analysis of 5-Aza treated [100 µM] (PA4) versus untreated (PA6) hyphal culture. (A) Biological process (BP). (B) Molecular function (MF). (C) Cellular component (CC). Analysis was conducted with goseq with the Wallenius method. All GOs listed with p adjusted value <0.01 and log2FC >1.1. (D) GO enrichment analysis of DE genes (p adjusted value <0.01 and log2FC >1.1). Analysis was conducted with GOEnrichment (p value <0.05).

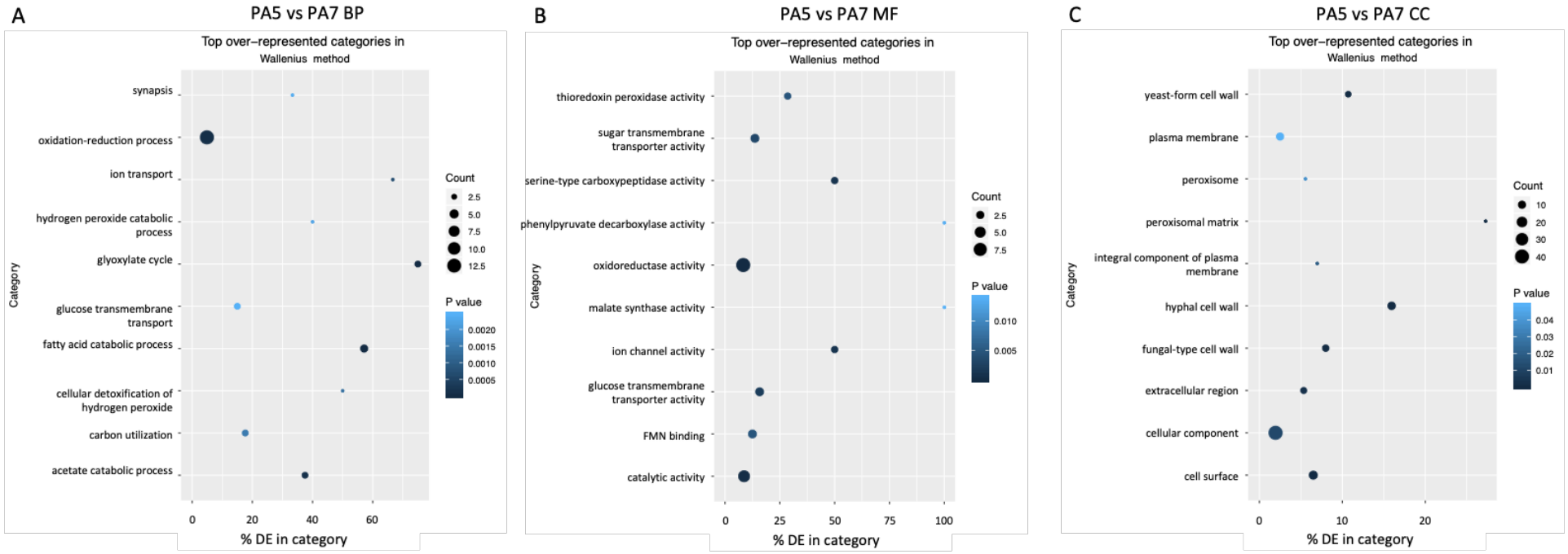

Figure 31: GO analysis with top GO terms of upregulated differentially expressed genes. GO analysis of 5-Aza treated [100 µM] (PA5) versus untreated (PA7) yeast culture. (A) Biological process (BP). (B) Molecular function (MF). (C) Cellular component (CC). Analysis was conducted with goseq with the Wallenius method. All GOs listed with p adjusted value <0.01 and log2FC >1.1.

3.2.4 5-Aza affects differential regulation of morphology-specific genes

To further investigate our hypothesis, that inhibition of DNA demethylation would lead to enhanced transcription of genes promoting hyphal growth, we specifically looked at their regulation under 5-Aza treatment. One part of these genes is represented by the "core filamentation response network" (Martin *et al.*, 2013; Romo *et al.*, 2019), which includes *ALS3*, *ECE1*, *HGT2*, *HWP1*, *IHD1*, *RBT1*, *DCK1* and *orf19.2457*. Further, we added genes coding for hyphae relevant transcription factors (*UME6*, *FLO8*, and *CZF1*), genes relevant in our specific conditions with different temperature and pH to induce yeast or hyphal development (*RIM101* and *HSP90*), genes encoding hyphal cell-wall proteins (*RBT1* and *HWP1*), and two yeast specific genes (*RHD3* and *YWP1,* Table 14)

Table 14: Selected genes relevant for development of hyphal and yeast morphology.

Gene name	ID*	Position	Function
Expected as upregulated under hyphae inducing conditions			
HGT2	C1_02110C	434412 – 436049	Putative MFS glucose transporter, Spider biofilm induced
orf19.2457	C1_05920W	1236305 – 1238380	Protein of unknown function, Spider biofilm induced
UME6	C1_06280C	1314438 – 1316969	TF, controls transition to FG
CPH1	C1_07370C	1590522 – 1592492	TF, regulates galactose metabolism genes, filamentation on solid media, pheromone-stimulated biofilms, rat catheter biofilm repressed
RIM101	C1_14340C	3158465 – 3160450	TF, required for alkaline-induced HG
DCK1	C2_04050C	847533 – 853277	Regulated by Nrg1, required for embedded filamentous growth, (not upregulated in liquid cultures), Spider biofilm induced
TEC1	C3_04530C	949762 – 951993	TF, hyphal gene regulation, required for biofilm formation on distinct media
ECE1	C4_03470C	726514 – 727329	Candidalysin, hyphae-specific protein, farnesol-induced, Spider biofilm induced
RBT1	C4_03520C	745166 – 747331	Cell wall protein, serum, hyphal and alkaline induced
HWP1	C4_03570W	762835 – 764739	Hyphal cell wall protein, Spider biofilm induced
CZF1	C4_06820C	1518979 – 1520136	TF, HG regulator, Spider biofilm induced
IHD1	C6_03850C	838281 – 839459	GPI-anchored protein, hyphae-induced

FLO8	C6_04350C	959560 – 961938	TF, required for hyphal formation, regulates hyphal gene expression
HSP90	C7_02030W	439525 – 441648	Essential chaperone, temperature-induced morphogenesis, localizes to surface of hypha – not yeast cells
CYR1	C7_03070C	662700 – 667772	Adenylyl cyclase, involved in regulation of filamentation
ALS3	CR_07070C	1532277 – 1535744	Cell wall adhesin, endothelial invasion, induced in Spider biofilm
EFG1	CR_07890W	1723489 – 1725146	TF, hyphal growth, cell-wall gene regulation
Expected as downregulated under hyphae inducing conditions			
TUP1	C1_00060W	12163 – 13701	Represses FG
RPG1A	C1_12770W	2782398 – 2785190	Putative translation initiation factor, Spider biofilm repressed and upon phagocytosis
YWP1	C2_08590W	1746839 – 1748440	Yeast wall protein, Spider biofilm repressed
SSN6	C3_07020W	1607932 – 1611174	HG regulator, Repressed during HG (HG regulator)
RHD3	C4_04050C	867681 – 868295	Yeast-associated cell wall protein, Spider biofilm repressed
RBF1	C6_02840C	586391 – 587995	TF, mutation leads to accelerated induction of hyphal growth
NRG1	C7_04230W	918812 – 919744	TF, regulates hyphal gene induction genes, Spider biofilm repressed
RFG1	CR_02640W	600287 – 602089	Transcriptional repressor of filamentous growth and hyphal genes

*Last letter of ID corresponds to DNA strand (W= Watson strand = +strand; C= Crick strand = -strand). Information on genes extracted from CGD (candidagenome.org).

Based on this list, analysis showed a significant upregulation of *TEC1* (log2FC +0.66), *HWP1* (+0.82), *CPH1* (+1.11) and *IHD1* (+2.47) in the 5-Aza treated yeast precultures (p adjusted value <0.01) compared to the untreated yeast precultures. The yeast cell wall protein gene *RHD3* (-1.45) was significantly downregulated in this condition, as well as *DCK1* (-0.83) (Figure 32, A). *DCK1* is a hyphae specific gene, but only becomes relevant in embedded filamentous growth but not in liquid cultures.

In the subcultures of the untreated experimental arm (Figure 32, D and E), many of the selected genes were significantly regulated. Amongst those of the hyphal culture there were a few hyphae promoting genes, which were slightly downregulated (<-0.8, but also the hyphal

TF *EFG1* (-1.84). Further, as expected, many hyphal genes were strongly upregulated, like for example *UME6* (+5.17), *ALS3* (+4.35), *RBT1* (+5.32), *IHD1* (+6.6), *ECE1* (+7.78), and *HWP1* (+5.08). Also, in the yeast subcultures many of the investigated genes were differentially regulated, interestingly including the downregulation of the yeast wall protein gene *YWP1* (-5.27). Typical hyphae promoting genes in general were not that much upregulated like in the hyphae cultures and showed a much lower log2FC, but the hyphal cell wall protein gene *RBT1* was upregulated by +2.91 and the TF *UME6* by +3.29. Nevertheless, some hyphae promoting genes were downregulated, like *RIM101* (-0.64) and *EFG1* (-1.79). *RBF1* (+0.64) as yeast specific TF was upregulated, as well as *RPG1A* (+2.49), which is also found in yeast cells.

In the subcultures of the 5-Aza treated experimental arm (Figure 32, B and C), fewer genes were differentially regulated compared to the untreated arm. Nevertheless, transcription of some hyphae promoting genes was strongly increased in the hyphae cultures, e.g., *UME6* (+3.56), *ALS3* (+3.27), or *ECE1* (+7.26). Further, as expected, transcription of *NRG1* (a suppressor of hyphal development) was downregulated (-2.48) as well as the yeast wall protein gene *YWP1* (-3.60). Strikingly, in the yeast subcultures the yeast specific gene *RPG1A* was not that much upregulated and the hyphal gene repressor NRG1 was more downregulated (-1.45) than in the untreated arm. Further, typical hyphal genes were much stronger upregulated: *ECE1* (+3.43) and *RBT1* (+4.10), even though upregulation did not have the same extent, like in the hyphae culture.

It is important to be aware at this point, that the two compared culture conditions, represented cultures in different growth phases and like this a contra intuitive regulation of distinct morphology promoting genes could be possible. Even more important is the analysis of samples that are in the same growth phase.

In the 5-Aza treated arm only a few hyphae relevant genes in the hyphal cultures were upregulated compared to the yeast cultures (Figure 32, F). In contrast, in the untreated experimental part much more hyphae promoting genes were significantly upregulated and also to a greater extent (Figure 32, G). The same referred to the downregulation of hyphae suppressive or yeast growth promoting genes, showing the deregulating effect of 5-Aza and a shift to more hyphae promoting genes.

Regarding same morphologies in treated and untreated condition, we only found one gene being differentially regulated in the treated hyphae cultures (Figure 32, H), which was the hyphal growth repressor Nrg1 with a log2FC of +0.91. Hence, no strong difference was observed between these two hyphal cultures concerning these specific genes. However, in the treated yeast cultures compared to untreated yeast cultures we saw a strong upregulation of four hyphae specific genes - *RBT1* (+2.58), *IHD1* (+3.94), *ECE1* (+3.71), and *HWP1* (+2.58) - indicating again a remarkable effect of 5-Aza on hyphae promoting genes in the yeast cultures (Figure 32, I).

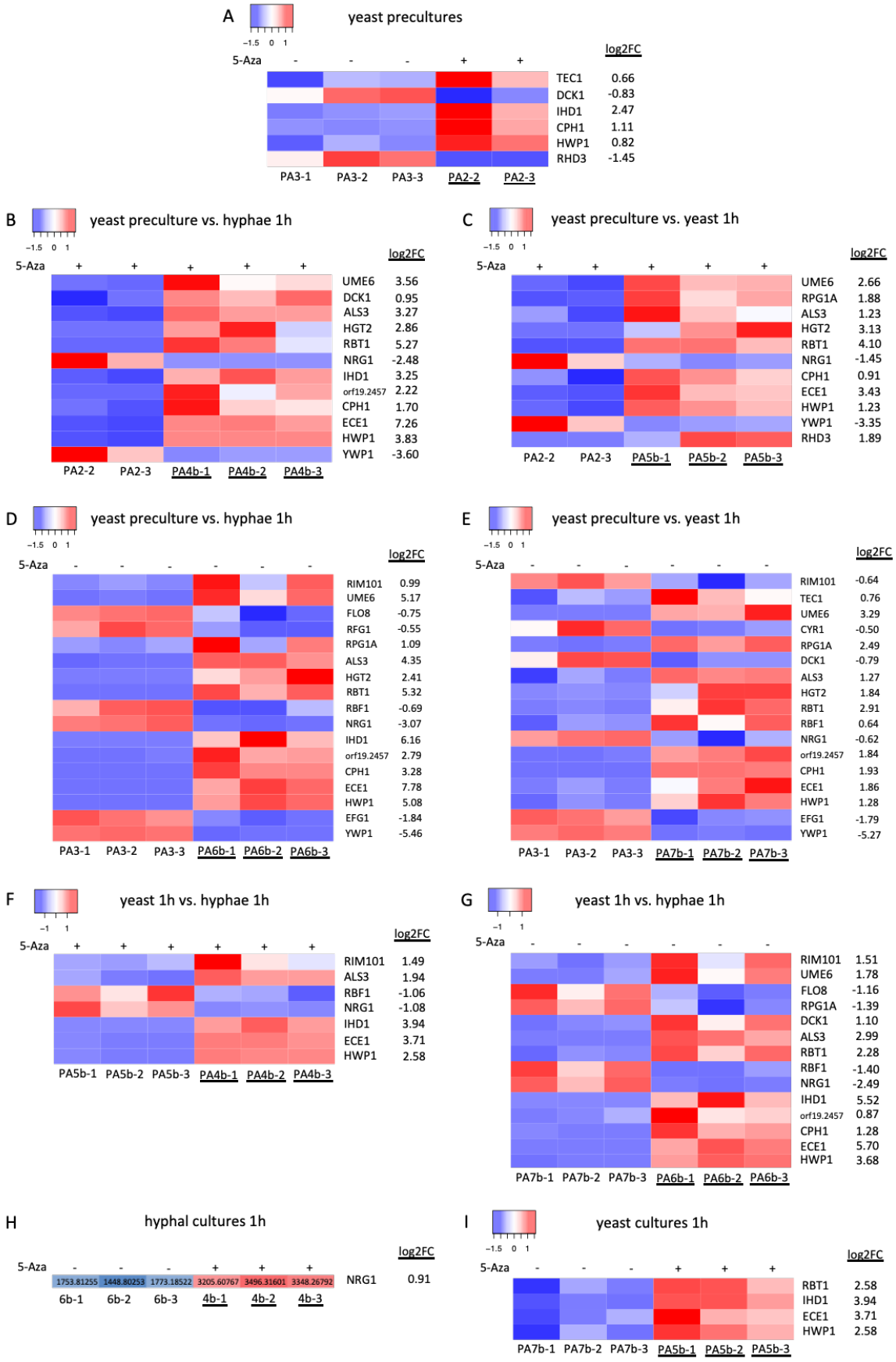

Figure 32: Selected morphologically relevant genes significantly regulated. All genes listed with p adjusted value <0.01. Average log2FC refers to underlined samples. Treated precultures contain 1mM 5-Aza, treated 1h cultures contain 100 µM 5-Aza.

3.3 5-Aza treatment does not affect morphology in *C. albicans* filamentous reference strains, but in an attenuated strain

For further morphological characterisation of 5-Aza-treated and untreated samples, different reference strains were plated onto Spider medium. This medium is known for its hyphal growth inducing effect, which is based on beef extract peptides, including peptides found in human blood (Daniels *et al.*, 2013). Spider medium is often used to, e.g., investigate filamentation capacity of gene deletion mutants (Noble *et al.*, 2010).

In this experimental setup, samples were incubated for 24 hours with or without 5-Aza [5mM] under yeast inducing conditions in liquid Lee's medium with low pH and temperature (pH 4.5, 30 °C). Hyphal growth was then monitored over several days in a spot assay on Spider medium under hyphae inducing conditions at 37°C. This experiment was conducted with different reference strains of *Candida albicans* - SC5314, DSM 11949, and DSM 11225. Further the oral isolate 529L (Rahman *et al.*, 2007), received from Prof. Julian Naglik (King's College, London), was included in our experiments.

In a first spot assay with strain SC5314 with 5-Aza [1mM], independently of the treatment, all spots of different cell densities developed hyphae at the same time and to the same extent during observation (Figure 33, A). A 5-fold higher concentration of 5mM 5-Aza did not result in a divergent growth pattern for three *C. albicans* reference strains (SC5314, DSM 11225, and DSM 11949) but for the filamentous growth-attenuated strain 529L, which showed hyphal development after 5-Aza treatment (Figure 33, B). Further, microscopic analysis confirmed that 5-Aza does not change the morphological appearance of *C. albicans* reference strains SC5314, DSM11225, and DSM 11949, but of strain 529L on solid Spider medium (Figure 33, C).

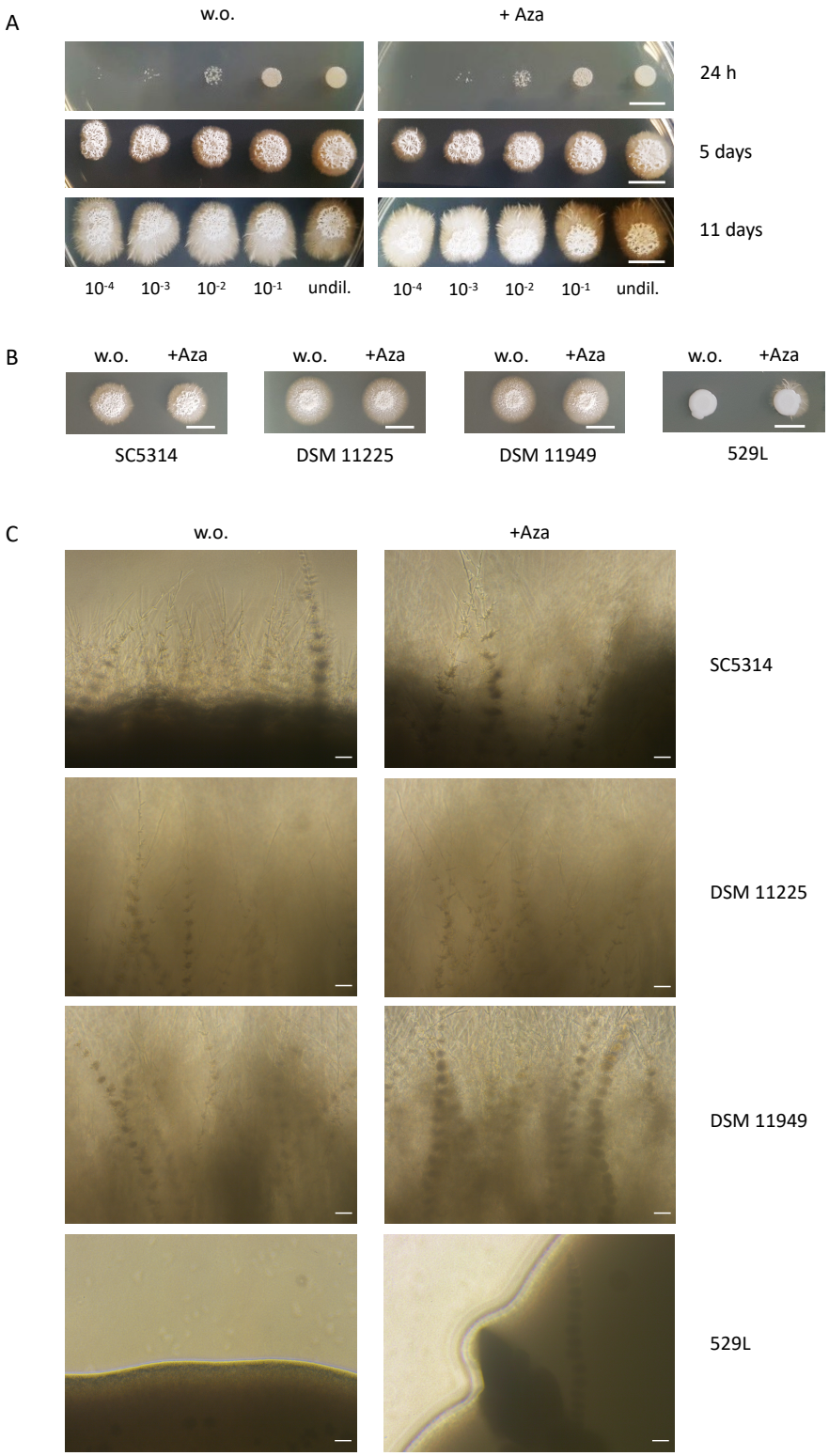

Figure 33: Hyphal formation of different *C. albicans* reference strains on Spider medium. Cell suspensions were spotted on Spider agar 24 h after incubation of cells without and with 5-Aza. Plates were incubated at 37°C to support hyphal growth. (A) SC5314 cell suspensions were treated with 1 mM 5-Aza. Spots show dilutions of 10^{-4} to 10^{-1} (left to right) of a McFarland 2.0 suspension (right). Scalebar 1 cm. (B) Cell suspensions (McFarland 2.0) of SC5314, DSM 11225, DSM 11949, and 529L were spotted 24 h after incubation of cells without and with 5-Aza [5mM]. Pictures were taken 7 days after incubation at 37°C. Scalebar 1 cm. (C) Microscopic analysis of SC5314, DSM 11225, DSM 11949, and 529L at 72 hours after spotting cell suspensions treated with 5 mM 5-Aza (exemplarily for the whole testing period, showing no difference between treated and untreated samples for the first three samples, but the attenuated strain 529L produced hyphae after 5-Aza treatment). Pictures show edge of a respective colony. Scalebar 50 µm.

3.4 Attenuated clinical isolates of *C. albicans*

3.4.1 5-Aza promotes hyphal growth in attenuated clinical *C. albicans* isolates

As morphological differences between 5-Aza treated and untreated samples could be observed for a known attenuated *C. albicans* reference strain, we tested whether the morphological outcome could be altered by 5-Aza treatment also of fresh clinical isolates. The isolates originated from a first screening for morphology on Spider medium. From 50 isolates two attenuated of each clinical specimen type were collected (respiratory, oral, urine, stool, invasive, and blood). Additionally, one blood isolate was chosen, which showed strong hyphal growth, like the reference strain SC5314. These two filamenting strains served as positive controls (2.2.11.1, Figure 12). The growth pattern was stably maintained in 86.5% of isolates after freeze and thaw cycles. Further, this screening revealed that 5-Aza treatment altered the phenotype of isolates that previously developed only small or no filaments at all, but did not affect the phenotype of those isolates already showing strong filamentous growth prior to treatment.

As in the previous experiment with *C. albicans* reference strains (section 3.3), clinical isolates were incubated for 24 hours with and without 5 mM 5-Aza and spotted onto Spider medium in three biologically independent replicates. After growth for 7 days under these hyphae-inducing conditions, a clear difference between treated and untreated samples was visible: untreated samples maintained their attenuated phenotype, whereas 5-Aza-treated samples developed already macroscopically visible filaments (Figure 34). This result was mostly consistent in all three replicates. Only one blood isolate (PEU3790) did not show filamentation after 5-Aza treatment at all. As expected, reference strain SC5314 and the filamenting blood isolate PEU3700 always showed the same strongly filamenting phenotype, irrespectively of the treatment.

After this 7 days timepoint, filamenting sections of the colonies were subcultured again on Spider medium in order to check if the filamenting phenotype of the previously attenuated isolates was maintained. This could also be an indication, that 5-Aza leads to an epigenetic regulation of the respective genes. The resulting colonies showed the same phenotype as before and fully filamenting clones could be isolated from 5-Aza treated samples. Only the attenuated blood isolate PEU3790 continuously did not show filamentation. Only in the third

experiment the 5-Aza treated spot showed few filaments, but clones with a stable phenotype could not be isolated by subculturing from these cultures.

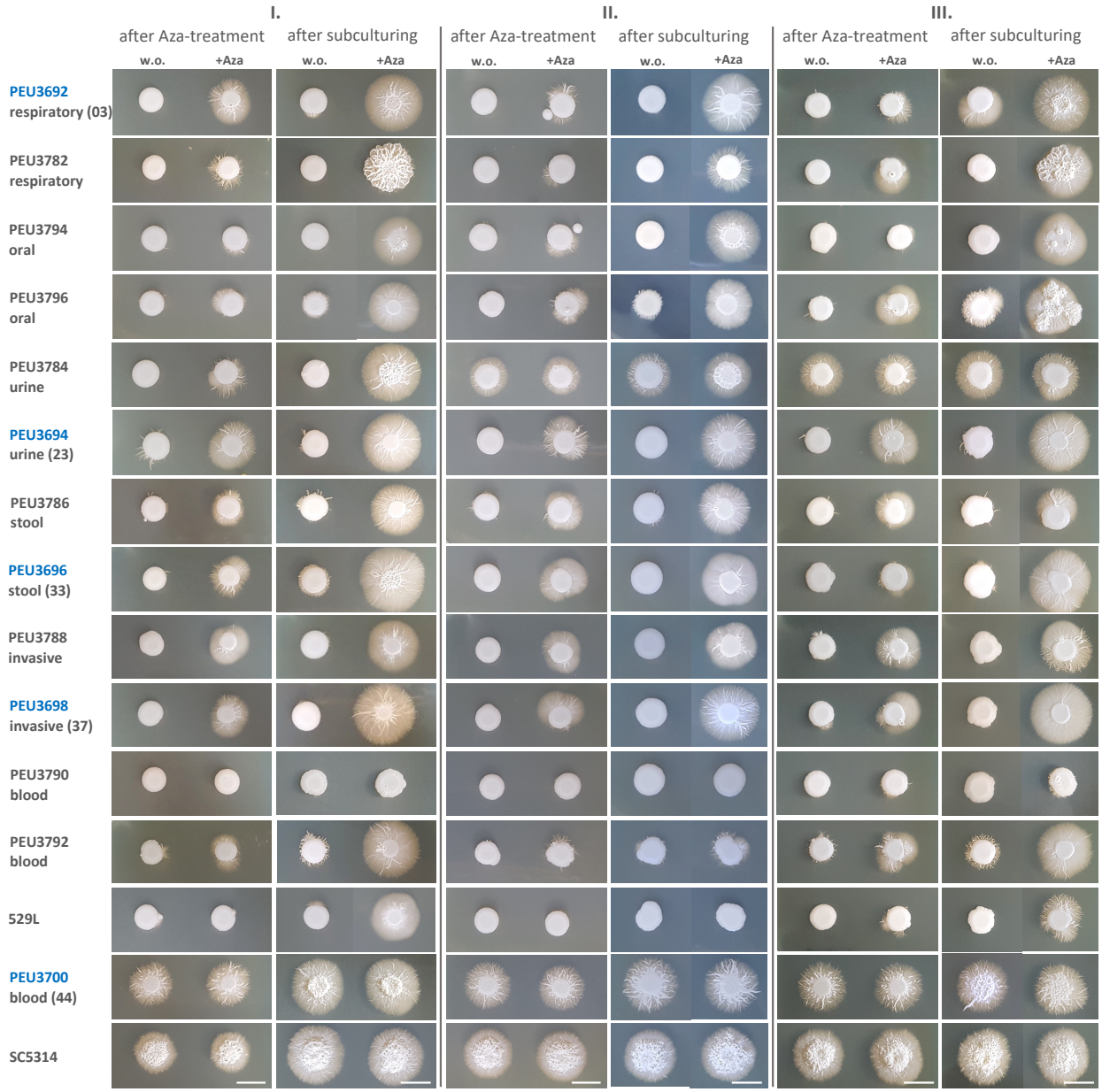

Figure 34: Spot assay of *C. albicans* clinical isolates after treatment with 5-Azacytidine. Clinical isolates originated from respiratory, oral, urine, stool, and blood samples. Three independent replicates of the experiment are shown. Each experiment included spotting of the 5-Aza treated (5mM) and untreated cell suspensions on Spider medium plates and a subculture of the colonies after 7 days on the same medium. The strongly filamenting blood isolate PEU 3700 and reference strain SC5314 were used as positive controls. Pictures were taken after 7 days of incubation at 37°C for hyphal growth induction. Scalebar is 1 cm. Isolates used for further experiments (03, 23, 33, 37, and 44) are indicated.

Microscopic analysis as well confirmed the difference between colonies of untreated and 5-Aza treated cells (Figure 35). In SC5314 during the second day of incubation, filamentous growth became visible on the edge of the colonies, and on the third day filaments could be found around the whole colony. In contrast, in untreated samples however filamentous growth mostly was not visible during the first days and became visible only rarely in a few spots of the colony after some days (Figure 35, PEU3698 - 7d). These filaments grew more slowely and often stopped growing after some days compared to a filamentous strain like SC5314.

Interestingly, colonies from both, untreated and treated cells showed zones of dense growth already in the early phase of incubation as dark spots underneath the colonies. In colonies from treated cells filamentation appeared to start from these spots. However, in most instances these zones did not produce visible filaments in untreated samples. On the other hand, in 5-Aza treated cells from attenuated strains filamentous growth was already visible around days 2-3. In the following days this growth then became dense, spreading around the whole colony, comparable to strain SC5314.

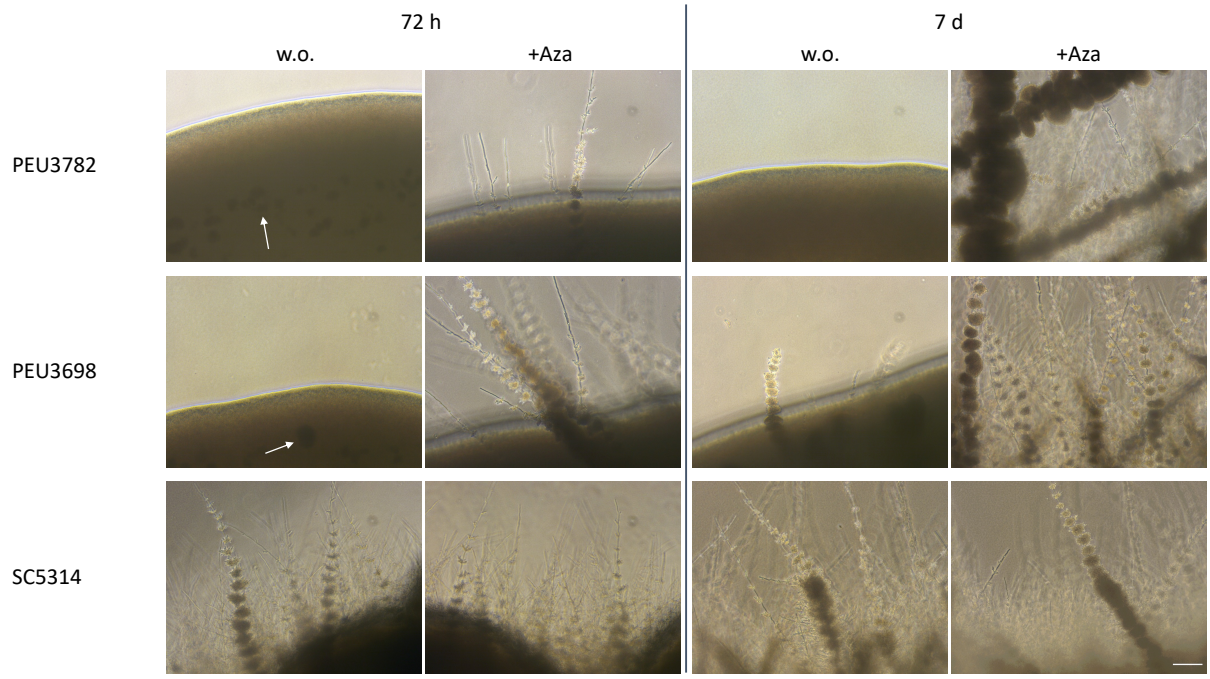

Figure 35: Microscopic analysis of 5-Aza treated attenuated clinical isolates. Pictures of PEU3782 and PEU3698 are representative for all attenuated samples that show filamentous growth after 5-Aza treatment. Scalebar 100 µm. Dark spots in colonies are marked with white arrows.

Next, the growth of colonies was quantified by measurement of the colony size seven days after 5-Aza treatment for each of the three replicates (Figure 34). The colony surface area of untreated samples ranged between 0.62 to 0.76 cm^2 in average. However, ten of twelve 5-Aza treated clinical isolates had a larger colony surface area than their untreated corresponding sample, ranging from 0.99 to 1.91 cm^2 in average. Only for one isolate (PEU3784) this effect of 5-Aza could not reproducibly be shown, as the second and third replicate also showed strong filamentation for the untreated sample. This isolate was the only one changing its morphology without 5-Aza-tretment during the whole experiment. Also, again no effect of 5-Aza was observed towards PEU3790. Both positive controls showed strongest filamentation in both, the untreated as well as in the treated sample. Significant differences between treated and untreated samples were observed for 7 of 12 clinical isolates. The overall significance indicating the dependence of filamentation on 5-Aza treatment in this setting was $p < 0.01$ (Figure 36).

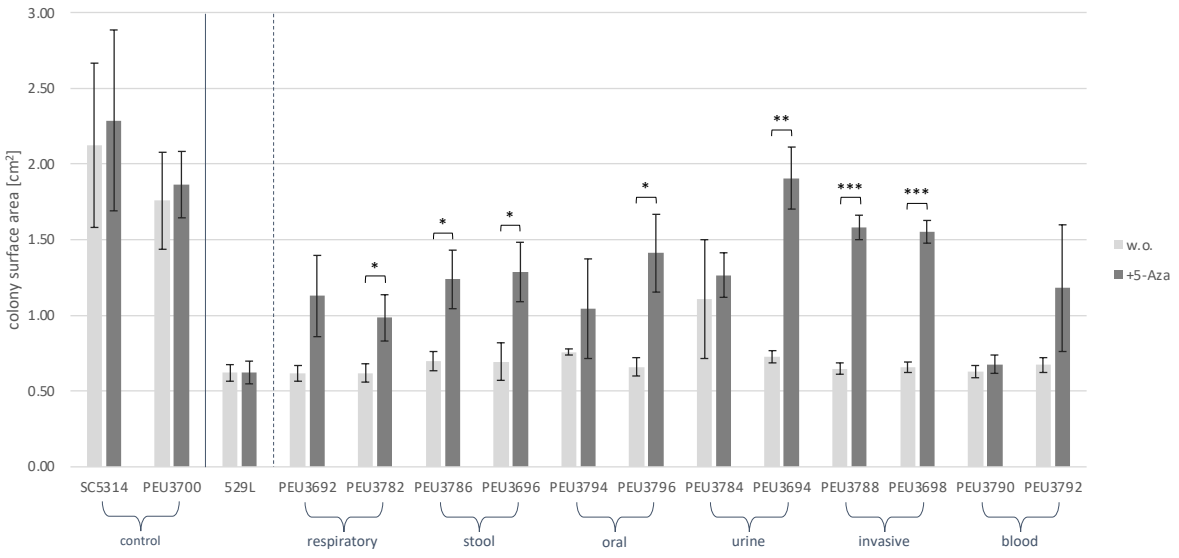

Figure 36: Colony surface area of untreated and 5-Aza treated attenuated clinical isolates. The colony surface area (seven days after 5-Aza treatment) was measured from different clinical attenuated isolates, the attenuated strain 529L, and two strongly filamenting positive controls (SC5314 and isolate PEU3790). Results shown are the mean of 3 biological replicates. Degree of significance between untreated and treated sample is shown by asterisks for each isolate. Combined p value < 0.01 (harmonic mean, 0.0024) for all clinical isolates.

3.4.1.1 Cell damage capacity of untreated and 5-Aza treated clinical isolates of *C. albicans*

Filamentous growth generally coincides with increased host cell damage. Whether this was the case for clones raised from 5-Aza treated colonies was tested on four of the attenuated clinical isolates and their corresponding 5-Aza treated filamenting samples. These were sent to the laboratories of our collaboration partners Prof. Julian Naglik, Dr. Jonathan Richardson, and Antzela Zavou (King's College, London), where the following experiments were conducted. The samples originated from four clinical isolates of different clinical specimen types (respiratory, urine, stool, and invasive) and three untreated morphologically attenuated plus three individually 5-Aza treated filamenting samples of isolate 529L, originating from three different liquid cultures (C1, C2, and C3; Figure 37). Reference strains SC5314 and BWP17 (untreated) served as positive controls in the experiment.

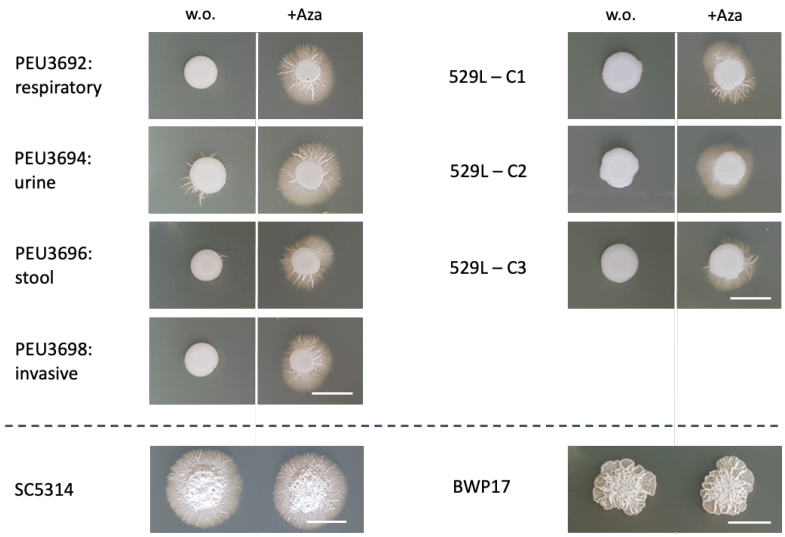

Figure 37: *C. albicans* clinical isolates used for cell invasion assay. The clinical isolates originated from different clinical specimen types. Pictures show spot assay on Spider medium after treatment with 5-Aza [5 mM] and growth for seven days in comparison to reference strain SC5314 and BWP17. 529L is represented by three independent cultures (C1, C2, and C3). Scalebar 1 cm.

Reaction of human host cells to confrontation with selected clinical isolates was measured indirectly by several parameters that are typical indicators: lactate dehydrogenase (LDH), a cytosolic enzyme that is released in case of cellular damage; G-CSF, a peptide hormone stimulating the growth of granulocytes, as well as stimulating the activity of existing granulocytes; GM-CSF, a glycoprotein stimulating the differentiation of precursor cells into

granulocytes and macrophages; interleukin 6 (IL-6), a pleiotropic cytokine and a marker for cell damage; and IL-1 alpha and IL-1 beta, two proinflammatory cytokines.

In detail, the LDH concentration was on the level of the negative control ("vehicle") for all 529L isolates tested, when testing a low MOI of 0.01, independently of their treatment with 5-Aza (Figure 38). At an MOI of 0.1 the six 529L samples were slightly above the concentration of the negative control, but still very low. In fresh clinical isolates, comparable low LDH concentration at an MOI of 0.01 was measured for all but the 5-Aza treated urine sample, which showed a nearly 2-fold higher LDH concentration. At a higher fungal inoculum (MOI 0.1) three of four clinical isolates (urine (PEU3694), stool (PEU3696), and invasive (PEU3698)) showed an increase in LDH concentration in the untreated and treated samples. The respiratory clinical sample (PEU3692) resulted in a low LDH concentration only, even below the concentration of the 529L samples. Two samples presented a remarkable increase of LDH in the cell culture, the 5-Aza treated sample of the urine isolate PEU3694 and the 5-Aza treated sample of the invasive isolate PEU3698. They showed a significant increase with a 2-fold LDH concentration compared to their corresponding untreated sample.

The concentration of G-CSF was slightly increased in all 529L samples and the respiratory isolate PEU3692. The three clinical isolates showed a higher concentration here as well, but not to a large degree. Again, only the 5-Aza treated urine sample PEU3694 led to a stronger increase of G-CSF.

GM-CSF was only slightly increased in the 5-Aza treated sample of the urine isolate PEU3694. All other samples did not show a considerable increase compared to the negative control.

A remarkably higher concentration of IL-6 was observed for the 5-Aza treated sample of isolate PEU3694. Only a negligible concentration of the cytokine could be determined for the two samples of the respiratory isolate PEU3692. Further, all samples of 529L and the rest of the clinical isolates showed a similarly lower level of IL-6.

IL-1 alpha and IL-1 beta, were generally low in all samples, only for the 5-Aza treated samples of the urine isolate PEU3694 and the invasive isolate PEU3698 a visible increase of IL-1 alpha and a slight increase of IL-1 beta was observed.

In the case of strain 529L, no significant increase for any of these parameters could be detected, neither in untreated nor in 5-Aza treated clones.

Recapitulated, even though 5-Aza treatment led to strong filamentation in the beforehand attenuated isolates, it only provided two of our four clinical isolates with stronger invasion

capabilities. We could not observe any increase in virulence markers for 529L after 5-Aza treatment.

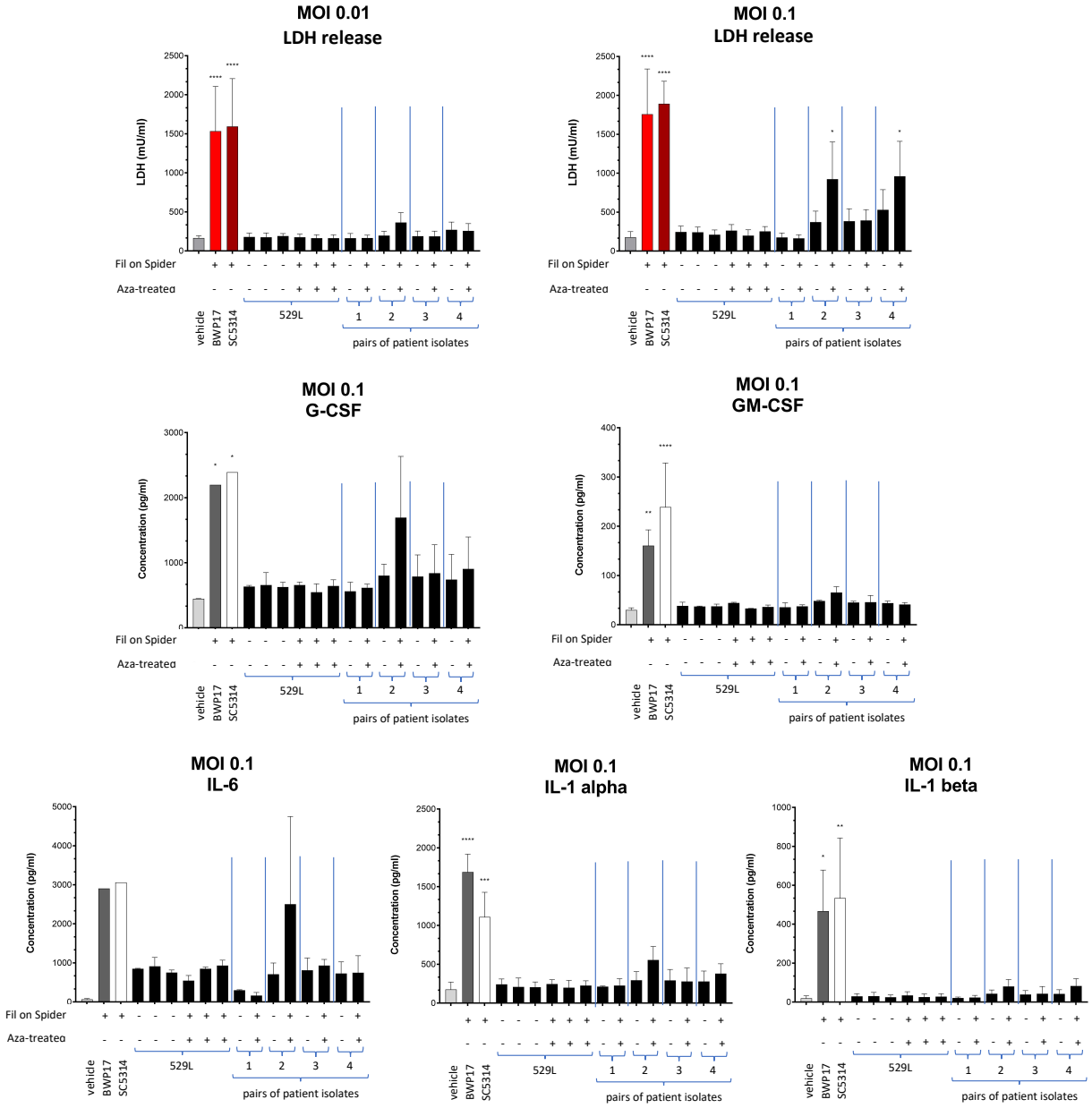

Figure 38: Cell damage assay of untreated and 5-Aza treated clinical isolates. LDH concentration was measured in three replicates; G-CSF, GM-CSF, IL-6, IL-1 alpha, and IL-1 beta were measured in 2 replicates. 1 = PEU3692 (respiratory), 2 = PEU3694 (urine), 3 = PEU2696 (stool), 4 = PEU3698 (invasive). The reference strains SC5314 and BWP17 served as positive controls. Experiment conducted and data provided by Dr. Jonathan Richardson, Prof. Julian Naglik, and Antzela Zavou (King's College, London).

3.4.2 Screening of *C. albicans* clinical isolates for filamentation

The freshly collected clinical isolates from our routine diagnostic unit (*i.e.*, respiratory, stool, oral, urine, invasive, and blood) were screened for their morphology on Spider medium, with the primary intention to select strongly attenuated samples for our 5-Aza screening (section 3.4.1). Further, we aimed to analyse the interdependency of sample origin and morphology, as we assumed the origin could play a role in the long-term morphological characteristics of an isolate, maybe even on the level of genetic imprinting.

We aimed at collecting 30 fresh clinical isolates for each group of origin. Only the number of blood isolates had to be augmented with frozen samples from our collection, as blood infections with *C. albicans* did not occur that frequently during the time of collection.

The spot assay on Spider medium revealed that from each origin we could isolate strongly filamenting as well as completely attenuated samples, which did not produce any hyphae at all in a hyphal growth supporting environment (Spider medium, 37°C for 7 days) (Figure 39).

The isolates were grouped into three categories depending on the degree of filamentation on Spider medium: attenuated (blue), intermediate (grey), and strongly filamenting (orange). Colonies were categorised as ‘attenuated’ with a smooth colony surface and no or countable short filaments around the colony, ‘intermediate’ with multiple but short filaments growing at the side of the colony and not covering all sides completely, and ‘strong’ with long filaments all around the colony.

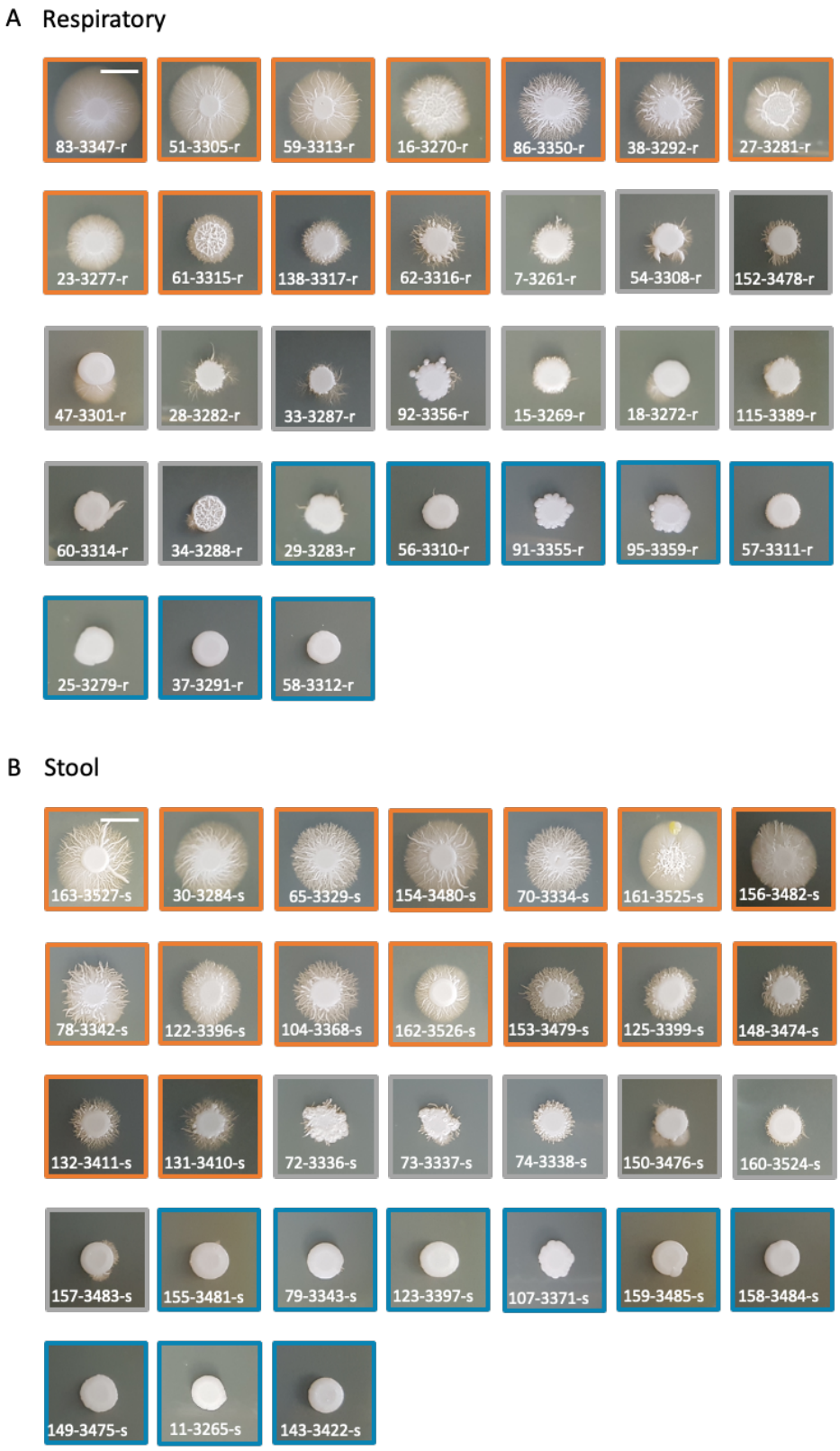

Figure 39: Clinical isolates of *C. albicans* of different clinical specimen types spotted on Spider agar. The isolates came from (A) respiratory tract, (B) stool, (C) oral cavity, (D) urine, (E) invasive samples (swabs from intraoperative sites), and from (F) blood samples. Plates were incubated for 7 days at 37°C to support hyphal growth. Samples are categorized by filamentation, colony size, and surface appearance, where orange frames indicate strong hyphal formation, grey frames intermediate hyphal formation, and blue frames morphologically attenuated colonies. Sample ID: No. in clinical sample collection - No. of the sample in PEU collection - clinical specimen type. Scalebar in every first picture of each sample group is 1 cm. Pictures were taken 7 days after inoculation.

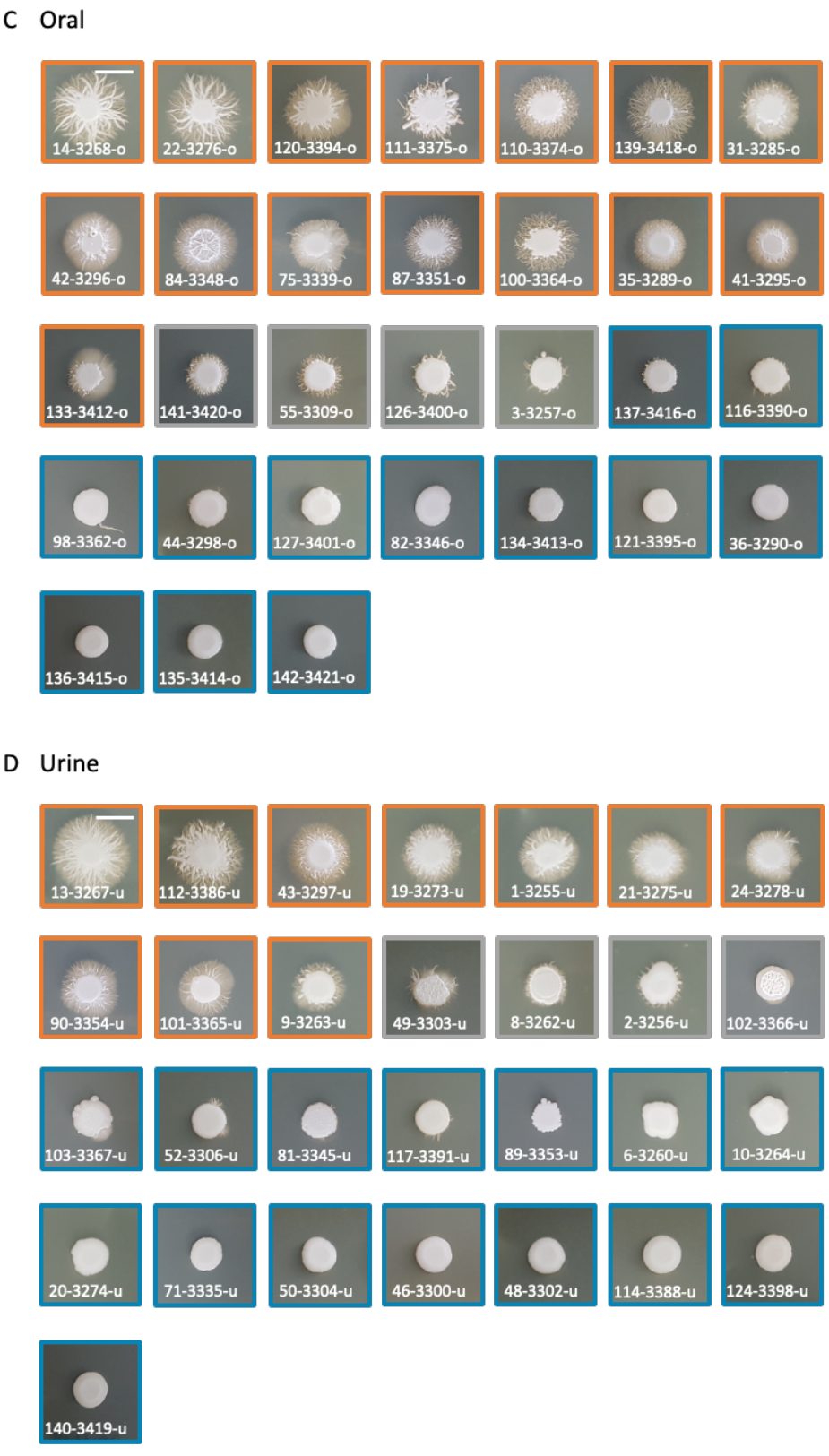

Continued from previous page.

Figure 40: Clinical isolates of *C. albicans* of different clinical specimen types spotted on Spider agar.(C) oral cavity, (D) urine.

E Invasive

F Blood

Continued from previous page.

Figure 40: Clinical isolates of *C. albicans* of different clinical specimen types spotted on Spider agar. (E) invasive, (F) blood.

Depending on the origin, we discovered different proportions of isolates, that could be assigned to the three different categories (Figure 40, A). The group of isolates filamenting most frequently and strongly were found to originate from stool and oral isolates, with 50% and 48.4% respectively. Urine, invasive and blood isolates on the contrary mostly showed an attenuated phenotype, with 51.7%, 59.4%, and 53.3% respectively. The blood culture isolates additionally had the lowest number of highly filamenting isolates with 23.3%. The least attenuated isolates were found from respiratory isolates with 25.8%.

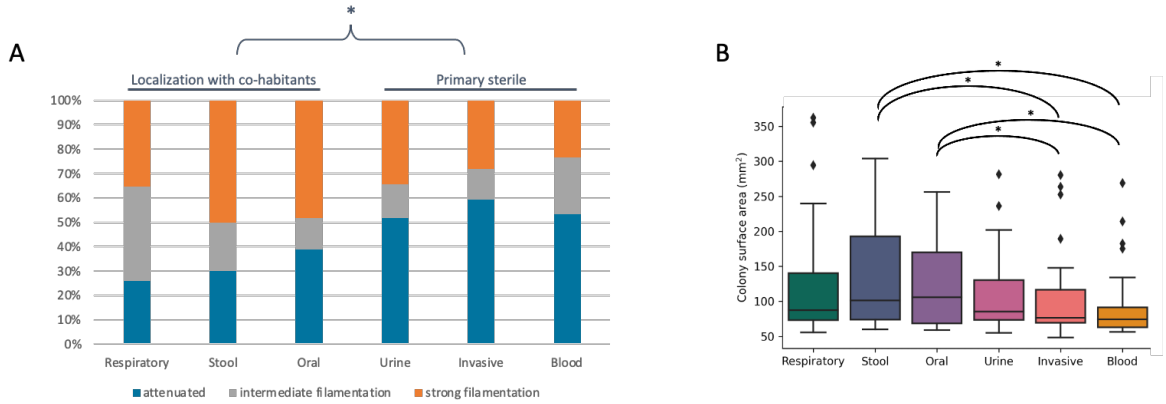

Figure 40: Rates of attenuation among clinical *C. albicans* isolates. (A) Clinical isolates were categorized by their ability to form filaments on Spider medium. Significance between non-sterile (respiratory, stool, and oral) and primary sterile conditions (urine, invasive, and blood) for attenuation $p < 0.05$ (student's *t*-test, p-value = 0.0105). (B) The cell surface area of isolates of different clinical specimen types was measured with Fiji (ImageJ) software. Significance between specific groups: stool or oral isolate groups, each compared either with invasive or blood isolate groups $p < 0.05$ (student's *t*-test).

Further, the isolates' growth was analysed quantitatively by measuring the colony surface area after 7 days of growth on spider agar (Figure 40, B). The fastest growing colonies were found in stool and oral samples with most colonies ranging between 100 and 200 mm^2 or 170 mm^2 in case of the oral samples, followed by respiratory (85 – 130 mm^2) and urine samples (80 – 120 mm^2), whereas the respiratory samples included the biggest colonies (over 350 mm^2) of the study. In contrast, invasive (75 – 110 mm^2) and blood culture isolates (70 – 90 mm^2) frequently produced only small colonies without or only few filaments and showed only a few large filamenting colonies.

3.4.3 Filamentous and attenuated clinical isolates show differences in the capability to damage host cells

It is generally accepted that one of the most important aspects of cell damage is the ability of a strain to form hyphae, as this morphology brings up specific invasive properties. Based on the results from 5-Aza treatment of selected isolates (section 3.4.1), we wanted to know how well filamentation vs. attenuation correlated with ability to damage host cells. For this purpose, we investigated 34 isolates showing strong filamentation on Spider medium and 35 isolates that were highly attenuated and did not show any hyphal growth in our screening. Samples were again tested by our collaboration partners on an oral epithelial cell line (TR146), which were infected for 24 hours with MOI 0.01.

The two groups showed significant differences in LDH concentration (Figure 41): 18 of 34 samples of the filamentous group (A) correlate with a significant higher LDH concentration in the cell culture, whereas only 5 of 35 attenuated samples (B) showed a significant higher LDH concentration (p value < 0.01). Interestingly, in group A all the urine samples showed a significant higher LDH concentration, whereas other groups contained both, isolates resulting in high as well as with low host cell damage. Only the blood culture samples also contained only samples showing low LDH concentration, but here only two samples were tested, thus those might not be representative for the whole specimen type. Interestingly, the invasive group did not significantly contain an increased number of isolates that caused increased cell damage.

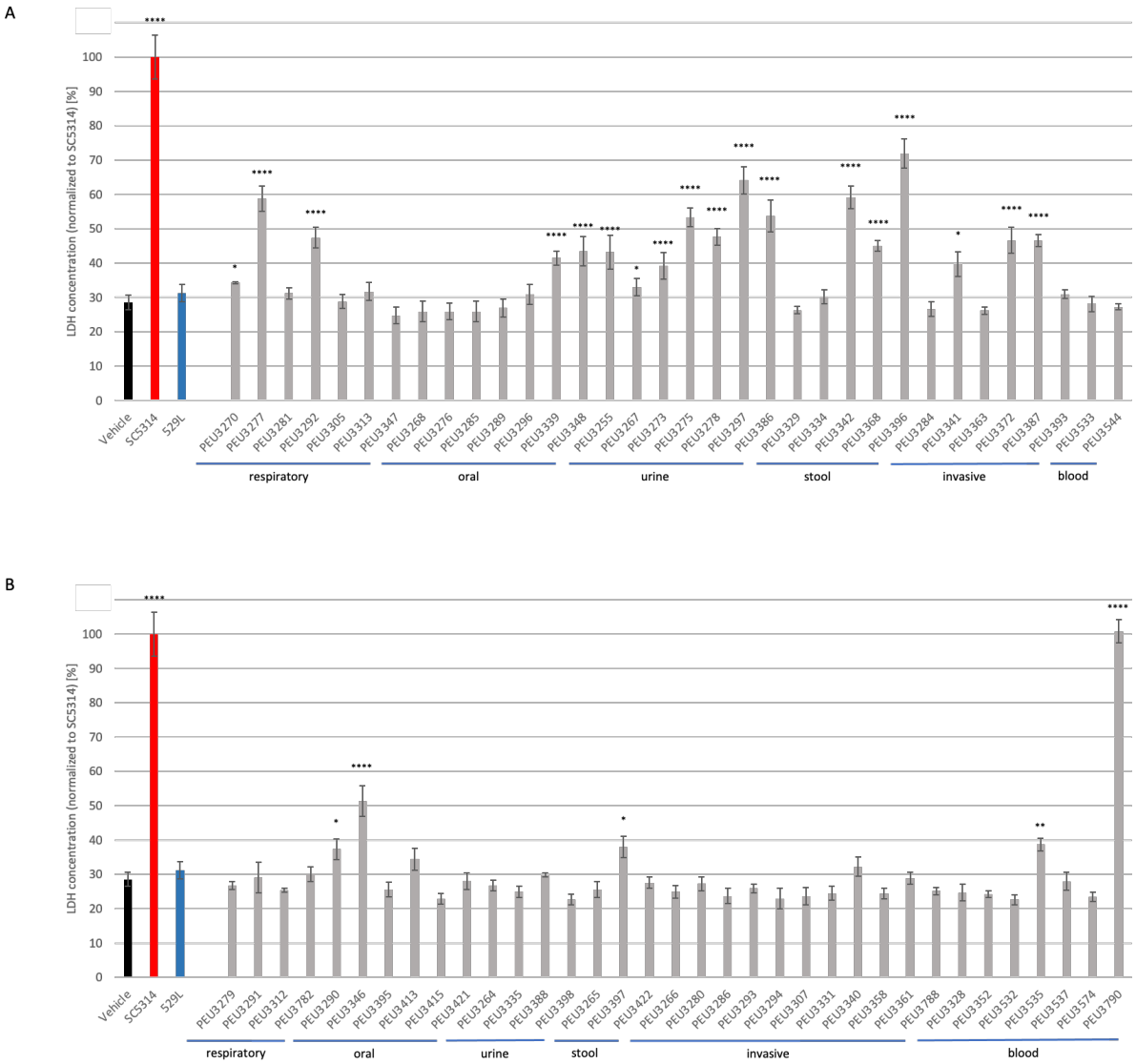

Figure 41: LDH concentration after infection of oral epithelial cells with clinical isolates. Isolates from different clinical specimen type were screened for their phenotype on Spider medium, beforehand. LDH screening was conducted by Prof. J. Naglik, Dr. J. Richardson, and Antzela Zavou (King's College, London). LDH concentration after infection with clinical isolates showing (A) strong filamentous growth and (B) attenuated growth without any filaments on Spider medium. Measurement conducted 24 hours p.i., MOI = 0.01. SC5314 (red) served as positive control and the strain 529L (blue) as negative control. Asterisks represent significance in comparison to vehicle (black) (one way ANOVA and Tukey's multiple comparison test). Significance between both groups: p value < 0.01 (one way ANOVA).

For all strains marked as significant (Figure 41) hyphal growth was observed in YPD broth at 30°C after 24h.

3.4.4 Passage through the mammalian gut alters morphological and invasive outcome of reference strain SC5314

The reference wild type strain SC5314 is known as a highly filamenting strain in each lab working with *C. albicans*. Further it is known as a highly virulent and strongly invasive strain (Lüttich *et al.*, 2013). Nevertheless, if our hypothesis of the connection of morphology and DNA methylation - or epigenetics in general - would be true, it should be possible to change the genetic imprinting in SC5314. As a lab strain, it is usually subcultivated under the same non-competitive conditions, and obtaining all necessary nutrients. In a competitive environment, where the strain must adapt to defence mechanisms of other microbes and lack of nutrients, it would have to change its genetic program again, which could possibly lead to variations in its morphology.

For this experiment we obtained *C. albicans* samples from a gut passage experiment from Prof. Ilse Jacobsen, Wibke Krüger and Sarah Vielreicher (Hans-Knöll-Institut, Jena) (Figure 42).

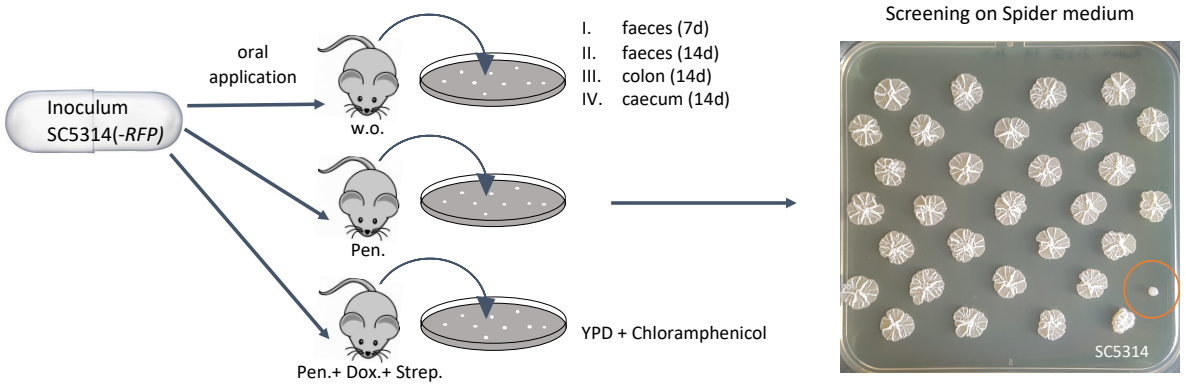

Figure 42: Global experimental setup for gut passage in mice and morphological screening of SC5314. Samples derived from an experiment conducted by our cooperation partner Prof. Ilse Jacobsen, Wibke Krüger und Sarah Vielreicher (Hans-Knöll-Institut, Jena). The samples we obtained, were collected as follows: three differently treated groups of mice (1. control, 2. penicillin, and 3. penicillin + doxycycline + streptomycin) were infected with SC5314-*RFP*. Faeces from 7 and 14 days p.i., and content of colon and caecum 14 days p.i. were plated on YPD plates with chloramphenicol. In our hands colonies were picked from these agar plates, spotted on Spider agar plates, and incubated for 7 days at 37°C for hyphal induction. Plates were then screened for attenuated colonies. SC5314 was spotted as positive control. Red circle exemplarily marks colony of interest.

Colonies obtained from three independent experiments were screened: two of which used SC5314-*RFP* as inoculum and the other the unmodified SC5314 without *RFP* (Table 15). From these experiments we received plates with colonies from faeces, colon, or caecum content.

Table 15: Statistics for spot assay on Spider medium.

Experiment	A (SC5314-*RFP*)	B (SC5314)	C (SC5314-*RFP*)
No. of colonies	4213	2528	2986
Attenuated colonies	0.69%*	0.75%	0.70%*

*only *RFP* positive colonies stated

Intriguingly, attenuated colonies became visible (Figure 42). To clarify if these colonies really derived from the inoculum (and are not naturally occurring *C. albicans* isolates, or another organism), we performed PCR with primers amplifying the *RFP* gene. In experiment A, from 12 of 41 the *RFP* fragment could not be amplified, so these isolates could have been naturally occurring *C. albicans* isolates or had eliminated the marker gene from the genome. Nevertheless, in experiment C all selected colonies were positive for *RFP*.

If this change in morphology really was due to a change in epigenetic DNA methylation, it should be possible to alter the morphology of the attenuated isolates again by 5-Aza treatment. Indeed, we were able to increase filamentous growth by treating the isolates for 24 hours with 5 mM 5-Aza. Further, the colonies as well grew very differently depending on the grade of attenuation they had had before. The two isolates showing the strongest attenuation throughout the experiments (Figure 43) were chosen for a further host cell damage assay conducted by our cooperation partners Prof. Julian Naglik, Dr. Jonathan Richardson, and Antzela Zavou (King's College, London).

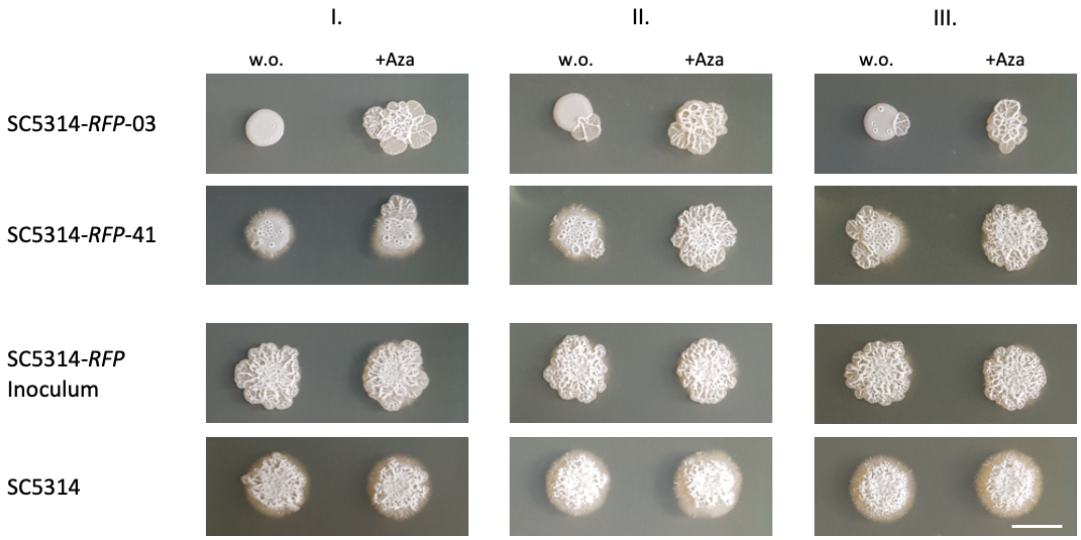

Figure 43: Isolates of SC5314 after gut passage. Pictures show three independent experiments. Samples were treated with 5mM 5-Aza for 24 hours before spotting (McFarland 2.0) on Spider medium. First and second row: attenuated isolates from screening on Spider agar. Third row: inoculum SC5314-RFP before gut passage (Jena strain collection); fourth row: our lab reference strain (Göttingen strain collection). Pictures were taken after 5 days of incubation at 37°C. Scalebar 1 cm.

Both samples originated from faeces collection seven days after infection from two mice that were treated with penicillin. For the analysis, the subcultures after 5-Aza treatment (untreated and treated) were used, both originating from the first Spider spot assay.

Surprisingly, the attenuated samples indeed caused significantly less host cell damage than the inoculum, especially strain PEU3801, which was also more attenuated than strain PEU3804 (Figure 44, A). And intriguingly the 5-Aza treated strains gained back their cell damage capability, nearly to the same extent as the inoculum. Fitting to this observation the *ECE1* gene expression also dropped significantly in the attenuated isolates compared to the inoculum and was at least partially restored again in the 5-Aza treated samples, even though PEU3801+Aza did not show the same expression rate as the inoculum, whereas PEU3804+Aza showed an even higher expression (Figure 44, B).

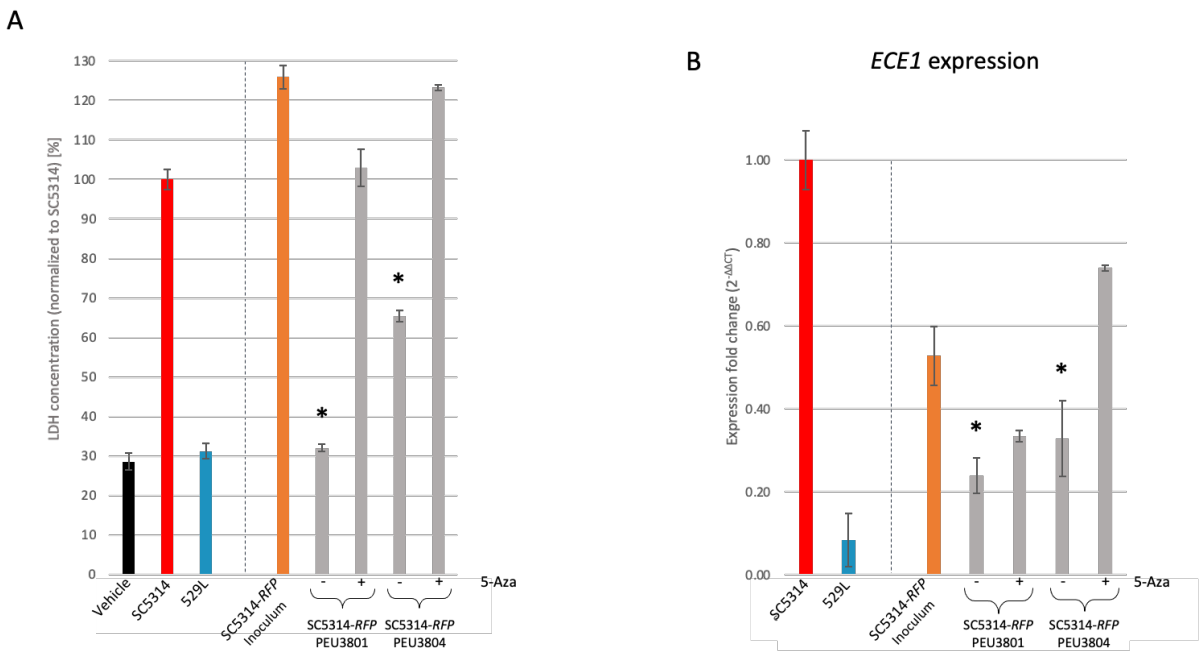

Figure 44: Cell damage capacity and *ECE1* expression of SC5314-*RFP* and its derivates. 5-Aza treated attenuated derivates of SC5314-*RFP* (from Prof. Ilse Jacobsen) (Figure 44) were tested in an LDH assay (A) and for their *ECE1* expression (B). Data provided by Prof. Julian Naglik, Dr. Jonathan Richardson, and Antzela Zavou (King's College, London). Significance for untreated samples $p < 0.05$ (student's *t*-test).

3.5 DNA methylation in clinical isolates of *C. albicans*

For our analysis of DNA methylation patterns in fresh clinical isolates we used those strains, that had been investigated for their capability to invade host cells. As such, we could analyse differences between different clinical isolates as well as having opportunity to compare strains with a higher capability for cell invasion (PEU3694+Aza and PEU3698+Aza) with those that have a low cell invasion capability. Further, we added the highly filamenting blood strain PEU3700 to our analysis, which showed a similar phenotype like SC5314 in our previous investigations on Spider medium. Furthermore, we again used the strongly attenuated strain 529L, and reference strain SC5314 (Figure 45).

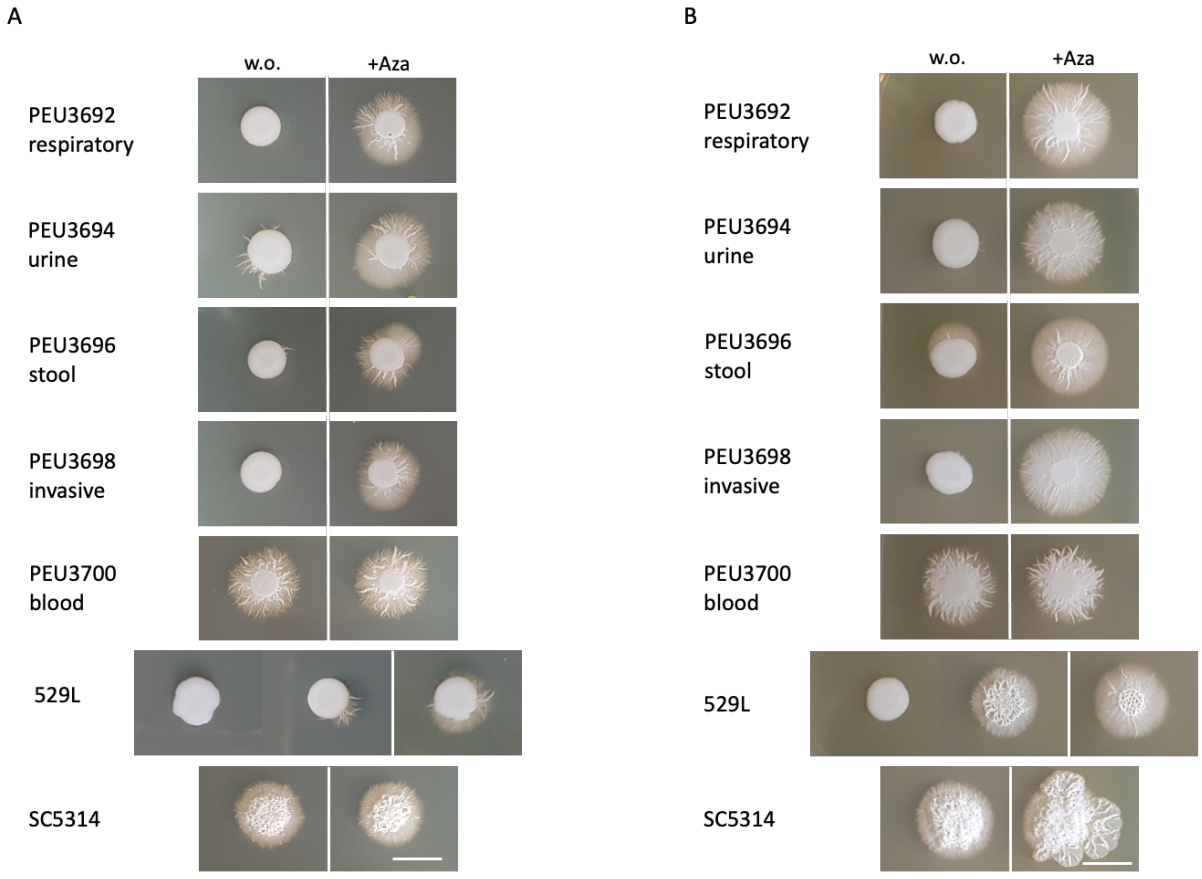

Figure 45: Spot assay of samples used for WGBS. (A) Samples were treated with 5-Aza [5mM] for 24 h before spotting on Spider medium and incubating for seven days. (B) Samples from frozen stocks directly taken from (A). Spotted two days after thawing without further treatment. All pictures taken after 7 days. 529L is represented with two untreated strains, one without filaments and one filamenting on Spider medium. Scalebar 1 cm.

For each strain we used a direct subculture from the Spider spot assay of the untreated and the 5-Aza treated culture, which was thawed from a cryo stock (Figure 45, B). In case of 529L

we added a third sample from a spot that developed hyphae on Spider medium without 5-Aza treatment. Spotting on Spider medium after thawing showed a clear conservation of the 5-Aza induced phenotype and even a stronger hyphal growth. This could also be shown for the untreated filamenting 529L sample. Even strain SC5314 showed a stronger hyphal growth after one freeze and thaw cycle, with the additional interesting observation, that the 5-Aza treated sample also showed stronger hyphal growth compared to the untreated sample on the agar surface.

WGBS of clinical isolates was performed in collaboration with Prof. Toni Gabaldón and Ester Saus (BSC-CNS and IRB, Barcelona, Spain). Sequencing reads were 100 bp PE.

Variance analysis for genome coverage and GC content again did not show any remarkable discrepancies in our data (Supplementary Figure 5). Between 65.5% and 82.1% of the reads could be mapped to the nuclear genome of SC5314, with a calculated coverage between 92 and 183 for all samples. Further, like in our previous WGBS analysis, we had a very reliable coverage for all samples for our further downstream analysis, ranging between 92 and 183 (Supplementary Table 4). Exemplary visualization of the coverage of all nuclear chromosomes of sample PEU3692w.o. showed an average coverage between 70 and 110 and like this confirmed the calculated average coverage. Also comparable to our previous experiment (Figure 46) higher coverage rates were observable in the subtelomeric regions, which might be due to the higher GC content in these parts, potentially leading to better read mapping.

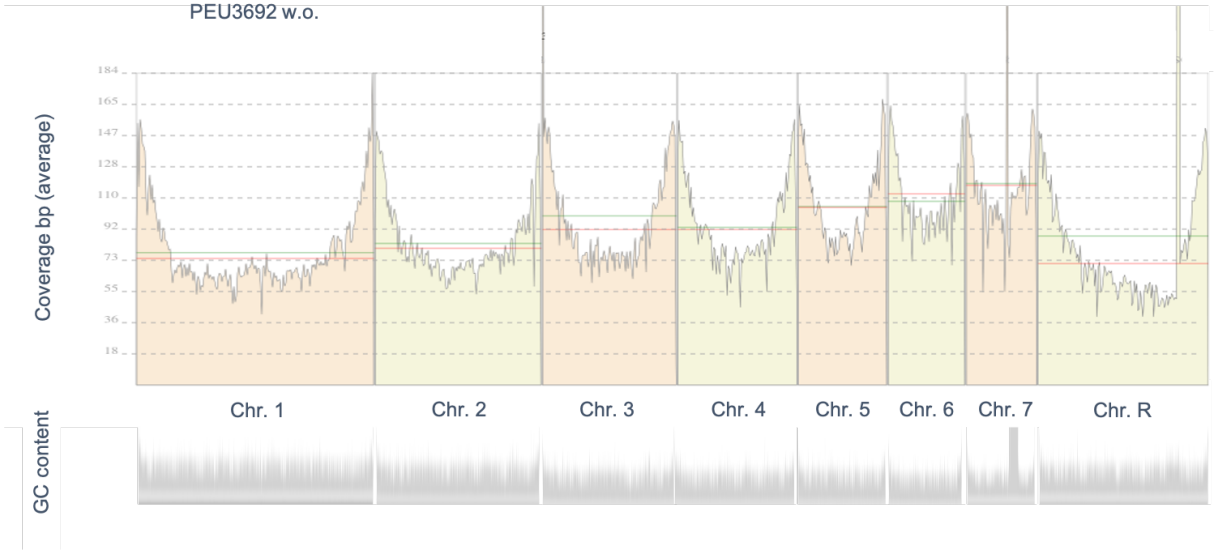

Figure 46: Read Coverage of WGBS reads. Exemplarily the coverage of the respiratory clinical isolate PEU3692 w.o. treatment is shown for all eight chromosomes.

Especially the mapping of strain 529L revealed more missing data in the further downstream analysis than the other clinical isolates. As the full genome for this strain is available (GenBank accession number ASHC00000000 (Cuomo *et al.*, 2019)), we mapped 529L additionally to its own genome. As expected, mapping 529L sequence reads to its own genome resulted in higher mapping rates and less unmapped or multi-mapped reads (Table 16). For reasons of comparability and as not all annotations needed were available at the time of analysis, we further analysed 529L like the other strains, by mapping on the SC5314 genome.

Table 16: Mapping statistics for strain 529L

Sample ID	Description	Total reads (after trimming)	Reads uniquely mapping (%)	Reads unmapped [%]	Reads mapped >1 [%]	Calculated Coverage[1]
529L mapped to the SC5314 genome:						
529Lwo_nucl	attenuated	18 293 164	12 009 262 (65.6)	31.6	2.8	114
529LwoSpF_nucl	filamenting	19 422 574	12 863 635 (66.2)	31.0	2.8	122
529L+Aza_nucl	filamenting	22 056 681	14 452 119 (65.5)	31.8	2.6	137
529L mapped to its own sequenced genome:						
529Lwo_nucl	attenuated	18 293 164	12 699 205 (69.4)	28.1	2.5	120
529LwoSpF_nuc	filamenting	19 422 574	13 624 735 (70.1)	27.3	2.5	129
529L+Aza_nucl	filamenting	22 056 681	15 254 477 (69.2)	28.5	2.4	144

[1] Coverage was calculated after quality trimming and mapping of paired end reads to nuclear (15 433 330 bp) haploid genome (coverage $=\frac{uniquely\ mapped\ reads * 95\ bp}{haploid\ genome}$)

In summary, methylation analysis revealed a much lower methylation content of all samples analysed above of only 0.07% to 0.1%, as compared to our previous experiments (0.49% - 0.54% and 0.69% - 0.78%). This depended on methylation context and sample (Supplementary Table 4). Analysis of methylation in the different contexts confirmed the observation of our previous experiments of a higher methylation content in the non-palindromic CHH context. Differently to or previous analysis only the CpG methylation content was slightly lower, whereas CHG methylation occurred as often as CHH methylation in all samples analysed.

Table 17: Methylation content in different sequence contexts

Sample ID	Description	CpG (%)	CHG (%)	CHH (%)
PEU3692wo_nucl	attenuated	0.08	0.10	0.10
PEU3692+Aza_nucl	filamenting	0.08	0.10	0.10
PEU3694wo_nucl	attenuated	0.08	0.10	0.10
PEU3694+Aza_nucl	filamenting	0.08	0.10	0.10
PEU3696wo_nucl	attenuated	0.08	0.10	0.10
PEU3696+Aza_nucl	filamenting	0.08	0.09	0.09
PEU3698wo_nucl	attenuated	0.08	0.10	0.10
PEU3698+Aza_nucl	filamenting	0.08	0.10	0.10
PEU3700wo_nucl	filamenting	0.09	0.11	0.11
PEU3700+Aza_nucl	filamenting	0.09	0.11	0.11
529Lwo_nucl	attenuated	0.08	0.10	0.10
529LwoSpF_nucl	filamenting	0.08	0.10	0.10
529L+Aza_nucl	filamenting	0.07	0.08	0.08
SC5314wo_nucl	filamenting	0.08	0.09	0.09
SC5314+Aza_nucl	filamenting	0.08	0.09	0.09
529L mapped to own genome:				
529Lwo_nucl	attenuated	0.08	0.10	0.10
529LwoSpF_nucl	filamenting	0.08	0.10	0.10
529L+Aza_nucl	filamenting	0.07	0.08	0.08

3.5.1 Augmentation of mapping rates for clinical isolates

As a result of the increased mapping rates observed for 529L mapped onto its own reference genome, we determined the genetic distances of the other clinical isolates to the reference strain. Multilocus sequence typing (MLST) analysis was performed (Table 18). Indeed, three strains showed novel MLST profiles (PEU 3692, PEU3694, and PEU3696) which were contributed to the pubMLST database (https://pubmlst.org/organisms/candida-albicans). The allele profiles of the two other strains showed direct concordance with diploid sequence type (dST) profiles previously described: strain PEU3698 was concordant to dST24 and strain PEU3700 to dST124. Additionally, the dST ID for 529L was determined for the genome used for methylation analysis (accession number in GenBank ASHC00000000), which, as compared to the official database entry, showed small variations.

Table 18: MLST gene allele code and dST ID

Strain	*AAT1a*	*ACC1*	*ADP1*	*MP1b*	*SYA1*	*VPS13*	*ZWF1b*	dST ID
PEU3692	3	2	6	2	2	6	5	3638
PEU3694	2	5	5	4	239	6	12	3639
PEU3696	2	5	5	175	4	6	20	3640
PEU3698	2	5	5	2	2	24	5	24
PEU3700	8	14	8	4	7	10	8	124
529L (genome)	53	3	10	36	116	201	10*	1214*

*best hit

Phylogenetic placement of the clinical isolates illustrated the closer proximity of strain PEU3694 to SC5314, followed by strains PEU3696, PEU3698, PEU3692 and PEU3700 (Figure 47). This ranking matches well with the amount of missing data visualized in our methylation analysis for CDSs over the whole genome of our clinical isolates, when mapped to SC5314 (Figure 48, A; white areas in heatmaps).

In order to augment mapping for these isolates in the future, they were sent for genome sequencing to our cooperation partner Prof. Toni Gabaldon (BSC-CNS and IRB, Barcelona, Spain). These results were, however, not available at the point of writing.

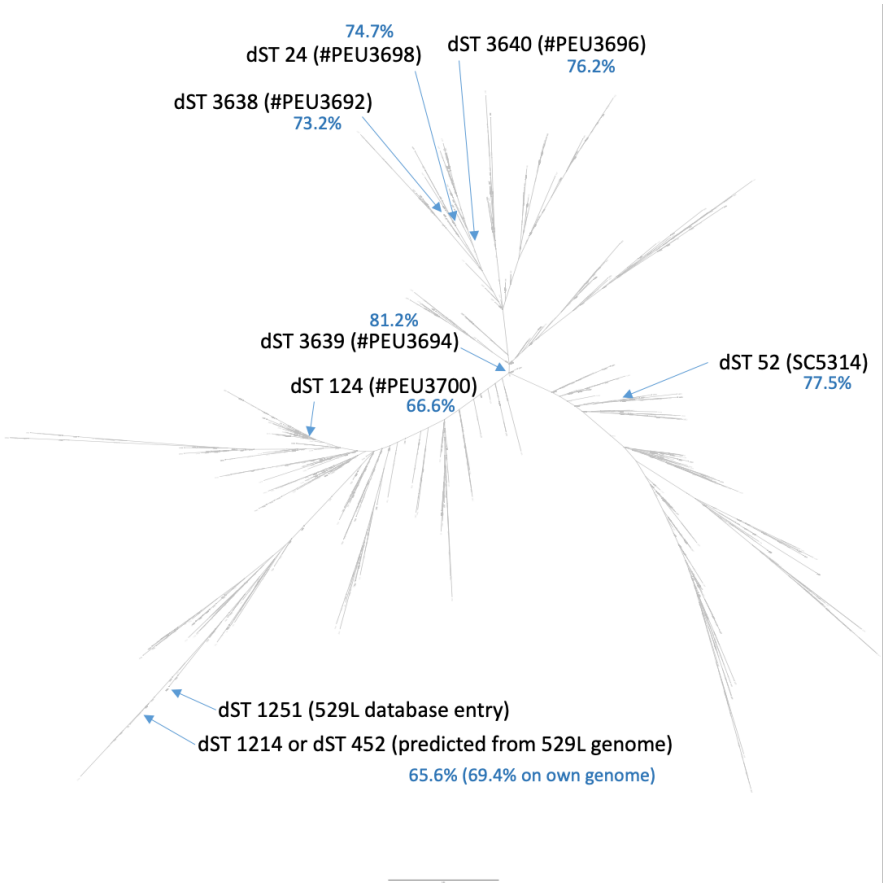

Figure 47: Placement of clinical isolates in phylogenetic tree of *C. albicans* by MLST allele profile. Clinical isolates were mapped in comparison to reference strain SC5314 and isolate 529L. Created with RAxML 8.1 from concatenated *C. albicans* MLST data (N=3639 sequences) after outlier (N=3) removal. Mapping rates of the isolates to SC5314 reference genome are stated in blue.

3.5.2 Degree of methylation in mitochondria

Methylation calling (CpG, CHG, and CHH) of the different clinical isolates showed that the overall 5mC methylation level was between 0.02% and 0.08% (Figure 48), which was considerably lower (approximately 1/20 for SC5314) as compared to our previous WGBS sequencing data, obtained from other sequencing facilities.

Especially the mitochondrial sequences seemed to be visually free of DNA methylation. Only some very specific areas showed methylation at all (Figure 48, F), which may reflect a mapping problem. Sample 529L showed methylation to a greater degree in the 5' and the 3' region, as well as inside the CDS. Otherwise, also the data for this sample showed mitochondrial DNA to be mostly free of methylation. This observation could indicate that our previous two analyses

on SC5314 data reflected incomplete bisulfite conversion of the DNA before sequencing, and that this analysis now uncovered the real methylation level in *C. albicans*.

3.5.3 Differences in methylation as a result of 5-Aza treatment

Through treatment of fungal cell cultures with the DNA methyltransferase inhibitor 5-Aza, we expected to see a global reduction of methylation. This was the case for the isolates PEU3692, PEU3694, PEU3698 (less pronounced), and 529L (Figure 48, A), but not for isolate PEU3696, where methylation was on the same level in untreated and 5-Aza treated sample. The highly filamenting isolates PEU3700 and SC5314 also did not show a reduction of methylation, in contrast, methylation level was even a bit higher when treated with 5-Aza. This effect could be observed in the CDSs (A), subtelomeric CDSs (B), lncRNA genes (D), as well as tRNA genes (E). Interestingly, in all these features the methylation level of the untreated but partly filamenting sample 529L always ranged in the middle between the methylation level of the untreated attenuated sample and the treated filamenting sample, indicating a dependence of morphology and methylation.

When comparing the fresh clinical isolates with reference strain SC5314, we saw that the global methylation level, best represented by CDSs and lncRNAs (Figure 48, A+D), was much lower in SC5314 compared to the fresh clinical isolates, with a baseline of 0.03% versus 0.055% to 0.08%, respectively. Basic methylation level of attenuated 529L without treatment was highest (0.08%).

No difference was observed between the global methylation level of the untreated attenuated clinical isolates as compared to the untreated highly filamenting isolate PEU3700.

In general, the methylation signatures of the different features were comparable to our previous experiments in SC5314, characterized by peaks in the direct 5’ and 3’ region of the protein CDSs (A), and less distinct and on lower level in the subtelomeric CDSs (B). In contrast specific and therefore stronger methylation peaks in LTRs and retrotransposons (C) were observable, and higher methylation levels over the whole lncRNA coding sequences compared to their 5’ and 3’ regions (D). Within tRNA coding sequences we observed a drop in the overall methylation level, but single strong peaks in the middle part in most of the isolates, showing stronger methylation of specific parts of the sequence (E). This was true for most of the clinical isolates, but differing in the manifestation. In PEU3692, in the filamenting isolate PEU3700, as

well as in SC5314, methylation in the tRNA coding sequence was not that distinct. Isolate 529L conversely showed a very strong methylation of the tRNA coding sequence in the untreated attenuated sample, as well as methylation of the direct and broader 5’ and 3’ region. Further, a slightly decrease of methylation in the coding sequence and loss of the peak in the direct 5’ region can be observed in the untreated, partly filamenting sample. In the 5-Aza treated 529L sample methylation was mainly observed at the baseline level (0.05%), peaking in the 5’ region.

Especially for 529L the heatmaps revealed a lot of missing data (white areas), when mapping to the SC5314 reference genome. Mapping to its own genome improved the heatmaps and plots and showed methylation signatures more precisely (Figure 49), while it did not change the overall detection level of methylation.

Figure 48: Mean 5mC DNA methylation levels of different features and adjacent regions. All samples mapped to SC5314 reference genome. Features are scaled to average length from transcriptional start side (TSS) to transcriptional end side (TES): (A) coding sequences (CDS) of the nucleus 1400 bp. (B) Subtelomeric CDSs include the first and last 50000 bp of each chromosome. (C) LTRs and retrotransposons 1800 bp. Adjacent regions -/+ 1kb. Colour bars show level of methylation in percent. Summary plots show mean of methylation of all features plotted. Bin size is 25 bp. Missing data is white. The first sample PEU3692 is always in descending order concerning mean methylation level, gene order was applied to the following samples.

Continued from previous page:

Figure 48: (D) lncRNAs 800 bp. (E) tRNAs 300 bp. (F) mitochondrial coding sequences (mCDS) 550 bp.

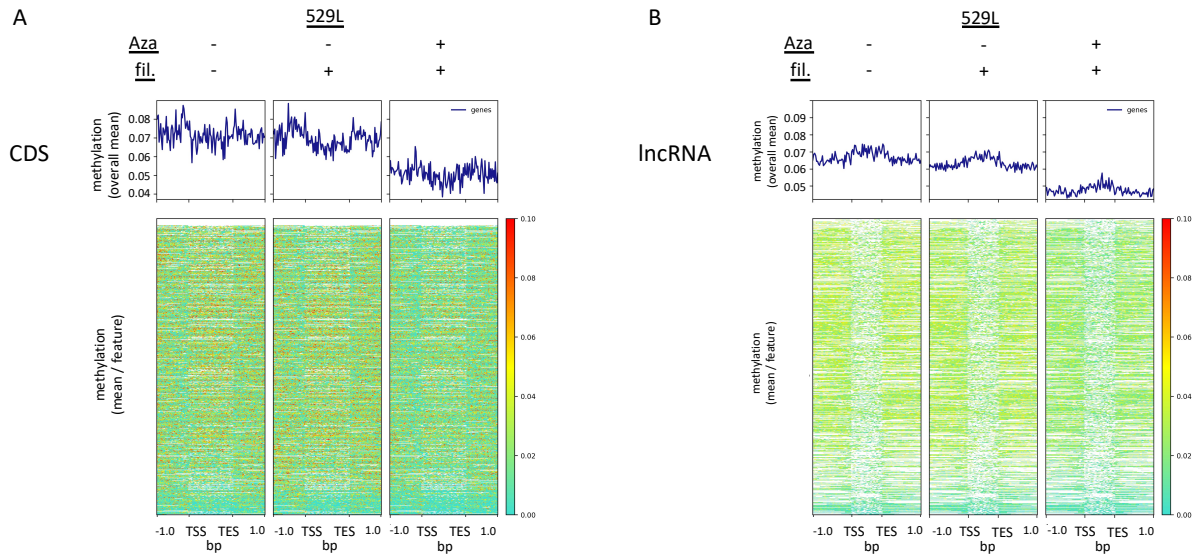

Figure 49: Mean 5mC DNA methylation levels of CDS and lncRNA in 529L. Samples mapped to 529L genome. (A) coding sequence (CDS) of the nucleus 1400 bp. (B) lncRNA 800 bp. Colour bars show level of methylation in percent. Summary plots show mean of methylation of all features plotted. Bin size is 25 bp. Missing data is white. The first sample 529L w.o. is always in descending order concerning mean methylation level, gene order was applied to the following samples. Compared to the 529L samples mapped to the SC5314 genome (Figure 48) much less missing data is observed here.

Correlation analysis of the average methylation scores disclosed some very interesting relations between the samples (Figure 50): First, the highest correlation was found for the filamenting clinical blood isolate PEU3700wo and its corresponding 5-Aza treated sample. A similar high correlation was found for the two SC5314 samples. Intriguingly, these two filamenting isolates also showed a high correlation amongst each other.

Attenuated isolates did not show the same high correlation to their corresponding 5-Aza treated sample. In contrast, 5-Aza treated samples correlated more with the filamenting clinical isolate PEU3700, whereas their corresponding untreated sample showed a larger distance. The only exception was isolate PEU3696, which also correlated well with its 5-Aza treated samples.

Another interesting observation was the cluster of the three 529L samples, showing also a correlation amongst each other, despite their different phenotype and 5-Aza treatment.

Compared to the Pearson correlation shown here, with the Spearman correlation (data not shown) the correlation amongst the 529L samples was even stronger (Spearman is less driven by outliers, but also less sensitive).

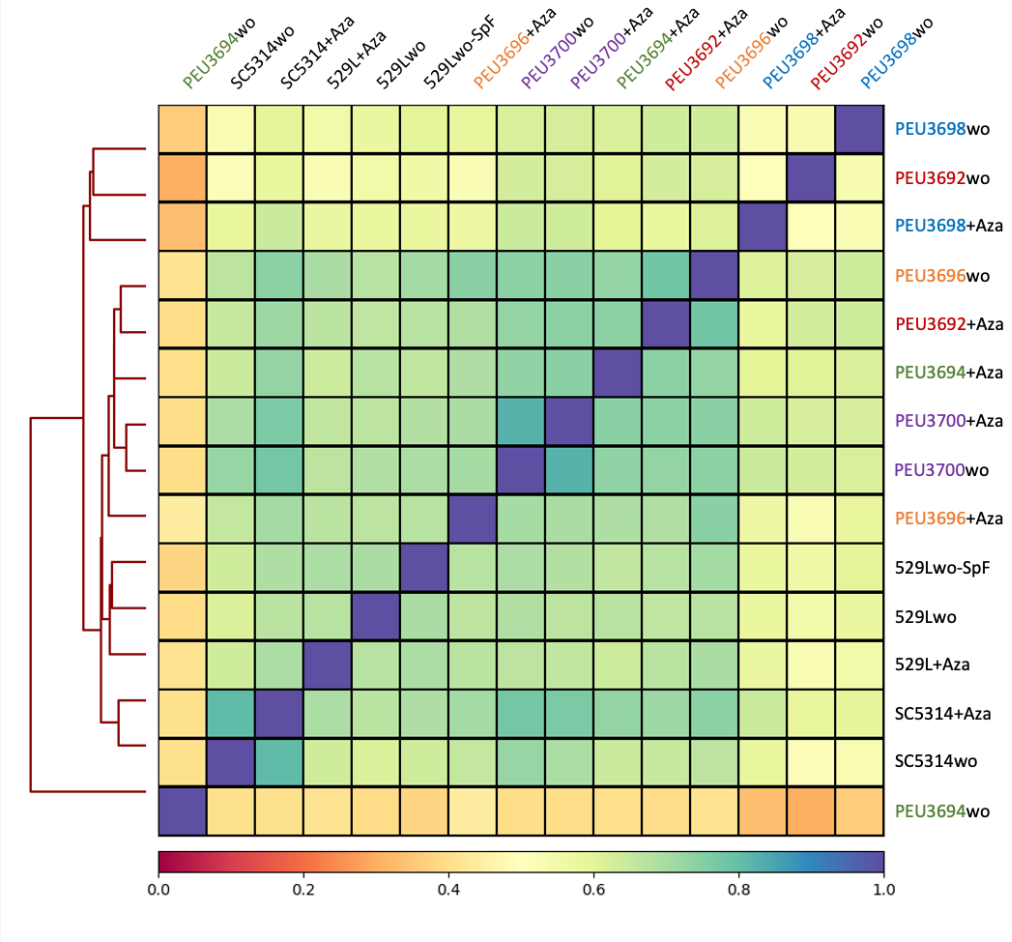

Figure 50: Correlation of methylation sites in clinical isolates. Correlation coefficients (colour bar) were calculated with Pearson method on 10 kb bins of the genome.

Visualization of methylation sites (Figure 51) in hyphae relevant genes of clinical isolates revealed a reduction of methylation sites of 5-Aza treated compared to untreated samples in the respective regions. Further, it could be observed that some regions were specifically targeted in all samples, whereas promotor regions were less methylated than other regions. Also differences between the genes could be shown: especially *ECE1* showed only few methylation sites in all samples sequenced. In contrast *HWP1* and *ALS3* had more methylation sites, but *ALS3* was also less methylated in the center of the gene. Additionally, differences in the occucence of methylation sites between the different isolates were noticeable.

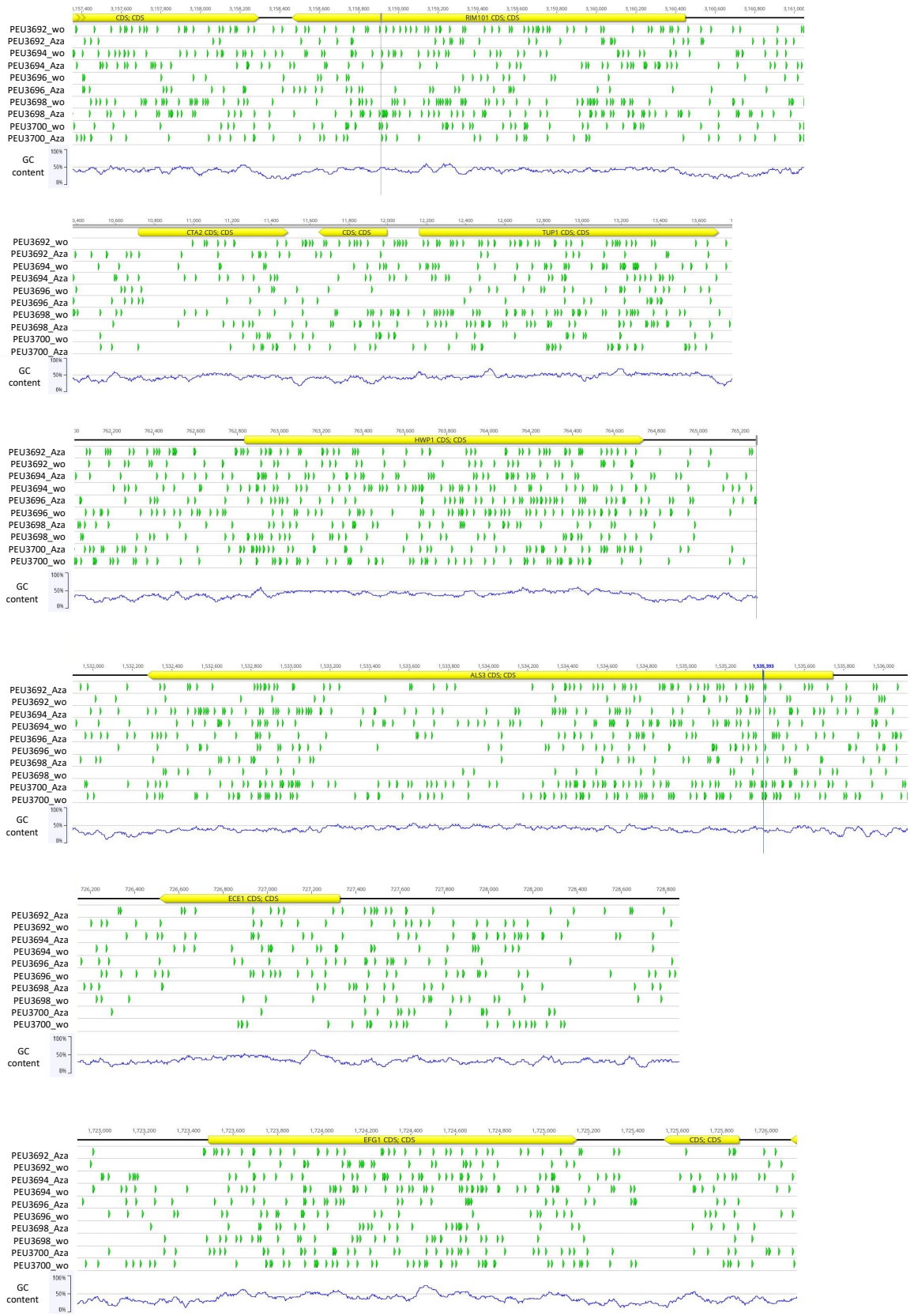

Figure 51: Distribution of 5mC methylation sites in hyphae relevant genes. 5mC methylation sites (green) are shown for all clinical isolates analysed by WGBS, located on forward and reverse DNA strand.

3.6 Rates of 5mC DNA methylation across different *C. albicans* isolates and other fungal species

To obtain an independent quantification of the 5mC DNA methylation level in the investigated isolates of *C. albicans* a 5mC-specific ELISA immunoassay was applied. This assay uses a primary anti-5-mC monoclonal antibody for the specific detection of 5mC in single stranded DNA and has a detection limit of ≥ 0.5% mC / 100 ng single stranded DNA, which was just about the level of methylation observed in our WGS experiments. Therefore, the maximum possible amount of 200 ng per sample was used. The DNA of THP1 human monocytes and *Lentinula edodes* (shiitake fungus) served as positive controls. All samples of the WGBS analysis of clinical isolates (3.5), including their corresponding 5-Aza treated samples were analysed. Further, SC5314-*RFP* and its attenuated isolate PEU3801 were included in the sample set, along with *C. auris*, *C. glabrata*, *C. parapsilosis*, *C. tropicalis*, *Cryptococcus neoformans*, *Cryptococcus diffluens*, *Saccharomyces cerevisiae*, *Aspergillus flavus*, and *Aspergillus fumigatus* clinical isolates from our PEU collection.

Among *C. albicans* strains, a low-level methylation near the detection limit was detectable in six of nine, namely PEU3692, PEU3696, PEU3698, PEU3700, 529L, and the SC5314-*RFP* inoculum (Figure 52). Also, all 5-Aza treated correspondent samples showed methylation in these samples, except for 529L+Aza. In all of these samples methylation was very low and ranged between 0.009% (PEU3700+Aza) and 0.04% (PEU3692+Aza). No methylation was detectable in SC5314 (Göttingen strain collection), PEU3694, and the SC5314-*RFP* derived isolate from the gut passage, PEU3801. Interestingly this was the case for both, untreated and 5-Aza treated sample of each isolate. Further *Candida* species showing methylation were *C. auris*, and *C. tropicalis*. The highest level was observed for *Cryptococcus neoformans* (0.439%). No methylation was observed for *S. cerevisiae* or *C. glabrata*, and surprisingly also not for *A. flavus* and *A. fumigatus*.

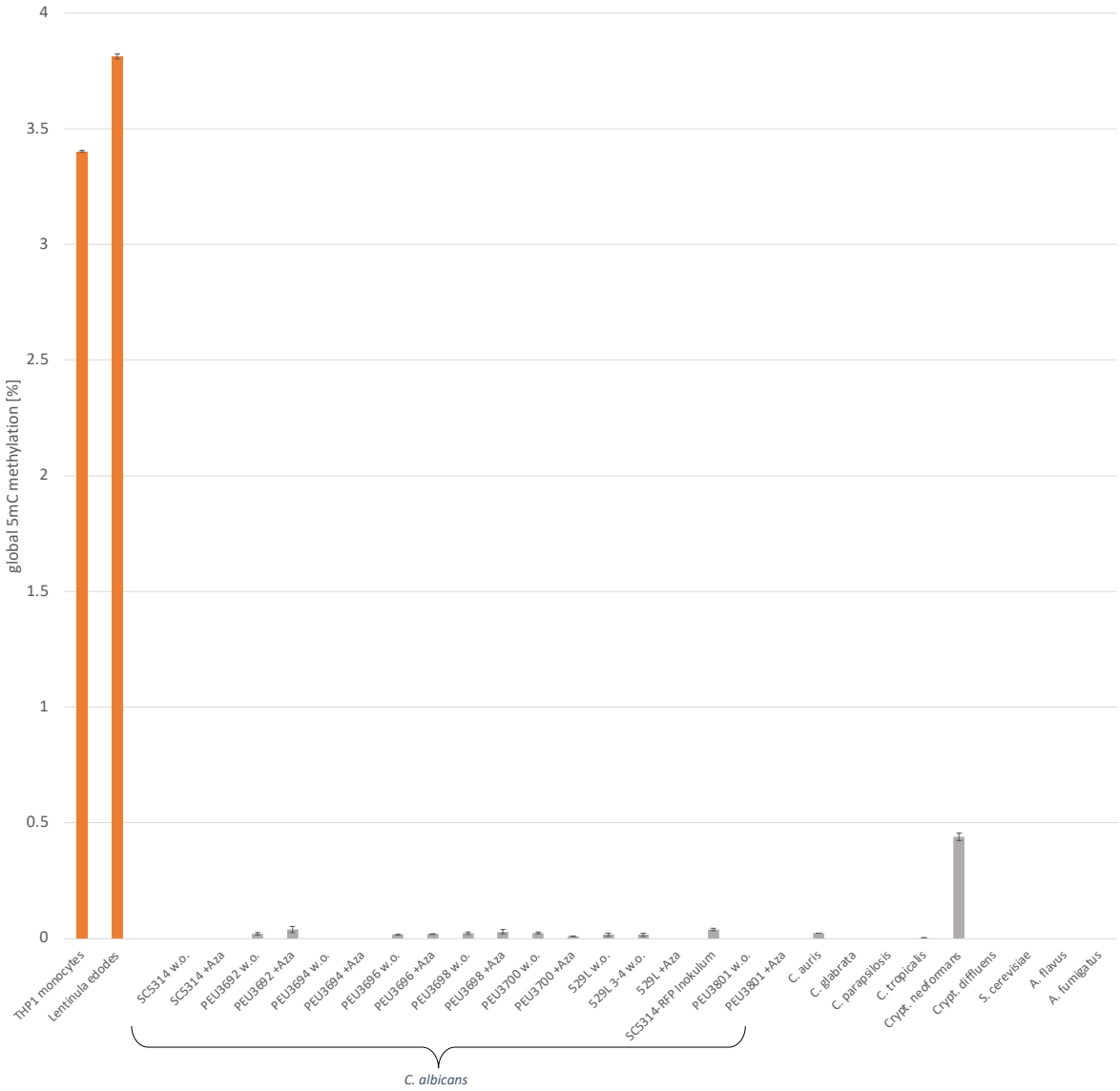

Figure 52: 5mC ELISA immunoassay of different isolates of *C. albicans* and further fungal species. Concentrations of 5mC were calculated using the logarithmic equation of the standard curve. All samples were measured as duplicates.

4 DISCUSSION

Epigenetic modifications induced by environmental triggers play a central role in gene regulation. These modifications can lead to transient or stable inherited changes in gene expression (reviewed by Gómez-Díaz *et al.*, 2012). Different covalent modifications are known to contribute to gene regulation: histone modifications such as methylation, phosphorylation, and acetylation, as well as direct modifications of DNA bases. The interaction of histone and DNA modifications can lead to a specific chromatin structure differentially mediating transcription of genes. The downstream effect can be different in different organisms (groups). While histones and their modifications are well conserved in the tree of life, covalent methylation of cytosines in DNA is not and enzymes promoting this DNA modification are diverse in different species. Additionally, DNMTs differ in the way they methylate DNA, resulting in two groups, *de novo* and maintenance methyltransferases.

A phylogenetic analysis of 528 fungal species revealed that *de novo* DNMTs that can be found in vertebrates, insects, and plants, like Dnmt3 or related enzymes (e.g., DRM2 in plants), are not present in fungi (Bewick *et al.*, 2019). Instead, fungi generally encode four different DNA methyltransferases: DNMT5, RID, DIM-2, and DNMT1. The latter, DNMT1, is regarded as the "classical" maintenance DNMTase, known from higher species. These 5mC methyltransferases are found in diverse combinations in the different fungal subphyla. In Ascomycota mainly RID, DIM-2, and DNMT5 are present in diverse combinations, but DNMT1 is found only rarely. However, the Saccharomycotina clade represents an example of extreme losses, as no 5mC DNMTases were detectable in the species investigated in that study. Accordingly, *C. albicans* also shows none of the typical fungal DNMTs (Bewick *et al.*, 2019). Our own attempts searching genetic features related to known DNMTs did not find any matches either (data not shown).

Consequently, 5mC modifications are not consistently found in all fungal species, and especially the Ascomycota clade only includes only few species that show substantial 5mC DNA methylation, like *Neurospora crassa* or *Pseudogymnoascus destructans*. The latter with an astonishing 5mC content of up to 30% in intergenic regions (Bewick *et al.*, 2019).

In contrast to these findings, the few studies investigating DNA methylation in *C. albicans* had indicate the presence of 5mC in the DNA of this fungal species. Low contents of 5mC have

been detected through different methods, including mass spectrometry (Russell *et al.*, 1987) and methyl-CpG affinity chromatography of fractionated DNA and subsequent PCR of specific genes with bisulfite treated DNA (Mishra, Baum and Carbon, 2011). The screening study of Bewick *et al.* (2019) mentioned above therefore intensively investigated the 5mC content of diverse fungal species by whole genome bisulfite sequencing (WGBS). There, the methylation state of the nuclear genome of *C. albicans* showed a global CpG, CHG, and CHH methylation content lower than ~0.3%, also when specified in intergenic regions, exons, and introns.

This very low content of methylation in *C. albicans* is common in fungi. Many other fungal species, especially amongst Ascomycota, showed a comparable low content of methylation in this study, like *Candida auris*, *Clavispora lusitaniae*, or *Aspergillus flavus*. And many other studies previously observed low methylation contents in fungi (Zemach *et al.*, 2010; Wang *et al.*, 2015; Li *et al.*, 2017; Catania *et al.*, 2020; Hosseini *et al.*, 2020). For *Aspergillus flavus* different studies come to different results depending on the detection technique applied and its state of methylation still is not fully resolved yet (Gowher, Ehrlich and Jeltsch, 2001; Liu *et al.*, 2012).

Outside of transposable elements, the functional role of such modifications remains unclear in the literature.

4.1 DNA methylation is reproducibly found on a low level in *C. albicans* nuclear, but not mitochondrial DNA

Given that previous research showed the presence of 5mC DNA methylation in *C. albicans*, our aim was to gain a deeper understanding of DNA methylation in this species and investigate its impact on gene transcription and phylogenetic plasticity.

Applying WGBS to investigate DNA methylation on single-base resolution, we were able to reproduce the findings of a very low global methylation content in *C. albicans* (Russell *et al.*, 1987; Bewick *et al.*, 2019). However, we detected different contents of 5mC in our three WGBS experiments. In all of them the reference strain SC5314 was sequenced, making all three experiments comparable. For SC5314 the global 5mC content ranged between 0.03 - 0.78%, which is a difference of 1:26. These discrepancies may be due to incomplete bisulfite conversion, which was >99.5% for our first analysis (GATC) and resulted in average

methylation contents of 0.52 - 0.54%. The second experiment had a conversion rate of only >99.2 - 99.3% (Eurofins) and the observed methylation contents were higher with 0.78% on average. In our last experiment (WGBS by Prof. Toni Gabaldón) we observed a methylation content of only 0.1% on average and locally 0.03 – 0.15% at a bisulfite conversion rate of >99.6%. Intriguingly, in the last analysis mitochondrial CDSs as well as their adjacent regions (+/- 1kb) were nearly completely free of methylation, different to our previous two analyses. Thus, we conclude that *C. albicans* is lacking DNA methylation in the mitochondrion. This observation is concordant with a similar debate in other organisms, where different research groups still come to opposing results (Mechta *et al.*, 2017; Patil *et al.*, 2019). For human and mouse DNA it could be shown that a digestion of mitochondrial DNA (mtDNA) with the restriction enzyme BamHI prior to bisulfite sequencing decreased the bisulfite unconversion rate. This indicates that the supercoiled structure of the mtDNA might be the reason for reduced access for bisulfite conversion (Mechta *et al.*, 2017). In fungi mtDNA methylation is viewed ambiguously as well, as for example shown in a study on the basidiomycete *Agaricus bisporus* (Li and Horgen, 1993). In some studies, mtDNA sequences serve already as non-methylated bisulfite conversion control besides the normally used unmethylated lambda phage DNA. One example for this is the comprehensive study on DNA methylation in different fungal species by Bewick and coworkers (Bewick *et al.*, 2019). In contrast, a recent study especially investigated mtDNA methylation in *C. albicans* and showed results of a mean per cytosine methylation of 99% in strains SC5314 and L757 (Bartelli, Bruno and Briones, 2018). This very high level is not only contrary to our findings, but also to general findings about the low global content of DNA methylation in fungi as described above. Our three independent WGBS experiments strongly indicate a level of mtDNA methylation *below* the level of nuclear DNA methylation, and with our last experiment we find the absence of mtDNA methylation in *C. albicans* to be rather reliable. Thus, we conclude that the DNA methylation content observed in the mitochondrial DNA of our first two studies, could be seen as baseline and everything detected above represents the real methylation content in *C. albicans*. Applying this idea, we obtain similar results for the level of methylation in all three experiments, ranging between ~0.03 – 0.15%, depending on the investigated feature.

Interestingly, fresh clinical isolates diverged a bit in their average methylation content by ~0.01 – 0.02%, and were a bit higher than SC5314. Local methylation levels reaced up to 0.2%. A mean methylation content of 0.1% and 0.05% was already postulated by Russel *et al*.

(Russell *et al.*, 1987), who investigated the global 5mC content of yeast and hyphal DNA of *C. albicans* by mass-spectrometry. These issues illustrate the importance of an ideally complete bisulfite conversion for organisms with such a low degree of methylation. Further, we think that for *C. albicans* the mtDNA methylation should always be analysed separately, to control for complete bisulfite conversion, and calculate background levels.

Comparable to previous analysis, we found DNA methylation in all sequence contexts (CpG, CHG, and CHH) (Mishra, Baum and Carbon, 2011; Bewick *et al.*, 2019). Methylation in CpG contexts was slightly less frequent than CHG and CHH, which is also concordant to the observations of Mishra *et al*. (2011), who found that methylation occurred more often in CpA and CpT contexts.

We confirmed the low methylation level in different *C. albicans* samples by an ELISA immunoassay, which also could reproduce known methylation levels for other fungal species, like *C. neoformans* and *L. edodes* (DongLai *et al.*, 2018; Catania *et al.*, 2020). No methylation above the detection level was observed for *S. cerevisiae* or *A. flavus*, both species for which methylation is still questionable (Liu *et al.*, 2012; Capuano *et al.*, 2014; Bewick *et al.*, 2019).

As most of our *Candida albicans* samples - and most other fungi investigated- indicated methylation contents near the detection limit of this test, it was only used for a rough estimation. Nevertheless, in contrast to the other fungi analysed, presence of low-level DNA methylation could indeed be confirmed in most of our samples.

4.2 *C. albicans* shows characteristic patterns of DNA methylation in different features

Next, we sought to identify specific methylation patterns over the whole genome. Therefore, we looked at DNA methylation of specific features in each sample. Our results revealed, that *C. albicans* indeed harbours characteristic patterns of DNA methylation, which are known from other fungal species.

A totally new observation to our knowledge is the detection of typical methylation patterns in the 5’ and 3’ flanking regions of coding sequences (CDS) (Figure 18, Figure 20, and Figure 48). These patterns were found in all three of our WGBS experiments and in all samples sequenced, irrespective of their treatment or morphology. In detail, peaks of methylation

were observed 5' and 3' of CDSs, which dropped inside the CDSs themselves to constant lower levels. This is consistent with similar methylation patterns found for *Neurospora* spp. and other fungal species (Bewick *et al.*, 2019; Hosseini *et al.*, 2020). Especially methylation in the direct 5' region can been associated to promoter methylation in other species, as there higher methylation in promoter regions correlates with low or no expression of the respective gene (Suzuki and Bird, 2008). From specific bacteria it is known, that certain promoters are active only during the hemi-methylation interval that follows DNA replication (Casadesús and Low, 2006). A very interesting observation in *N. crassa* is that methylation 5' of CDSs did not inhibit transcription initiation, but elongation (Rountree and Selker, 1997).

In our data, the level of methylation in the CDSs' flanking regions was less pronounced in subtelomeric regions (50 kb), where the DNA is comparatively G/C-rich (Lynch *et al.*, 2010). Subtelomeric regions often can be found in a heterochromatic state, which is also the case in *C. albicans* (Dunn and Anderson, 2019). Heterochromatin states are usually accompanied by DNA methylation in other species, for example in *N. crassa* (Lewis *et al.*, 2009). As many repetitive regions, especially retrotransposons, are present in the subtelomeric regions (Dunn and Anderson, 2019), we speculated that methylation in subtelomeric regions might concentrate more on these repetitive sequences and less on CDSs. Further, many critical genes associated to biofilm formation, growth in hyphae-inducing media, and genes with assigned roles in virulence, which we would expect not to be silenced, can be found in the subtelomeric regions (e.g., *TUP1*, *RIM101*, *RBT5*, *HGT2*, and *CPH2*; Dunn and Anderson, 2019 and our own unpublished observation). Consequently, we predict that reduced methylation in subtelomeric regions could correlate with higher gene expression, however, more detailed investigations on our transcriptomic data of subtelomeric genes are necessary to test this hypothesis.

Indeed, retrotransposons and other repetitive regions were found to be methylated at above background levels in our samples. This is also the case in many other species (Suzuki and Bird, 2008). Methylation in transposable elements is generally though seen as a genome defence mechanism, as their uncontrolled replication in the genome could result in gene damage, increasing genome sizes and chromosome instability. A loss of methylation in these regions is associated with increased mobilization of TEs (Zemach *et al.*, 2010; Su, Han and Zhao, 2011). In many fungal species TEs are the main target of methylation (Jeon *et al.*, 2015; Bewick *et al.*, 2019; Hosseini *et al.*, 2020). From our data we observed a methylation level nearly double of

the level of other features in most of our samples, locally up to 0.2%. Thus, we conclude also in *C. albicans* the effect of methylation of TEs may be transcriptional silencing.

A very interesting observation in our data was the detection of methylation in DNA coding for long non-protein encoding RNAs (lncRNAs). lncRNAs themselves play important roles in several cellular processes and are regulating gene expression on different levels. Also, an involvement in epigenetic control had been observed by affecting histone modification or chromatin remodelling (Khalil *et al.*, 2009). Further, direct interactions with DNMTs have been reported (reviewed by Zhao, Sun and Wang, 2016). As lncRNAs are involved in many fundamental processes, a strict control for these functional RNAs is necessary and could be the reason for the methylation of their coding DNA locus. Interestingly, their regulation seems to work differently as compared to the protein CDSs in *C. albicans*, as their patterns of methylation are completely opposing. In humans it was shown, that lncRNAs can be activated by either loss of CpG methylation in their promotor region, or by hypermethylation in their gene-body (Li *et al.*, 2020).

Methylation of tRNA DNA loci was not as consistent as in the other features in our samples and a global pattern could not be generalized. Nevertheless, methylation of the 5' and / or 3' flanking regions seemed to play a role, as well as methylation of the gene body itself. In humans hypermethylation of tRNA genomic loci could be correlated to ageing (Acton *et al.*, 2021). In *C. albicans* an ageing cell is characterized by multiple bud-scars on the cell surface, increased cell size, cell wall thickness, and slower doubling time (Bhattacharya, Bouklas and Fries, 2021). A similar correlation between hypermethylation of specific regions and age could be conceivable, as methylation could accumulate in cells, which divide more slowly.

As these patterns could be found in all of our samples, it is obvious that specific patterns of methylation and with this the mechanism of DNA methylation is conserved across isolates of *C. albicans*. Further, as shown in previous research and here, DNA methylation in fungi is not restricted to repeat sequences (Mishra, Baum and Carbon, 2011; Wang *et al.*, 2015; Li *et al.*, 2017; Bewick *et al.*, 2019).

4.3 DNA methylation in different morphologies of SC5314

To test our hypothesis, that DNA methylation might be involved in morphological differentiation in *C. albicans*, we specifically analysed DNA methylation in yeast and hyphal morphology of strain SC5314 by WGBS. The change from yeast to hyphal growth was induced by a change in pH and temperature, a classical experimental setup (Figure 11). In contrast to previous findings of a higher methylation content in yeast compared to hyphal morphology (~0.1% to ~0.05%, respectively (Russell *et al.*, 1987)), substantial differences between both morphologies in the average 5mC content were detectable neither in the 1h p.i. nor the 6h p.i. cultures. Other studies had observed different patterns of methylation during dimorphic transition in *Mucor rouxii*, *Yarrowia lipolytica*, and *Ustilago maydis* (Reyna-López, Simpson and Ruiz-Herrera, 1997), and also in *C. albicans* it was previously found for single genes involved in phenotypic switching, that different methylation patterns in the gene-body of yeasts exist, as compared to hyphal morphology (Mishra, Baum and Carbon, 2011).

Indeed, in a direct bisulfite sequencing experiment of locus *C1_00050C* next to the hyphal gene repressor *TUP1*, repeated methylation patterns in regions of up to 13 nucleotides in different cultures were detectable. Whereas yeast cultures had these clusters in the central part as well as also at the beginning and end of the genes (including the stop codon area), later hyphal cultures (2h and 6h p.i.) only showed methylation in the central part of the gene body. This observation indicated a shift of methylation from the sides of the gene more to the centre during transition from yeast to hyphal morphology. Additionally, less methylated sequences were observed in the later hyphal culture samples (33.3% compared to previous 47 and 50%). Thus, not a loss of methylation throughout the whole genome could change the expression level of a gene, but a different locus of the methylated cytosine in the respective gene or its close proximity.

This would be in line with our WGBS observation, that we did not observe differences in the methylation levels of the adjacent gene regions between both morphologies. Shifts of methylation either to the centre or to the end of the CDS (or further into the adjacent regions) depending on the gene could equalize the overall methylation level in these regions. Interestingly, this could also explain a to our data contrary observation. Mishra and co-workers did not look at 5mC methylation in intergenic regions, but mainly in the gene bodies of *C. albicans*, in 55 fragments of different regions across the SC5314 genome (Mishra, Baum and Carbon, 2011). Some of the investigated regions only cover parts of genes, resulting in an

incomplete picture. Further, their analysis could be biased by their pull-down method, as they purified fractionated DNA by affinity chromatography with methyl-CpG binding protein. As methylation was found in all sequence contexts and especially in CpA and CpT context, this method might also affect their results.

Further the context of methylation could play a role for gene expression, as we observed in our direct bisulfite sequencing experiment: in the yeast morphology the CpA and CpT context were predominant with multiple adenines upstream, whereas in the hyphal morphology the CpT context was very dominant with additional Cs in the closer proximity up- and downstream of the methylated C. A preliminary analysis (data not shown) already suggests confirmation of this trend across the WGBS data.

The observation of a methylated region of 10 - 15 bp instead of one single methylated cytosine, might be due to the mechanism by which cytosines are methylated in *C. albicans*. From humans and other species with predominant palindromic CpG methylation it is known, that their maintenance DNMTs recognize hemi methylated CpG sites and methylate the opposite unmethylated CpG motif (Bostick *et al.*, 2007). Thus, cytosines at a distance of – for example - 10 nucleotides could still have the same regulatory function. However, in a CHH context maintenance methylation would have to take place across a wider area, an activity for which no precedence exists, to the best of our knowledge.

Even though we could not find obvious differences in the overall methylation patterns between the different morphologies in our WGBS experiment with SC5314, two interesting observations could be made regarding the correlation of methylation: first, biological replicates of the same sample formed clusters showing their similarity in methylation and second, a stronger correlation of late-stage culture samples (16h yeast preculture and 6h p.i.) was observed compared to the 1h yeast and hyphal culture samples, irrespective of their morphology. Thus, methylation patterns seem to be more diverse directly after a new stimulus and equalize over time. In the heatmaps a similar observation can be made: 1h samples showed more diffuse peaks of methylation, whereas their correspondent 6h samples originating from the same culture showed a clearer pattern of methylation in the different features (Figure 20).

This change in methylation patterns has been described as “epigenetic drift”, the divergence of the epigenome in cells of multicellular organisms over time (Teschendorff, West and Beck,

2013), but also as a process of dysregulation in human cell culture (Franzen *et al.*, 2021). Here however, we see a more directed change in our late *C. albicans* cell cultures, leading to more similar methylation patterns across the genome. Again, this difference to human cells could only be explained by substantially different mechanisms by which DNA is methylated in *C. albicans*.

4.4 DNA demethylation by 5-Aza leads to expression of hypha specific genes in yeast morphology induced cultures

As a DNMTase in *C. albicans* is still unknown, and with this a potential knockout target is lacking, we used the cytidine analogue and DNA methyltransferase inhibitor 5-Azacytidine instead to investigate the impact of DNA demethylation on morphology. The effect of 5-Aza is already proven in different *in vitro* studies (Christman, 2002; Stresemann and Lyko, 2008), and it is used as a demethylating therapy in myelodysplastic syndrome (Šorm *et al.*, 1964; Gore *et al.*, 2006; Raj, 2006; Qiu *et al.*, 2010). Further, in *C. albicans* it had already been observed, that 5-Aza accelerates germ tube formation in hyphae induced cells (Pancaldi *et al.*, 1988). A side-effect of 5-Aza is its incorporation also into RNA besides DNA, which can lead to inhibition of protein biosynthesis and in the following to cell death (Kihslinger and Godley, 2007). Additionally, a mutagenic effect of the breakdown product of 5-Aza has been observed in human cells (Lamparska *et al.*, 2012).

By randomly demethylating DNA by 5-Aza treatment, we expected a global reduction of methylation, and thus deregulation of diverse genes and with this a random activation of genes, amongst those genes responsible for hyphal development.

Our observation was indeed a strong upregulation of genes in a 5-Aza treated [1mM] yeast culture. Primarily these genes were responsible for DNA repair, which was not unexpected. If 5-Aza could also cause double strand breaks, like shown for its derivate Decitabine (Stresemann and Lyko, 2008)) and replication, as well as for detoxification, like for example the very strongly upregulated formate dehydrogenases (*FDH1* +5.82, *C5_03770C* +7.60, and *C2_10070W* +6.85). Their substrate formate is formed, when the structure of 5-Aza breaks down to an open ring structure, either as a consequence of the covalent bond to a DNA

methyltransferase or due to its instability in aqueous phases (Christman, 2002). Interestingly, *FDH1* normally is repressed by Efg1 in yeast cells (Pierce and Kumamoto, 2012).

Further, the isocitrate lyase *ICL1*, which is a glyoxylate cycle gene (alternative carbon metabolism) required for fungal virulence and commensalism (Lorenz and Fink, 2001; Vico *et al.*, 2021) was strongly upregulated. This gene is localized in peroxisomes (overrepresented in our GO analysis) and might be involved in oxidative degradation of 5-Aza breakdown products. Indeed, several hyphae relevant genes were upregulated in the 5-Aza treated yeast cultures, especially in the freshly induced 1 h cultures. These genes were also present in the parallel hyphal cultures, but not in the untreated yeast cultures. Gene ontology analysis additionally revealed an upregulation of genes involved in “hyphal cell wall”, “fungal type cell wall” and “extracellular region”, but also “yeast form cell wall” (with less counts than “hyphal cell wall”) in the 5-Aza treated yeast cultures compared to the untreated yeast cultures. These observations indicate an effect of 5-Aza on morphology related gene regulation. Only a small difference in differential gene expression was observed between 5-Aza treated and untreated hyphal culture, which additionally indicates a hyphal-directed effect by 5-Aza demethylation, consequently those genes being not that much increased in the hyphal morphology. A further interesting observation in our gene ontology analysis of the 5-Aza treated yeast subculture was the downregulation of “mitochondrial tRNA methylation”. This result could be a hint for incorporation of 5-Aza into RNA and producing a negative feedback loop by binding a potential tRNA methyltransferase, as shown for DNMT2 in humans (Schaefer *et al.*, 2009).

4.5 Demethylation by 5-Aza leads to strong hyphal development in previously attenuated clinical isolates

The effect of 5-Aza on morphology of SC5314 in our liquid culture experiment was not as strong as expected and we only saw slightly enlarged cells in the yeast culture with a possible tendency towards a more pseudohyphae-like morphology. These findings were in contrast to the findings of Pancaldi *et al*. (1988), who found that 5-Aza significantly accelerates yeast mycelium conversion.

Following this up by investigating hyphal formation on Spider agar, a correlation between the correspondence to 5-Aza and the untreated phenotype could be observed: while the

previously strong filamenting strain SC5314 as well as two other filamenting reference strains did not show any change in morphology after 5-Aza treatment, the attenuated strain 529L, started producing filaments after 5-Aza treatment. This observation also may further explain the results of Pancaldi *et al*. (1988) who used a strain "isolated from a clinical specimen", for which the filamentation/attenuation phenotype is not indicated in the publication. In general, an important consideration when investigating any context in an organism is, that reference strains have usually been kept in a non-natural environment over extended times, where they are repeatedly subcultured, re-frozen, have access to nutrient-rich agars, and are not exposed to interactions with competing strains, or the immune system of a host. This problem is also known for bacterial reference strains, which have lost typical pathophysiological characteristics, because of changes in their genotype over time (Fux *et al.*, 2005). Thus, we should ask as well, if these circumstances could also alter the epigenetic heritage of an organism in a way, that it could lead to a non-natural altered outcome of a study.

As a consequence to this idea and to the result of the 5-Aza treatment of strain 529L (a relatively new clinical isolate) the investigation of fresh clinical isolates was of special interest for us. Indeed, we were able to reproducibly induce significant filamentation in previously attenuated fresh clinical isolates through 5-Aza treatment.

Nevertheless, as observed for the reference strains, already strongly filamenting isolates were not altered in their phenotype by 5-Aza. This is in concordance to our transcriptomic data, where 5-Aza leads to a strong change in the yeast, but not in the hyphal morphology, indicating that alterations by 5-Aza affect similar pathways necessary for hyphal development. As random mutations usually do not lead to such reproducible changes and further also include mutations leading to growth defects - which we could not observe - we conclude that changes in the DNA methylation pattern are likely to be causative for the observed changes in morphology.

4.6 DNA demethylation by 5-Aza can lead to a higher cell damage capacity of previously attenuated clinical isolates

In a cell damage assay four of our clinical isolates – PEU3692, PEU3694, PEU3696, and PEU3698, each 5-Aza treated and untreated - were tested for their capacity to cause cell damage in a human cell line. Additionally, treated and untreated samples of 529L were tested. In 529L, 5-Aza did not alter the cell damage capacity, which fits to the recently published observation, that the reason for reduced virulence of this strain is an alternative candidalysin allele leading to impaired secretion of the encoded peptide (Liu *et al.*, 2021). In contrast, two of our four originally attenuated clinical isolates showed significantly increased concentrations of LDH after 5-Aza treatment compared to the untreated samples. Thus, 5-Aza treatment led to a higher cell damage capacity in these strains, which could be due to an upregulation of *ECE1* and further involved genes, as we could show for the 5-Aza treated yeast cultures of SC5314.

4.7 5-Aza induced filamentation leads to a local reduction of methylation and higher inter-sample correlation

The same samples discussed above were used for DNA methylation analysis of 5-Aza treated and untreated attenuated stages. Additionally, the epigenome of a filamentous clinical isolate (PEU3700) was sequenced, for comparison to SC5314. All sequences were mapped to the SC5314 reference genome (assembly 22, candidagenome.org), as no own genome was available for the isolates. Mapping and downstream analysis revealed several gaps and missing data in the different samples, its quantity roughly correlating to the phylogenetic distance to strain SC5314. This indicates the benefit to sequence the genome of a strain in parallel to WGBS, which was also shown by the mapping of 529L sequences to its own genome. Nevertheless, a higher methylation rate could be observed for the clinical isolates as compared to SC5314. No global reduction of DNA methylation by 5-Aza could be observed in any of the clinical isolates or strain SC5314; only strain 529L showed a reduction of ~20% in the 5-Aza treated sample (0.08% vs 0.1% in CHH and CHG, and 0.07% vs 0.08% in CpG contexts).

Locally in the different features we saw a different picture, as we observed that the level of methylation in the different feature loci was also different between the isolates (Figure 48). We further observed that 5-Aza had local impacts on the methylation level in some of the isolates, but not all. Three of four previously attenuated isolates showed a lower level of methylation after 5-Aza treatment, only the fourth had the same level. On average, a reduction of methylation in the attenuated samples by 5-Aza treatment can therefore indeed be assumed. This reduction was most obvious for strain 529L. Interestingly, the filamentous 5-Aza-*un*treated isolate of 529L also showed a slightly lower level of methylation as compared to its attenuated progenitor, again pointing towards a functional correlation of morphology and reduction in methylation. Similarly, a reduction of methylation by 5-Aza in 529L resulted in even stronger hyphal development. Hence, the data of all attenuated strains taken together strengthened our hypothesis that a demethylation in coding sequences and other features correlates with, and possibly allows for, stronger hyphal development. In contrast, both filamentous isolates, PEU3700 as well as SC5314 had an even higher level of methylation locally (but not globally) after 5-Aza treatment. This observation is a bit curious. Yet, Pearson correlation analysis showed a strong and significant correlation between methylation in the filamentous samples and their respective 5-Aza treated sample and also amongst each other. In contrast, attenuated samples did not correlate that well with their respective 5-Aza treated sample, but instead their 5-Aza treated samples (all but one) correlated well with each other as well as with treated and untreated filamentous samples (Figure 50). Again, this result strongly indicates a relation between demethylation by 5-Aza and the original hyphal morphology, as 5-Aza treatment seems to “imitate” the methylation pattern of the hyphal morphology. Further, methylation patterns in non-filamenting samples seemed to be more different to each other.

Unanticipated was the low degree of demethylation by 5-Aza, i.e. the fact that methylation was not fully absent after prolonged treatment. One explanation could be a too fast degradation of 5 -Aza in our medium, leading to incomplete inhibition. As 5-Aza treatment usually was conducted under yeast inducing conditions, we used Lee’s medium at a pH of 4.5. A slightly acidic pH of 6 is normally recommended for 5-Aza preparation, but a pH of 4.5 is also in a range where enough of the compound should be stably available in solution (Argemí and Saurina, 2007).

However, it could also point towards unviability of cells devoid of DNA-methylation, which would be in line with a concept shown for Cryptococcus, where DNA methalytion patterns (albeit at CpG) have been conserved over evolutionary times in the absence of a de novo methylase activity (Catania *et al.*, 2020)

4.8 The body site of isolation determines the predominant phenotype in *C. albicans* and its cell damage capacity

In a side-experiment we were able to show that the phenotype of clinical isolates on Spider medium is significantly depending on the source of its isolation: attenuated isolates are predominantly found in primary sterile environments like urine, blood and invasive samples. Outliers in these samples could be assigned to patients with coinfections in nearly all cases and further to three oncological patients, who received anti-cancer chemotherapy, which however, did not include 5-Aza. One oncological patient further was coinfected with different pathogenic bacteria. Thus, extremely filamenting isolates in normally primary sterile environments in fact did not originate from sterile environments, which could have triggered the more filamentous phenotype. Interestingly, all these phenotypes are stable in most of the cases, as shown for our attenuated strains, that were used in different experiments over several months.

Strong filamentation in clinical isolates also significantly correlated with a stronger cell damage capacity compared to completely attenuated samples. However, not all filamentous samples showed hyphal formation in the hands of our cooperation partners, who tested the phenotype in a different medium (liquid YPD), and vice-versa a few attenuated samples showed hyphal development in cell culture media in their hands, indicating a relative stability of those phenotypes only.

In sum, the environment and co-habitats where these strains were isolated from, obviously leave an epigenetic imprint on transcriptional programs, where we assume DNA methylation is a crucial part of.

4.9 Passage through the mammalian gut leads to an epigenetically induced phenotypic switch in SC5314

With this assumption in mind, we hypothesized a possible change of the highly filamentous morphology of SC5314 by passage through a mammalian host. It was already shown that passage through a mammalian gastrointestinal environment triggers a developmental switch to a commensal-specific “GUT” cell type (Pande, Chen and Noble, 2013). Further, the yeast as well filamentous morphologies had been found in different parts of the gut (Witchley *et al.*, 2019). We were able to repeatedly identify ~0.7% of attenuated SC5314 isolates after gut passage in three independent experiments. This number is much higher than the assumed mutation rate in *C. albicans* (Ene *et al.*, 2018) and for this reason we hypothesized that this phenotypic switch must be due to epigenetic imprinting. In contrast to our fresh clinical isolates, this phenotype became weaker in the following *in vitro* experiments, where most of the colonies started to form filaments again. This supports our idea of an epigenetic phenotypical switch, as the time of persistence in the host seems to play a role in the stability of the phenotype. These samplings of SC5314 were obtained at maximum 14 days p.i.. With *C. albicans* infections usually stemming from within the host, patients suffering of a *Candida albicans* infection likely harbored their particular strain since many months or even years, resulting in a stronger manifestation of adaptation to the host environment. Besides the microbial environment that might trigger an epigenetic adaptation, the immune system of the host might play an additional role and could be the cause for the significantly stronger attenuation observed in blood and invasive samples, as the immune system can reach microbes in these environments more easily. Further it had been shown, that specific gut bacteria are able to activate the host immune response to keep up the *C. albicans* colonization resistance (Fan *et al.*, 2015).

A further strong indicator for an *epi*genetic involvement in the phenotypic switch of SC5314 from filamentation to attenuation after gut passage, is the restorability of the filamentous phenotype by 5-Aza treatment. Both variants of two of the attenuated isolates – non-filamenting and filamenting by 5-Aza treatment – were also tested for their cell damage capacity, where both attenuated isolates caused significantly less host cell damage, depending on their grade of attenuation. 5-Aza treatment, accordingly to previous experiments with clinical isolates, resulted in increasing host cell damage nearly reaching the capacity of the

inoculum. Finally, also a loss- and gain-of-function for both morphological states could be observed: while the attenuated isolates had a decreased *ECE1* expression compared to the inoculum, the *ECE1* expression could be restored (in the first sample partially, the second sample even stronger than before) by 5-Aza treatment. This experiment is a further indication for an alteration in gene expression not depending on mutation (neither in the host, nor by 5-Aza), but by an *epi*genetic event, as these changes are easily reversible. Further, it is rather unlikely - albeit not impossible - that a mutation could lead to a gain-of-function in two independent samples and lead to a similar expression profile of one specific gene.

4.10 Potential candidates for DNA methyltransferases in *C. albicans*

C. albicans definitely is one of the morphologically most variable pathogens found in mammals. Its perfect adaption to its environment enables the fungus to continuously persist in the host and to avoid the host immune system. This plasticity requires rapid alterations of the gene expression profiles, which *C. albicans* achieves by an elaborate system of signalling pathways. Different epigenetic modifications determine accessibility of genes, their regulatory regions, and promoters for transcription factors, polymerases and other factors and enzymes involved in gene regulation. Given the pattern of methylation detected adjacent to CDSs in our research, a regulatory role for DNA methylation in gene expression in *C. albicans* seems to be very likely. From other organisms it is known, that DNA methylation can also specifically be found in transcription factor binding sites and new observations even bring up the idea that TFs could also prohibit DNA methylation (Héberlé and Bardet, 2019; Martin-Trujillo *et al.*, 2020).

Other regulatory mechanisms involve different non-coding functional RNAs (ncRNAs) which gained attention in the last years and had also been observed for *C. albicans* (Drinnenberg *et al.*, 2009). Amongst those the small ncRNAs (miRNAs) were shown to take influence on gene expression by targeting and modifying mRNAs and this way leading to gene-silencing (Guil and Esteller, 2009). Many of those ncRNAs (miRNAs, siRNA, piRNAs and lncRNAs) had been shown to directly play a role in epigenetic modification processes as well, like histone modification, heterochromatin formation, and DNA methylation targeting of DNMTs (reviewed in Wei *et al.*, 2017). RNA directed DNA methylation had been shown for fungi as well (Zemach *et al.*, 2010).

The question is, how can *C. albicans* establish DNA methylation in its genome, while no DNMTase could be found yet? And how can it distinguish between CDSs, TEs, and lncRNAs, which are obviously methylated in different ways? Other fungal species exhibiting such a low methylation content were observed to contain up to three different kinds of the typical fungal DNMTases, like *Aureobasidium pullulans* or the plant pathogen *Leptospheria maculans* (Bewick *et al.*, 2019). *Cryptococcus neoformans* harbors symmetric CpG methylation and it was found that DNA is methylated by a single maintenance methyltransferase (DNMT5), as its deletion leads to loss of DNA methylation (Catania *et al.*, 2020).

In *C. albicans* another mechanism of methylation has to be assumed. A potential candidate for a DNA methyltransferase might also be an enzyme, which originally methylates other nucleotide molecules. In this context, Bewick *et al.* (2019) showed, that DNMT2 – a tRNA methyltransferase – is related to the DNA methyltransferase DNMT5, which is found in some Ascomycetes, however not in *C. albicans*. Apparently DNMT2 exhibits residual DNA methyltransferase activity in some contexts/species to a small degree (Hermann, Schmitt and Jeltsch, 2003; Jeltsch, Nellen and Lyko, 2006).

The only known tRNA 5C-methyltransferase in *C. albicans* is Ncl1. Its orthologue of *S. cerevisiae* methylates the cytosine in the wobble position of $tRNA^{LEU}$(CAA) of its anticodon. Interestingly, an increase of oxidative stress leads to an increase of Ncl1 activity in *S. cerevisiae*, and loss of *NCL1* results in hypersensitivity to oxidative stress (Chan *et al.*, 2012). Our transcriptomic data for *C. albicans* strongly reveals that 5-Aza leads to oxidative stress response by upregulation of genes involved in oxidation-reduction processes. Thus, this response could derive from degradation of Ncl1 by a 5-Aza incorporation in DNA or in RNA. A potential hypothesis would be, that *C. albicans* Ncl1, besides methylating tRNA, also might methylate DNA to a small degree. An increase of oxidative-stress by 5-Aza could also lead to an increase of Ncl1 activity and thus to an increase of DNA methylation – which would explain the only slight decrease of methylation after 5-Aza treatment.

Such an activity could also explain the very low methylation level, and possibly the patterns observed, if active DNA were targeted. Additionally, the anticodon of the $tRNA^{LEU}$ (CAA) supports the idea, that Ncl1 could also recognize similar sites in the DNA of *C. albicans*, as a slight predominance of methylation in the CHH context is present. Moreover, our bisulfite sequencing experiment showed a predominance of CAA methylation in the yeast morphology.

4.11 Conclusion and outlook

As in many other fungal species DNA methylation is found only at a very low level in *C. albicans*. Our data shows for the first time, that DNA methylation in *C. albicans* occurs in clusters in different features of the *C. albicans* genome. In the absence of classic potential DNA methyltransferases in the *C. albicans* genome, especially the patterns adjacent to CDSs still resemble the ones found in other fungi with known DNMTase activity, such as in *N. crassa*. Also, a stronger methylation in transposable elements is in concordance with the findings in many other fungi, where methylation of these regions is seen as a genome defence mechanism. Further, lncRNAs were found to be specifically methylated, but unlike the patterns found at CDSs, suggesting a differential regulation of these regions.

The analysis of different isolates treated with the demethylating agent 5-Azacytidine strongly indicates a relation between methylation and morphology on different levels, as morphologic, transcriptomic, and methylation correlation analysis revealed a significant tendency to develop a hyphal phenotype. Thus, demethylation by 5-Aza treatment seems to "imitate" a hyphal specific methylation pattern. As seen in our initial experiment, in the hyphal morphology this could imply a shift of methylation away from the CDSs' adjacent regions, possibly indicating a regulation of TF binding sites by methylation. In the future differential methylated regions (DMR) analysis will be used to test this hypothesis in more detail.

Further, a significant impact of the host natural environment on clinical isolates as well as on SC5314 was observed, significantly influencing cell invasion capacity. In SC5314 attenuation through factors present in the host environment also implied a reduction in its cell invasion capacity and in *ECE1* expression, a key hyphae-associated virulence gene (encoding the Candidalysin peptide). Both could be restored by 5-Aza treatment, again strongly indicating an involvement of DNA methylation in gene regulation.

Besides further analysis on our sequencing data, addressing questions like a correlation between expression of specific genes and their DNA methylation patterns, we aim to perform transcriptomic analysis of the clinical isolates (with and without 5-Aza treatment) already investigated by WGBS. Further, we aim to delete the potential DNMTase candidate gene *NCL1* in a clinical isolate and SC5314 and investigate their methylome as well as transcriptome to explore its potential role as a DNA-active enzyme.

4.11.1 Clinical aspects of 5-Aza treatment

Fungal infections are a consistent problem for oncological patients and the main cause for morbidity and mortality during chemotherapeutic treatment (Mousset *et al.*, 2014), with *C. albicans* as one of the major causes for opportunistic microbial infections in these patients (Teoh and Pavelka, 2016). Our results indicate a further problem during chemotherapeutic treatment with demethylating agents, as in general it is not clear what kind of effect an application of these kind of substances could have on pathogenic microorganisms residing in the human body. The concentration of 5-Azacytidine normally reachable in the blood of a patient during chemotherapy is ~0.5 – 11 µM and the drug elimination half life time 48 – 72 h (Marcucci *et al.*, 2005; Liu *et al.*, 2006). This concentration is only ~1/100 – 1/500 lower than the concentration used in our experiments, however with a longer exposure time (as our medium was exchanged and cells were washed after 24 hours). Thus, a similar effect as shown in our experiments appears possible, inducing a switch of previously attenuated to more virulent *C. albicans* cells. These would have a significantly higher potential for invasive growth as also shown above. Consequently, an antifungal therapy prior to chemotherapy represents an important consideration, especially in the application of demethylating chemotherapies.

5 REFERENCES

Acton, R. J. *et al.* (2021) 'The genomic loci of specific human tRNA genes exhibit ageing-related DNA hypermethylation', *Nature Communications*. Nature Publishing Group, 12(1), p. 2655. doi: 10.1038/s41467-021-22639-6.

Afgan, E. *et al.* (2018) 'The Galaxy platform for accessible, reproducible and collaborative biomedical analyses: 2018 update.', *Nucleic acids research*. Oxford University Press, 46(W1), pp. W537–W544. doi: 10.1093/nar/gky379.

Alby, K., Schaefer, D. and Bennett, R. J. (2009) 'Homothallic and heterothallic mating in the opportunistic pathogen Candida albicans', *Nature 2009 460:7257*. Nature Publishing Group, 460(7257), pp. 890–893. doi: 10.1038/nature08252.

Anderson, J., Mihalik, R. and Soll, D. R. (1990) 'Ultrastructure and antigenicity of the unique cell wall pimple of the Candida opaque phenotype.', *Journal of bacteriology*. American Society for Microbiology (ASM), 172(1), pp. 224–35. doi: 10.1128/jb.172.1.224-235.1990.

Anderson, M. Z. *et al.* (2019) 'A "parameiosis" drives depolyploidization and homologous recombination in Candida albicans', *Nature Communications*. Nature Publishing Group, 10(1), p. 4388. doi: 10.1038/s41467-019-12376-2.

Aoki, Y. *et al.* (1998) '[Rbf1 (RPG-box binding factor), a transcription factor involved in yeast-hyphal transition of Candida albicans].', *Nihon Ishinkin Gakkai zasshi = Japanese journal of medical mycology*. Nihon Ishinkin Gakkai Zasshi, 39(2), pp. 67–71. doi: 10.3314/jjmm.39.67.

Aramayo, R. and Selker, E. U. (2013) 'Neurospora crassa, a model system for epigenetics research.', *Cold Spring Harbor perspectives in biology*. Cold Spring Harbor Laboratory Press, 5(10), p. a017921. doi: 10.1101/cshperspect.a017921.

Arendrup, M. C. and Patterson, T. F. (2017) 'Multidrug-Resistant Candida: Epidemiology, Molecular Mechanisms, and Treatment', *The Journal of Infectious Diseases*. Oxford Academic, 216(suppl_3), pp. S445–S451. doi: 10.1093/INFDIS/JIX131.

Argemí, A. and Saurina, J. (2007) 'Study of the degradation of 5-azacytidine as a model of unstable drugs using a stopped-flow method and further data analysis with multivariate curve resolution', *Talanta*, 74(2), pp. 176–182. doi: 10.1016/j.talanta.2007.05.053.

Bader, O. *et al.* (2011) 'Improved clinical laboratory identification of human pathogenic yeasts by matrix-assisted laser desorption ionization time-of-flight mass spectrometry', *Clinical Microbiology and Infection*. Elsevier, 17(9), pp. 1359–1365. doi: 10.1111/J.1469-0691.2010.03398.X.

Ball, M. P. *et al.* (2009) 'Targeted and genome-scale strategies reveal gene-body methylation signatures in human cells.', *Nature biotechnology*. Nat Biotechnol, 27(4), pp. 361–8. doi: 10.1038/nbt.1533.

Bannister, A. J. *et al.* (2001) 'Selective recognition of methylated lysine 9 on histone H3 by the HP1 chromo domain.', *Nature*. Nature, 410(6824), pp. 120–4. doi: 10.1038/35065138.

Bannister, A. J. and Kouzarides, T. (2011) 'Regulation of chromatin by histone modifications', *Cell Research*. Nature Publishing Group, 21(3), pp. 381–395. doi: 10.1038/cr.2011.22.

El Barkani, A. *et al.* (2000) 'Dominant active alleles of RIM101 (PRR2) bypass the pH restriction on filamentation of Candida albicans.', *Molecular and cellular biology*. American Society for Microbiology (ASM), (2013), pp. 4635–47. doi: 10.1128/MCB.20.13.4635-4647.2000.

Bartelli, T. F., Bruno, D. C. F. and Briones, M. R. S. (2018) 'Evidence for Mitochondrial Genome Methylation in the Yeast Candida albicans: A Potential Novel Epigenetic Mechanism Affecting Adaptation and Pathogenicity?', *Frontiers in genetics*. Frontiers Media SA, 9, p. 166. doi: 10.3389/fgene.2018.00166.

Bauer, W. R. *et al.* (1994) 'Nucleosome structural changes due to acetylation.', *Journal of molecular biology*. J Mol Biol, 236(3), pp. 685–90. doi: 10.1006/jmbi.1994.1180.

Bennett, R. J. and Johnson, A. D. (2003) 'Completion of a parasexual cycle in Candida albicans by induced chromosome loss in tetraploid strains.', *The EMBO journal*. European Molecular Biology Organization, 22(10), pp. 2505–15. doi: 10.1093/emboj/cdg235.

Berman, J. (2006) 'Morphogenesis and cell cycle progression in Candida albicans', *Current Opinion in Microbiology*, 9(6), pp. 595–601. doi: 10.1016/j.mib.2006.10.007.

Bernhard, M. *et al.* (2014) 'Yeast on-target lysis (YOTL), a procedure for making auxiliary mass spectrum data sets for clinical routine identification of yeasts.', *Journal of clinical microbiology*. American Society for Microbiology (ASM), 52(12), pp. 4163–7. doi: 10.1128/JCM.02128-14.

Bewick, A. J. *et al.* (2017) 'Evolution of DNA Methylation across Insects.', *Molecular biology and evolution*. Mol Biol Evol, 34(3), pp. 654–665. doi: 10.1093/molbev/msw264.

Bewick, A. J. *et al.* (2019) 'Diversity of cytosine methylation across the fungal tree of life', *Nature Ecology and Evolution*, 3(3), pp. 479–490. doi: 10.1038/s41559-019-0810-9.

Bewick, A. J. and Schmitz, R. J. (2017) 'Gene body DNA methylation in plants.', *Current opinion in plant biology*. Curr Opin Plant Biol, 36, pp. 103–110. doi: 10.1016/j.pbi.2016.12.007.

Bhattacharya, S., Bouklas, T. and Fries, B. C. (2021) 'Replicative aging in pathogenic fungi', *Journal of Fungi*, 7(1), pp. 1–14. doi: 10.3390/jof7010006.

Bird, A. (2002) 'DNA methylation patterns and epigenetic memory', *Genes and Development*. Cold Spring Harbor Laboratory Press, pp. 6–21. doi: 10.1101/gad.947102.

Biswas, S., Van Dijck, P. and Datta, A. (2007) 'Environmental sensing and signal transduction pathways regulating morphopathogenic determinants of Candida albicans.', *Microbiology and molecular biology reviews : MMBR*. Microbiol Mol Biol Rev, 71(2), pp. 348–76. doi: 10.1128/MMBR.00009-06.

Bolger, A. M., Lohse, M. and Usadel, B. (2014) 'Trimmomatic: a flexible trimmer for Illumina sequence data', *Bioinformatics*. Oxford Academic, 30(15), pp. 2114–2120. doi: 10.1093/bioinformatics/btu170.

Bostick, M. *et al.* (2007) 'UHRF1 Plays a Role in Maintaining DNA Methylation in Mammalian Cells', *Science*. American Association for the Advancement of Science , 317(5845), pp. 1760–1764. doi: 10.1126/science.1147939.

Bougnoux, M.-E. *et al.* (2003) 'Collaborative consensus for optimized multilocus sequence typing of Candida albicans.', *Journal of clinical microbiology*. J Clin Microbiol, 41(11), pp. 5265–6. doi: 10.1128/JCM.41.11.5265-5266.2003.

Bourc'his, D. *et al.* (2001) 'Dnmt3L and the establishment of maternal genomic imprints.', *Science (New York, N.Y.)*. Science, 294(5551), pp. 2536–9. doi: 10.1126/science.1065848.

Braun, B. R. *et al.* (2005) 'A Human-Curated Annotation of the Candida albicans Genome', *PLoS Genetics*. Edited by M. Snyder. Public Library of Science, 1(1), p. e1. doi: 10.1371/journal.pgen.0010001.

Braun, B. R. and Johnson, A. D. (1997) 'Control of filament formation in Candida albicans by the transcriptional repressor TUP1', *Science*. Science, 277(5322), pp. 105–109. doi: 10.1126/science.277.5322.105.

Braun, B. R. and Johnson, A. D. (2000) 'TUP1, CPH1 and EFG1 make independent contributions to filamentation in candida albicans.', *Genetics*. Oxford University Press, 155(1), pp. 57–67. doi: 10.1093/genetics/155.1.57.

Butler, G. *et al.* (2009) 'Evolution of pathogenicity and sexual reproduction in eight Candida genomes'. doi: 10.1038/nature08064.

Cambareri, E. *et al.* (1989) 'Repeat-induced G-C to A-T mutations in Neurospora', *Science*, 244(4912), pp. 1571–1575. doi: 10.1126/science.2544994.

Cao, X. and Jacobsen, S. E. (2002) 'Role of the arabidopsis DRM methyltransferases in de novo DNA methylation and gene silencing.', *Current biology : CB*. Curr Biol, 12(13), pp. 1138–44. doi: 10.1016/s0960-9822(02)00925-9.

Capuano, F. *et al.* (2014) 'Cytosine DNA methylation is found in Drosophila melanogaster but absent in Saccharomyces cerevisiae, Schizosaccharomyces pombe, and other yeast species.', *Analytical chemistry*. Anal Chem, 86(8), pp. 3697–702. doi: 10.1021/ac500447w.

Carninci, P. *et al.* (2006) 'Genome-wide analysis of mammalian promoter architecture and evolution.', *Nature genetics*. Nat Genet, 38(6), pp. 626–35. doi: 10.1038/ng1789.

Casadesús, J. and Low, D. (2006) 'Epigenetic gene regulation in the bacterial world.', *Microbiology and molecular biology reviews : MMBR*. American Society for Microbiology (ASM), 70(3), pp. 830–56. doi: 10.1128/MMBR.00016-06.

Catania, S. *et al.* (2017) 'Evolutionary persistence of DNA methylation for millions of years after ancient loss of a de novo methyltransferase', *bioRxiv*. Cold Spring Harbor Laboratory, p. 149385. doi: 10.1101/149385.

Catania, S. *et al.* (2020) 'Evolutionary Persistence of DNA Methylation for Millions of Years after Ancient Loss of a De Novo Methyltransferase', *Cell*. NIH Public Access, 180(2), pp. 263-277.e20. doi: 10.1016/j.cell.2019.12.012.

Chan, C. T. Y. *et al.* (2012) 'Reprogramming of tRNA modifications controls the oxidative stress response by codon-biased translation of proteins', *Nature Communications*. Nature Publishing Group, 3(1), p. 937. doi: 10.1038/ncomms1938.

Chen, L. *et al.* (1991) 'Direct identification of the active-site nucleophile in a DNA (cytosine-5)-methyltransferase.', *Biochemistry*. Biochemistry, 30(46), pp. 11018–25. doi: 10.1021/bi00110a002.

Ching, T.-T. *et al.* (2005) 'Epigenome analyses using BAC microarrays identify evolutionary conservation of tissue-specific methylation of SHANK3', *Nature Genetics*. Nature Publishing Group, 37(6), pp. 645–651. doi: 10.1038/ng1563.

Chiu, C.-P. and Blau, H. M. (1985) '5-azacytidine permits gene activation in a previously noninducible cell type', *Cell*. Cell Press, 40(2), pp. 417–424. doi: 10.1016/0092-8674(85)90155-2.

Chowdhary, A., Sharma, C. and Meis, J. F. (2017) 'Candida auris: A rapidly emerging cause of hospital-acquired multidrug-resistant fungal infections globally', *PLOS Pathogens*. Public Library of Science, 13(5), p. e1006290. doi: 10.1371/JOURNAL.PPAT.1006290.

Christman, J. K. (2002) '5-Azacytidine and 5-aza-2'-deoxycytidine as inhibitors of DNA methylation: mechanistic studies and their implications for cancer therapy', *Oncogene*. Nature Publishing Group, 21(35), pp. 5483–5495. doi: 10.1038/sj.onc.1205699.

Cleary, I. A. *et al.* (2016) 'Examination of the pathogenic potential of Candida albicans filamentous cells in an animal model of haematogenously disseminated candidiasis', *FEMS Yeast Research*, 16, p. 11. doi: 10.1093/femsyr/fow011.

Crooks, G. E. *et al.* (2004) 'WebLogo: A sequence logo generator', *Genome Research*. Cold Spring Harbor Laboratory Press, 14(6), pp. 1188–1190. doi: 10.1101/gr.849004.

Cuomo, C. A. *et al.* (2019) 'Genome Sequence for Candida albicans Clinical Oral Isolate 529L.', *Microbiology resource announcements*. American Society for Microbiology (ASM), 8(25). doi: 10.1128/MRA.00554-19.

D'enfert, C. and Janbon, G. (2016) 'Biofilm formation in Candida glabrata: What have we learnt from functional genomics approaches?', *FEMS Yeast Research*, 16, p. 111. doi: 10.1093/femsyr/fov111.

Daniels, K. J. *et al.* (2013) 'Impact of Environmental Conditions on the Form and Function of Candida albicans Biofilms', *Eukaryotic Cell*. American Society for Microbiology (ASM), 12(10), p. 1389. doi: 10.1128/EC.00127-13.

Davis-Hanna, A. *et al.* (2008) 'Farnesol and dodecanol effects on the Candida albicans Ras1-cAMP signalling pathway and the regulation of morphogenesis.', *Molecular microbiology*. Mol Microbiol, 67(1), pp. 47–62. doi: 10.1111/j.1365-2958.2007.06013.x.

Davis, D. (2003) 'Adaptation to environmental pH in Candida albicans and its relation to pathogenesis', *Current Genetics*. Springer, 44(1), pp. 58–58. doi: 10.1007/s00294-003-0431-2.

Davis, D., Wilson, R. B. and Mitchell, A. P. (2000) 'RIM101-dependent and-independent pathways govern pH responses in Candida albicans.', *Molecular and cellular biology*. Mol Cell Biol, 20(3), pp. 971–8. doi: 10.1128/MCB.20.3.971-978.2000.

Dhayalan, A. *et al.* (2010) 'The Dnmt3a PWWP domain reads histone 3 lysine 36 trimethylation and guides DNA methylation.', *The Journal of biological chemistry*. J Biol Chem, 285(34), pp. 26114–20. doi: 10.1074/jbc.M109.089433.

Doedt, T. *et al.* (2004) 'APSES proteins regulate morphogenesis and metabolism in Candida albicans', *Molecular Biology of the Cell*. American Society for Cell Biology, 15(7), pp. 3167–3180. doi: 10.1091/mbc.E03-11-0782.

Domcke, S. *et al.* (2015) 'Competition between DNA methylation and transcription factors determines binding of NRF1.', *Nature*. Nature, 528(7583), pp. 575–9. doi: 10.1038/nature16462.

Dongari-Bagtzoglou, A. *et al.* (2009) 'Characterization of Mucosal Candida albicans Biofilms', *PLoS ONE*. Public Library of Science, 4(11), p. 7967. doi: 10.1371/JOURNAL.PONE.0007967.

DongLai, X. *et al.* (2018) *Evaluation of 20 Lentinula edodes strains using ISSR and F-MSAP markers*, *Jiangsu Journal of Agricultural Sciences*. Fujian Sheng nong ye ke xue yuan.

Dotis, J. *et al.* (2012) 'Epidemiology, risk factors and outcome of Candida parapsilosis bloodstream infection in children.', *The Pediatric infectious disease journal*. NIH Public Access, 31(6), pp. 557–60. doi: 10.1097/INF.0b013e31824da7fe.

Drinnenberg, I. A. *et al.* (2009) 'RNAi in Budding Yeast', *Science*, 326(5952), pp. 544–550. doi: 10.1126/science.1176945.

Du, J. *et al.* (2015) 'DNA methylation pathways and their crosstalk with histone methylation.', *Nature reviews. Molecular cell biology*. NIH Public Access, 16(9), pp. 519–32. doi: 10.1038/nrm4043.

Duc, C. *et al.* (2015) 'The histone chaperone complex HIR maintains nucleosome occupancy and counterbalances impaired histone deposition in CAF-1 complex mutants.', *The Plant journal : for cell and molecular biology*. Plant J, 81(5), pp. 707–22. doi: 10.1111/tpj.12758.

Dumesic, P. A. *et al.* (2020) 'ATP Hydrolysis by the SNF2 Domain of Dnmt5 Is Coupled to Both Specific Recognition and Modification of Hemimethylated DNA', *Molecular Cell*. Cell Press, 79(1), pp. 127-139.e4. doi: 10.1016/J.MOLCEL.2020.04.029.

Dunn, M. F., Ramírez-Trujillo, J. A. and Hernández-Lucas, I. (2009) 'Major roles of isocitrate lyase and malate synthase in bacterial and fungal pathogenesis', *Microbiology*. Microbiology Society, pp. 3166–3175. doi: 10.1099/mic.0.030858-0.

Dunn, M. J. and Anderson, M. Z. (2019) 'To repeat or not to repeat: Repetitive sequences regulate genome stability in candida albicans', *Genes*, 10(11). doi: 10.3390/genes10110866.

Eckhardt, F. *et al.* (2006) 'DNA methylation profiling of human chromosomes 6, 20 and 22.', *Nature genetics*. Nat Genet, 38(12), pp. 1378–85. doi: 10.1038/ng1909.

Ene, I. V *et al.* (2018) 'Global analysis of mutations driving microevolution of a heterozygous diploid fungal pathogen.', *Proceedings of the National Academy of Sciences of the United States of America*. National Academy of Sciences, 115(37), pp. E8688–E8697. doi: 10.1073/pnas.1806002115.

Fan, D. *et al.* (2015) 'Activation of HIF-1α and LL-37 by commensal bacteria inhibits Candida albicans colonization', *Nature medicine*. NIH Public Access, 21(7), p. 808. doi: 10.1038/NM.3871.

Fan, L.-H. *et al.* (2019) 'Absence of mitochondrial DNA methylation in mouse oocyte maturation, aging and early embryo development', *Biochemical and Biophysical Research Communications*. Academic Press, 513(4), pp. 912–918. doi: 10.1016/J.BBRC.2019.04.100.

Fitzpatrick, D. A. *et al.* (2006) 'A fungal phylogeny based on 42 complete genomes derived from supertree and combined gene analysis'. doi: 10.1186/1471-2148-6-99.

Flanagan, J. M. and Wild, L. (2007) 'An epigenetic role for noncoding RNAs and intragenic DNA methylation', *Genome Biology*. BioMed Central, 8(6), p. 307. doi: 10.1186/gb-2007-8-6-307.

Flores-Sierra, J. *et al.* (2016) 'The trans fatty acid elaidate affects the global DNA methylation profile of cultured cells and in vivo', *Lipids in Health and Disease*. BioMed Central, 15(1), p. 75. doi: 10.1186/s12944-016-0243-2.

Flores, K. *et al.* (2012) 'Genome-wide association between DNA methylation and alternative splicing in an invertebrate.', *BMC genomics*. BioMed Central, 13, p. 480. doi: 10.1186/1471-2164-13-480.

Fonzi, W. A. *et al.* (1998) *The pH of the Host Niche Controls Gene*, *Infect. Immun*.

Forche, A. *et al.* (2008) 'The Parasexual Cycle in Candida albicans Provides an Alternative Pathway to Meiosis for the Formation of Recombinant Strains', *PLoS Biology*. Edited by J. Heitman. Public Library of Science, 6(5), p. e110. doi: 10.1371/journal.pbio.0060110.

Formighieri, E. F. *et al.* (2008) 'The mitochondrial genome of the phytopathogenic basidiomycete Moniliophthora perniciosa is 109 kb in size and contains a stable integrated plasmid', *Mycological Research*, 112(10), pp. 1136–1152. doi: 10.1016/j.mycres.2008.04.014.

Franzen, J. *et al.* (2021) 'DNA methylation changes during long-term in vitro cell culture are caused by epigenetic drift', *Communications Biology*. Nature Publishing Group, 4(1), p. 598. doi: 10.1038/s42003-021-02116-y.

Fuso, A. (2018) 'Non-CpG Methylation Revised', *Epigenomes*. MDPI AG, 2(4), p. 22. doi: 10.3390/epigenomes2040022.

Fux, C. A. *et al.* (2005) 'Can laboratory reference strains mirror "real-world" pathogenesis?', *Trends in microbiology*. Trends Microbiol, 13(2), pp. 58–63. doi: 10.1016/j.tim.2004.11.001.

Ghoshal, K. *et al.* (2005) '5-Aza-deoxycytidine induces selective degradation of DNA methyltransferase 1 by a proteasomal pathway that requires the KEN box, bromo-adjacent homology domain, and nuclear localization signal.', *Molecular and cellular biology*. Mol Cell Biol, 25(11), pp. 4727–41. doi: 10.1128/MCB.25.11.4727-4741.2005.

Gladyshev, E. and Kleckner, N. (2017) 'DNA sequence homology induces cytosine-to-thymine mutation by a heterochromatin-related pathway in Neurospora.', *Nature genetics*. NIH Public Access, 49(6), pp. 887–894. doi: 10.1038/ng.3857.

Goll, M. G. and Halpern, M. E. (2011) 'DNA methylation in zebrafish.', *Progress in molecular biology and translational science*. Prog Mol Biol Transl Sci, 101, pp. 193–218. doi: 10.1016/B978-0-12-387685-0.00005-6.

Gómez-Díaz, E. *et al.* (2012) 'Epigenetics of Host-Pathogen Interactions: The Road Ahead and the Road Behind', *PLoS Pathogens*, 8(11). doi: 10.1371/journal.ppat.1003007.

Gore, S. D. *et al.* (2006) 'Combined DNA methyltransferase and histone deacetylase inhibition in the treatment of myeloid neoplasms', *Cancer Research*. Cancer Res, 66(12), pp. 6361–6369. doi: 10.1158/0008-5472.CAN-06-0080.

Gow, N. A. ., Brown, A. J. . and Odds, F. C. (2002) 'Fungal morphogenesis and host invasion', *Current Opinion in Microbiology*. Elsevier Current Trends, pp. 366–371. doi: 10.1016/S1369-5274(02)00338-7.

Gowher, H., Ehrlich, K. C. and Jeltsch, A. (2001) 'DNA from *Aspergillus flavus* contains 5-methylcytosine', *FEMS Microbiology Letters*. Oxford University Press, 205(1), pp. 151–155. doi: 10.1111/j.1574-6968.2001.tb10939.x.

Grayburn, W. S. and Selker, E. U. (1989) 'A natural case of RIP: degeneration of the DNA sequence in an ancestral tandem duplication.', *Molecular and cellular biology*. Mol Cell Biol, 9(10), pp. 4416–21. doi: 10.1128/mcb.9.10.4416-4421.1989.

Greenberg, J. R. *et al.* (2005) 'Candida albicans SOU1 encodes a sorbose reductase required for L-sorbose utilization.', *Yeast (Chichester, England)*. Yeast, 22(12), pp. 957–69. doi: 10.1002/yea.1282.

Grubb, S. E. W. *et al.* (2009) 'Adhesion of Candida albicans to endothelial cells under physiological conditions of flow.', *Infection and immunity*. Infect Immun, 77(9), pp. 3872–8. doi: 10.1128/IAI.00518-09.

Gu, Y. *et al.* (2019) 'Promoter methylation of the candidate tumor suppressor gene TCF21 in myelodysplastic syndrome and acute myeloid leukemia', *American Journal of Translational Research*. e-Century Publishing Corporation, 11(6), pp. 3450–3460.

Guil, S. and Esteller, M. (2009) 'DNA methylomes, histone codes and miRNAs: tying it all together.', *The international journal of biochemistry & cell biology*. Int J Biochem Cell Biol, 41(1), pp. 87–95. doi: 10.1016/j.biocel.2008.09.005.

Gutierrez-Arcelus, M. *et al.* (2013) 'Passive and active DNA methylation and the interplay with genetic variation in gene regulation.', *eLife*. Elife, 2, p. e00523. doi: 10.7554/eLife.00523.

Hallen-Adams, H. E. and Suhr, M. J. (2017) 'Fungi in the healthy human gastrointestinal tract', *Virulence*. Taylor & Francis, pp. 352–358. doi: 10.1080/21505594.2016.1247140.

Harshman, S. W. *et al.* (2013) 'H1 histones: current perspectives and challenges.', *Nucleic acids research*. Oxford University Press, 41(21), pp. 9593–609. doi: 10.1093/nar/gkt700.

Hazen, K. C. *et al.* (2003) 'Comparison of the Susceptibilities of Candida spp. to Fluconazole and Voriconazole in a 4-Year Global Evaluation Using Disk Diffusion', *Journal of Clinical Microbiology*. American Society for Microbiology (ASM), 41(12), p. 5623. doi: 10.1128/JCM.41.12.5623-5632.2003.

Héberlé, É. and Bardet, A. F. (2019) 'Sensitivity of transcription factors to DNA methylation.', *Essays in biochemistry*. Portland Press Ltd, 63(6), pp. 727–741. doi: 10.1042/EBC20190033.

Hermann, A., Schmitt, S. and Jeltsch, A. (2003) 'The Human Dnmt2 Has Residual DNA-(Cytosine-C5) Methyltransferase Activity', *Journal of Biological Chemistry*. Elsevier, 278(34), pp. 31717–31721. doi: 10.1074/jbc.M305448200.

Hernando-Herraez, I. *et al.* (2015) 'DNA Methylation: Insights into Human Evolution', *PLOS Genetics*. Edited by R. J. Oakey. Public Library of Science, 11(12), p. e1005661. doi: 10.1371/journal.pgen.1005661.

Hongs, L. *et al.* (1993) *Studies of the DNA binding properties of histone H4 amino terminus. Thermal denaturation studies reveal that acetylation markedly reduces the binding constant of the H4 â€œtailâ€ to DNA.*, *THE JOURNAL OF BIOLOGICAL CHEMISTRY*. doi: 10.1016/S0021-9258(18)54150-8.

Hosseini, S. *et al.* (2020) 'Comparative analysis of genome-wide DNA methylation in Neurospora.', *Epigenetics*. Taylor & Francis, 15(9), pp. 972–987. doi: 10.1080/15592294.2020.1741758.

Hu, C.-W. *et al.* (2015) 'Trace analysis of methylated and hydroxymethylated cytosines in DNA by isotope-dilution LC-MS/MS: first evidence of DNA methylation in Caenorhabditis elegans.', *The Biochemical journal*. Biochem J, 465(1), pp. 39–47. doi: 10.1042/BJ20140844.

Huang, Y. W. *et al.* (2011) 'An overview of epigenetics and chemoprevention', *FEBS Letters*, pp. 2129–2136. doi: 10.1016/j.febslet.2010.11.002.

Huff, J. T. and Zilberman, D. (2014) 'Dnmt1-independent CG methylation contributes to nucleosome positioning in diverse eukaryotes.', *Cell*. NIH Public Access, 156(6), pp. 1286–1297. doi: 10.1016/j.cell.2014.01.029.

Hunt, B. G. *et al.* (2013) 'The function of intragenic DNA methylation: insights from insect epigenomes.', *Integrative and comparative biology*. Integr Comp Biol, 53(2), pp. 319–28. doi: 10.1093/icb/ict003.

Illingworth, R. *et al.* (2008) 'A Novel CpG Island Set Identifies Tissue-Specific Methylation at Developmental Gene Loci', *PLoS Biology*. Edited by E. T. Liu. Public Library of Science, 6(1), p. e22. doi: 10.1371/journal.pbio.0060022.

Ito, S. *et al.* (2011) 'Tet proteins can convert 5-methylcytosine to 5-formylcytosine and 5-carboxylcytosine.', *Science (New York, N.Y.)*. Science, 333(6047), pp. 1300–3. doi: 10.1126/science.1210597.

Iyer, L. M. *et al.* (2009) 'Prediction of novel families of enzymes involved in oxidative and other complex modifications of bases in nucleic acids.', *Cell cycle (Georgetown, Tex.)*. Cell Cycle, 8(11), pp. 1698–710. doi: 10.4161/cc.8.11.8580.

Iyer, L. M. *et al.* (2014) 'Lineage-specific expansions of TET/JBP genes and a new class of DNA transposons shape fungal genomic and epigenetic landscapes.', *Proceedings of the National Academy of Sciences of the United States of America*. National Academy of Sciences, 111(5), pp. 1676–83. doi: 10.1073/pnas.1321818111.

Jackson, J. P. *et al.* (2002) 'Control of CpNpG DNA methylation by the KRYPTONITE histone H3 methyltransferase.', *Nature*. Nature, 416(6880), pp. 556–60. doi: 10.1038/nature731.

Jeltsch, A., Nellen, W. and Lyko, F. (2006) 'Two substrates are better than one: dual specificities for Dnmt2 methyltransferases.', *Trends in biochemical sciences*. Trends Biochem Sci, 31(6), pp. 306–8. doi: 10.1016/j.tibs.2006.04.005.

Jenull, S. *et al.* (2017) 'The Candida albicans HIR histone chaperone regulates the yeast-to-hyphae transition by controlling the sensitivity to morphogenesis signals', *Scientific Reports*, 7(1). doi: 10.1038/s41598-017-08239-9.

Jenuwein, T. and Allis, C. D. (2001) 'Translating the histone code.', *Science (New York, N.Y.)*. Science, 293(5532), pp. 1074–80. doi: 10.1126/science.1063127.

Jeon, J. *et al.* (2015) 'Genome-wide profiling of DNA methylation provides insights into epigenetic regulation of fungal development in a plant pathogenic fungus, Magnaporthe oryzae', *Scientific Reports*. Nature Publishing Group, 5(1), p. 8567. doi: 10.1038/srep08567.

Jin, C. *et al.* (2009) 'H3.3/H2A.Z double variant-containing nucleosomes mark "nucleosome-free regions" of active promoters and other regulatory regions.', *Nature genetics*. Nat Genet, 41(8), pp. 941–5. doi: 10.1038/ng.409.

Jolley, K. A., Bray, J. E. and Maiden, M. C. J. (2018) 'Open-access bacterial population genomics: BIGSdb software, the PubMLST.org website and their applications.', *Wellcome open research*. Wellcome Open Res, 3, p. 124. doi: 10.12688/wellcomeopenres.14826.1.

Jones, P. A. and Laird, P. W. (1999) 'Cancer epigenetics comes of age.', *Nature genetics*. Nat Genet, 21(2), pp. 163–7. doi: 10.1038/5947.

Jones, P. A. and Taylor, S. M. (1980) 'Cellular differentiation, cytidine analogs and DNA methylation', *Cell*. Elsevier, 20(1), pp. 85–93. doi: 10.1016/0092-8674(80)90237-8.

Kebaara, B. W. *et al.* (2008) 'Candida albicans Tup1 is involved in farnesol-mediated inhibition of filamentous-growth induction.', *Eukaryotic cell*. American Society for Microbiology (ASM), 7(6), pp. 980–7. doi: 10.1128/EC.00357-07.

Khalaf, R. A. and Zitomer, R. S. (2001) 'The DNA binding protein Rfg1 is a repressor of filamentation in Candida albicans.', *Genetics*. Oxford University Press, 157(4), pp. 1503–12. doi: 10.1093/genetics/157.4.1503.

Khalil, A. M. *et al.* (2009) 'Many human large intergenic noncoding RNAs associate with chromatin-modifying complexes and affect gene expression.', *Proceedings of the National Academy of Sciences of the United States of America*. National Academy of Sciences, 106(28), pp. 11667–72. doi: 10.1073/pnas.0904715106.

Kihslinger, J. E. and Godley, L. A. (2007) 'The use of hypomethylating agents in the treatment of hematologic malignancies', *Leukemia & Lymphoma*. Taylor & Francis, 48(9), pp. 1676–1695. doi: 10.1080/10428190701493910.

Kim, D., Langmead, B. and Salzberg, S. L. (2015) 'HISAT: a fast spliced aligner with low memory requirements', *Nature Methods*. Nature Publishing Group, 12(4), pp. 357–360. doi: 10.1038/nmeth.3317.

Kimura, K. *et al.* (2006) 'Diversification of transcriptional modulation: large-scale identification and characterization of putative alternative promoters of human genes.', *Genome research*. Genome Res, 16(1), pp. 55–65. doi: 10.1101/gr.4039406.

Koehler, P. *et al.* (2019) 'Morbidity and mortality of candidaemia in Europe: an epidemiologic meta-analysis', *Clinical Microbiology and Infection*. Elsevier Ltd, 25(10), pp. 1200–1212. doi: 10.1016/j.cmi.2019.04.024.

Kojic, E. M. and Darouiche, R. O. (2004) 'Candida Infections of Medical Devices', *Clinical Microbiology Reviews*. American Society for Microbiology (ASM), 17(2), p. 255. doi: 10.1128/CMR.17.2.255-267.2004.

Kouzarides, T. (2007) 'Chromatin modifications and their function.', *Cell*. Elsevier, 128(4), pp. 693–705. doi: 10.1016/j.cell.2007.02.005.

Kouzminova, E. and Selker, E. U. (2001) 'dim-2 encodes a DNA methyltransferase responsible for all known cytosine methylation in Neurospora.', *The EMBO journal*. European Molecular Biology Organization, 20(15), pp. 4309–23. doi: 10.1093/emboj/20.15.4309.

Krueger, F. and Andrews, S. R. (2011) 'Bismark: a flexible aligner and methylation caller for Bisulfite-Seq applications', *BIOINFORMATICS APPLICATIONS NOTE*, 27(11), pp. 1571–1572. doi: 10.1093/bioinformatics/btr167.

Kulis, M. *et al.* (2012) 'Epigenomic analysis detects widespread gene-body DNA hypomethylation in chronic lymphocytic leukemia.', *Nature genetics*. Nat Genet, 44(11), pp. 1236–42. doi: 10.1038/ng.2443.

Kurtzman, C. P. and Robnett, C. J. (2013) 'Relationships among genera of the Saccharomycotina (Ascomycota) from multigene phylogenetic analysis of type species', *FEMS Yeast Research*. FEMS Yeast Res, 13(1), pp. 23–33. doi: 10.1111/1567-1364.12006.

Lackey, E. *et al.* (2013) 'Comparative evolution of morphological regulatory functions in Candida species', *Eukaryotic Cell*. Eukaryot Cell, 12(10), pp. 1356–1368. doi: 10.1128/EC.00164-13.

Lamparska, K. *et al.* (2012) '2'-Deoxyriboguanylurea, the primary breakdown product of 5-aza-2'-deoxyribocytidine, is a mutagen, an epimutagen, an inhibitor of DNA methyltransferases and an inducer of 5-azacytidine-type fragile sites', *Nucleic Acids Research*. Oxford University Press, 40(19), pp. 9788–9801. doi: 10.1093/nar/gks706.

Laurent, L. *et al.* (2010) 'Dynamic changes in the human methylome during differentiation.', *Genome research*. Cold Spring Harbor Laboratory Press, 20(3), pp. 320–31. doi: 10.1101/gr.101907.109.

Leberer, E. *et al.* (2008) 'Ras links cellular morphogenesis to virulence by regulation of the MAP kinase and cAMP signalling pathways in the pathogenic fungus Candida albicans', *Molecular Microbiology*. John Wiley & Sons, Ltd, 42(3), pp. 673–687. doi: 10.1046/j.1365-2958.2001.02672.x.

Lee, D. W. *et al.* (2008) 'A cytosine methyltransferase homologue is essential for sexual development in Aspergillus nidulans', *PLoS ONE*, 3(6), pp. 1–10. doi: 10.1371/journal.pone.0002531.

Lee, D. Y. *et al.* (1993) 'A positive role for histone acetylation in transcription factor access to nucleosomal DNA.', *Cell*. Cell, 72(1), pp. 73–84. doi: 10.1016/0092-8674(93)90051-q.

Lee, J. E. *et al.* (2015) 'Ssn6 has dual roles in Candida albicans filament development through the interaction with Rpd31', *FEBS Letters*, 589(4). doi: 10.1016/j.febslet.2015.01.011.

Lee, K. L., Buckley, H. R. and Campbell, C. C. (1975) 'An amino acid liquid synthetic medium for the development of mycellal and yeast forms of candida albicans', *Medical Mycology*, 13(2), pp. 148–153. doi: 10.1080/00362177585190271.

Lew, D. J. and Reed, S. I. (1995) 'Cell cycle control of morphogenesis in budding yeast', *Current Opinion in Genetics & Development*. Elsevier Current Trends, 5(1), pp. 17–23. doi: 10.1016/S0959-437X(95)90048-9.

Lewis, Z. A. *et al.* (2009) 'Relics of repeat-induced point mutation direct heterochromatin formation in Neurospora crassa.', *Genome research*. Genome Res, 19(3), pp. 427–37. doi: 10.1101/gr.086231.108.

Li, A. and Horgen, P. A. (1993) 'Evidence for Cytosine Methylation in Ribosomal RNA Genes and in a Family of Dispersed Repetitive DNA Elements in Agaricus bisporus and Selected Other Agaricus Species', *Experimental Mycology*, pp. 356–361. doi: 10.1006/emyc.1993.1034.

Li, E., Beard, C. and Jaenisch, R. (1993) 'Role for DNA methylation in genomic imprinting.', *Nature*. Nature, 366(6453), pp. 362–5. doi: 10.1038/366362a0.

Li, E., Bestor, T. H. and Jaenisch, R. (1992) 'Targeted mutation of the DNA methyltransferase gene results in embryonic lethality.', *Cell*. Cell, 69(6), pp. 915–26. doi: 10.1016/0092-8674(92)90611-f.

Li, H. *et al.* (2009) 'The Sequence Alignment/Map format and SAMtools.', *Bioinformatics (Oxford, England)*. Bioinformatics, 25(16), pp. 2078–9. doi: 10.1093/bioinformatics/btp352.

Li, W. *et al.* (2017) 'Differential DNA methylation may contribute to temporal and spatial regulation of gene expression and the development of mycelia and conidia in entomopathogenic fungus Metarhizium robertsii', *Fungal Biology*. Elsevier Ltd, 121(3), pp. 293–303. doi: 10.1016/j.funbio.2017.01.002.

Li, Z. *et al.* (2020) 'DNA methylation and gene expression profiles characterize epigenetic regulation of lncRNAs in colon adenocarcinoma', *Journal of Cellular Biochemistry*, 121(3), pp. 2406–2415. doi: 10.1002/jcb.29463.

Liao, Y., Smyth, G. K. and Shi, W. (2014) 'featureCounts: an efficient general purpose program for assigning sequence reads to genomic features', *Bioinformatics*. Oxford Academic, 30(7), pp. 923–930. doi: 10.1093/bioinformatics/btt656.

Lindroth, A. M. *et al.* (2001) 'Requirement of CHROMOMETHYLASE3 for maintenance of CpXpG methylation.', *Science (New York, N.Y.)*. Science, 292(5524), pp. 2077–80. doi: 10.1126/science.1059745.

Lisch, D. (2009) 'Epigenetic regulation of transposable elements in plants.', *Annual review of plant biology*. Annu Rev Plant Biol, 60, pp. 43–66. doi: 10.1146/annurev.arplant.59.032607.092744.

Liu, J. *et al.* (2021) 'A variant ECE1 allele contributes to reduced pathogenicity of Candida albicans during vulvovaginal candidiasis', *PLoS Pathogens*, 17(9), pp. 1–24. doi: 10.1371/journal.ppat.1009884.

Liu, S.-Y. *et al.* (2012) 'Bisulfite Sequencing Reveals That Aspergillus flavus Holds a Hollow in DNA Methylation', *PLoS ONE*. Edited by M. Pellegrini. Public Library of Science, 7(1), p. e30349. doi: 10.1371/journal.pone.0030349.

Liu, Z. *et al.* (2006) 'Characterization of decomposition products and preclinical and low dose clinical pharmacokinetics of decitabine (5-aza-2'-deoxycytidine) by a new liquid chromatography/tandem mass spectrometry quantification method', *Rapid Communications in Mass Spectrometry*, 20(7), pp. 1117–1126. doi: 10.1002/rcm.2423.

Lo, H.-J. *et al.* (1997) 'Nonfilamentous C. albicans Mutants Are Avirulent', *Cell*. Elsevier, 90(5), pp. 939–949. doi: 10.1016/S0092-8674(00)80358-X.

Lockhart, S. R. *et al.* (2017) 'Simultaneous Emergence of Multidrug-Resistant Candida auris on 3 Continents Confirmed by Whole-Genome Sequencing and Epidemiological Analyses', *Clinical Infectious Diseases*. Oxford Academic, 64(2), pp. 134–140. doi: 10.1093/CID/CIW691.

Lorenz, M. C. and Fink, G. R. (2001) 'The glyoxylate cycle is required for fungal virulence.', *Nature*. Nature, 412(6842), pp. 83–6. doi: 10.1038/35083594.

Love, M. I., Huber, W. and Anders, S. (2014) 'Moderated estimation of fold change and dispersion for RNA-seq data with DESeq2', *Genome Biology*. BioMed Central Ltd., 15(12), p. 550. doi: 10.1186/s13059-014-0550-8.

Lu, Y. *et al.* (2008) 'Efg1-mediated recruitment of NuA4 to promoters is required for hypha-specific Swi/Snf binding and activation in Candida albicans.', *Molecular biology of the cell*. American Society for Cell Biology, 19(10), pp. 4260–72. doi: 10.1091/mbc.e08-02-0173.

Lu, Y. *et al.* (2011) 'Hyphal development in Candida albicans requires two temporally linked changes in promoter chromatin for initiation and maintenance.', *PLoS biology*. Public Library of Science, 9(7), p. e1001105. doi: 10.1371/journal.pbio.1001105.

Luger, K. *et al.* (1997) 'Crystal structure of the nucleosome core particle at 2.8 A resolution.', *Nature*. Nature, 389(6648), pp. 251–60. doi: 10.1038/38444.

Lüttich, A. *et al.* (2013) 'Serial passaging of Candida albicans in systemic murine infection suggests that the wild type strain SC5314 is well adapted to the murine kidney.', *PloS one*. Edited by D. R. Andes, 8(5), p. e64482. doi: 10.1371/journal.pone.0064482.

Lynch, D. B. *et al.* (2010) 'Chromosomal G + C content evolution in yeasts: Systematic interspecies differences, and GC-poor troughs at centromeres', *Genome Biology and Evolution*, 2(1), pp. 572–583. doi: 10.1093/gbe/evq042.

Maestrone, G. and Semar, R. (1968) 'Establishment and treatment of cutaneous Candida albicans infection in the rabbit', *Die Naturwissenschaften*, 55(2), pp. 87–88. doi: 10.1007/BF00599501.

Malagnac, F. *et al.* (1997) 'A gene essential for de novo methylation and development in Ascobolus reveals a novel type of eukaryotic DNA methyltransferase structure.', *Cell*. Cell, 91(2), pp. 281–90. doi: 10.1016/s0092-8674(00)80410-9.

Malani, A. N. *et al.* (2011) 'Is age a risk factor for Candida glabrata colonisation?', *Mycoses*. Mycoses, 54(6), pp. 531–7. doi: 10.1111/j.1439-0507.2010.01941.x.

Marcucci, G. *et al.* (2005) 'Bioavailability of azacitidine subcutaneous versus intravenous in patients with the myelodysplastic syndromes.', *Journal of clinical pharmacology*. J Clin Pharmacol, 45(5), pp. 597–602. doi: 10.1177/0091270004271947.

Martin-Trujillo, A. *et al.* (2020) 'Rare genetic variation at transcription factor binding sites modulates local DNA methylation profiles', *PLOS Genetics*. Edited by C. Relton. Public Library of Science, 16(11), p. e1009189. doi: 10.1371/journal.pgen.1009189.

Martin, M. (2011) 'Cutadapt removes adapter sequences from high-throughput sequencing reads', *EMBnet.journal*, 17(1), p. 10. doi: 10.14806/ej.17.1.200.

Martin, R. *et al.* (2013) 'A Core Filamentation Response Network in Candida albicans Is Restricted to Eight Genes', *PLoS ONE*. Public Library of Science, 8(3), p. e58613. doi: 10.1371/journal.pone.0058613.

Matzke, M. A. and Mosher, R. A. (2014) 'RNA-directed DNA methylation: an epigenetic pathway of increasing complexity.', *Nature reviews. Genetics*. Nat Rev Genet, 15(6), pp. 394–408. doi: 10.1038/nrg3683.

Maunakea, A. K. *et al.* (2010) 'Conserved role of intragenic DNA methylation in regulating alternative promoters', *Nature*, 466(7303), pp. 253–257. doi: 10.1038/nature09165.

Mccarty, T. P. and Pappas, P. G. (2015) 'Invasive Candidiasis', *Infectious Disease Clinics of NA*. doi: 10.1016/j.idc.2015.10.013.

Mechta, M. *et al.* (2017) 'Evidence suggesting absence of mitochondrial DNA methylation', *Frontiers in Genetics*. Frontiers, 8(NOV), p. 166. doi: 10.3389/fgene.2017.00166.

Meis, J. *et al.* (2000) 'A global evaluation of the susceptibility of Candida species to fluconazole by disk diffusion', *Diagnostic Microbiology and Infectious Disease*. Diagn Microbiol Infect Dis, 36(4), pp. 215–223. doi: 10.1016/S0732-8893(99)00152-2.

Meyer, W. *et al.* (2003) 'Molecular typing of IberoAmerican Cryptococcus neoformans isolates.', *Emerging infectious diseases*. Centers for Disease Control and Prevention, 9(2), pp. 189–95. doi: 10.3201/eid0902.020246.

Mishra, P. K., Baum, M. and Carbon, J. (2011) 'DNA methylation regulates phenotype-dependent transcriptional activity in Candida albicans', *Proceedings of the National Academy of Sciences*, 108(29), pp. 11965–11970. doi: 10.1073/pnas.1109631108.

Möller, M. *et al.* (2021) 'Recent loss of the Dim2 DNA methyltransferase decreases mutation rate in repeats and changes evolutionary trajectory in a fungal pathogen', *PLOS Genetics*. Edited by K. Krasileva. Public Library of Science, 17(3), p. e1009448. doi: 10.1371/journal.pgen.1009448.

Montero, L. M. *et al.* (1992) 'The distribution of 5-methylcytosine in the nuclear genome of plants.', *Nucleic acids research*. Oxford University Press, 20(12), pp. 3207–10. doi: 10.1093/nar/20.12.3207.

Mousset, S. *et al.* (2014) 'Treatment of invasive fungal infections in cancer patients-updated recommendations of the Infectious Diseases Working Party (AGIHO) of the German Society of Hematology and Oncology (DGHO).', *Annals of hematology*. Springer, 93(1), pp. 13–32. doi: 10.1007/s00277-013-1867-1.

Moyes, D. L. *et al.* (2016) 'Candidalysin is a fungal peptide toxin critical for mucosal infection', *Nature*. Nature Publishing Group, 532(7597), pp. 64–68. doi: 10.1038/nature17625.

Muñoz, J. F. *et al.* (2018) 'Genomic insights into multidrug-resistance, mating and virulence in Candida auris and related emerging species', *Nature Communications*, 9(1). doi: 10.1038/s41467-018-07779-6.

Murad, A. M. A. *et al.* (2001) 'NRG1 represses yeast-hypha morphogenesis and hypha-specific gene expression in Candida albicans', *EMBO Journal*. European Molecular Biology Organization, 20(17), pp. 4742–4752. doi: 10.1093/emboj/20.17.4742.

Nai, Y.-S. *et al.* (2021) 'Diversity of Fungal DNA Methyltransferases and Their Association With DNA Methylation Patterns', *Frontiers in Microbiology*. Frontiers, 11, p. 3614. doi: 10.3389/fmicb.2020.616922.

Nakayama, J. *et al.* (2001) 'Role of histone H3 lysine 9 methylation in epigenetic control of heterochromatin assembly.', *Science (New York, N.Y.)*. Science, 292(5514), pp. 110–3. doi: 10.1126/science.1060118.

Nobile, C. J. and Johnson, A. D. (2015) 'Candida albicans Biofilms and Human Disease', *Annual review of microbiology*. NIH Public Access, 69(1), p. 71. doi: 10.1146/ANNUREV-MICRO-091014-104330.

Noble, S. M. *et al.* (2010) 'Systematic screens of a Candida albicans homozygous deletion library decouple morphogenetic switching and pathogenicity.', *Nature genetics*. NIH Public Access, 42(7), pp. 590–8. doi: 10.1038/ng.605.

Noble, S. M., Gianetti, B. A. and Witchley, J. N. (2017a) 'Candida albicans cell-type switching and functional plasticity in the mammalian host', *Nature Reviews Microbiology*. Nature Publishing Group, 15(2), pp. 96–108. doi: 10.1038/nrmicro.2016.157.

Noble, S. M., Gianetti, B. A. and Witchley, J. N. (2017b) 'Candida albicans cell-type switching and functional plasticity in the mammalian host', *Nature Reviews Microbiology*. Nature Publishing Group, 15(2), pp. 96–108. doi: 10.1038/NRMICRO.2016.157.

Noble, S. M. and Johnson, A. D. (2007) 'Genetics of Candida albicans, a Diploid Human Fungal Pathogen', *http://dx.doi.org/10.1146/annurev.genet.41.042007.170146*. Annual Reviews , 41, pp. 193–211. doi: 10.1146/ANNUREV.GENET.41.042007.170146.

Norton, V. G. *et al.* (1989) 'Histone acetylation reduces nucleosome core particle linking number change.', *Cell*. Cell, 57(3), pp. 449–57. doi: 10.1016/0092-8674(89)90920-3.

Odds, F. C. *et al.* (2007) 'Molecular Phylogenetics of Candida albicans †', *EUKARYOTIC CELL*, 6(6), pp. 1041–1052. doi: 10.1128/EC.00041-07.

Ohtani, H. *et al.* (2020) 'Activation of a Subset of Evolutionarily Young Transposable Elements and Innate Immunity Are Linked to Clinical Responses to 5-Azacytidine', *Cancer Research*. American Association for Cancer Research, 80(12), pp. 2441–2450. doi: 10.1158/0008-5472.CAN-19-1696.

Okano, M. *et al.* (1999) 'DNA methyltransferases Dnmt3a and Dnmt3b are essential for de novo methylation and mammalian development.', *Cell*. Cell, 99(3), pp. 247–57. doi: 10.1016/s0092-8674(00)81656-6.

Ostrosky-Zeichner, L. *et al.* (2003) 'Antifungal Susceptibility Survey of 2,000 Bloodstream Candida Isolates in the United States', *Antimicrobial Agents and Chemotherapy*. American Society for Microbiology (ASM), 47(10), p. 3149. doi: 10.1128/AAC.47.10.3149-3154.2003.

Pain, A. *et al.* (2004) 'Insight into the genome of Aspergillus fumigatus: Analysis of a 922 kb region encompassing the nitrate assimilation gene cluster', *Fungal Genetics and Biology*, 41(4), pp. 443–453. doi: 10.1016/j.fgb.2003.12.003.

Palmer, L. E. *et al.* (2003) 'Maize genome sequencing by methylation filtration.', *Science (New York, N.Y.)*. Science, 302(5653), pp. 2115–7. doi: 10.1126/science.1091265.

Pancaldi, S. *et al.* (1988) '5-Azacytidine accelerates yeast-mycelium conversion in Candida albicans', *Cell Biology International Reports*. No longer published by Elsevier, 12(1), pp. 35–40. doi: 10.1016/0309-1651(88)90109-9.

Pande, K., Chen, C. and Noble, S. M. (2013) 'Passage through the mammalian gut triggers a phenotypic switch that promotes Candida albicans commensalism.', *Nature genetics*. NIH Public Access, 45(9), pp. 1088–91. doi: 10.1038/ng.2710.

Pappas, P. G. *et al.* (2018) 'Invasive candidiasis', *Nature Reviews Disease Primers*, 4. doi: 10.1038/nrdp.2018.26.

Patil, V. *et al.* (2019) 'Human mitochondrial DNA is extensively methylated in a non-CpG context', *Nucleic Acids Research*. Oxford Academic, 47(19), pp. 10072–10085. doi: 10.1093/nar/gkz762.

Paulsen, M. and Ferguson-Smith, A. C. (2001) 'DNA methylation in genomic imprinting, development, and disease', *The Journal of Pathology*, 195(1), pp. 97–110. doi: 10.1002/path.890.

Pfaller, M. A. and Diekema, D. J. (2007) 'Epidemiology of Invasive Candidiasis: a Persistent Public Health Problem', *CLINICAL MICROBIOLOGY REVIEWS*, 20(1), pp. 133–163. doi: 10.1128/CMR.00029-06.

Pierce, J. V and Kumamoto, C. A. (2012) 'Variation in Candida albicans EFG1 expression enables host-dependent changes in colonizing fungal populations.', *mBio*. American Society for Microbiology (ASM), 3(4), pp. e00117-12. doi: 10.1128/mBio.00117-12.

Qiu, X. *et al.* (2010) 'Equitoxic doses of 5-azacytidine and 5-aza-2'deoxycytidine induce diverse immediate and overlapping heritable changes in the transcriptome.', *PloS one*. Public Library of Science, 5(9). doi: 10.1371/journal.pone.0012994.

Rabinowicz, P. D. *et al.* (2003) 'Genes and transposons are differentially methylated in plants, but not in mammals.', *Genome research*. Cold Spring Harbor Laboratory Press, 13(12), pp. 2658–64. doi: 10.1101/gr.1784803.

Rahman, D. *et al.* (2007) 'Murine model of concurrent oral and vaginal Candida albicans colonization to study epithelial host-pathogen interactions'. doi: 10.1016/j.micinf.2007.01.012.

Raj, K. (2006) 'Azacytidine (Vidaza ®) in the treatment of myelodysplastic syndromes', 2(4), pp. 377–388.

Ramírez, F. *et al.* (2016) 'deepTools2: a next generation web server for deep-sequencing data analysis', *Nucleic acids research*. Nucleic Acids Res, 44(W1), pp. W160–W165. doi: 10.1093/nar/gkw257.

Reyna-López, G. E., Simpson, J. and Ruiz-Herrera, J. (1997) 'Differences in DNA methylation

patterns are detectable during the dimorphic transition of fungi by amplification of restriction polymorphisms', *Molecular and General Genetics*, 253(6), pp. 703–710. doi: 10.1007/s004380050374.

Richmond, T. J. *et al.* (1984) 'Structure of the nucleosome core particle at 7 A resolution.', *Nature*. Nature, 311(5986), pp. 532–7. doi: 10.1038/311532a0.

Robertson, K. D. (2005) 'DNA methylation and human disease.', *Nature reviews. Genetics*. Nat Rev Genet, 6(8), pp. 597–610. doi: 10.1038/nrg1655.

Romo, J. A. *et al.* (2019) 'Global Transcriptomic Analysis of the Candida albicans Response to Treatment with a Novel Inhibitor of Filamentation'. doi: 10.1128/mSphere.

Rountree, M. R. and Selker, E. U. (1997) 'DNA methylation inhibits elongation but not initiation of transcription in Neurospora crassa.', *Genes & development*. Cold Spring Harbor Laboratory Press, 11(18), pp. 2383–95.

Rountree, M. R. and Selker, E. U. (2010) 'DNA methylation and the formation of heterochromatin in Neurospora crassa', *Heredity*. Nature Publishing Group, 105(1), pp. 38–44. doi: 10.1038/hdy.2010.44.

Russell,', P. J. *et al.* (1987) *Differential DNA Methylation during the Vegetative Life Cycle of Neurospora crassat*, *JOURNAL OF BACTERIOLOGY*.

Russell, P. J. *et al.* (1987) 'Different Levels of DNA Methylation in yeast and Mycelial form of Candida albicans', *J. Bacteriology*, 169(9), pp. 4393–4395.

Rustchenko-Bulgac, E. P., Sherman, F. and Hicks, J. B. (1990) 'Chromosomal rearrangements associated with morphological mutants provide a means for genetic variation of Candida albicans.', *Journal of bacteriology*. J Bacteriol, 172(3), pp. 1276–83. doi: 10.1128/jb.172.3.1276-1283.1990.

SanMiguel, P. *et al.* (1996) 'Nested retrotransposons in the intergenic regions of the maize genome.', *Science (New York, N.Y.)*. Science, 274(5288), pp. 765–8. doi: 10.1126/science.274.5288.765.

Schaefer, M. *et al.* (2009) 'Azacytidine Inhibits RNA Methylation at DNMT2 Target Sites in Human Cancer Cell Lines', *Cancer Research*. American Association for Cancer Research, 69(20), pp. 8127–8132. doi: 10.1158/0008-5472.CAN-09-0458.

Schmitz, R. J., Lewis, Z. A. and Goll, M. G. (2019) 'DNA Methylation: Shared and Divergent Features across Eukaryotes.', *Trends in genetics : TIG*. NIH Public Access, 35(11), pp. 818–827. doi: 10.1016/j.tig.2019.07.007.

Selker, E. U. *et al.* (1987) 'Rearrangement of duplicated DNA in specialized cells of Neurospora.', *Cell*. Cell, 51(5), pp. 741–52. doi: 10.1016/0092-8674(87)90097-3.

Selker, E. U. *et al.* (2003) 'The methylated component of the *Neurospora crassa* genome', *Nature*, 422(6934), pp. 893–897. doi: 10.1038/nature01564.

Selker, E. U., Fritz, D. Y. and Singer, M. J. (1993) 'Dense nonsymmetrical DNA methylation resulting from repeat-induced point mutation in Neurospora.', *Science (New York, N.Y.)*. Science, 262(5140), pp. 1724–8. doi: 10.1126/science.8259516.

Selker, E. U. and Garrett, P. W. (1988) 'DNA sequence duplications trigger gene inactivation in Neurospora crassa.', *Proceedings of the National Academy of Sciences of the United States of America*. Proc Natl Acad Sci U S A, 85(18), pp. 6870–4. doi: 10.1073/pnas.85.18.6870.

Selmecki, A., Forche, A. and Berman, J. (2006) 'Aneuploidy and isochromosome formation in drug-resistant Candida albicans.', *Science (New York, N.Y.)*. NIH Public Access, 313(5785), pp. 367–70. doi: 10.1126/science.1128242.

Sharma, J. *et al.* (2019) 'Linking cellular morphogenesis with antifungal treatment and susceptibility in candida pathogens', *Journal of Fungi*. J Fungi (Basel), 5(1). doi: 10.3390/jof5010017.

Shi, D.-Q. *et al.* (2017) 'New Insights into 5hmC DNA Modification: Generation, Distribution and Function', *Frontiers in Genetics*. Frontiers, 8, p. 100. doi: 10.3389/fgene.2017.00100.

Singer, M. J., Marcotte, B. A. and Selker, E. U. (1995) 'DNA methylation associated with repeat-induced point mutation in Neurospora crassa.', *Molecular and cellular biology*. Mol Cell Biol, 15(10), pp. 5586–97. doi: 10.1128/MCB.15.10.5586.

Smith, Z. D. and Meissner, A. (2013) 'DNA methylation: roles in mammalian development', *Nature Reviews Genetics*. Nature Publishing Group, 14(3), pp. 204–220. doi: 10.1038/nrg3354.

Šorm, F. *et al.* (1964) '5-Azacytidine, a new, highly effective cancerostatic', *Experientia*. Experientia, 20(4), pp. 202–203. doi: 10.1007/BF02135399.

Stokes, C. *et al.* (2007) 'Lower filamentation rates of Candida dubliniensis contribute to its lower virulence in comparison with Candida albicans', *Fungal Genetics and Biology*. Academic Press, 44(9), pp. 920–931. doi: 10.1016/J.FGB.2006.11.014.

Stoldt, V. R. *et al.* (1997) 'Efg1p, an essential regulator of morphogenesis of the human pathogen Candida albicans, is a member of a conserved class of bHLH proteins regulating morphogenetic processes in fungi', *The EMBO Journal*. John Wiley & Sons, Ltd, 16(8), pp. 1982–1991. doi: 10.1093/EMBOJ/16.8.1982.

Stresemann, C. and Lyko, F. (2008) 'Modes of action of the DNA methyltransferase inhibitors azacytidine and decitabine', *Int. J. Cancer*, pp. 123–131. doi: 10.1002/ijc.23607.

Su, Z., Han, L. and Zhao, Z. (2011) 'Conservation and divergence of DNA methylation in eukaryotes: new insights from single base-resolution DNA methylomes.', *Epigenetics*. Taylor & Francis, 6(2), pp. 134–40. doi: 10.4161/epi.6.2.13875.

Sudbery, P. E. (2011) 'Growth of Candida albicans hyphae', *Nature Reviews Microbiology*. Nature Publishing Group, 9(10), pp. 737–748. doi: 10.1038/nrmicro2636.

Sudbery, P., Gow, N. and Berman, J. (2004) 'The distinct morphogenic states of Candida albicans', *Trends in Microbiology*, 12(7), pp. 317–324. doi: 10.1016/j.tim.2004.05.008.

Suzuki, M. M. and Bird, A. (2008) 'DNA methylation landscapes: provocative insights from epigenomics', *Nature Reviews Genetics*, 9(6), pp. 465–476. doi: 10.1038/nrg2341.

Tahiliani, M. *et al.* (2009) 'Conversion of 5-methylcytosine to 5-hydroxymethylcytosine in mammalian DNA by MLL partner TET1.', *Science (New York, N.Y.)*. Science, 324(5929), pp. 930–5. doi: 10.1126/science.1170116.

Tamaru, H. and Selker, E. U. (2001) 'A histone H3 methyltransferase controls DNA methylation in Neurospora crassa.', *Nature*. Nature, 414(6861), pp. 277–83. doi: 10.1038/35104508.

Tamaru, H. and Selker, E. U. (2003) 'Synthesis of signals for de novo DNA methylation in Neurospora crassa.', *Molecular and cellular biology*. American Society for Microbiology (ASM), 23(7), pp. 2379–94. doi: 10.1128/MCB.23.7.2379-2394.2003.

Tao, L. *et al.* (2014) 'Discovery of a "White-Gray-Opaque" Tristable Phenotypic Switching System in Candida albicans: Roles of Non-genetic Diversity in Host Adaptation', *PLoS Biology*. Edited by J. Heitman. Public Library of Science, 12(4), p. e1001830. doi: 10.1371/journal.pbio.1001830.

Teoh, F. and Pavelka, N. (2016) 'How Chemotherapy Increases the Risk of Systemic Candidiasis in Cancer Patients: Current Paradigm and Future Directions.', *Pathogens (Basel, Switzerland)*. Multidisciplinary Digital Publishing Institute (MDPI), 5(1). doi: 10.3390/pathogens5010006.

Teschendorff, A. E., West, J. and Beck, S. (2013) 'Age-associated epigenetic drift: implications, and a case of epigenetic thrift?', *Human molecular genetics*. Hum Mol Genet, 22(R1), pp. R7–R15. doi: 10.1093/hmg/ddt375.

Tortorano, A. M. *et al.* (2006) 'Candidaemia in Europe: epidemiology and resistance', *International Journal of Antimicrobial Agents*, 27, pp. 359–366. doi: 10.1016/j.ijantimicag.2006.01.002.

Tse, C. *et al.* (1998) 'Disruption of higher-order folding by core histone acetylation dramatically enhances transcription of nucleosomal arrays by RNA polymerase III.', *Molecular and cellular biology*. American Society for Microbiology (ASM), 18(8), pp. 4629–38. doi: 10.1128/MCB.18.8.4629.

Tsong, A. E. *et al.* (2003) *Evolution of a Combinatorial Transcriptional Circuit: A Case Study in Yeasts*, *Cell*.

Tzung, K.-W. *et al.* (2001) 'Genomic evidence for a complete sexual cycle in Candida albicans', *Proceedings of the National Academy of Sciences*. National Academy of Sciences, 98(6), pp. 3249–3253. doi: 10.1073/PNAS.061628798.

Valinluck, V. and Sowers, L. C. (2007) 'Endogenous Cytosine Damage Products Alter the Site Selectivity of Human DNA Maintenance Methyltransferase DNMT1', *Cancer Research*. American Association for Cancer Research, 67(3), pp. 946–950. doi: 10.1158/0008-5472.CAN-06-3123.

Vettese-Dadey, M. *et al.* (1996) 'Acetylation of histone H4 plays a primary role in enhancing transcription factor binding to nucleosomal DNA in vitro.', *The EMBO journal*, 15(10), pp. 2508–18.

Vico, S. H. *et al.* (2021) 'The Glyoxylate Cycle Is Involved in White-Opaque Switching in Candida albicans', *Journal of Fungi*. Multidisciplinary Digital Publishing Institute, 7(7), p. 502. doi: 10.3390/jof7070502.

Wang, E. T. *et al.* (2008) 'Alternative isoform regulation in human tissue transcriptomes', *Nature*. Nature Publishing Group, 456(7221), pp. 470–476. doi: 10.1038/nature07509.

Wang, J. M., Bennett, R. J. and Anderson, M. Z. (2018) 'The genome of the human pathogen Candida albicans is shaped by mutation and cryptic sexual recombination', *mBio*. American Society for Microbiology, 9(5). doi: 10.1128/MBIO.01205-18.

Wang, Y. L. *et al.* (2015) 'Genome-wide analysis of DNA methylation in the sexual stage of the insect pathogenic fungus Cordyceps militaris', *Fungal Biology*. Elsevier Ltd, 119(12), pp. 1246–1254. doi: 10.1016/j.funbio.2015.08.017.

Wassenegger, M. (2000) 'RNA-directed DNA methylation', *Plant Molecular Biology*. Springer, 43(2/3), pp. 203–220. doi: 10.1023/A:1006479327881.

Wei, J.-W. *et al.* (2017) 'Non-coding RNAs as regulators in epigenetics', *Oncology Reports*. Spandidos Publications, 37(1), pp. 3–9. doi: 10.3892/or.2016.5236.

Whiteway, M. and Bachewich, C. (2007) 'Morphogenesis in *Candida albicans*', *Annual Review of Microbiology*, 61(1), pp. 529–553. doi: 10.1146/annurev.micro.61.080706.093341.

Wilson, R. B., Davis, D. and Mitchell, A. P. (1999) 'Rapid hypothesis testing with Candida albicans through gene disruption with short homology regions.', *Journal of bacteriology*. J Bacteriol, 181(6), pp. 1868–74. doi: 10.1128/JB.181.6.1868-1874.1999.

Witchley, J. N. *et al.* (2019) 'Candida albicans Morphogenesis Programs Control the Balance between Gut Commensalism and Invasive Infection.', *Cell host & microbe*. NIH Public Access, 25(3), pp. 432-443.e6. doi: 10.1016/j.chom.2019.02.008.

Wojak, K.-P. *et al.* (2021) 'Host Age and Denture Wearing Jointly Contribute to Oral Colonization with Intrinsically Azole-Resistant Yeasts in the Elderly.', *Microorganisms*. Microorganisms, 9(8). doi: 10.3390/microorganisms9081627.

Xie, J. *et al.* (2013) 'White-Opaque Switching in Natural MTLa/α Isolates of Candida albicans: Evolutionary Implications for Roles in Host Adaptation, Pathogenesis, and Sex', *PLoS Biology*. Edited by J. Heitman. Public Library of Science, 11(3), p. e1001525. doi: 10.1371/journal.pbio.1001525.

Xu, C. and Corces, V. G. (2018) 'Nascent DNA methylome mapping reveals inheritance of hemimethylation at CTCF/cohesin sites.', *Science (New York, N.Y.)*. Science, 359(6380), pp. 1166–1170. doi: 10.1126/science.aan5480.

Xu, X.-L. *et al.* (2008) 'Bacterial Peptidoglycan Triggers Candida albicans Hyphal Growth by Directly Activating the Adenylyl Cyclase Cyr1p', *Cell Host & Microbe*, 4(1), pp. 28–39. doi: 10.1016/j.chom.2008.05.014.

Yang, K. *et al.* (2016) 'The DmtA methyltransferase contributes to Aspergillus flavus conidiation, sclerotial production, aflatoxin biosynthesis and virulence OPEN', *Nature Publishing Group*. doi: 10.1038/srep23259.

Yapar, N. (2014) 'Epidemiology and risk factors for invasive candidiasis', *Therapeutics and Clinical Risk Management*. Dove Press, 10(1), pp. 95–105. doi: 10.2147/TCRM.S40160.

Young, L. Y., Lorenz, M. C. and Heitman, J. (2000) 'A STE12 homolog is required for mating but dispensable for filamentation in candida lusitaniae.', *Genetics*. Oxford University Press, 155(1), p. 17.

Young, M. D. *et al.* (2010) 'Gene ontology analysis for RNA-seq: accounting for selection bias', *Genome Biology*. BioMed Central, 11(2), p. R14. doi: 10.1186/gb-2010-11-2-r14.

Yue, H. *et al.* (2018) 'Filamentation in Candida auris, an emerging fungal pathogen of humans: passage through the mammalian body induces a heritable phenotypic switch', *Emerging Microbes and Infections*. Emerg Microbes Infect, 7(1). doi: 10.1038/s41426-018-0187-x.

Zemach, A. *et al.* (2010) 'Genome-wide evolutionary analysis of eukaryotic DNA methylation.', *Science (New York, N.Y.)*. American Association for the Advancement of Science, 328(5980), pp. 916–9. doi: 10.1126/science.1186366.

Zervou, F. N. *et al.* (2017) 'T2 Magnetic Resonance for Fungal Diagnosis', *Methods in Molecular Biology*. Humana Press, New York, NY, 1508, pp. 305–319. doi: 10.1007/978-1-4939-6515-1_18.

Zhang, X. *et al.* (2006) 'Genome-wide high-resolution mapping and functional analysis of DNA methylation in arabidopsis.', *Cell*. Cell, 126(6), pp. 1189–201. doi: 10.1016/j.cell.2006.08.003.

Zhao, Y., Sun, H. and Wang, H. (2016) 'Long noncoding RNAs in DNA methylation: new players stepping into the old game.', *Cell & bioscience*. BioMed Central, 6, p. 45. doi: 10.1186/s13578-016-0109-3.

Zhu, H., Wang, G. and Qian, J. (2016) 'Transcription factors as readers and effectors of DNA methylation.', *Nature reviews. Genetics*. Nat Rev Genet, 17(9), pp. 551–65. doi: 10.1038/nrg.2016.83.

6 APPENDIX

6.1 *C. albicans* clinical isolates

Supplementary Table 1: Sources of clinical isolates used for morphology screening on Spider medium.

PEU#	Source	PEU#	Source
3255	Urine catheter	**3287**	Respiratory
3256	Urine	**3288**	Respiratory
3257	Sputum	**3289**	Oral
3258	Invasive	**3290**	Oral
3259	Blood	**3291**	Respiratory
3260	Urine catheter	**3292**	Respiratory
3261	Respiratory	**3293**	Invasive
3262	Urine	**3294**	Invasive
3263	Urine	**3295**	Oral
3264	Urine	**3296**	Oral
3265	Stool	**3297**	Urine catheter
3266	Invasive	**3298**	Oral
3267	Urine	**3299**	Invasive
3268	Oral	**3300**	Urine
3269	Respiratory	**3301**	Respiratory
3270	Respiratory	**3302**	Urine
3271	Invasive	**3303**	Urine
3272	Respiratory	**3304**	Urine
3273	Urine	**3305**	Respiratory
3274	Urine catheter	**3306**	Urine catheter
3275	Urine	**3307**	Invasive
3276	Oral	**3308**	Respiratory
3277	Respiratory	**3309**	Oral
3278	Urine	**3310**	Respiratory
3279	Respiratory	**3311**	Respiratory
3280	Invasive	**3312**	Respiratory
3281	Respiratory	**3313**	Respiratory
3282	Respiratory	**3314**	Respiratory
3283	Respiratory	**3315**	Respiratory
3284	Stool	**3316**	Respiratory
3285	Oral	**3328**	Blood
3286	Invasive	**3329**	Stool
3330	Invasive	**3371**	Stool

3331	Invasive	**3372**	Invasive
3332	Invasive	**3373**	Invasive
3333	Invasive	**3374**	Oral
3334	Stool	**3375**	Oral
3335	Urine	**3386**	Urine
3336	Stool	**3387**	Invasive
3337	Stool	**3388**	Urine catheter
3338	Stool	**3389**	Respiratory
3339	Oral	**3390**	Oral
3340	Invasive	**3371**	Stool
3341	Invasive	**3372**	Invasive
3342	Stool	**3373**	Invasive
3343	Stool	**3374**	Oral
3344	Blood	**3375**	Oral
3345	Urine	**3386**	Urine
3346	Oral	**3387**	Invasive
3347	Respiratory	**3388**	Urine catheter
3348	Oral	**3389**	Respiratory
3349	Invasive	**3390**	Oral
3350	Respiratory	**3371**	Stool
3351	Oral	**3372**	Invasive
3352	Blood	**3373**	Invasive
3353	Urine	**3374**	Oral
3354	Urine catheter	**3375**	Oral
3355	Respiratory	**3386**	Urine
3356	Respiratory	**3387**	Invasive
3357	Blood	**3388**	Urine catheter
3358	Invasive	**3389**	Respiratory
3359	Respiratory	**3390**	Oral
3360	Invasive	**3391**	Urine
3361	Oral	**3392**	Invasive
3362	Oral	**3393**	Invasive
3363	Invasive	**3394**	Oral
3364	Oral	**3395**	Oral
3365	Urine	**3396**	Stool
3366	Urine	**3397**	Stool
3367	Urine	**3398**	Urine
3368	Stool	**3399**	Stool
3369	Blood	**3400**	Oral
3370	Invasive	**3401**	Oral
3407	Invasive	**3529**	Invasive

3408	Invasive	**3530**	Blood
3409	Invasive	**3531**	Blood
3410	Stool	**3532**	Blood
3411	Stool	**3533**	Blood
3412	Oral	**3534**	Blood
3413	Oral	**3535**	Blood
3414	Oral	**3536**	Blood
3415	Oral	**3537**	Blood
3416	Oral	**3538**	Blood
3417	Respiratory	**3539**	Blood
3418	Oral	**3540**	Blood
3419	Urine	**3541**	Blood
3420	Oral	**3542**	Blood
3421	Oral	**3543**	Blood
3422	Stool	**3544**	Blood
3470	Blood	**3545**	Blood
3471	Blood	**3573**	Blood
3472	Invasive	**3574**	Blood
3473	Invasive	**3575**	Blood
3474	Stool	**3576**	Blood
3475	Stool	**3578**	Blood
3476	Stool	**3648**	Blood
3477	Invasive	**3649**	Blood
3478	Respiratory	**3650**	Blood
3479	Stool	**3651**	Blood
3480	Stool	**3652**	Blood
3481	Stool	**3653**	Blood
3482	Stool	**3654**	Blood
3483	Stool	**3655**	Blood
3484	Stool	**3656**	Blood
3485	Stool	**3657**	Blood
3524	Stool	**3688**	Blood
3525	Stool	**3689**	Blood
3526	Stool	**3690**	Blood
3527	Stool	**3691**	Blood
3528	Blood		

6.2 WGBS - technical parameters and data quality

6.2.1 Yeast versus hyphae one-to-one sample analysis

Sequencing reads were obtained from GATC Biotech AG. After quality trimming, a mapping rate for uniquely mapping reads of 84.5% and 83.6% for the nuclear genome of yeast and hyphal sample respectively, was obtained (Supplementary Table 2). Unmapped reads of each sample were again mapped to the mitochondrial genome, out of which 9.4% and 11% could be mapped, representing 1.26% and 1.55% of all reads of the yeast and hyphal samples, respectively.

Supplementary Table 2: Sample statistics from MultiQC analysis after mapping.

Sample ID	Total number of reads (after trimming)	Reads uniquely mapping [%]	Reads unmapped [%]	Reads mapped >1 [%]	Calculated fold-Coverage[1]
Ca_yeast_nucl	37 643 737	31 817 075 (84.5)	13.5	2.0	247.39
Ca_yeast_mito[2]	5 826 662	549 437 (9.4)	83.5	7.1	1631.18
Ca_hyphae_nucl	30 934 391	25 845 887 (83.6)	14.4	2.1	200.96
Ca_hyphae_mito[2]	5 088 504	558 704 (11.0)	80.6	8.4	1658.70

[1] Coverage was calculated after quality trimming and mapping of paired end reads to haploid nuclear (15 433 330 bp) or mitochondrial (40 420 bp) genome (coverage = $\frac{uniquely\ mapped\ reads * 120\ bp}{haploid\ genome}$).

[2] Unmapped reads from the first mapping to the nuclear genome, mapped to the mitochondrial genome.

The calculated read coverage in the nuclear genome was 247-fold for the yeast sample and 201-fold for the hyphal sample. Visualization of read coverage showed an approximate average coverage between 185- and 300-fold for the yeast culture (Supplementary Figure 1) and 160- to 250-fold for the hyphal culture, verifying the average calculated value. Mitochondrial coverage was ~1600-fold for both samples.

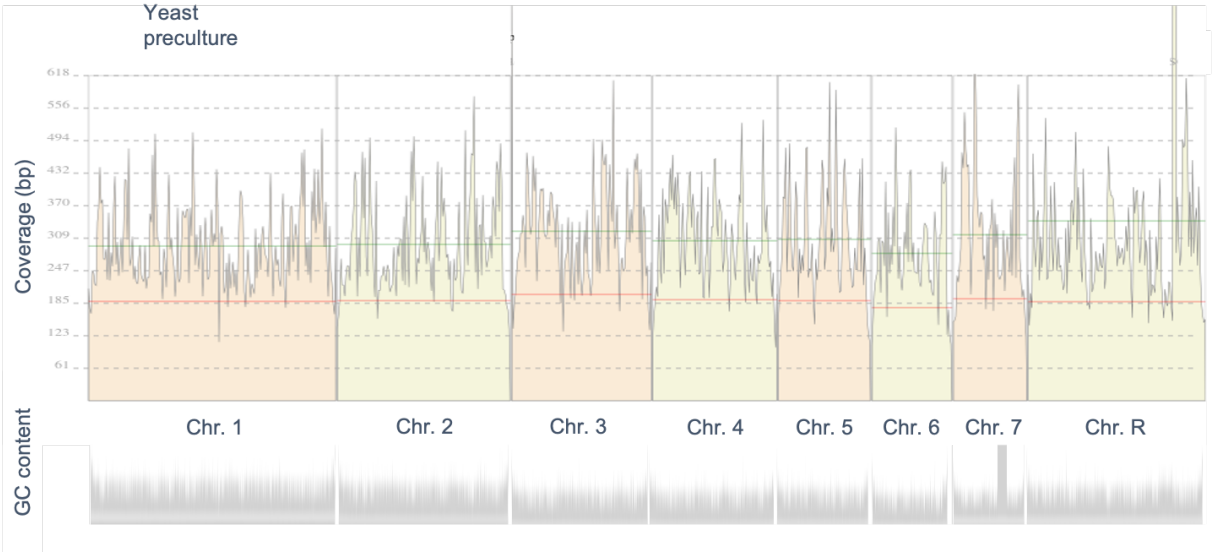

Supplementary Figure 1: Read Coverage of WGBS reads. Exemplarily the coverage of the yeast sample is shown for all eight chromosomes.

To exclude possible variances in mapping between the two samples, average GC content and coverage in defined regions (1000 bins) of both samples were plotted against each other. Both samples showed an overlapping pattern, with most reads showing a GC content of 30 to 35% (corresponding to the average GC content of the genome of 33.5%) and a coverage between 50 to 100 in this area (Supplementary Figure 2, A). Further the coverage of both samples over the whole genome was plotted against each other, resulting in a high correlation coefficient (Supplementary Figure 2, B), indicating that observed differences between the stages are not due to mapping artifacts.

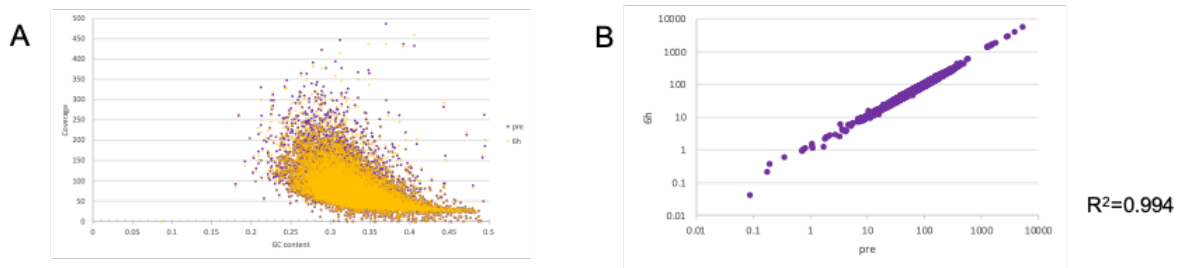

Supplementary Figure 2: Variance analysis of mapped reads. (A) Plot of GC content against coverage in regions of 1000 bins for both samples. (B) Plot of the coverage of both samples with correlation coefficient.

6.2.2 Yeast versus hyphae - timecourse

Sequences were again mapped to nuclear and mitochondrial genome separately. Between 45.7% and 71.6% of the trimmed reads could be mapped uniquely to the nuclear genome (Supplementary Table 3), which is much less than in the previous experiment, even though we used the same pipeline for quality trimming. As we obtained a very good coverage with these reads, it was not an issue for our further downstream data analyses.

Calculated coverage ranged between 92- and 260-fold for the nuclear genome, the coverage of the mitochondrial genome was up to 10-fold higher.

Supplementary Table 3: Sample statistics from MultiQC Analysis after mapping.

Sample ID (replicate 1 and 2)	description	Total number of reads (after trimming)	Reads uniquely mapping [%]	Reads unmapped [%]	Reads mapped >1 [%]	Calculated Coverage[1]
PA3-1_nucl	yeast	27 727 931	18 622 240 (67.2)	31.1	1.7	176
PA3-1_mito[2]	16h	9 105 691	615 870 (6.8)	87.3	5.9	2225
PA3-3_nucl	yeast	25 586 925	14 310 746 (55.9)	42.5	1.6	135
PA3-3_mito[2]	16h	11 276 179	593 260 (5.3)	90.5	4.2	2143
PA6b-1_nucl	hyphae	20 574 628	9 734 379 (47.3)	51.4	1.3	92
PA6b-1_mito[2]	1h	10 840 249	305 212 (2.8)	94.6	2.5	1102
PA6b-3_nucl	hyphae	24 038 633	10 990 795 (45.7)	53.0	1.3	104
PA6b-3_mito[2]	1h	13 047 838	370 559 (2.8)	95.0	2.1	1338
PA6e-1_nucl	hyphae	36 815 463	27 468 766 (74.6)	23.7	1.7	260
PA6e-1_mito[2]	6h	9 346 697	853 802 (9.1)	83.1	7.8	3084
PA6e-3_nucl	hyphae	30 928 112	22 048 052 (71.3)	26.9	1.8	209
PA6e-3_mito[2]	6h	8 880 060	625 292 (7.0)	86.5	6.5	2259
PA7b-1_nucl	yeast	19 477 654	10 969 382 (56.3)	41.9	1.8	104
PA7b-1_mito[2]	1h	8 508 272	295 193(3.5)	93.3	3.2	1066
PA7b-3_nucl	yeast	40 190 184	21 350 844 (53.1)	45.3	1.6	202
PA7b-3_mito[2]	1h	18 839 340	746 664 (4.0)	93.5	2.6	2697
PA7e-1_nucl	yeast	27 125 340	19 409 139 (71.6)	26.6	1.8	184
PA7e-1_mito[2]	6h	7 716 201	765 620 (9.9)	81.3	8.8	2765
PA7e-3_nucl	yeast	27 669 892	20 609 419 (74.5)	23.6	1.9	195
PA7e-3_mito[2]	6h	7 060 473	674000 (9.5)	82.8	7.7	2435

[1] coverage was calculated after quality trimming and mapping of paired end reads to nuclear (15 433 330 bp) or mitochondrial (40 420 bp) haploid genome (coverage = $\frac{uniquely\ mapped\ reads * 146\ bp}{haploid\ genome}$).

[2] Unmapped reads from the first mapping to the nuclear genome mapped to the mitochondrial genome

Visualization of the read coverage in the eight nuclear chromosomes again revealed the average calculated value, exemplarily demonstrated for the yeast-1h-sample (Supplementary Figure 3), which had an average calculated value of 104 and ranged between 80 and 115 in the plot. Coverage was higher in the subtelomeric regions.

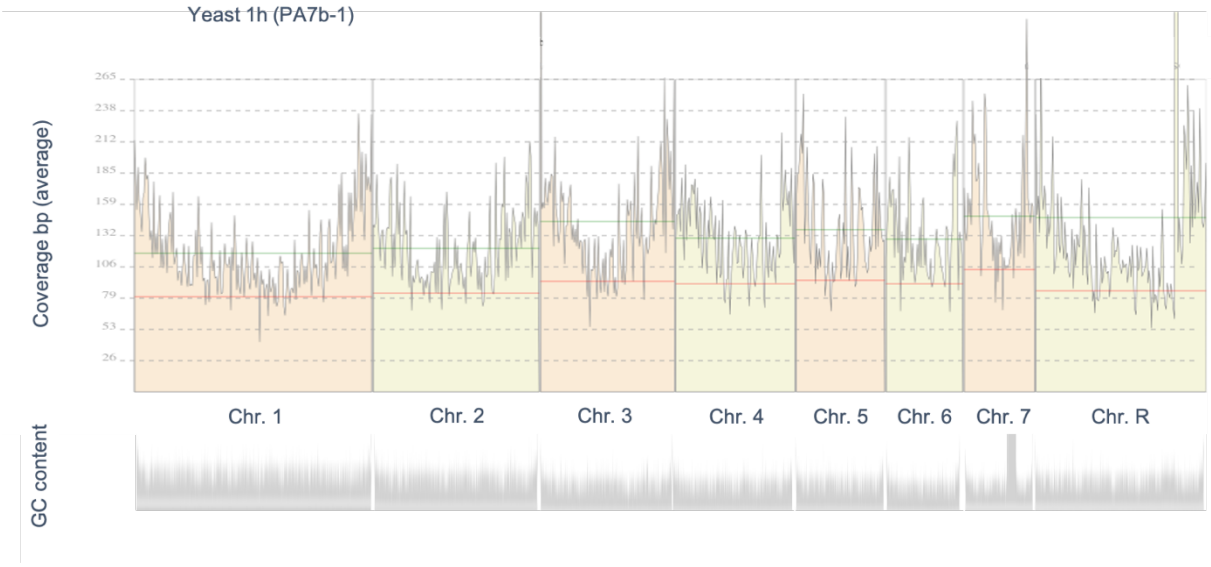

Supplementary Figure 3: Read Coverage of WGBS reads. Exemplarily the coverage of the yeast-1h-sample is shown for all eight chromosomes.

Variance analysis was conducted for the two replicates of each sample. All samples showed a high correlation amongst their replicates concerning the dependence of GC content and coverage. Further, a high correlation coefficient was observed for all replicates concerning coverage analysis over the whole genome (Supplementary Figure 4).

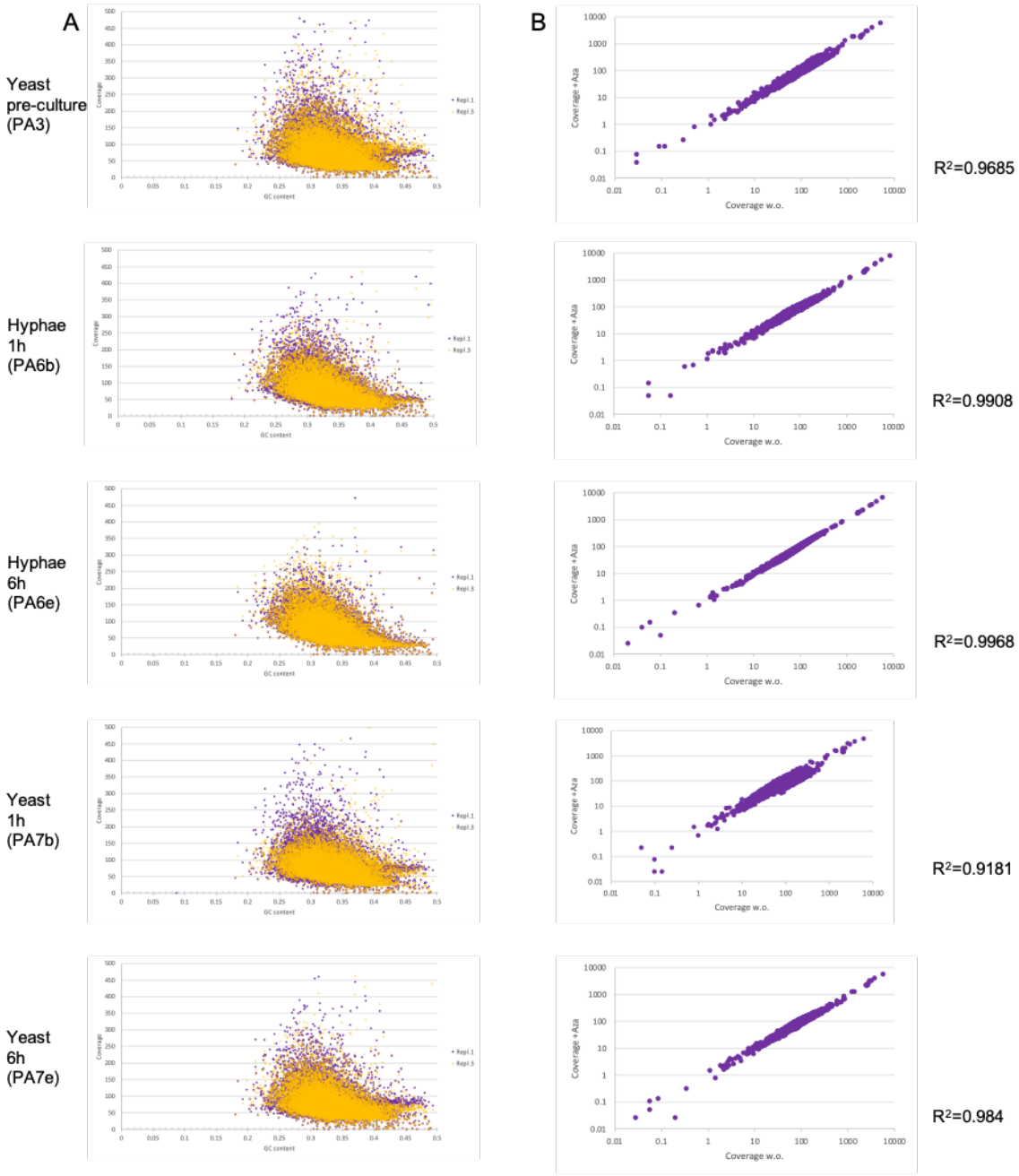

Supplementary Figure 4: Variance analysis of mapped reads.(A) Plot of GC content against coverage in regions of 1000 bins for both samples. (B) Plot of the coverage of both samples with correlation coefficient. For each sample respective replicates were plotted against each other.

6.2.3 Untreated and 5-Aza treated fresh clinical isolates

Also the clinical isolates' sequences were mapped to nuclear and mitochondrial genome separately. Between 65.5% and 81.2% of the trimmed reads could be mapped uniquely to the nuclear genome (Supplementary Table 4). Additionally, strain 529L was mapped to its own genome, resulting in a higher coverage rate.

Calculated coverage ranged between 83- and 155-fold for the nuclear genome of the samples mapped to SC5314. Again, the coverage of the mitochondrial genome was up to 10-fold higher.

Supplementary Table 4: Sample statistics from MultiQC Analysis after mapping.

Sample ID	Description	Total number of reads (after trimming)	Reads uniquely mapping [%]	Reads unmapped [%]	Reads mapped >1 [%]	Calculated Coverage[1]	CpG (%)	CHG (%)	CHH (%)
PEU3692wo_nucl	attenuated	13 335 358	9 761 292 (73.2)	24.1	2.7	92	0.08	0.10	0.10
PEU3692_mito[2]		3 574 066	183 764 (5.1)	92.6	2.2	664	0.1	0.1	0.1
PEU3692+Aza_nucl	filamenting	22 389 666	16 253 574 (72.6)	24.4	3.0	154	0.08	0.10	0.10
PEU3692+Aza_mito[2]		6 136 092	274863 (4.5)	93.5	2.0	993	0.1	0.1	0.1
PEU3694wo_nucl	attenuated	16 370 603	13 291 847 (81.2)	15.9	2.9	126	0.08	0.10	0.10
PEU3694wo_mito[2]		3 078 756	167 907 (5.5)	92.2	2.3	606	0.1	0.1	0.1
PEU3694+Aza_nucl	filamenting	19 999 329	16 423 131 (82.1)	15.1	2.8	155	0.08	0.10	0.10
PEU3694+Aza_mito[2]		3 576 198	237 475 (6.6)	90.6	2.8	858	0.1	0.1	0.1
PEU3696wo_nucl	attenuated	19 524 258	14 871 183 (76.2)	21.1	2.7	141	0.08	0.10	0.10
PEU3696wo_mito[2]		4 653 075	317 845 (6.8)	90.3	2.9	1148	0.1	0.1	0.1
PEU3696+Aza_nucl	filamenting	20 323 827	14 741 849 (72.5)	24.4	3.1	139	0.08	0.09	0.09
PEU3696+Aza_mito[2]		5 581 978	359 760 (6.4)	90.8	2.8	1299	0.1	0.1	0.1
PEU3698wo_nucl	attenuated	11 749 591	8 772 994 (74.7)	21.6	3.8	83	0.08	0.10	0.10
PEU3698wo_mito[2]		2 976 597	161 294 (5.4)	92.2	2.4	583	0.1	0.1	0.1
PEU3698+Aza_nucl	filamenting	13 205 913	10 135 969 (76.8)	20.4	2.8	96	0.08	0.10	0.10
PEU3698+Aza_mito[2]		3 069 944	178 632 (5.8)	91.7	2.5	645	0.1	0.1	0.1
PEU3700wo_nucl	filamenting	24 035 145	16 002 180 (66.6)	30.8	2.6	151	0.09	0.11	0.11
PEU3700wo_mito[2]		8 032 965	292 841 (3.6)	95.0	1.3	1058	0.1	0.1	0.1
PEU3700+Aza_nucl	filamenting	21 065 568	14 962 953 (71.0)	26.1	2.8	142	0.09	0.11	0.11
PEU3700+Aza_mito[2]		6 102 615	271 408 (4.4)	93.9	1.6	980	0.1	0.1	0.1

529Lwo_nucl	attenuated	18 293 164	12 009 262 (65.6)	31.6	2.8	114	0.08	0.10	0.10
529Lwo_mito[2]		6 283 902	275 184 (4.4)	94.2	1.4	994	0.1	0.1	0.1
529LwoSpF_nucl	filamenting	19 422 574	12 863 635 (66.2)	31.0	2.8	122	0.08	0.10	0.10
529L_woSpF_mito[2]		6 558 939	252 639 (3.9)	94.9	1.3	913	0.1	0.1	0.1
529L+Aza_nucl	filamenting	22 056 681	14 452 119 (65.5)	31.8	2.6	137	0.07	0.08	0.08
529L_+Aza_mito[2]		7 604 562	382 333 (5.0)	93.3	1.7	1381	0.1	0.1	0.1
SC5314wo_nucl	filamenting	24 991 617	19 371 888 (77.5)	19.3	3.2	183	0.08	0.09	0.09
SC5314wo_mito[2]		5 619 729	401 975 (7.2)	89.8	3.0	1452	0.1	0.1	0.1
SC5314+Aza_nucl	filamenting	21 782 701	16 961 818 (77.9)	18.8	3.3	160	0.08	0.09	0.09
SC5314+Aza_mito[2]		10 892 004	382 345 (7.9)	88.7	3.4	1381	0.1	0.1	0.1
529L mapped to its own sequenced genome:									
529Lwo_nucl	attenuated	18 293 164	12 699 205 (69.4)	28.1	2.5	120	0.08	0.10	0.10
529Lwo_mito[2]		5 593 959	275 184 (4.9)	93.5	1.6	994	0.1	0.1	0.1
529LwoSpF_nucl	filamenting	19 422 574	13 624 735 (70.1)	27.3	2.5	129	0.08	0.10	0.10
529L_woSpF_mito[2]		5 797 839	252 638 (4.4)	94.2	1.4	913	0.1	0.1	0.1
529L+Aza_nucl	filamenting	22 056 681	15 254 477 (69.2)	28.5	2.4	144	0.07	0.08	0.08
529L_+Aza_mito[2]		6 802 204	382 337 (5.6)	92.5	1.8	1381	0.1	0.1	0.1

[1] Coverage was calculated after quality trimming and mapping of paired end reads to nuclear (15 433 330 bp) or mitochondrial (40 420 bp) haploid genome (coverage $=\frac{uniquely\ mapped\ reads * 95\ bp}{haploid\ genome}$)

[2] Unmapped reads from the first mapping to the nuclear genome subsequently were mapped to the mitochondrial genome.

Variance analysis was conducted for untreated and 5-Aza treated sample of each isolate, or in case of 529L also to the third untreated filamenting sample. All samples showed a high correlation amongst their replicates concerning the dependence of GC content and coverage. Further, a high correlation coefficient was observed for all replicates concerning coverage analysis over the whole genome (Supplementary Figure 5).

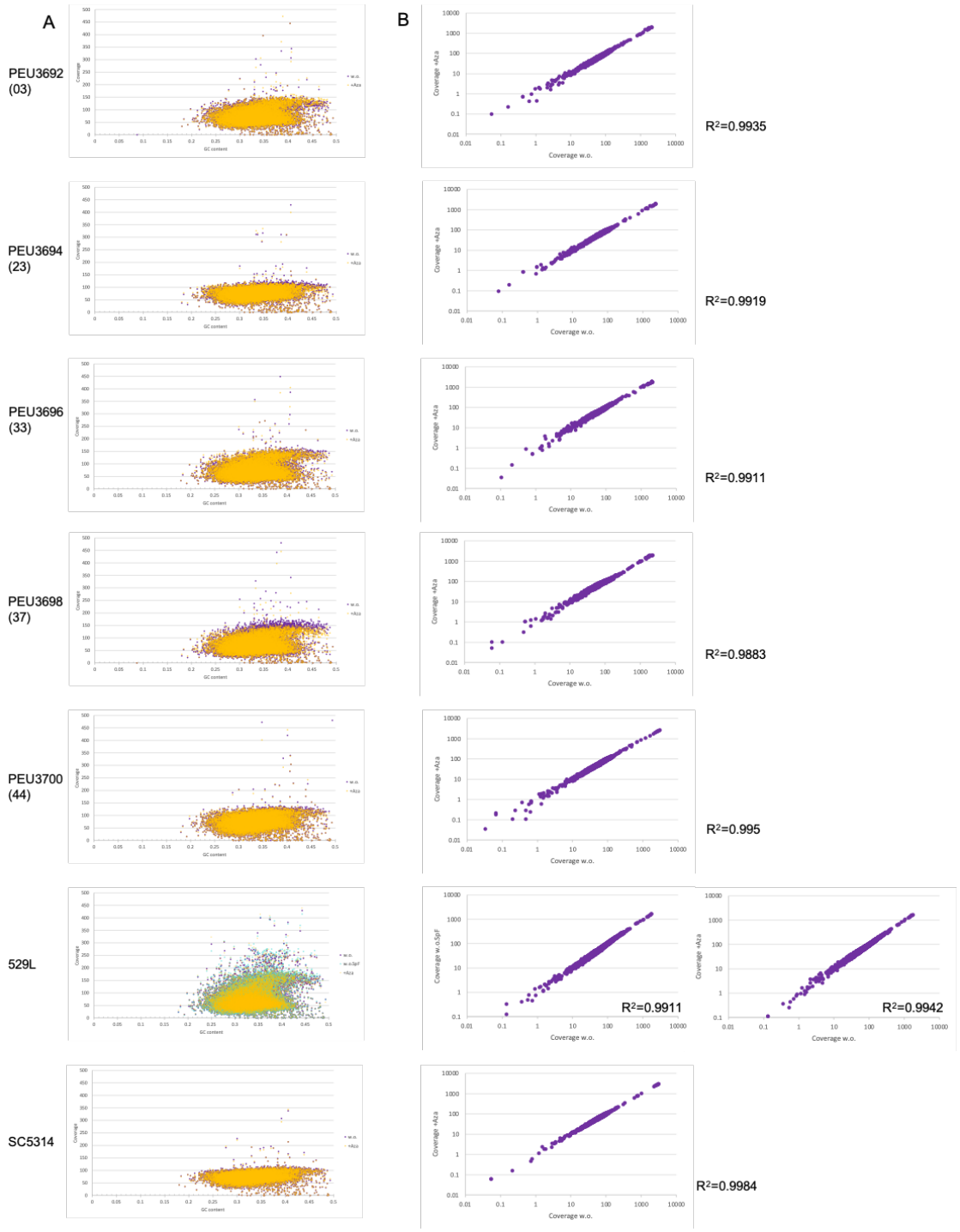

Supplementary Figure 5: Variance analysis of mapped reads. (A) Plot of GC content vs. coverage in regions of 1000 bins for both samples. (B) Plot of the coverage of both samples with correlation coefficient. For each sample respective replicates were plotted against each other.

6.3 RNAseq - technical parameters and data quality

Initial quality control of all samples in a fragment analyser showed that replicate PA2-1 did not have a good quality prior to RNA sequencing (very low concentration of 21 ng/µl – RNA integrity number (RIN) is questionable). Hence, this replicate of PA2 was removed from downstream analyses and will be replaced by another technical replicate of PA2-1 subsequently to this work. All other samples were of good quality (Supplementary Table 5). After quality analysis and trimming of RNAseq data, between 16.6 and 48.4 million single end reads with a mean read size still up to 51 bp were left for analyses. Uniquely mapped reads ranged between 92.02 and 94.86%. The assignment rate to known features of the *C. albicans* reference genome ranged around 90 to 94%, taking the uniquely mapped reads as a basis. Sample PA4b-1 had a lower rate (86.39 %), but showed a higher number of total reads than all other samples.

Supplementary Table 5: Samples for RNAseq transcriptome analysis of *C. albicans* SC5314.

Sample ID (-replicates)	RIN	Concentration [ng/µl]	5-Aza-treatment	Morphology	Total number of reads*	Reads uniquely mapping [%]	Reads unmapped [%]	Reads mapped >1 [%]	Feature-assigned reads (% to uniquely mapped)
(PA2-1)	(8.8)	(21)	(yes)	(yeast)	-	-	-	-	-
PA2-2	9.2	1207	yes	yeast	16 605 207	92.01	3.63	4.36	14 413 048 (94.34)
PA2-3	9.1	1145	yes	yeast	37 410 299	92.64	3.47	3.89	32 450 381 (93.63)
PA3-1	9.1	946	no	yeast	42 836 003	95.21	2.54	2.25	37 529 913 (92.02)
PA3-2	9.1	1216	no	yeast	38 356 893	94.84	2.61	2.55	34 241 864 (94.13)
PA3-3	8.5	1171	no	yeast	33 935 240	94.86	2.70	2.43	30 192 032 (93.79)
PA4b-1	10	130	yes	hyphae	48 288 706	93.61	2.32	4.07	39 051 188 (86.39)
PA4b-2	9.9	346	yes	hyphae	30 803 540	93.54	2.60	3.86	26 878 292 (93.28)
PA4b-3	9.6	495	yes	hyphae	38 632 703	94.00	2.72	3.28	34 031 609 (93.71)
PA5b-1	9.9	120	yes	yeast	27 692 766	92.75	2.40	4.85	23 848 390 (92.85)
PA5b-2	10	200	yes	yeast	36 712 337	93.61	2.36	4.03	31 716 617 (92.29)
PA5b-3	10	288	yes	yeast	21 769 326	93.05	2.47	4.48	18 955 642 (93.58)
PA6b-1	9.9	153	no	hyphae	41 533 941	93.25	2.37	4.38	36 079 254 (93.15)
PA6b-2	8.9	425	no	hyphae	31 452 499	93.98	2.49	3.54	26 624 735 (90.07)
PA6b-3	9.5	453	no	hyphae	35 991 827	93.38	2.42	4.20	31 482 581 (93.67)
PA7b-1	10	125	no	yeast	41 922 734	92.39	2.31	5.30	35 617 864 (91.96)
PA7b-2	9.9	453	no	yeast	38 534 122	93.36	2.33	4.31	33 157 174 (92.17)
PA7b-3	10	269	no	yeast	29 930 852	92.02	2.43	5.56	25 627 809 (93.05)

**after quality trimming*

Variance between the different cultures was analysed, to see if any hidden effect is present on the data. The starter cultures (treated vs. untreated yeast cultures) showed a strong variance (91%) in the first dimension, separating treated and untreated samples. However, 5% variance in the second dimension - representing the biological replicates - was considered very small (Supplementary Figure 6).

Next, variance between starter cultures and their subcultures (yeast or hyphal induction, with or without 5-Aza pressure) was analysed. In general, the preculture samples again clustered very closely together in the second dimension, while the 1h subcultures showed small variances between their biological replicates. This variance between the replicates was expected, as all three subculture replicates were handled by a different person. In the first dimension all analyses showed a variance between 84 and 99%, demonstrating a strong effect of 5-Aza treatment (Supplementary Figure 7, Supplementary Figure 8).

The 5-Aza effect was less strong when comparing treated and untreated subculture sample of one morphology. Especially for the hyphal culture a stronger variance was observed for the replicates than for the 5-Aza treatment (Supplementary Figure 9).

Further, variance between yeast and hyphal morphology within one treatment group showed the expected result of a strong variance in the first dimension, separating yeast and hyphal morphology, with a stronger variance between the replicates (16%) in the 5-Aza treatment group (Supplementary Figure 10).

A histogram for p-values (data not shown) showed a normal distribution for all conditions except for the treated and untreated hyphal sample. This was also an expectable result fitting to our hypothesis: 5-Aza presumably inhibits DNA methylation, leading to an increased expression of hyphal genes. Thus, a treatment should not cause a strong variance between treated and untreated hyphal culture.

In sum, data quality corresponded the expectations, fuse of the data for further biological analysis.

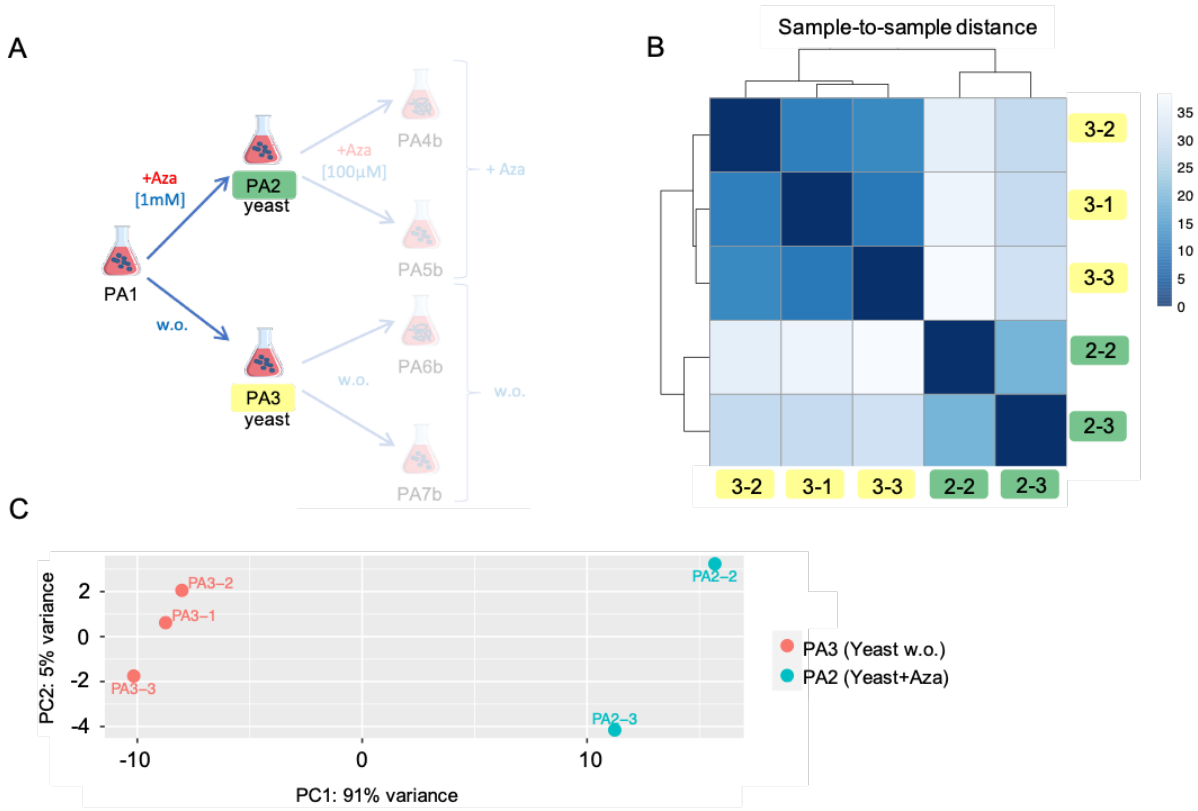

Supplementary Figure 6: Variance analysis of 5-Aza treated and untreated *C. albicans* yeast precultures. (A) Experimental setup with 5-Aza treated (PA2) and untreated (PA3) precultures coloured in green and yellow, respectively. (B) Heatmap of sample-to-sample distance matrix (Euclidean distance), where darker colour shows smaller distance and brighter colour shows a bigger distance. (C) PCA plot showing the variance between the two sample groups and amongst their replicates. Analysis was carried out with DESeq2, which calculates variances based on normalized counts.

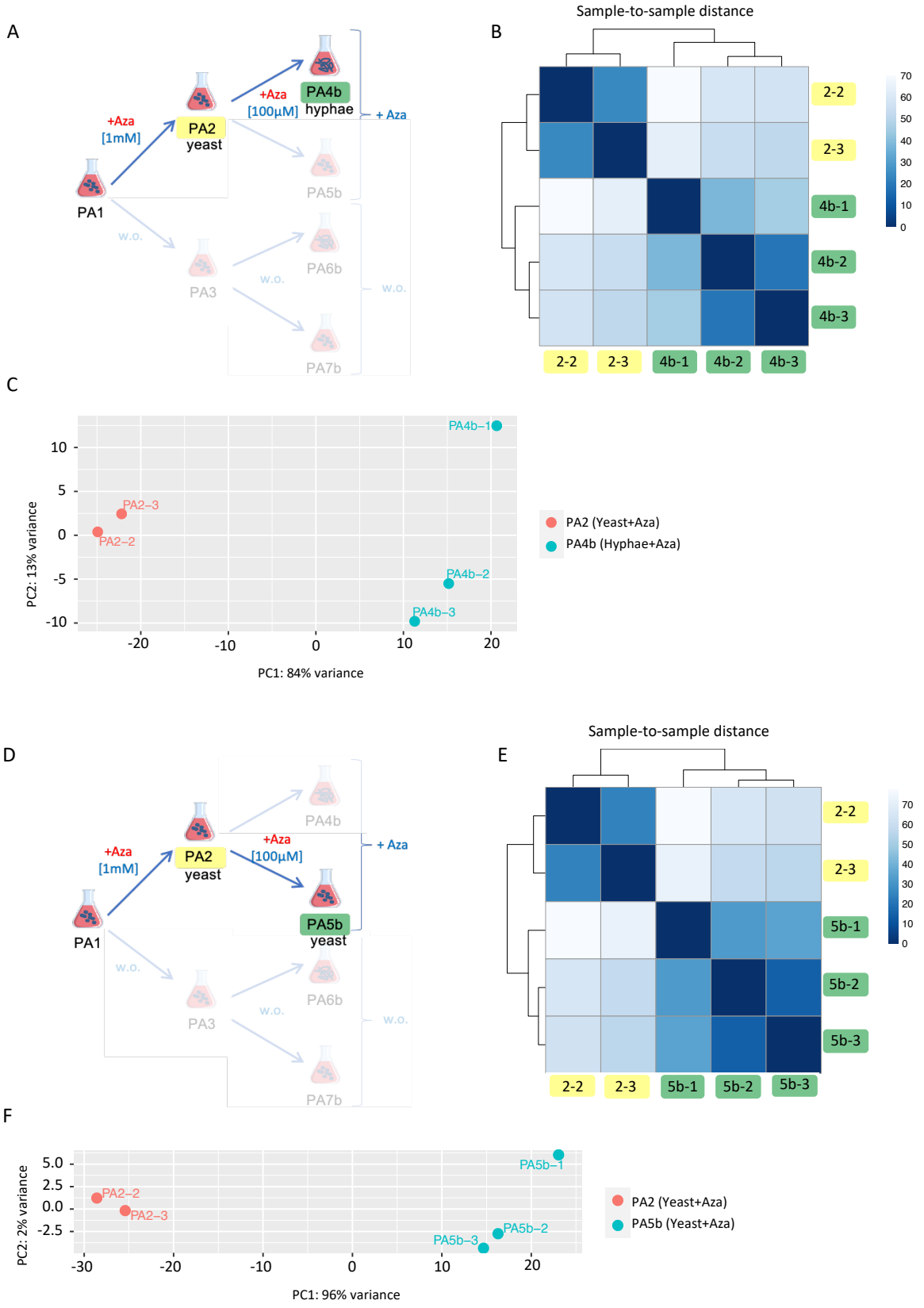

Supplementary Figure 7: Variance analysis of 5-Aza treated *C. albicans* precultures and their subcultures. (A) Experimental setup with culture group PA2 (yellow) in yeast morphology and treated with 1mM 5-Aza versus culture group PA4b (green) in hyphal morphology and treated with 100 µM 5-Aza. (D) Experimental setup with culture group PA2 (yellow) in yeast morphology and treated with 1mM 5-Aza versus culture group PA5b (green) in yeast morphology and treated with 100 µM 5-Aza. (B)+(E) Heatmap of sample-to-sample distance matrix (Euclidean distance). (C)+(F) PCA plot showing the variance between the two sample groups and amongst their replicates. Analysis was carried out with DESeq2, which calculates variances based on normalized counts.

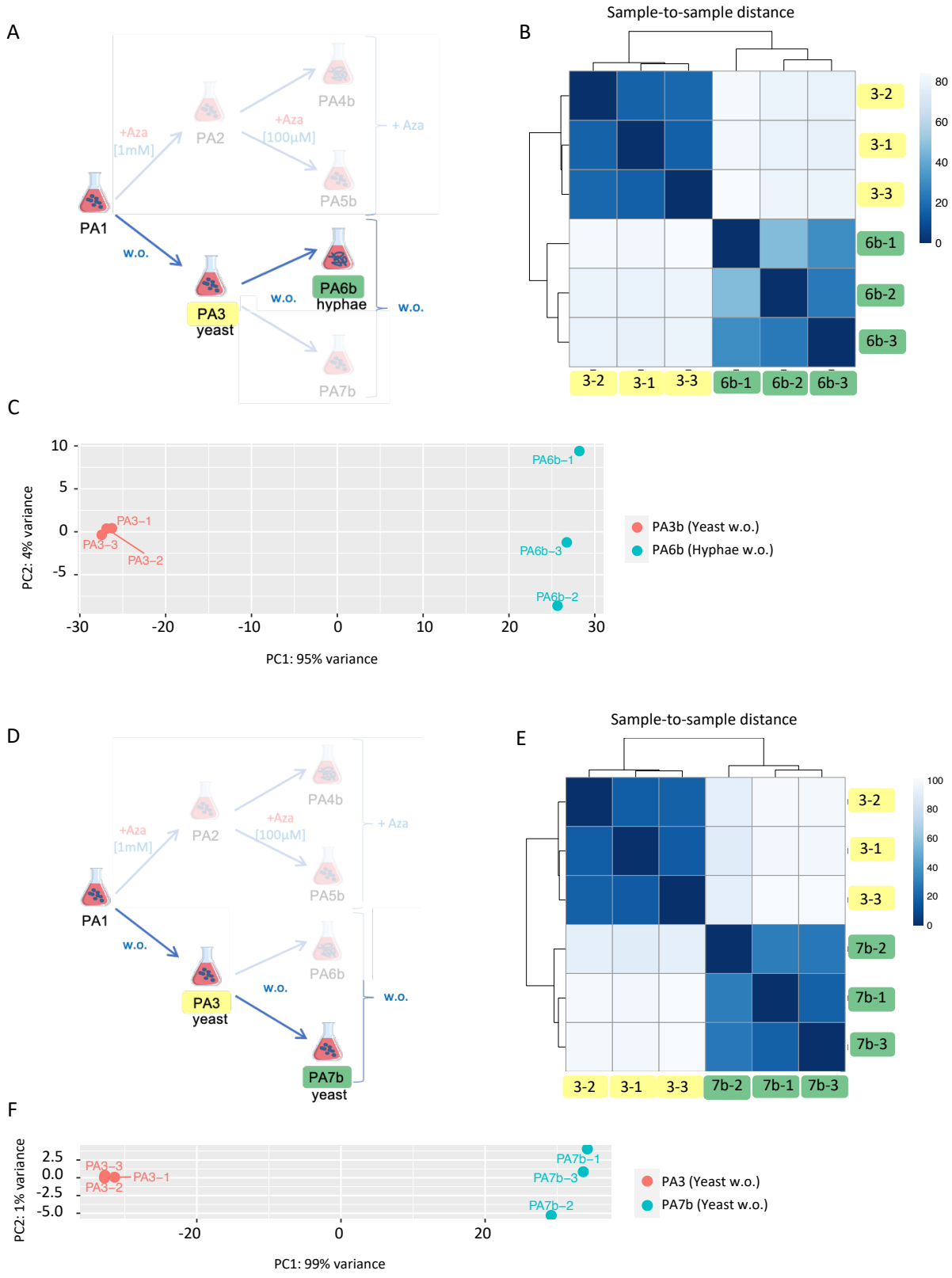

Supplementary Figure 8: Variance analysis of untreated *C. albicans* precultures and their subcultures. (A) Experimental setup with culture group PA3 (yellow) in yeast morphology culture group PA6b (green) in hyphal morphology. (D) Experimental setup with culture group PA3 (yellow) in yeast morphology versus culture group PA7b (green) in yeast morphology. All untreated. (B)+(E) Heatmap of sample-to-sample distance matrix (Euclidean distance). (C)+(F) PCA plot showing the variance between the two sample groups and amongst their replicates. Analysis was carried out with DESeq2, which calculates variances based on normalized counts.

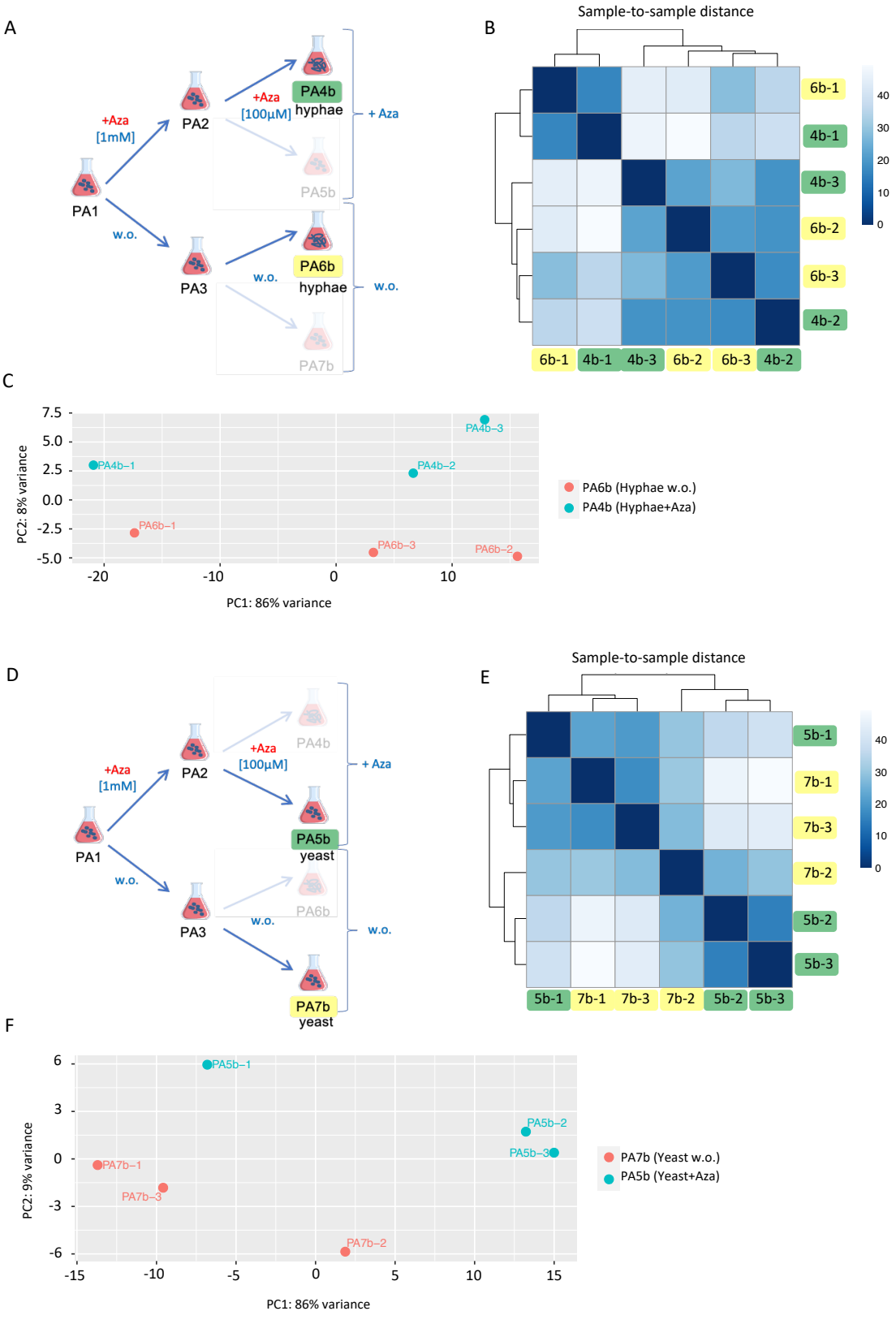

Supplementary Figure 9: Variance analysis of 5-Aza treated *C. albicans* 1h cultures and their corresponding untreated cultures. (A) Experimental setup with culture group PA4b (green) in hyphae morphology and treated with 100µM 5-Aza versus culture group PA7b (yellow) in hyphal morphology, untreated. (D) Experimental setup with culture group PA5b (green) in yeast morphology and treated with 100µM 5-Aza versus culture group PA7b (green) in yeast morphology, untreated. (B)+(E) Heatmap of sample-to-sample distance matrix (Euclidean distance). (C)+(F) PCA plot showing the variance between the two sample groups and amongst their replicates. Analysis was carried out with DESeq2, which calculates variances based on normalized counts.

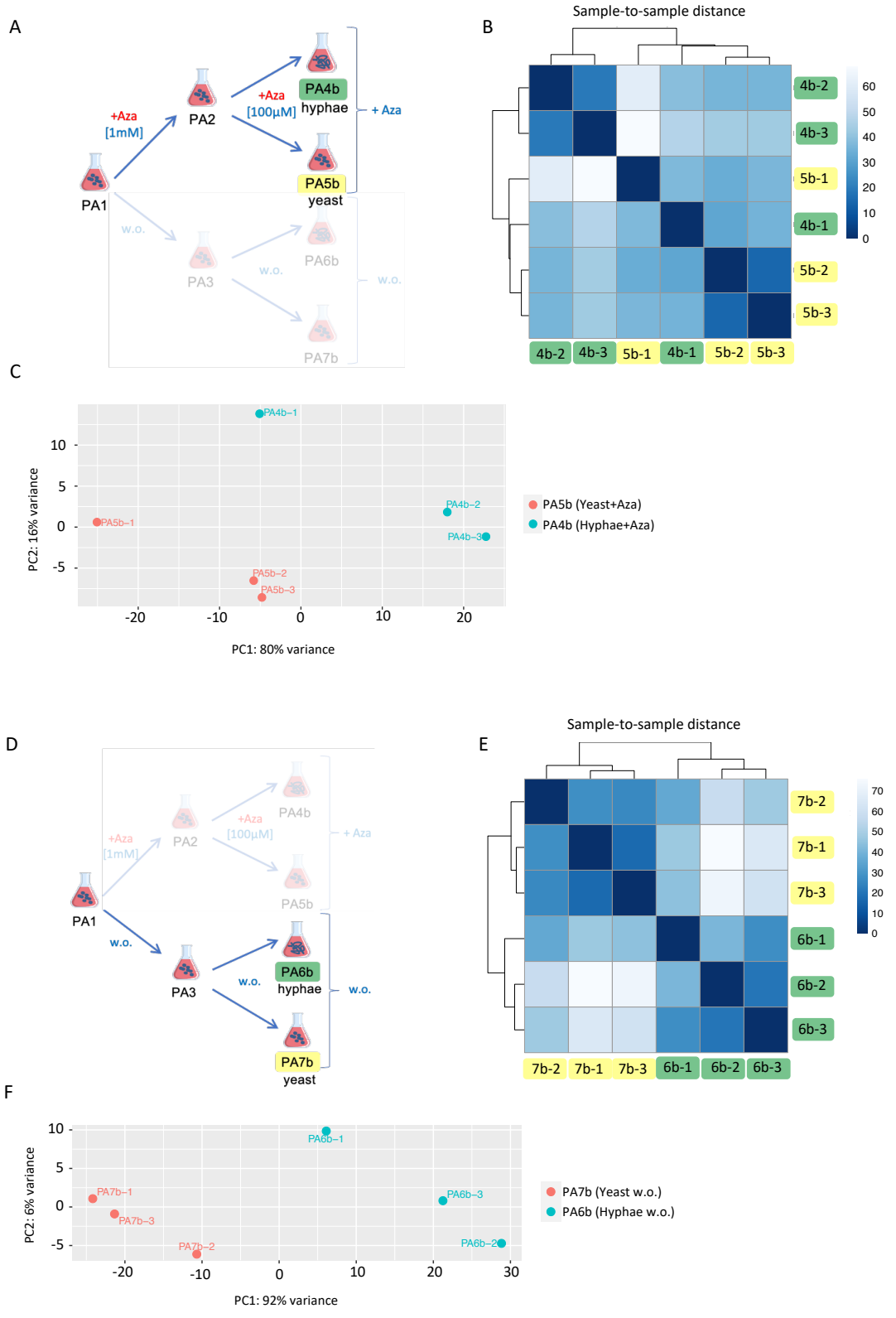

Supplementary Figure 10: Variance analysis of 5-Aza treated and untreated *C. albicans* hyphae and yeast cultures. (A) Experimental setup with culture group PA4b (green) in hyphae morphology and culture group PA5b (yellow) in yeast morphology. Both treated with 100 µM 5-Aza. (D) Experimental setup with culture group PA6b (green) in hyphae morphology and culture group PA7b (yellow) in yeast morphology. Both untreated. (B)+(E) Heatmap of sample-to-sample distance matrix (Euclidean distance). (C)+(F) PCA plot showing the variance between the two sample groups and amongst their replicates. Analysis was carried out with DESeq2, which calculates variances based on normalized counts.

6.3.1 Differentially expression (DE) analysis

Supplementary Table 6: Top 25 significantly up- and downregulated genes of 5-Aza treated versus untreated *C. albicans* yeast precultures (PA2 vs. PA3)

Gene	Log2FC	Function
upregulated		
C5_03770C	7.60	Protein similar to *Candida boidinii* formate dehydrogenase
C2_10070W	6.85	Predicted dehydrogenase
FDH1	5.82	Formate dehydrogenase, oxidizes formate to CO_2, stationary phase enriched
HSP31	4.51	Putative 30 kda heat shock protein
DUT1	4.20	dUTP pyrophosphatase, decreased in stationary phase yeast
ICL1	3.89	Isocitrate lyase, glyoxylate cycle enzyme, farnesol regulated, stationary phase enriched
C1_09670C	3.80	Has domain(s) with predicted DNA binding activity, role in DNA recombination, DNA repair, DNA replication and nucleus localization
POL1	3.67	Putative DNA directed DNA polymerase alpha
PGA6	3.56	GPI-anchored cell wall adhesin-like protein, induced by high iron, upregulated upon Als2 depletion, mRNA binds She3 and is localized to hyphal tips
MSH6	3.48	Protein similar to *S. cerevisiae* Msh6p, which is involved in mismatch repair
POL30	3.40	Proliferating cell nuclear antigen (PCNA), forms homotrimeric sliding clamp for DNA polymerases, stationary phase enriched protein
RFA2	3.32	Putative DNA replication factor A, RNA abundance regulated by cell cycle, tyrosol and cell density
RNR1	3.32	Ribonucleotide reductase large subunit, induced in low iron, farnesol upregulated in biofilm
MCD1	3.28	Alpha-kleisin cohesin complex subunit, for sister chromatid cohesion in mitosis and meiosis, periodic cell-cycle expression
IRR1	3.25	Putative cohesin complex subunit, cell-cycle regulated periodic mRNA expression
CTF8	3.16	Putative kinetochore protein with a predicted role in sister chromatid cohesion
CHA1	3.13	Similar to catabolic ser/thr dehydratases, repressed by Rim101, induced in low iron, filament induced
SMC1	3.05	Protein similar to chromosomal ATPases, cell-cycle regulated periodic mRNA expression
CR_08830W	3.03	Protein of unknown function, Spider biofilm induced
CR_07540C	3.02	Protein of unknown function, downregulated by fluphenazine treatment or in an azole-resistant strain that overexpresses CDR1 and CDR2
MPH1	2.97	Protein similar to *S. cerevisiae* Mph1p, which is a DNA helicase involved in DNA repair
TSA1B	2.96	Putative peroxidase, Tsa1p and Tsa1Bp role under oxidative/reductive stress
PRI2	2.96	Putative DNA primase, gene adjacent to and divergently transcribed with CDC68, Hap43-induced
C1_12910W	2.95	Protein of unknown function, Spider biofilm repressed
SUT1	2.95	Zn2Cys6 transcription factor involved in sterol uptake
downregulated		
OPT4	-2.81	Oligopeptide transporter, Hap43-repressed

C4_03960W	-2.76	Protein of unknown function, ORF added to Assembly 21 based on comparative genome analysis, protein detected by mass spec in stationary phase cultures
GPI14	-2.64	Catalytic subunit of glycosylphosphatidylinositol-alpha 1,4 mannosyltransferase I, involved in GPI anchor biosynthesis, regulated by Tsa1p, Tsa1Bp under H_2O_2 stress conditions
CRG1	-2.64	Methyltransferase involved in sphingolipid homeostasis, methylates a drug cantharidin, decreased expression in hyphae compared to yeast, Hap43-repressed gene
C7_03830C	-2.62	Ortholog(s) have role in posttranslational protein targeting to endoplasmic reticulum membrane and TRC complex, cytoplasm localization
OPT3	-2.49	Oligopeptide transporter, Hap43-repressed
RNR22	-2.33	Putative ribonucleoside diphosphate reductase, colony morphology-related gene regulation by Ssn6, transcript regulated by tyrosol and cell density, Hap43-repressed
GDH3	-2.27	NADP-glutamate dehydrogenase, Nrg1, Plc1 regulated, hypha, hypoxia, Efg1-repressed, exp and stationary phase protein
OPT2	-2.22	Oligopeptide transporter, macrophage/pseudohyphal-repressed after 16h, Hap43-repressed
CDA2	-2.20	Putative chitin deacetylase, transcription is positively regulated by Tbf1p
CR_04750W	-2.10	Protein of unknown function, Hap43-induced, rat catheter and Spider biofilm induced
URA1	-2.08	Dihydroorotate dehydrogenase, de novo pyrimidine biosynthesis, regulated by yeast-hypha switch
DBR1	-2.03	Debranchase, homozygous mutant accumulates lariat intermediates of mRNA splicing
C7_00910C	-2.02	Ortholog of S. cerevisiae Ioc4, a protein that influences gene expression through chromatin remodeling, oxidative stress-induced via Cap1
C6_02100W	-2.02	Secreted protein, Hap43-repressed, fluconazole-induced, regulated by Tsa1, Tsa1B under H2O2 stress conditions
AQY1	-2.02	Aquaporin water channel, osmotic shock resistance
BMT4	-2.01	Beta-mannosyltransferase, for elongation of beta-mannose chains on the acid-labile fraction of cell wall phosphopeptidomannan, 9-gene family member, regulated by Tsa1, Tsa1B
MNN14	-1.96	Predicted alpha-1,3-mannosyltransferase activity with a role in protein glycosylation, Hap43-repressed
C6_03360C	-1.95	Ortholog of C. dubliniensis CD36 : Cd36_63640, C. auris B8441 : B9J08_001441, Pichia stipitis Pignal : PICST_32878 and Candida guilliermondii ATCC 6260 : PGUG_03423
C2_07620W	-1.94	Has domain(s) with predicted guanyl-nucleotide exchange factor activity, role in regulation of Rho protein signal transduction and intracellular anatomical structure localization
GAP2	-1.93	General broad specificity amino acid permease, regulated by Nrg1, Tup1, colony morphology-related gene regulation by Ssn6
ALK6	-1.92	Putative cytochrome P-450 of N-alkane-induced detoxification
AMS1	-1.92	Putative alpha-mannosidase, transcript regulated by Nrg1
C7_02610C	-1.92	Putative Gag protein of retrotransposon Tca2
C3_01220W	-1.91	Putative transcription factor with zinc finger DNA-binding motif

Supplementary Table 7: Top 25 significantly up- and downregulated genes of 5-Aza treated hyphal subculture versus yeast preculture (PA4b vs. PA2)

Gene	Log2FC	Function
upregulated		
ECE1	7.26	Candidalysin, cytolytic peptide toxin essential for mucosal infection, hypha-specific protein, regulated by Rfg1, Nrg1, Tup1, Cph1, Efg1, Hog1, farnesol, phagocytosis, fluconazole-induced, rat catheter and Spider biofilm induced
SOD5	6.89	Cu-containing superoxide dismutase, protects against oxidative stress, induced by neutrophils, hyphal growth, osmotic/oxidative stress, Spider biofilm induced
SAP6	6.45	Biofilm-specific aspartyl protease, expressed during hyphal growth
PHR1	6.13	Cell surface glycosidase, may act on cell-wall beta-1,3-glucan prior to beta-1,6-glucan linkage, role in systemic, high pH or filamentation induced
HYR1	5.86	GPI-anchored hyphal cell wall protein, regulated by Rfg1, Efg1, Nrg1, Tup1, Cyr1, Bcr1, Hap43, Spider and flow model biofilm induced
CFL11	5.81	Superoxide-generating NADPH oxidase, produces extracellular burst of reactive oxygen species at growing cell tips during hyphal morphogenesis
C1_13100W_A	5.58	Putative adhesin-like protein, Spider biofilm induced
RBT1	5.27	Cell wall protein with similarity to Hwp1, predicted glycosylation, Tup1 repressed, farnesol, hyphal and alkaline induced, Rfg1, Rim101-regulated
HGT1	5.20	High-affinity MFS glucose transporter, likely essential for growth, protein newly produced during adaptation to the serum, Spider biofilm induced
PHO89	5.15	Putative phosphate permease, transcript regulated upon white-opaque switch, alkaline induced by Rim101, Spider biofilm induced
HGT12	5.09	Glucose, fructose, mannose transporter, major facilitator superfamily, role in macrophage-induced hyphal growth, detected at germ tube plasma membrane
SKN1	5.03	Protein with a role in beta-1,6-glucan synthesis, probable N-glycosylated type II membrane protein, transcript and mRNA length change induced by yeast-hypha transition, induced by Rim101, Spider biofilm induced
C1_06340W_A	4.10	Ortholog of C. dubliniensis CD36 : Cd36_05920, C. parapsilosis CDC317 : CPAR2_803860, C. auris B8441 : B9J08_000594, Pichia stipitis Pignal : PICST_30324 and Candida guilliermondii ATCC 6260 : PGUG_04439
SAP5	4.08	Biofilm-specific aspartyl protease, virulence role effected by URA3, expressed during infection, mRNA localized to hyphal tip via She3, Spider biofilm induced
MAL31	3.97	Putative high-affinity maltose transporter, transcript is upregulated in clinical isolates from HIV+ patients with oral candidiasis, alkaline induced, Spider biofilm induced
GCV2	3.90	Glycine decarboxylase P subunit, protein of glycine catabolism, repressed by Efg1, Hog1-induced, induced by Rim101 at acid pH
FAV1	3.89	Protein with weak similarity to S. cerevisiae Fus2p, induced by alpha pheromone mating factor in MTLa/MTLa opaque cells
C1_07220W_A	3.86	Protein of unknown function, Plc1p-regulated, expression induced early upon infection of reconstituted human epithelium, Spider biofilm induced
HWP1	3.83	Hyphal cell wall protein, host transglutaminase substrate, opaque-, a-specific, alpha-factor induced, at MTLa side of conjugation tube, Spider biofilm induced
PGA45	3.78	Putative GPI-anchored cell wall protein, regulated by Ssn6, Mob2-dependent hyphal regulation
ATO1	3.65	Putative fungal-specific transmembrane protein, induced by Rgt1, Spider biofilm induced

C4_03480C_A	3.64	Ortholog of C. dubliniensis CD36 : Cd36_43270 and Candida albicans WO-1 : CAWG_03460
UME6	3.56	Zn(II)2Cys6 transcription factor, has a long 5'-UTR that regulates translational efficiency and controls transition to filamentous growth
HGT20	3.54	Putative glucose transporter of the major facilitator superfamily, regulated by Nrg1
C1_05950C_A	3.53	Protein of unknown function, induced in high iron, repressed in core caspofungin response, ketoconazole-repressed, colony morphology-related gene regulation by Ssn6, possibly subject to Kex2 processing
downregulated		
RBR1	-9.01	Glycosylphosphatidylinositol (GPI)-anchored cell wall protein, required for filamentous growth at acidic pH, expression repressed by Rim101 and activated by Nrg1, Hap43-induced
C5_03770C_A	-8.79	Protein similar to Candida boidinii formate dehydrogenase, virulence-group-correlated expression, Hap43-repressed, Spider biofilm repressed
C5_04480C_A	-7.52	Has domain(s) with predicted nucleic acid binding, nucleotide binding activity
C2_00860C_A	-7.46	Protein of unknown function, Spider biofilm induced
C2_10070W_A	-7.43	Predicted dehydrogenase, transcript upregulated in an RHE model of oral candidiasis, virulence-group-correlated expression, Spider biofilm repressed
C1_10170W_A	-7.00	Putative adhesin-like protein, Hap43-repressed, rat catheter and Spider biofilm induced
HSP30	-6.97	Putative heat shock protein, fluconazole repressed, amphotericin B induced, Spider biofilm induced, rat catheter biofilm induced
CRZ2	-6.81	C2H2 transcription factor, Rim101-repressed at pH 8, required for yeast cell adherence to silicone substrate, Spider biofilm induced
AQY1	-6.73	Aquaporin water channel, osmotic shock resistance, Spider biofilm induced, required for RPMI biofilm formation
FMP45	-6.34	Predicted membrane protein induced during mating, alkaline repressed, Spider biofilm induced
C5_04980W_A	-6.29	Putative adhesin-like protein, induced by Mnl1 under weak acid stress, Spider biofilm induced
FET99	-6.29	Multicopper oxidase family protein, similar to S. cerevisiae Fet3, iron-repressed, regulated by Tup1, Rim101, Spider biofilm repressed
FDH1	-6.11	Formate dehydrogenase, oxidizes formate to CO2, Mig1 regulated, repressed by Efg1 in yeast, not hyphal conditions, stationary phase enriched, Spider biofilm induced
CR_02880W_A	-6.11	Protein of unknown function, Hap43-repressed, induced in core caspofungin response, regulated by yeast-hypha switch, Spider biofilm repressed
SOD3	-6.09	Cytosolic manganese-containing superoxide dismutase, protects against oxidative stress, Hap43-repressed, Spider biofilm induced
WH11	-6.04	White-phase yeast transcript, expression in opaques increases virulence/switching, Spider biofilm induced
AOX1	-5.98	Alternative oxidase, low abundance, constitutively expressed, one of two isoforms (Aox1p and Aox2p), involved in a cyanide-resistant respiratory pathway present in plants, protists, and some fungi
RTA3	-5.90	7-transmembrane receptor protein involved in regulation of asymmetric lipid distribution in plasma membrane

ALS4	-5.83	GPI-anchored adhesin, role in adhesion, germ tube induction, growth, temperature regulated, repressed during chlamydospore formation
ASR1	-5.83	Heat shock protein, transcript regulated by cAMP, osmotic stress, colony morphology-related regulated by Ssn6, stationary phase enriched, Spider biofilm induced
CSH1	-5.77	Aldo-keto reductase, role in fibronectin adhesion, cell surface hydrophobicity, regulated by temperature, growth phase, Spider biofilm induced
C7_03560W_A	-5.71	Protein of unknown function, Spider biofilm induced
C4_00990W_A	-5.58	NRAMP metal ion transporter domain-containing protein, induced by nitric oxide independent of Yhb1
IFD6	-5.35	Aldo-keto reductase, similar to aryl alcohol dehydrogenases, farnesol regulated, possibly essential, Spider biofilm induced
ZRT2	-5.17	Zinc transporter, essential for zinc uptake and acidic conditions tolerance, Spider biofilm induced

Supplementary Table 8: Top 25 significantly up- and downregulated genes of 5-Aza treated *C. albicans* yeast subculture versus yeast preculture (PA5b vs. PA2)

Gene	Log2FC	Function
upregulated		
C2_06930C_A	4.70	Ortholog of C. dubliniensis CD36 : Cd36_21220, C. parapsilosis CDC317 : CPAR2_406700, Candida tenuis NRRL Y-1498 : CANTEDRAFT_127772 and Candida tropicalis MYA-3404 : CTRG_01766
PUT1	4.52	Putative proline oxidase, alkaline upregulated by Rim101, flow model biofilm induced, Spider biofilm induced
HGT12	4.48	Glucose, fructose, mannose transporter, major facilitator superfamily, role in macrophage-induced hyphal growth, detected at germ tube plasma membrane by mass spectrometry, Snf3p-induced, 12 probable transmembrane segments
GAL7	4.39	Putative galactose-1-phoshphate uridyl transferase, downregulated by hypoxia, upregulated by ketoconazole, macrophage/pseudohyphal-repressed
GCV2	4.34	Glycine decarboxylase P subunit, protein of glycine catabolism, repressed by Efg1, Hog1-induced, induced by Rim101 at acid pH, transcript induced in elevated CO2, stationary phase enriched protein
PUT2	4.23	Putative delta-1-pyrroline-5-carboxylate dehydrogenase, alkaline upregulated, protein present in exponential and stationary growth phase yeast cultures, flow model biofilm induced, Spider biofilm induced
RBT1	4.10	Cell wall protein with similarity to Hwp1, required for virulence, predicted glycosylation, fluconazole, Tup1 repressed, farnesol, alpha factor, serum, hyphal and alkaline induced, Rfg1, Rim101-regulated
RPS7A	3.93	Ribosomal protein S7, genes encoding cytoplasmic ribosomal subunits, translation factors, and tRNA synthetases are downregulated upon phagocytosis by murine macrophage, Spider biofilm repressed
C1_08520C_A	3.73	Ortholog(s) have structural constituent of ribosome activity and mitochondrial large ribosomal subunit localization
GCV1	3.61	Putative T subunit of glycine decarboxylase, transcript negatively regulated by Sfu1, Spider biofilm repressed
C5_01550C_A	3.58	Predicted protein of unknown function, overlaps orf19.4149.1

HGT10	3.57	Glycerol permease involved in glycerol uptake, member of the major facilitator superfamily, induced by osmotic stress, at low glucose in rich media, during cell wall regeneration, 12 membrane spans, Hap43p-induced gene
MRV5	3.56	Planktonic growth-induced gene
RPL35	3.51	Ribosomal protein, downregulation correlates with clinical development of fluconazole resistance, colony morphology-related gene regulation by Ssn6, Hap43-induced, Spider biofilm repressed
C5_03410C_A	3.51	Ortholog(s) have structural constituent of ribosome activity and mitochondrial large ribosomal subunit localization
C1_13100W_A	3.50	Putative adhesin-like protein, Spider biofilm induced
C5_01540W_A	3.49	Protein component of the small (40S) ribosomal subunit, Spider biofilm repressed
SER2	3.46	Ortholog(s) have phosphoserine phosphatase activity and role in L-serine biosynthetic process
MRPL10	3.44	Putative mitochondrial large subunit ribosomal protein, colony morphology-related gene regulation by Ssn6
ECE1	3.43	Candidalysin, cytolytic peptide toxin essential for mucosal infection, hypha-specific protein, regulated by Rfg1, Nrg1, Tup1, Cph1, Efg1, Hog1, farnesol, phagocytosis, fluconazole-induced, rat catheter and Spider biofilm induced
PGA45	3.38	Putative GPI-anchored cell wall protein, repressed in core caspofungin response, Hog1-induced, regulated by Ssn6, Mob2-dependent hyphal regulation, flow model biofilm induced
C2_03950W_A	3.37	Putative ribosomal protein, large subunit, mitochondrial precursor, repressed by prostaglandins, Spider biofilm repressed
C5_00820W_A	3.37	Ortholog(s) have structural constituent of ribosome activity and mitochondrial large ribosomal subunit localization
RPS12	3.35	Acidic ribosomal protein S12, regulated by Gcn4, activated by Tbf1, repressed by amino acid starvation (3-AT), protein abundance is affected by URA3 expression in CAI-4 strain background, sumoylation target, Spider biofilm repressed
C1_02330C_A	3.34	Ribosomal 60S subunit protein, Spider biofilm repressed
downregulated		
IFD6	-7.68	Aldo-keto reductase, similar to aryl alcohol dehydrogenases, protein increase correlates with MDR1 overexpression (not CDR1 or CDR2) in fluconazole-resistant clinical isolates, farnesol regulated, possibly essential, Spider biofilm induced
ASR1	-7.44	Heat shock protein, transcript regulated by cAMP, osmotic stress, ciclopirox olamine, ketoconazole, repressed by Cyr1, Ras1, colony morphology-related regulated by Ssn6, stationary phase enriched, Hap43-induced, Spider biofilm induced
CSH1	-7.39	Aldo-keto reductase, role in fibronectin adhesion, cell surface hydrophobicity, regulated by temperature, growth phase, benomyl, macrophage interaction, azole resistance associated, Spider biofilm induced, rat catheter biofilm repressed
C5_03770C_A	-7.37	Protein similar to Candida boidinii formate dehydrogenase, virulence-group-correlated expression, Hap43-repressed, Spider biofilm repressed
C1_10170W_A	-7.31	Putative adhesin-like protein, Hap43-repressed, rat catheter and Spider biofilm induced
C5_04480C_A	-7.24	Has domain(s) with predicted nucleic acid binding, nucleotide binding activity

RBR1	-7.13	Glycosylphosphatidylinositol (GPI)-anchored cell wall protein, required for filamentous growth at acidic pH, expression repressed by Rim101 and activated by Nrg1, Hap43-induced
C2_08260W_A	-7.09	Protein of unknown function, Hap43-repressed gene, by Rgt1, repressed in Spider biofilms by Bcr1, Tec1, Brg1, Rob1 and induced by Efg1, Ndt80, Spider biofilm induced
C1_04010C_A	-6.99	Protein with a NADP-dependent oxidoreductase domain, transcript induced by ketoconazole, rat catheter and Spider biofilm induced
C5_04980W_A	-6.90	Putative adhesin-like protein, induced by Mnl1 under weak acid stress, rat catheter and Spider biofilm induced
RBT5	-6.85	GPI-linked cell wall protein, hemoglobin utilization, Rfg1, Rim101, Tbf1, Fe regulated, Sfu1, Hog1, Tup1, serum, alkaline pH, antifungal drugs, geldamycin repressed, Hap43 induced, required for RPMI biofilms, Spider biofilm induced
WH11	-6.79	White-phase yeast transcript, expression in opaques increases virulence/switching, mutant switches as WT, Hap43, hypoxia, ketoconazol induced, required for RPMI biofilm, Bcr1-induced in RPMI a/a biofilm, rat catheter, Spider biofilm induced
HSP30	-6.70	Putative heat shock protein, fluconazole repressed, amphotericin B induced, Spider biofilm induced, rat catheter biofilm induced
AQY1	-6.58	Aquaporin water channel, osmotic shock resistance, WT freeze tolerance, virulent in mice, flucytosine repressed, flow model/RPMI/Spider/rat catheter biofilm induced, required for RPMI biofilm formation, Bcr1-induced in a/a RPMI biofilms
SOD3	-6.48	Cytosolic manganese-containing superoxide dismutase, protects against oxidative stress, repressed by ciclopirox olamine, induced during stationary phase when SOD1 expression is low, Hap43-repressed, Spider and flow model biofilm induced
FMP45	-6.39	Predicted membrane protein induced during mating, mutation confers hypersensitivity to toxic ergosterol analog, to amphotericin B, alkaline repressed, repressed by alpha pheromone in SpiderM medium, rat catheter, Spider biofilm induced
C1_11200W_A	-6.37	Predicted mucin-like protein, ketoconazole-induced, fluconazole-repressed, induced in cyr1 mutant, colony morphology-related gene regulation by Ssn6, flow model biofilm induced, Spider biofilm induced
ARG3	-6.29	Putative ornithine carbamoyltransferase, Gcn4-regulated, Hap43-induced, repressed in alkalinizing medium, rat catheter and Spider biofilm induced
FDH1	-6.23	Formate dehydrogenase, oxidizes formate to CO2, Mig1 regulated, induced by macrophages, fluconazole-repressed, repressed by Efg1 in yeast, not hyphal conditions, stationary phase enriched, rat catheter and Spider biofilm induced
C3_06040W_A	-6.21	CCCH zinc finger protein, Spider biofilm induced
C5_02110W_A	-6.19	Putative heat shock protein, decreased expression in hyphae, transcription is increased in populations of cells exposed to fluconazole over multiple generations, overexpression increases resistance to farnesol and azoles
GST2	-6.18	Glutathione S transferase, induced by benomyl and in populations of cells exposed to fluconazole over multiple generations, regulated by Nrg1, Tup1, induced by nitric oxide, stationary phase enriched, Spider biofilm induced
LAP3	-6.14	Putative aminopeptidase, positively regulated by Sfu1, clade-associated gene expression, virulence-group-correlated expression, induced by alpha pheromone in SpiderM medium, Hap43-induced, Spider and flow model biofilm induced

GLX3	-6.10	Glutathione-independent glyoxalase, binds human immunoglobulin E, alkaline, fluconazole, Hog1 repressed, hypoxia, oxidative stress via Cap1, Hap43 induced, stationary-phase enriched, rat catheter, Spider biofilm induced
AOX1	-5.99	Alternative oxidase, low abundance, constitutively expressed, one of two isoforms (Aox1p and Aox2p), involved in a cyanide-resistant respiratory pathway present in plants, protists, and some fungi, absent in S. cerevisiae, Hap43p-repressed

Supplementary Table 9: Top 25 significantly up- and downregulated genes of untreated hyphal subculture versus yeast preculture (PA6b vs. PA3)

Gene	Log2FC	Function
upregulated		
ECE1	7.79	Candidalysin, cytolytic peptide toxin essential for mucosal infection, hypha-specific protein, regulated by Rfg1, Nrg1, Tup1, Cph1, Efg1, Hog1, farnesol, phagocytosis, fluconazole-induced, rat catheter and Spider biofilm induced
SOD5	7.48	Cu-containing superoxide dismutase, protects against oxidative stress, induced by neutrophils, hyphal growth, caspofungin, osmotic/oxidative stress, oralpharyngeal candidiasis induced, rat catheter and Spider biofilm induced
PHR1	6.93	Cell surface glycosidase, may act on cell-wall beta-1,3-glucan prior to beta-1,6-glucan linkage, role in systemic, not vaginal virulence (neutral, not low pH), high pH or filamentation induced, Bcr1-repressed in RPMI a/a biofilm
SAP6	6.39	Biofilm-specific aspartyl protease, expressed during hyphal growth, oral carriage, infection, virulence role affecte by URA3, N-glycosylated, rat catheter biofilm induced
CFL11	6.30	Superoxide-generating NADPH oxidase, produces extracellular burst of reactive oxygen species at growing cell tips during hyphal morphogenesis, flucytosine repressed, possibly adherence-induced, rat catheter biofilm repressed
IHD1	6.16	GPI-anchored protein, alkaline, hypha-induced, regulated by Nrg1, Rfg1, Tup1 and Tsa1, Tsa1B in minimal media at 37, oralpharyngeal candidasis induced , Spider biofilm induced, regulated in Spider biofilms by Tec1, Efg1, Ndt80, Rob1, Brg1
HYR1	6.10	GPI-anchored hyphal cell wall protein, macrophage-induced, repressed by neutrophils, resistance to killing by neutrophils, azoles, regulated by Rfg1, Efg1, Nrg1, Tup1, Cyr1, Bcr1, Hap43, Spider and flow model biofilm induced
GCV2	6.08	Glycine decarboxylase P subunit, protein of glycine catabolism, repressed by Efg1, Hog1-induced, induced by Rim101 at acid pH, transcript induced in elevated CO2, stationary phase enriched protein
IDP2	6.06	Isocitrate dehydrogenase, white-opaque switch regulated, morphology-regulation by Ssn6, protein in exponential and stationary phase yeast, Hap43-repressed, Spider biofilm repressed by Bcr1, Tec1, Ndt80, Rob1, Brg1, Spider biofilm induced
SKN1	6.06	Protein with a role in beta-1,6-glucan synthesis, probable N-glycosylated type II membrane protein, transcript and mRNA length change induced by yeast-hypha transition, induced by Rim101, caspofungin, rat catheter and Spider biofilm induced
C1_13100W_A	6.04	Putative adhesin-like protein, Spider biofilm induced

C1_06340W_A	6.02	Ortholog of C. dubliniensis CD36 : Cd36_05920, C. parapsilosis CDC317 : CPAR2_803860, C. auris B8441 : B9J08_000594, Pichia stipitis Pignal : PICST_30324 and Candida guilliermondii ATCC 6260 : PGUG_04439
ATO1	5.62	Putative fungal-specific transmembrane protein, induced by Rgt1, Spider biofilm induced
HGT1	5.55	High-affinity MFS glucose transporter, induced by progesterone, chloramphenicol, benomyl, likely essential for growth, protein newly produced during adaptation to the serum, rat catheter and Spider biofilm induced
CTF8	5.43	Putative kinetochore protein with a predicted role in sister chromatid cohesion, repressed during the mating process, flow model biofilm induced
GCV1	5.37	Putative T subunit of glycine decarboxylase, transcript negatively regulated by Sfu1, Spider biofilm repressed
RBT1	5.32	Cell wall protein with similarity to Hwp1, required for virulence, predicted glycosylation, fluconazole, Tup1 repressed, farnesol, alpha factor, serum, hyphal and alkaline induced, Rfg1, Rim101-regulated
UME6	5.17	Zn(II)2Cys6 transcription factor, has a long 5'-UTR that regulates translational efficiency and controls transition to filamentous growth, stability controlled by Grr1p, Ubr1p, Ptc2p in response to CO2 and O2 levels
C6_02210W_A	5.12	Protein of unknown function, oxidative stress-induced via Cap1, induced by alpha pheromone in SpiderM medium
PHO89	5.09	Putative phosphate permease, transcript regulated upon white-opaque switch, alkaline induced by Rim101, possibly adherence-induced, F-12/CO2 model, rat catheter and Spider biofilm induced
HWP1	5.08	Hyphal cell wall protein, host transglutaminase substrate, opaque-, a-specific, alpha-factor induced, at MTLa side of conjugation tube, virulence complicated by URA3 effects, Bcr1-repressed in RPMI a/a biofilms, Spider biofilm induced
C4_03480C_A	4.95	Ortholog of C. dubliniensis CD36 : Cd36_43270 and Candida albicans WO-1 : CAWG_03460
FAV1	4.87	Protein with weak similarity to S. cerevisiae Fus2p, induced by alpha pheromone mating factor in MTLa/MTLa opaque cells
HGT20	4.81	Putative glucose transporter of the major facilitator superfamily, the C. albicans glucose transporter family comprises 20 members, 12 probable membrane-spanning segments, regulated by Nrg1
C2_06930C_A	4.74	Ortholog of C. dubliniensis CD36 : Cd36_21220, C. parapsilosis CDC317 : CPAR2_406700, Candida tenuis NRRL Y-1498 : CANTEDRAFT_127772 and Candida tropicalis MYA-3404 : CTRG_01766
downregulated		
C1_10170W_A	-10.92	Putative adhesin-like protein, Hap43-repressed, rat catheter and Spider biofilm induced
WH11	-10.31	White-phase yeast transcript, expression in opaques increases virulence/switching, mutant switches as WT, Hap43, hypoxia, ketoconazol induced, required for RPMI biofilm, Bcr1-induced in RPMI a/a biofilm, rat catheter, Spider biofilm induced
AQY1	-10.21	Aquaporin water channel, osmotic shock resistance, WT freeze tolerance, virulent in mice, flucytosine repressed, flow model/RPMI/Spider/rat catheter biofilm induced, required for RPMI biofilm formation, Bcr1-induced in a/a RPMI biofilms

CRZ2	-9.19	C2H2 transcription factor, involved in regulation of early adaptation to murine GI tract, Rim101-repressed at pH 8, required for yeast cell adherence to silicone substrate, Spider biofilm induced
C2_00860C_A	-9.07	Protein of unknown function, Spider biofilm induced
IFD6	-9.01	Aldo-keto reductase, similar to aryl alcohol dehydrogenases, protein increase correlates with MDR1 overexpression (not CDR1 or CDR2) in fluconazole-resistant clinical isolates, farnesol regulated, possibly essential, Spider biofilm induced
C7_03560W_A	-8.97	Protein of unknown function, expression decreases by benomyl treatment or in an azole-resistant strain overexpressing MDR1, Spider biofilm induced
HSP30	-8.88	Putative heat shock protein, fluconazole repressed, amphotericin B induced, Spider biofilm induced, rat catheter biofilm induced
RBR1	-8.68	Glycosylphosphatidylinositol (GPI)-anchored cell wall protein, required for filamentous growth at acidic pH, expression repressed by Rim101 and activated by Nrg1, Hap43-induced
FET99	-8.54	Multicopper oxidase family protein, similar to S. cerevisiae Fet3, does not complement S. cerevisiae fet3 mutant growth under low-iron, iron-repressed, regulated by Tup1, Rim101, flow model biofilm induced, Spider biofilm repressed
CSH1	-8.32	Aldo-keto reductase, role in fibronectin adhesion, cell surface hydrophobicity, regulated by temperature, growth phase, benomyl, macrophage interaction, azole resistance associated, Spider biofilm induced, rat catheter biofilm repressed
FMP45	-8.22	Predicted membrane protein induced during mating, mutation confers hypersensitivity to toxic ergosterol analog, to amphotericin B, alkaline repressed, repressed by alpha pheromone in SpiderM medium, rat catheter, Spider biofilm induced
CR_08880C_A	-7.95	Protein of unknown function, rat catheter and Spider biofilm induced
C5_04480C_A	-7.83	Has domain(s) with predicted nucleic acid binding, nucleotide binding activity
C2_08260W_A	-7.37	Protein of unknown function, Hap43-repressed gene, by Rgt1, repressed in Spider biofilms by Bcr1, Tec1, Brg1, Rob1 and induced by Efg1, Ndt80, Spider biofilm induced
GLX3	-7.24	Glutathione-independent glyoxalase, binds human immunoglobulin E, alkaline, fluconazole, Hog1 repressed, hypoxia, oxidative stress via Cap1, Hap43 induced, stationary-phase enriched, rat catheter, Spider biofilm induced
HSP70	-7.14	Putative hsp70 chaperone, role in entry into host cells, heat-shock, amphotericin B, cadmium, ketoconazole-induced, surface localized in yeast and hyphae, antigenic in host, farnesol-downregulated in biofilm, Spider biofilm induced
CR_09140C_A	-6.94	Protein with a role in directing meiotic recombination events to homologous chromatids, induced by ciclopirox olamine, positively regulated by Sfu1, Hog1, fluconazole-repressed, Hap43-induced, Spider biofilm induced
HSP12	-6.81	Heat-shock protein, induced by osmotic/oxidative/cadmium stress, fluphenazine treatment, low iron, CDR1 and CDR2 overexpression, or ssn6 or ssk1 null mutation, overexpression increases resistance to farnesol and azoles
BMT4	-6.77	Beta-mannosyltransferase, for elongation of beta-mannose chains on the acid-labile fraction of cell wall phosphopeptidomannan, 9-gene family member, regulated by Tsa1, Tsa1B, flow model biofilm induced, rat catheter biofilm repressed

C1_04010C_A	-6.64	Protein with a NADP-dependent oxidoreductase domain, transcript induced by ketoconazole, rat catheter and Spider biofilm induced
ASR2	-6.56	Adenylyl cyclase and stress responsive protein, induced in cyr1 or ras1 mutant, stationary phase enriched protein, Spider biofilm induced
GAP2	-6.53	General broad specificity amino acid permease, ketoconazole, flucytosine repressed, Ssy1-dependent histidine induction, regulated by Nrg1, Tup1, colony morphology-related gene regulation by Ssn6, Spider and flow model biofilm induced
C3_02750W_A	-6.50	Protein with a ribonuclease III domain, flow model biofilm induced, Spider biofilm induced
C5_02110W_A	-6.49	Putative heat shock protein, decreased expression in hyphae, transcription is increased in populations of cells exposed to fluconazole over multiple generations, overexpression increases resistance to farnesol and azoles

Supplementary Table 10: Top 25 significantly up- and downregulated genes of untreated yeast subculture versus yeast preculture (PA7b vs. PA3)

Gene	Log2FC	Function
upregulated		
C2_06930C_A	6.62	Ortholog of C. dubliniensis CD36 : Cd36_21220, C. parapsilosis CDC317 : CPAR2_406700, Candida tenuis NRRL Y-1498 : CANTEDRAFT_127772 and Candida tropicalis MYA-3404 : CTRG_01766
GCV2	6.34	Glycine decarboxylase P subunit, protein of glycine catabolism, repressed by Efg1, Hog1-induced, induced by Rim101 at acid pH, transcript induced in elevated CO2, stationary phase enriched protein
CTF8	6.20	Putative kinetochore protein with a predicted role in sister chromatid cohesion, repressed during the mating process, flow model biofilm induced
PRI2	5.47	Putative DNA primase, gene adjacent to and divergently transcribed with CDC68, Hap43-induced, Spider biofilm repressed
C5_04140W_A	5.33	Protein of unknown function, decreased transcription is observed upon fluphenazine treatment or in an azole-resistant strain that overexpresses CDR1 and CDR2, transcription is repressed in response to alpha pheromone in SpiderM medium
GCV1	5.18	Putative T subunit of glycine decarboxylase, transcript negatively regulated by Sfu1, Spider biofilm repressed
MCD1	5.15	Alpha-kleisin cohesin complex subunit, for sister chromatid cohesion in mitosis and meiosis, repressed by alpha pheromone in SpiderM medium, periodic cell-cycle expression, Hap43-repressed, rat catheter and Spider biofilm repressed
OGG1	5.14	Mitochondrial glycosylase/lyase, repairs oxidative damage to mitochondrial DNA, contributes to UVA resistance, role in base-excision repair, Spider biofilm induced
IDP2	5.11	Isocitrate dehydrogenase, white-opaque switch regulated, morphology-regulation by Ssn6, protein in exponential and stationary phase yeast, Hap43-repressed, Spider biofilm repressed by Bcr1, Tec1, Ndt80, Rob1, Brg1, Spider biofilm induced
ESC4	5.10	Protein similar to S. cerevisiae Esc4, a protein that represses transposition, transposon mutation affects filamentation, rat catheter biofilm repressed

C1_07490C_A	5.05	Ortholog(s) have DNA-directed DNA polymerase activity, role in DNA replication initiation, telomere capping and alpha DNA polymerase:primase complex, nuclear envelope, nucleus localization
FAD3	4.90	Omega-3 fatty acid desaturase, production of alpha-linolenic acid, a major component of membranes, caspofungin induced, Plc1-regulated, colony morphology-related gene regulation by Ssn6, Spider biofilm induced, flow model biofilm repressed
GAL7	4.81	Putative galactose-1-phoshphate uridyl transferase, downregulated by hypoxia, upregulated by ketoconazole, macrophage/pseudohyphal-repressed
C2_09180W_A	4.72	Putative ribonuclease H2 subunit, required for RNase H2 activity, repressed in Spider biofilms by Bcr1, Tec1, Brg1, Rob1
CHT2	4.64	GPI-linked chitinase, required for normal filamentous growth, repressed in core caspofungin response, fluconazole, Cyr1, Efg1, pH-regulated, mRNA binds She3 and is localized to yeast-form buds and hyphal tips, Spider biofilm repressed
POL1	4.50	Putative DNA directed DNA polymerase alpha, RNA abundance regulated by cell cycle, tyrosol and cell density, rat catheter biofilm induced
MCM6	4.48	Putative MCM DNA replication initiation complex component, mRNA expression peak at cell-cycle M/G1 phase, regulated by tyrosol and cell density, repressed by alpha pheromone in SpiderM medium, Hap43-induced gene
DUT1	4.45	dUTP pyrophosphatase, cell-cycle regulated if expressed in S. cerevisiae, upstream MluI and SCB elements, 17-beta-estradiol, ethynyl estradiol, macrophage induced, decreased in stationary phase yeast, rat catheter, Spider biofilm repressed
GIN1	4.35	Protein involved in regulation of DNA-damage-induced filamentous growth, putative component of DNA replication checkpoint, ortholog of S. cerevisiae Mrc1p, an S-phase checkpoint protein, Hap43p-induced gene
C1_12910W_A	4.33	Protein of unknown function, Spider biofilm repressed
SMC5	4.31	Protein similar to S. cerevisiae Smc5p, which is involved in DNA repair, transposon mutation affects filamentous growth
PUT2	4.31	Putative delta-1-pyrroline-5-carboxylate dehydrogenase, alkaline upregulated, protein present in exponential and stationary growth phase yeast cultures, flow model biofilm induced, Spider biofilm induced
C1_03870C_A	4.31	Predicted heme-binding stress-related protein, Tn mutation affects filamentous growth, induced during chlamydospore formation in C. albicans and C. dubliniensis, Spider biofilm induced
DPB2	4.29	Probable subunit of DNA polymerase II (DNA polymerase epsilon), similar to S. cerevisiae Dpb2p, essential for viability, rat catheter biofilm induced
GAL1	4.26	Galactokinase, galactose, Mig1, Tup1, Hap43 regulated, fluconazole, ketoconazole-induced, stationary phase enriched protein, GlcNAc-induced protein, farnesol, hypoxia-repressed in biofilm, rat catheter and Spider biofilm induced
downregulated		
IFD6	-10.77	Aldo-keto reductase, similar to aryl alcohol dehydrogenases, protein increase correlates with MDR1 overexpression (not CDR1 or CDR2) in fluconazole-resistant clinical isolates, farnesol regulated, possibly essential, Spider biofilm induced
WH11	-10.51	White-phase yeast transcript, expression in opaques increases virulence/switching, mutant switches as WT, Hap43, hypoxia, ketoconazol

		induced, required for RPMI biofilm, Bcr1-induced in RPMI a/a biofilm, rat catheter, Spider biofilm induced
C1_10170W_A	-10.31	Putative adhesin-like protein, Hap43-repressed, rat catheter and Spider biofilm induced
AQY1	-9.86	Aquaporin water channel, osmotic shock resistance, WT freeze tolerance, virulent in mice, flucytosine repressed, flow model/RPMI/Spider/rat catheter biofilm induced, required for RPMI biofilm formation, Bcr1-induced in a/a RPMI biofilms
HSP30	-9.71	Putative heat shock protein, fluconazole repressed, amphotericin B induced, Spider biofilm induced, rat catheter biofilm induced
C2_08260W_A	-9.24	Protein of unknown function, Hap43-repressed gene, by Rgt1, repressed in Spider biofilms by Bcr1, Tec1, Brg1, Rob1 and induced by Efg1, Ndt80, Spider biofilm induced
C1_11200W_A	-9.06	Predicted mucin-like protein, ketoconazole-induced, fluconazole-repressed, induced in cyr1 mutant, colony morphology-related gene regulation by Ssn6, flow model biofilm induced, Spider biofilm induced
RBT5	-8.97	GPI-linked cell wall protein, hemoglobin utilization, Rfg1, Rim101, Tbf1, Fe regulated, Sfu1, Hog1, Tup1, serum, alkaline pH, antifungal drugs, geldamycin repressed, Hap43 induced, required for RPMI biofilms, Spider biofilm induced
CSH1	-8.95	Aldo-keto reductase, role in fibronectin adhesion, cell surface hydrophobicity, regulated by temperature, growth phase, benomyl, macrophage interaction, azole resistance associated, Spider biofilm induced, rat catheter biofilm repressed
CR_08880C_A	-8.88	Protein of unknown function, rat catheter and Spider biofilm induced
HSP70	-8.87	Putative hsp70 chaperone, role in entry into host cells, heat-shock, amphotericin B, cadmium, ketoconazole-induced, surface localized in yeast and hyphae, antigenic in host, farnesol-downregulated in biofilm, Spider biofilm induced
C5_04480C_A	-8.81	Has domain(s) with predicted nucleic acid binding, nucleotide binding activity
GLX3	-8.64	Glutathione-independent glyoxalase, binds human immunoglobulin E, alkaline, fluconazole, Hog1 repressed, hypoxia, oxidative stress via Cap1, Hap43 induced, stationary-phase enriched, rat catheter, Spider biofilm induced
AMS1	-8.58	Putative alpha-mannosidase, transcript regulated by Nrg1, induced during cell wall regeneration, flow model biofilm induced, Spider biofilm induced
FMP45	-8.55	Predicted membrane protein induced during mating, mutation confers hypersensitivity to toxic ergosterol analog, to amphotericin B, alkaline repressed, repressed by alpha pheromone in SpiderM medium, rat catheter, Spider biofilm induced
C3_01540W_A	-8.43	Plasma-membrane-localized protein, filament induced, Hog1, ketoconazole, fluconazole and hypoxia-induced, regulated by Nrg1, Tup1, Upc2, induced by prostaglandins, flow model biofilm induced, rat catheter and Spider biofilm repressed
ASR1	-8.34	Heat shock protein, transcript regulated by cAMP, osmotic stress, ciclopirox olamine, ketoconazole, repressed by Cyr1, Ras1, colony morphology-related regulated by Ssn6, stationary phase enriched, Hap43-induced, Spider biofilm induced
GST2	-8.28	Glutathione S transferase, induced by benomyl and in populations of cells exposed to fluconazole over multiple generations, regulated by Nrg1, Tup1, induced by nitric oxide, stationary phase enriched, Spider biofilm induced

HSP12	-8.17	Heat-shock protein, induced by osmotic/oxidative/cadmium stress, fluphenazine treatment, low iron, CDR1 and CDR2 overexpression, or ssn6 or ssk1 null mutation, overexpression increases resistance to farnesol and azoles
AHP1	-8.16	Alkyl hydroperoxide reductase, immunogenic, fluconazole-induced, amphotericin B, caspofungin, alkaline repressed, core stress response induced, Ssk1/Nrg1/Tup1/Ssn6/Hog1 regulated, flow model biofilm induced, rat catheter biofilm repressed
LAP3	-8.13	Putative aminopeptidase, positively regulated by Sfu1, clade-associated gene expression, virulence-group-correlated expression, induced by alpha pheromone in SpiderM medium, Hap43-induced, Spider and flow model biofilm induced
C3_06040W_A	-7.96	CCCH zinc finger protein, Spider biofilm induced
C1_04010C_A	-7.93	Protein with a NADP-dependent oxidoreductase domain, transcript induced by ketoconazole, rat catheter and Spider biofilm induced
C2_07630C_A	-7.91	Possible stress protein, increased transcription associated with CDR1 and CDR2 overexpression or fluphenazine treatment, regulated by Sfu1, Nrg1, Tup1, stationary phase enriched protein, Spider biofilm induced
PRC2	-7.84	Putative carboxypeptidase, induced by human neutrophils, Spider biofilm induced

Supplementary Table 11: Top 25 significantly up- and downregulated genes of treated hyphal subculture versus untreated hyphal subculture (PA4b vs. PA6b)

Gene	Log2FC	Function
upregulated		
ICL1	1.85	Isocitrate lyase, glyoxylate cycle enzyme, required for virulence in mice, induced upon phagocytosis by macrophage, farnesol regulated, Pex5-dependent peroxisomal localization, stationary phase enriched, rat catheter, Spider biofilm induced
TNA1	1.67	Putative nicotinic acid transporter, detected at germ tube plasma membrane by mass spectrometry, transcript induced upon phagocytosis by macrophage, rat catheter biofilm induced
C2_01630W_A	1.55	2-hydroxyacid dehydrogenase domain-containing protein, Hap43-repressed gene, induced by alpha pheromone in Spider medium

Supplementary Table 12: Top 25 significantly up- and downregulated genes of treated yeast subculture versus untreated yeast subculture (PA5b vs. PA7b)

Gene	Log2FC	Function
upregulated		
ICL1	2.68	Isocitrate lyase, glyoxylate cycle enzyme, required for virulence in mice, induced upon phagocytosis by macrophage, farnesol regulated, Pex5-dependent peroxisomal localization, stationary phase enriched, rat catheter, Spider biofilm induced

BTA1	2.28	Ortholog of C. dubliniensis CD36 : Cd36_10780, C. parapsilosis CDC317 : CPAR2_208080, C. auris B8441 : B9J08_003841 and Candida tenuis NRRL Y-1498 : CANTEDRAFT_120956
AHP1	2.16	Alkyl hydroperoxide reductase, immunogenic, fluconazole-induced, amphotericin B, caspofungin, alkaline repressed, core stress response induced, Ssk1/Nrg1/Tup1/Ssn6/Hog1 regulated, flow model biofilm induced, rat catheter biofilm repressed
SFC1	2.11	Putative succinate-fumarate transporter, involved in repression of growth on sorbose, alkaline induced, rat catheter biofilm induced, Spider biofilm induced
C4_05730W_A	2.06	Adhesin-like protein, regulated by Tsa1, Tsa1B in minimal media at 37 deg, clade-associated gene expression, induced by alpha pheromone in SpiderM medium, Hap43-induced, Spider biofilm repressed
ALD6	2.02	Putative aldehyde dehydrogenase, stationary phase enriched protein, expression regulated upon white-opaque switch, rat catheter biofilm induced, rat catheter and Spider biofilm induced
ARO10	1.96	Aromatic decarboxylase, Ehrlich fusel oil pathway of aromatic alcohol biosynthesis, alkaline repressed, protein abundance affected by URA3 expression in CAI-4 strain, Spider biofilm induced
CR_04820W_A	1.89	Protein of unknown function, Hap43-induced, rat catheter and Spider biofilm induced
HSP31	1.88	Putative 30 kda heat shock protein, repressed during the mating process, rat catheter biofilm induced
HGT1	1.87	High-affinity MFS glucose transporter, induced by progesterone, chloramphenicol, benomyl, likely essential for growth, protein newly produced during adaptation to the serum, rat catheter and Spider biofilm induced
PHO100	1.87	Putative inducible acid phosphatase, DTT-extractable and observed in culture supernatant in low-phosphate conditions, slight effect on murine virulence, virulence-group-correlated expression, N-glycosylated, F-12/CO2 early biofilm induced
KRE62	1.85	Putative subunit of glucan synthase, macrophage-induced gene, Bcr1-regulated in a/a RPMI biofilms
HGT12	1.85	Glucose, fructose, mannose transporter, major facilitator superfamily, role in macrophage-induced hyphal growth, detected at germ tube plasma membrane by mass spectrometry, Snf3p-induced, 12 probable transmembrane segments
C2_07840W_A	1.82	Has domain(s) with predicted N,N-dimethylaniline monooxygenase activity, NADP binding, flavin adenine dinucleotide binding activity
MLS1	1.82	Malate synthase, glyoxylate cycle enzyme, no mammalian homolog, regulated upon white-opaque switch, phagocytosis, strong oxidative stress induced, stationary phase enriched, flow model biofilm repressed, rat catheter, Spider biofilm induced
CIP1	1.80	Possible oxidoreductase, transcript induced by cadmium but not other heavy metals, heat shock, yeast-hypha switch, oxidative stress (via Cap1), or macrophage interaction, stationary phase enriched protein, Spider biofilm induced
CR_08670C_A	1.79	Protein with an enoyl-CoA hydratase related domain, Spider biofilm induced
ATO1	1.73	Putative fungal-specific transmembrane protein, induced by Rgt1, Spider biofilm induced
C5_02220C_A	1.68	Putative polyphosphate phosphatase, role in hydrolysis of diphosphorylated inositol polyphosphates and diadenosine polyphosphates, Spider biofilm induced

C7_03150W_A	1.66	Protein of unknown function, rat catheter and Spider biofilm induced
OYE32	1.64	NAD(P)H oxidoreductase family protein, induced by nitric oxide, amphotericin B, oxidative stress via Cap1, upregulation associated with MDR1 overexpression or benomyl treatment, macrophage-downregulated protein, Spider biofilm induced
ALD5	1.62	NAD-aldehyde dehydrogenase, decreased expression in fluconazole-resistant isolate, or in hyphae, biofilm induced, fluconazole-downregulated, protein abundance is affected by URA3 expression in the CAI-4 strain, stationary phase enriched
C6_02210W_A	1.62	Protein of unknown function, oxidative stress-induced via Cap1, induced by alpha pheromone in SpiderM medium
OYE22	1.61	Putative NADPH dehydrogenase, rat catheter biofilm induced
C5_02800C_A	1.60	Ortholog of C. dubliniensis CD36 : Cd36_52590, C. parapsilosis CDC317 : CPAR2_100565, Debaryomyces hansenii CBS767 : DEHA2G06908g and Candida guilliermondii ATCC 6260 : PGUG_02858
downregulated		
IMG2	-2.37	Mitochondrial ribosomal protein of the large subunit, rat catheter biofilm induced
CR_07840C_A	-2.01	Protein of unknown function, flow model biofilm induced, Spider biofilm induced, induced by Mnl1 under weak acid stress, transcript detected in high-resolution tiling arrays
C6_01360W_A	-1.86	Protein of unknown function, ketoconazole-repressed
PMP1	-1.83	Protein similar to S. cerevisiae small proteolipid associated with plasma membrane ATPase Pma1p, null mutant exhibits no obvious defects
C1_12280C_A	-1.66	Putative mitochondrial ribosomal protein of the large subunit, Hap43-induced, mutants are viable, protein level decreases in stationary phase
C4_02460W_A	-1.64	Ortholog(s) have HDEL sequence binding activity, role in endoplasmic reticulum to Golgi vesicle-mediated transport and integral component of endoplasmic reticulum membrane localization
CR_06650C_A	-1.58	Protein of unknown function, flow model, rat catheter, Spider biofilm induced
C3_06130W_A	-1.56	Ortholog of Candida albicans WO-1 : CAWG_02922
C1_07660W_A	-1.50	Protein of unknown function, transcript is upregulated in clinical isolates from HIV+ patients with oral candidiasis
C4_01330W_A	1.50	Protein of unknown function, Spider biofilm induced
HGT19	1.52	Putative MFS glucose/myo-inositol transporter, 20 member family, 12 transmembrane segments, extended N terminus, expressed in rich medium, Hap43, phagocytosis, rat catheter, Spider and flow model biofilm induced
C4_00850C_A	1.52	Putative secreted acid sphingomyelin phosphodiesterase, possible Kex2p substrate
C4_06150C_A	1.52	Ortholog(s) have double-stranded DNA binding activity, role in homologous chromosome pairing at meiosis, reciprocal meiotic recombination and condensed nuclear chromosome localization
C6_02550W_A	1.53	Ortholog of C. dubliniensis CD36 : Cd36_62790, C. parapsilosis CDC317 : CPAR2_601680, C. auris B8441 : B9J08_001637 and Candida tenuis NRRL Y-1498 : cten_CGOB_00252
HSP30	1.53	Putative heat shock protein, fluconazole repressed, amphotericin B induced, Spider biofilm induced, rat catheter biofilm induced

C5_04390C_A	1.53	Putative protein of unknown function, transcription is activated in the presence of elevated CO2
CR_07300W_A	1.55	Protein similar to ferric reductase Fre10p, possibly an essential gene, disruptants not obtained by UAU1 method
FAA2-1	1.56	Predicted long chain fatty acid CoA ligase, upregulated upon phagocytosis, induced by nitric oxide independent of Yhb1
C1_12140W_A	1.56	Ortholog of C. dubliniensis CD36 : Cd36_11370, C. parapsilosis CDC317 : CPAR2_207480, C. auris B8441 : B9J08_001721 and Candida tenuis NRRL Y-1498 : CANTEDRAFT_120384
C6_02450W_A	1.57	Ortholog of S. pombe SPCC550.08, an N-acetyltransferase, transcript induced during growth in the mouse cecum
SPR1	1.58	Putative GPI-anchored protein, similar but not orthologous to S. cerevisiae Spr1, a sporulation-specific exo-1,3-beta-glucanase, mutant is viable
PGA17	1.59	Putative GPI-anchored protein, exogenously expressed protein substrate for Kex2 processing in vitro, repressed by alpha pheromone in SpiderM medium, macrophage-induced, induced in oralpharyngeal candidiasis, Spider biofilm induced
HYR1	1.59	GPI-anchored hyphal cell wall protein, macrophage-induced, repressed by neutrophils, resistance to killing by neutrophils, azoles, regulated by Rfg1, Efg1, Nrg1, Tup1, Cyr1, Bcr1, Hap43, Spider and flow model biofilm induced
C2_06630C_A	1.59	Ortholog of C. parapsilosis CDC317 : CPAR2_104640, Candida orthopsilosis Co 90-125 : CORT_0B05695 and Candida orthopsilosis NEW ASSEMBLY : CORT1B05695
C5_02800C_A	1.60	Ortholog of C. dubliniensis CD36 : Cd36_52590, C. parapsilosis CDC317 : CPAR2_100565, Debaryomyces hansenii CBS767 : DEHA2G06908g and Candida guilliermondii ATCC 6260 : PGUG_02858

6.3.2 Gene ontology analysis

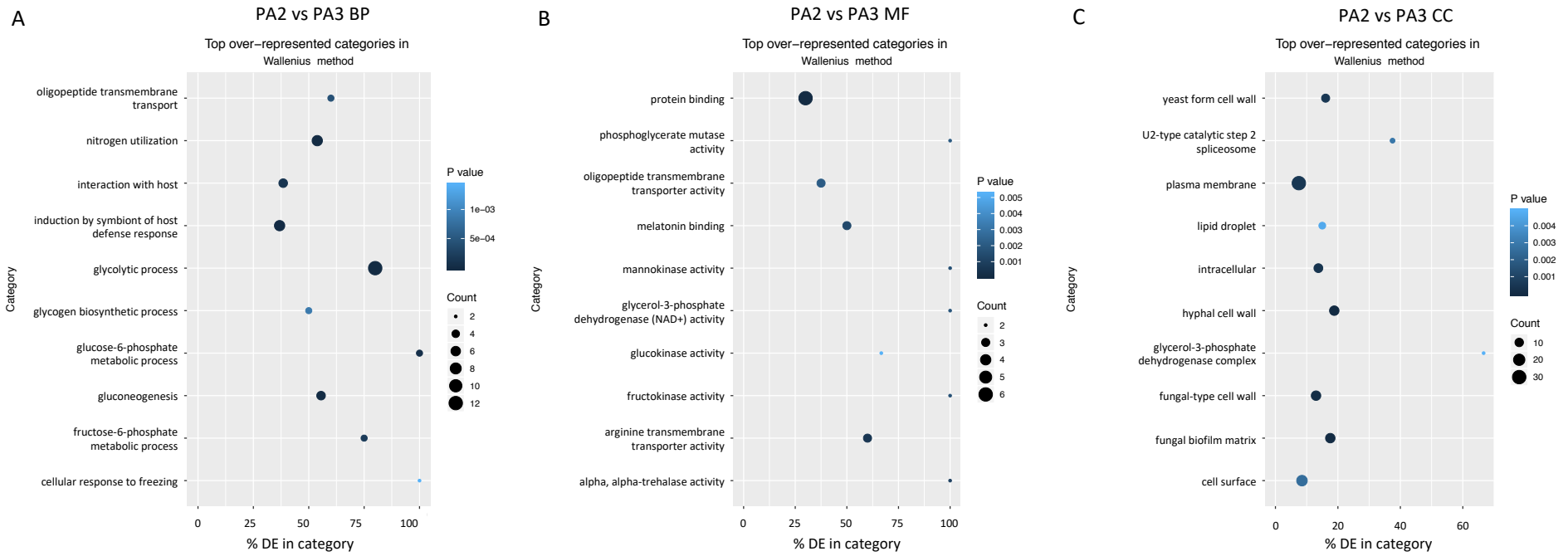

Supplementary Figure 11: GO analysis of sub-ontologies with top GO terms of downregulated differentially expressed genes of 5-Aza treated [1mM] (PA2) versus untreated (PA3) yeast precultures. (A) Biological process (BP). (B) Molecular function (MF). (C) Cellular component (CC). Analysis was conducted with goseq with Wallenius method. All GOs listed with p adjusted value <0.01, log2FC <-1.1.

Supplementary Figure 12: GO analysis of sub-ontologies with top GO terms of downregulated differentially expressed genes of 5-Aza treated [100 µM] (PA5) versus untreated (PA7) yeast subcultures. (A) Biological process (BP). (B) Molecular function (MF). (C) Cellular component (CC). Analysis was conducted with goseq with Wallenius method. All GOs listed with p adjusted value <0.01.

Supplementary Table 13: DE GO terms up BP PA2+3

category	over-represented p value	numDEInCat	numInCat	term
GO:0006281	5.45E-11	25	77	DNA repair
GO:0006271	1.18E-10	12	17	DNA strand elongation involved in DNA replication
GO:0006260	2.62E-10	13	21	DNA replication
GO:1902975	8.72E-10	9	10	mitotic DNA replication initiation
GO:0000727	3.13E-09	13	25	double-strand break repair via break-induced replication
GO:0007064	1.05E-07	12	26	mitotic sister chromatid cohesion
GO:0006270	2.99E-07	12	28	DNA replication initiation
GO:0006279	5.19E-07	7	9	premeiotic DNA replication
GO:0043137	1.64E-06	5	5	DNA replication, removal of RNA primer
GO:0043570	1.96E-06	6	7	maintenance of DNA repeat elements
GO:0006312	2.89E-06	7	11	mitotic recombination
GO:0045733	3.49E-06	6	8	acetate catabolic process
GO:0048478	5.16E-06	6	8	replication fork protection
GO:0006272	6.30E-06	6	9	leading strand elongation
GO:0006493	1.00E-05	7	13	protein O-linked glycosylation
GO:0006261	1.05E-05	8	17	DNA-dependent DNA replication
GO:0006099	1.35E-05	8	19	tricarboxylic acid cycle
GO:0000710	1.39E-05	6	9	meiotic mismatch repair
GO:0006268	1.65E-05	6	9	DNA unwinding involved in DNA replication
GO:0006097	2.76E-05	4	4	glyoxylate cycle
GO:0000724	3.08E-05	9	24	double-strand break repair via homologous recombination
GO:0006302	4.66E-05	10	29	double-strand break repair
GO:0015976	8.30E-05	7	17	carbon utilization
GO:0042276	8.87E-05	6	12	error-prone translesion synthesis
GO:0035753	0.000140	5	9	maintenance of DNA trinucleotide repeats
GO:0031297	0.000166	5	8	replication fork processing
GO:0043111	0.000199	4	5	replication fork arrest
GO:0007076	0.000250	6	13	mitotic chromosome condensation
GO:0000162	0.000260	4	6	tryptophan biosynthetic process
GO:0000709	0.000281	3	3	meiotic joint molecule formation
GO:0030466	0.000324	10	37	chromatin silencing at silent mating-type cassette
GO:0030491	0.000340	4	6	heteroduplex formation
GO:0006555	0.000344	3	3	methionine metabolic process
GO:0055114	0.000351	33	265	oxidation-reduction process
GO:0006273	0.000441	3	3	lagging strand elongation
GO:0010458	0.000443	5	10	exit from mitosis
GO:0036297	0.000476	5	10	interstrand cross-link repair
GO:0006298	0.000493	6	15	mismatch repair
GO:0007534	0.000597	4	6	gene conversion at mating-type locus
GO:0006974	0.000636	12	59	cellular response to DNA damage stimulus
GO:0006546	0.000660	4	7	glycine catabolic process
GO:0009062	0.000806	4	7	fatty acid catabolic process
GO:0000105	0.000957	4	8	histidine biosynthetic process

GO:0031204	0.001019	4	8	posttranslational protein targeting to membrane, translocation
GO:0006102	0.001029	3	4	isocitrate metabolic process
GO:0000278	0.001088	5	11	mitotic cell cycle
GO:0070868	0.001219	3	4	heterochromatin organization involved in chromatin silencing
GO:0009073	0.001283	4	8	aromatic amino acid family biosynthetic process
GO:0031122	0.001337	4	8	cytoplasmic microtubule organization
GO:0034087	0.001487	5	13	establishment of mitotic sister chromatid cohesion
GO:0051097	0.001858	3	4	negative regulation of helicase activity
GO:0006267	0.001875	6	19	pre-replicative complex assembly involved in nuclear cell cycle DNA replication
GO:0007097	0.001929	4	8	nuclear migration
GO:0006301	0.002009	5	14	postreplication repair
GO:0033260	0.002017	3	4	nuclear DNA replication
GO:0071932	0.002239	3	4	replication fork reversal
GO:0000729	0.002289	4	8	DNA double-strand break processing
GO:0000733	0.002501	4	9	DNA strand renaturation
GO:0006335	0.002599	3	5	DNA replication-dependent nucleosome assembly
GO:0030447	0.002616	48	442	filamentous growth
GO:0006111	0.002620	2	2	regulation of gluconeogenesis
GO:0006277	0.002776	3	5	DNA amplification
GO:0006165	0.002791	2	2	nucleoside diphosphate phosphorylation
GO:0006401	0.002822	4	10	RNA catabolic process
GO:0044879	0.003062	3	4	morphogenesis checkpoint
GO:0000070	0.003321	7	27	mitotic sister chromatid segregation
GO:0007004	0.003586	4	10	telomere maintenance via telomerase
GO:0070787	0.003632	3	5	conidiophore development
GO:0006084	0.003778	3	5	acetyl-CoA metabolic process
GO:0070783	0.003808	6	21	growth of unicellular organism as a thread of attached cells
GO:0000022	0.003924	4	10	mitotic spindle elongation
GO:0006104	0.004006	2	2	succinyl-CoA metabolic process
GO:0032119	0.004094	2	2	sequestering of zinc ion
GO:0009070	0.004425	2	2	serine family amino acid biosynthetic process
GO:0090307	0.004464	4	10	mitotic spindle assembly
GO:0007131	0.004546	8	37	reciprocal meiotic recombination
GO:0006235	0.004633	2	2	dTTP biosynthetic process
GO:0043392	0.004957	3	6	negative regulation of DNA binding
GO:1903459	0.005050	2	2	mitotic DNA replication lagging strand elongation
GO:0006278	0.005063	4	10	RNA-dependent DNA biosynthetic process
GO:0015749	0.005361	2	2	monosaccharide transmembrane transport
GO:0060903	0.005372	2	2	positive regulation of meiosis I
GO:0051256	0.005410	2	2	mitotic spindle midzone assembly
GO:1903466	0.005461	2	2	regulation of mitotic DNA replication initiation
GO:0006012	0.005467	3	6	galactose metabolic process
GO:0072428	0.005595	2	2	signal transduction involved in intra-S DNA damage checkpoint
GO:0045184	0.005642	3	6	establishment of protein localization
GO:0051417	0.005832	2	2	microtubule nucleation by spindle pole body

GO:1904161	0.005929	2	2	DNA synthesis involved in UV-damage excision repair
GO:0006265	0.006099	4	11	DNA topological change
GO:0000734	0.006137	2	2	gene conversion at mating-type locus, DNA repair synthesis
GO:1902969	0.006158	3	6	mitotic DNA replication
GO:2000218	0.006196	2	2	negative regulation of invasive growth in response to glucose limitation
GO:0006289	0.006474	7	32	nucleotide-excision repair
GO:1900101	0.006494	3	6	regulation of endoplasmic reticulum unfolded protein response
GO:1905775	0.006758	2	2	negative regulation of DNA helicase activity
GO:0006284	0.006982	4	11	base-excision repair
GO:0097046	0.007037	2	2	replication fork progression beyond termination site
GO:0051304	0.007433	2	2	chromosome separation
GO:0071139	0.007433	2	2	resolution of recombination intermediates
GO:0046020	0.007575	3	6	negative regulation of transcription from RNA polymerase II promoter by pheromones
GO:0032297	0.007706	2	2	negative regulation of DNA-dependent DNA replication initiation
GO:0010032	0.007820	2	2	meiotic chromosome condensation
GO:0051307	0.007820	2	2	meiotic chromosome separation
GO:0009272	0.008476	7	34	fungal-type cell wall biogenesis
GO:0045004	0.008870	2	2	DNA replication proofreading
GO:0071963	0.009190	5	19	establishment or maintenance of cell polarity regulating cell shape
GO:0000921	0.009279	4	13	septin ring assembly
GO:0000723	0.009371	8	42	telomere maintenance
GO:0030011	0.009625	4	12	maintenance of cell polarity
GO:0001302	0.010307	7	35	replicative cell aging
GO:0031145	0.011112	4	13	anaphase-promoting complex-dependent catabolic process
GO:0009298	0.011149	2	3	GDP-mannose biosynthetic process
GO:0006033	0.011180	2	3	chitin localization
GO:0007052	0.011628	5	22	mitotic spindle organization
GO:0006311	0.011871	2	3	meiotic gene conversion
GO:0033314	0.013542	4	13	mitotic DNA replication checkpoint
GO:0000280	0.013883	3	7	nuclear division
GO:0033499	0.014260	2	3	galactose catabolic process via UDP-galactose
GO:0006310	0.014734	5	21	DNA recombination
GO:0098863	0.014917	2	3	nuclear migration by microtubule mediated pushing forces
GO:0070058	0.015161	3	7	tRNA gene clustering
GO:0030473	0.015178	4	13	nuclear migration along microtubule
GO:0009086	0.015206	4	15	methionine biosynthetic process
GO:0040001	0.015251	2	3	establishment of mitotic spindle localization
GO:0042148	0.015413	2	3	strand invasion
GO:0046785	0.016259	2	3	microtubule polymerization
GO:1990571	0.016495	2	3	meiotic centromere clustering
GO:0006269	0.016545	2	3	DNA replication, synthesis of RNA primer
GO:0097271	0.016595	3	8	protein localization to bud neck

GO:0007533	0.017337	3	8	mating type switching
GO:2000001	0.017550	2	3	regulation of DNA damage checkpoint
GO:0061692	0.017978	2	4	cellular detoxification of hydrogen peroxide
GO:1902983	0.018434	2	3	DNA strand elongation involved in mitotic DNA replication
GO:0031589	0.019101	3	8	cell-substrate adhesion
GO:0000032	0.019765	4	16	cell wall mannoprotein biosynthetic process
GO:0031134	0.019966	3	8	sister chromatid biorientation
GO:0060258	0.020033	3	9	negative regulation of filamentous growth
GO:1903461	0.020100	2	3	Okazaki fragment processing involved in mitotic DNA replication
GO:0019878	0.021346	3	9	lysine biosynthetic process via aminoadipic acid
GO:0070987	0.021489	3	9	error-free translesion synthesis
GO:0061780	0.021692	2	3	mitotic cohesin loading
GO:0062022	0.021692	2	3	mitotic cohesin ssDNA (lagging strand) loading
GO:0000725	0.021692	3	8	recombinational repair
GO:1903342	0.021946	2	3	negative regulation of meiotic DNA double-strand break formation
GO:0071168	0.022347	2	3	protein localization to chromatin
GO:0090114	0.022976	2	4	COPII-coated vesicle budding
GO:0006348	0.023542	8	49	chromatin silencing at telomere
GO:0045047	0.023579	3	11	protein targeting to ER
GO:0006544	0.024414	2	4	glycine metabolic process
GO:0007130	0.024714	3	9	synaptonemal complex assembly
GO:0070914	0.025316	3	10	UV-damage excision repair
GO:0045861	0.026439	2	4	negative regulation of proteolysis
GO:0015867	0.026444	2	4	ATP transport
GO:0042744	0.027166	2	5	hydrogen peroxide catabolic process
GO:0032527	0.028248	2	4	protein exit from endoplasmic reticulum
GO:1902977	0.028556	2	4	mitotic DNA replication preinitiation complex assembly
GO:0036170	0.029258	23	207	filamentous growth of a population of unicellular organisms in response to starvation
GO:0070550	0.029426	3	9	rDNA condensation
GO:1990426	0.029504	2	4	mitotic recombination-dependent replication fork processing
GO:0006487	0.030640	6	36	protein N-linked glycosylation
GO:0035269	0.030945	3	10	protein O-linked mannosylation
GO:0042981	0.031169	2	4	regulation of apoptotic process
GO:0045860	0.031357	2	5	positive regulation of protein kinase activity
GO:0000132	0.032299	3	9	establishment of mitotic spindle orientation
GO:0000735	0.032766	2	4	removal of nonhomologous ends
GO:0061414	0.033935	2	4	positive regulation of transcription from RNA polymerase II promoter by a nonfermentable carbon source
GO:1990683	0.034676	2	4	DNA double-strand break attachment to nuclear envelope
GO:0031860	0.036092	2	4	telomeric 3' overhang formation
GO:0006635	0.037356	3	11	fatty acid beta-oxidation
GO:0009097	0.037893	2	5	isoleucine biosynthetic process

GO:0000910	0.038792	3	11	cytokinesis
GO:0031497	0.039114	2	5	chromatin assembly
GO:0009082	0.040298	2	5	branched-chain amino acid biosynthetic process
GO:0015031	0.041144	4	22	protein transport
GO:0045144	0.043270	2	5	meiotic sister chromatid segregation
GO:0006488	0.043488	3	13	dolichol-linked oligosaccharide biosynthetic process
GO:0043504	0.043710	2	5	mitochondrial DNA repair
GO:0006730	0.046260	3	12	one-carbon metabolic process
GO:0019348	0.046975	1	1	dolichol metabolic process
GO:0036091	0.047002	2	6	positive regulation of transcription from RNA polymerase II promoter in response to oxidative stress
GO:0008645	0.047186	2	5	hexose transmembrane transport
GO:0051228	0.048886	2	5	mitotic spindle disassembly
GO:0030448	0.049349	12	96	hyphal growth
GO:0045722	0.049766	2	5	positive regulation of gluconeogenesis

Supplementary Table 14: DE GO terms up MF PA2+3

category	over-represented p value	numDEInCat	numInCat	term
GO:0003697	6.48E-19	28	53	single-stranded DNA binding
GO:0003690	9.55E-11	19	46	double-stranded DNA binding
GO:0017116	3.14E-06	7	11	single-stranded DNA-dependent ATP-dependent DNA helicase activity
GO:0009378	3.97E-06	5	5	four-way junction helicase activity
GO:0003688	4.42E-06	11	30	DNA replication origin binding
GO:0030337	1.45E-05	4	4	DNA polymerase processivity factor activity
GO:0051287	3.17E-05	8	21	NAD binding
GO:0003887	4.18E-05	7	14	DNA-directed DNA polymerase activity
GO:0005200	6.54E-05	6	12	structural constituent of cytoskeleton
GO:0004582	0.000125	3	3	dolichyl-phosphate beta-D-mannosyltransferase activity
GO:0004550	0.000241	3	3	nucleoside diphosphate kinase activity
GO:0008310	0.000376	3	3	single-stranded DNA 3'-5' exodeoxyribonuclease activity
GO:0045145	0.000453	3	3	single-stranded DNA 5'-3' exodeoxyribonuclease activity
GO:0005524	0.000492	48	386	ATP binding
GO:0033679	0.000531	3	3	3'-5' DNA/RNA helicase activity
GO:1990518	0.000531	3	3	single-stranded DNA-dependent ATP-dependent 3'-5' DNA helicase activity
GO:0043515	0.000593	3	3	kinetochore binding
GO:0003682	0.000899	16	91	chromatin binding
GO:0030170	0.001523	9	41	pyridoxal phosphate binding
GO:0004523	0.001938	3	5	RNA-DNA hybrid ribonuclease activity
GO:0016887	0.001978	17	102	ATPase activity
GO:0032135	0.002035	3	4	DNA insertion or deletion binding

GO:0000400	0.003077	4	9	four-way junction DNA binding
GO:0017108	0.003638	3	5	5'-flap endonuclease activity
GO:0008094	0.003774	5	14	DNA-dependent ATPase activity
GO:1905334	0.003820	2	2	Swi5-Sfr1 complex binding
GO:0003678	0.003932	5	14	DNA helicase activity
GO:0004774	0.004006	2	2	succinate-CoA ligase activity
GO:0004775	0.004006	2	2	succinate-CoA ligase (ADP-forming) activity
GO:0003849	0.004021	2	2	3-deoxy-7-phosphoheptulonate synthase activity
GO:0004450	0.004395	2	2	isocitrate dehydrogenase (NADP+) activity
GO:0008379	0.004590	3	7	thioredoxin peroxidase activity
GO:0048487	0.004763	2	2	beta-tubulin binding
GO:0004049	0.005066	2	2	anthranilate synthase activity
GO:0003942	0.005204	2	2	N-acetyl-gamma-glutamyl-phosphate reductase activity
GO:0015145	0.005361	2	2	monosaccharide transmembrane transporter activity
GO:0000150	0.006224	3	6	recombinase activity
GO:0003994	0.006305	2	2	aconitate hydratase activity
GO:1904931	0.006472	2	2	MCM complex binding
GO:0032138	0.007214	2	2	single base insertion or deletion binding
GO:0000404	0.008280	3	6	heteroduplex DNA loop binding
GO:0005525	0.008320	12	83	GTP binding
GO:0004601	0.008790	2	3	peroxidase activity
GO:0051920	0.009103	2	3	peroxiredoxin activity
GO:0008569	0.009436	2	2	ATP-dependent microtubule motor activity, minus-end-directed
GO:0000403	0.009594	3	6	Y-form DNA binding
GO:0042602	0.010525	2	3	riboflavin reductase (NADPH) activity
GO:0019789	0.015253	3	8	SUMO transferase activity
GO:0003896	0.016545	2	3	DNA primase activity
GO:0008017	0.016730	6	30	microtubule binding
GO:0003684	0.017602	5	22	damaged DNA binding
GO:0032139	0.018560	2	3	dinucleotide insertion or deletion binding
GO:0004169	0.018813	3	8	dolichyl-phosphate-mannose-protein mannosyltransferase activity
GO:0003727	0.018909	3	9	single-stranded RNA binding
GO:0032137	0.020050	2	3	guanine/thymine mispair binding
GO:0043138	0.021651	4	14	3'-5' DNA helicase activity
GO:0004375	0.025156	2	4	glycine dehydrogenase (decarboxylating) activity
GO:0004568	0.026653	2	4	chitinase activity
GO:0008574	0.027574	2	4	ATP-dependent microtubule motor activity, plus-end-directed
GO:0016616	0.029804	3	11	oxidoreductase activity, acting on the CH-OH group of donors, NAD or NADP as acceptor
GO:0004712	0.029911	2	4	protein serine/threonine/tyrosine kinase activity
GO:0030985	0.042519	2	5	high molecular weight kininogen binding
GO:0008409	0.047208	2	5	5'-3' exonuclease activity
GO:0030976	0.050352	2	5	thiamine pyrophosphate binding

Supplementary Table 15: DE GO terms up CC PA2+3

category	over-represented p value	numDEInCat	numInCat	term
GO:0031298	8.24E-10	13	24	replication fork protection complex
GO:0071162	1.96E-09	9	11	CMG complex
GO:0035861	1.31E-08	14	31	site of double-strand break
GO:0042555	2.71E-07	6	6	MCM complex
GO:0031261	8.80E-07	10	22	DNA replication preinitiation complex
GO:0043596	9.56E-07	9	17	nuclear replication fork
GO:0005881	1.51E-05	7	13	cytoplasmic microtubule
GO:0005634	1.70E-05	86	788	nucleus
GO:0008622	2.91E-05	4	4	epsilon DNA polymerase complex
GO:0005658	3.48E-05	4	4	alpha DNA polymerase:primase complex
GO:0042645	3.82E-05	8	21	mitochondrial nucleoid
GO:0000784	5.82E-05	8	19	nuclear chromosome, telomeric region
GO:0000790	0.000106	24	146	nuclear chromatin
GO:0005940	0.000114	6	12	septin ring
GO:0005656	0.000131	7	17	nuclear pre-replicative complex
GO:0000794	0.000180	7	20	condensed nuclear chromosome
GO:0005876	0.000201	6	14	spindle microtubule
GO:0032299	0.000212	3	3	ribonuclease H2 complex
GO:0030915	0.000290	4	6	Smc5-Smc6 complex
GO:0043625	0.000389	3	3	delta DNA polymerase complex
GO:0031390	0.000476	4	7	Ctf18 RFC-like complex
GO:0097373	0.000531	3	3	MCM core complex
GO:0000775	0.000835	7	23	chromosome, centromeric region
GO:0005657	0.001161	5	11	replication fork
GO:0005874	0.001216	3	4	microtubule
GO:0034990	0.002230	3	4	nuclear mitotic cohesin complex
GO:0000778	0.002854	7	27	condensed nuclear chromosome kinetochore
GO:0005782	0.004346	4	11	peroxisomal matrix
GO:0005662	0.004414	2	2	DNA replication factor A complex
GO:0045298	0.004580	2	2	tubulin complex
GO:0005950	0.005066	2	2	anthranilate synthase complex
GO:0031431	0.005372	2	2	Dbf4-dependent protein kinase complex
GO:1990526	0.005453	2	2	Ste12p-Dig1p-Dig2p complex
GO:0005576	0.006159	17	132	extracellular region
GO:0032389	0.006402	2	2	MutLalpha complex
GO:0097582	0.006447	2	2	dolichyl-phosphate-mannose-protein mannosyltransferase Pmt1p-Pmt2p dimer complex
GO:0012505	0.006454	3	6	endomembrane system
GO:0000781	0.006824	4	11	chromosome, telomeric region
GO:0032301	0.007214	2	2	MutSalpha complex
GO:0009986	0.008714	23	200	cell surface
GO:0000144	0.012003	4	13	cellular bud neck septin ring
GO:0033186	0.013822	2	3	CAF-1 complex
GO:0005739	0.014077	29	288	mitochondrion
GO:0005787	0.014455	2	4	signal peptidase complex
GO:0000228	0.015722	5	20	nuclear chromosome

GO:0033309	0.016389	2	3	SBF transcription complex
GO:0000811	0.016438	2	4	GINS complex
GO:0005680	0.018063	4	15	anaphase-promoting complex
GO:0030127	0.018458	3	8	COPII vesicle coat
GO:0000235	0.020298	2	3	astral microtubule
GO:0031207	0.021032	2	4	Sec62/Sec63 complex
GO:0032160	0.023098	2	4	septin filament array
GO:0030121	0.026348	2	4	AP-1 adaptor complex
GO:0000785	0.029461	3	10	chromatin
GO:0005788	0.029947	3	10	endoplasmic reticulum lumen
GO:0062040	0.031017	9	74	fungal biofilm matrix
GO:0030907	0.032142	2	4	MBF transcription complex
GO:0071957	0.033038	2	4	old mitotic spindle pole body
GO:0005816	0.033631	6	33	spindle pole body
GO:0034506	0.035036	2	4	chromosome, centromeric core domain
GO:0031389	0.036532	2	5	Rad17 RFC-like complex
GO:0031105	0.037919	2	5	septin complex
GO:0005663	0.038238	2	5	DNA replication factor C complex
GO:0005622	0.038267	10	80	intracellular
GO:0031391	0.038282	2	5	Elg1 RFC-like complex
GO:0072687	0.041436	2	5	meiotic spindle
GO:0005829	0.046689	27	279	cytosol
GO:0009277	0.050040	12	100	fungal-type cell wall

Supplementary Table 16: DE GO terms up BP PA4+6

category	over-represented p value	numDEInCat	numInCat	term
GO:1903222	0.001522	1	1	quinolinic acid transmembrane transport
GO:0015749	0.003041	1	2	monosaccharide transmembrane transport
GO:0046942	0.003042	1	2	carboxylic acid transport
GO:0009437	0.004477	1	3	carnitine metabolic process
GO:0051180	0.004559	1	3	vitamin transport
GO:0006097	0.006011	1	4	glyoxylate cycle
GO:0006084	0.007507	1	5	acetyl-CoA metabolic process
GO:0006066	0.007532	1	5	alcohol metabolic process
GO:0008645	0.007567	1	5	hexose transmembrane transport
GO:0009062	0.010355	1	7	fatty acid catabolic process
GO:0045733	0.011949	1	8	acetate catabolic process
GO:0006820	0.022612	1	15	anion transport
GO:0015976	0.025245	1	17	carbon utilization
GO:0009405	0.055341	2	266	pathogenesis
GO:1990961	0.057447	1	40	drug transmembrane export
GO:0055114	0.057491	2	265	oxidation-reduction process
GO:0036244	0.073464	1	52	cellular response to neutral pH
GO:0036178	0.086195	1	61	filamentous growth of a population of unicellular organisms in response to neutral pH

Supplementary Table 17: DE GO terms up MF PA4+6

category	over-represented p value	numDEInCat	numInCat	term
GO:0004451	0.001522	1	1	isocitrate lyase activity
GO:0015663	0.001522	1	1	nicotinamide mononucleotide transmembrane transporter activity
GO:0015145	0.003041	1	2	monosaccharide transmembrane transporter activity
GO:0046943	0.003042	1	2	carboxylic acid transmembrane transporter activity
GO:0004092	0.004477	1	3	carnitine O-acetyltransferase activity
GO:0016616	0.016537	1	11	oxidoreductase activity, acting on the CH-OH group of donors, NAD or NADP as acceptor
GO:0015296	0.024103	1	16	anion:cation symporter activity
GO:0051287	0.031459	1	21	NAD binding
GO:0005507	0.032568	1	22	copper ion binding

Supplementary Table 18: DE GO terms up CC PA4+6

category	over-represented p value	numDEInCat	numInCat	term
GO:0005777	0.002752	2	54	peroxisome
GO:0005782	0.016621	1	11	peroxisomal matrix

Supplementary Table 19: DE GO terms up BP PA5+7

category	over-represented p value	numDEInCat	numInCat	term
GO:0009062	1.05E-06	4	7	fatty acid catabolic process
GO:0006097	9.78E-06	3	4	glyoxylate cycle
GO:0055114	8.14E-05	13	265	oxidation-reduction process
GO:0045733	0.000130	3	8	acetate catabolic process
GO:0006811	0.000655	2	3	ion transport
GO:0061692	0.001337	2	4	cellular detoxification of hydrogen peroxide
GO:0015976	0.001532	3	17	carbon utilization
GO:0042744	0.002243	2	5	hydrogen peroxide catabolic process
GO:0007129	0.002370	2	6	synapsis
GO:1904659	0.002457	3	20	glucose transmembrane transport
GO:0033554	0.002526	3	19	cellular response to stress
GO:0008643	0.003700	3	23	carbohydrate transport
GO:0045454	0.010045	3	31	cell redox homeostasis
GO:1990166	0.010468	1	1	protein localization to site of double-strand break
GO:0042760	0.012128	1	1	very long-chain fatty acid catabolic process
GO:0000950	0.013545	1	1	branched-chain amino acid catabolic process to alcohol via Ehrlich pathway
GO:0000951	0.013545	1	1	methionine catabolic process to 3-methylthiopropanol
GO:0000302	0.014228	1	1	response to reactive oxygen species

GO:0001315	0.014228	1	1	age-dependent response to reactive oxygen species
GO:0034276	0.014370	1	1	kynurenic acid biosynthetic process
GO:0006151	0.014647	1	1	xanthine oxidation
GO:0051701	0.014812	2	13	interaction with host
GO:0042821	0.014814	1	1	pyridoxal biosynthetic process
GO:0015741	0.015003	1	1	fumarate transport
GO:0015744	0.015003	1	1	succinate transport
GO:0015959	0.015448	1	1	diadenosine polyphosphate metabolic process
GO:0015961	0.015448	1	1	diadenosine polyphosphate catabolic process
GO:1901906	0.015448	1	1	diadenosine pentaphosphate metabolic process
GO:1901907	0.015448	1	1	diadenosine pentaphosphate catabolic process
GO:1901909	0.015448	1	1	diadenosine hexaphosphate catabolic process
GO:1901911	0.015448	1	1	adenosine 5'-(hexahydrogen pentaphosphate) catabolic process
GO:0034599	0.023109	5	115	cellular response to oxidative stress
GO:0019413	0.024804	1	2	acetate biosynthetic process
GO:0009405	0.026676	8	266	pathogenesis
GO:0006559	0.027206	1	2	L-phenylalanine catabolic process
GO:0006552	0.027555	1	2	leucine catabolic process
GO:0042743	0.028229	1	2	hydrogen peroxide metabolic process
GO:0045916	0.028764	1	2	negative regulation of complement activation
GO:0032119	0.029111	1	2	sequestering of zinc ion
GO:0020028	0.030242	1	2	endocytic hemoglobin import
GO:0071543	0.030311	1	2	diphosphoinositol polyphosphate metabolic process
GO:0032780	0.030486	1	2	negative regulation of ATPase activity
GO:1903614	0.031164	1	2	negative regulation of protein tyrosine phosphatase activity
GO:0051594	0.039024	1	3	detection of glucose
GO:0051603	0.039268	1	3	proteolysis involved in cellular protein catabolic process
GO:0006569	0.041156	1	3	tryptophan catabolic process
GO:0031638	0.041505	1	3	zymogen activation
GO:0046938	0.041540	1	3	phytochelatin biosynthetic process
GO:0031669	0.042211	1	3	cellular response to nutrient levels
GO:0019243	0.044591	1	3	methylglyoxal catabolic process to D-lactate via S-lactoyl-glutathione

Supplementary Table 20: DE GO terms up MF PA5+7

category	over-represented p value	numDEInCat	numInCat	term
GO:0016491	2.31E-05	9	108	oxidoreductase activity
GO:0003824	0.000419	6	69	catalytic activity
GO:0005216	0.001076	2	4	ion channel activity
GO:0004185	0.001111	2	4	serine-type carboxypeptidase activity
GO:0005355	0.002086	3	19	glucose transmembrane transporter activity
GO:0051119	0.003228	3	22	sugar transmembrane transporter activity
GO:0008379	0.004685	2	7	thioredoxin peroxidase activity

GO:0010181	0.004767	3	24	FMN binding
GO:0050177	0.013545	1	1	phenylpyruvate decarboxylase activity
GO:0004474	0.013923	1	1	malate synthase activity
GO:0004451	0.013928	1	1	isocitrate lyase activity
GO:0004491	0.013970	1	1	methylmalonate-semialdehyde dehydrogenase (acylating) activity
GO:0015149	0.014041	1	1	hexose transmembrane transporter activity
GO:0015578	0.014041	1	1	mannose transmembrane transporter activity
GO:0004030	0.014165	1	1	aldehyde dehydrogenase [NAD(P)+] activity
GO:0004096	0.014228	1	1	catalase activity
GO:0016212	0.014370	1	1	kynurenine-oxoglutarate transaminase activity
GO:0004055	0.014531	1	1	argininosuccinate synthase activity
GO:0097641	0.014647	1	1	alpha-ketoglutarate-dependent xanthine dioxygenase activity
GO:0004076	0.014710	1	1	biotin synthase activity
GO:0050236	0.014814	1	1	pyridoxine:NADP 4-dehydrogenase activity
GO:0005469	0.015003	1	1	succinate:fumarate antiporter activity
GO:0019172	0.015274	1	1	glyoxalase III activity
GO:0008486	0.015448	1	1	diphosphoinositol-polyphosphate diphosphatase activity
GO:0034431	0.015448	1	1	bis(5'-adenosyl)-hexaphosphatase activity
GO:0034432	0.015448	1	1	bis(5'-adenosyl)-pentaphosphatase activity
GO:0008785	0.015512	1	1	alkyl hydroperoxide reductase activity
GO:0004767	0.026107	1	2	sphingomyelin phosphodiesterase activity
GO:0003857	0.026136	1	2	3-hydroxyacyl-CoA dehydrogenase activity
GO:0004623	0.027054	1	2	phospholipase A2 activity
GO:0004300	0.027360	1	2	enoyl-CoA hydratase activity
GO:0003852	0.027429	1	2	2-isopropylmalate synthase activity
GO:0004180	0.027560	1	2	carboxypeptidase activity
GO:0005353	0.027794	1	2	fructose transmembrane transporter activity
GO:0009013	0.028122	1	2	succinate-semialdehyde dehydrogenase [NAD(P)+] activity
GO:0004061	0.029304	1	2	arylformamidase activity
GO:1990174	0.029863	1	2	phosphodiesterase decapping endonuclease activity
GO:0004499	0.041888	1	3	N,N-dimethylaniline monooxygenase activity
GO:0050072	0.041988	1	3	m7G(5')pppN diphosphatase activity
GO:0004029	0.042476	1	3	aldehyde dehydrogenase (NAD) activity
GO:0000298	0.042860	1	3	endopolyphosphatase activity
GO:0051920	0.045024	1	3	peroxiredoxin activity
GO:0004601	0.045226	1	3	peroxidase activity
GO:0044183	0.045960	1	3	protein binding involved in protein folding

Supplementary Table 21: DE GO terms up CC PA5+7

category	over-represented p value	numDEInCat	numInCat	term
GO:0030446	2.66E-09	11	69	hyphal cell wall
GO:0009986	3.07E-06	13	200	cell surface
GO:0009277	5.39E-05	8	100	fungal-type cell wall
GO:0030445	0.000136	6	56	yeast-form cell wall
GO:0005782	0.000436	3	11	peroxisomal matrix
GO:0005576	0.002464	7	131	extracellular region
GO:0005575	0.011642	41	2103	cellular_component
GO:0005887	0.019105	3	43	integral component of plasma membrane
GO:0005777	0.038075	3	54	peroxisome
GO:0005886	0.048899	10	400	plasma membrane

6.3.3 GO pathway enrichment analysis

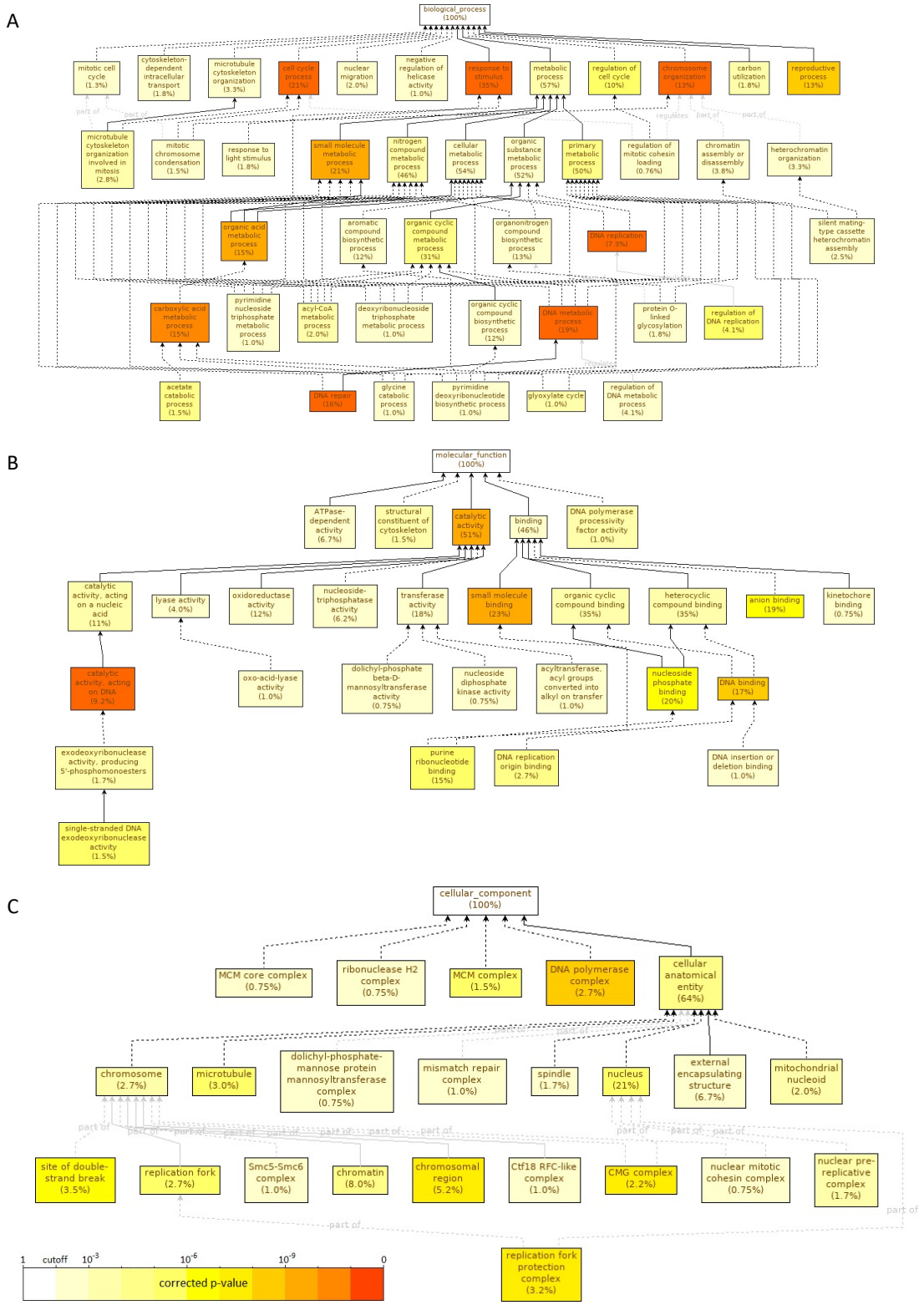

Supplementary Figure 13: GO enrichment analysis of upregulated differentially expressed genes (p adjusted value <0.01 and log2FC >1.1) of 5-Aza treated [1mM] (PA2) versus untreated (PA3) yeast precultures. (A) Biological process. (B) Molecular function. (C) Cellular component. Analysis was conducted with GOEnrichment (p value <0.01).

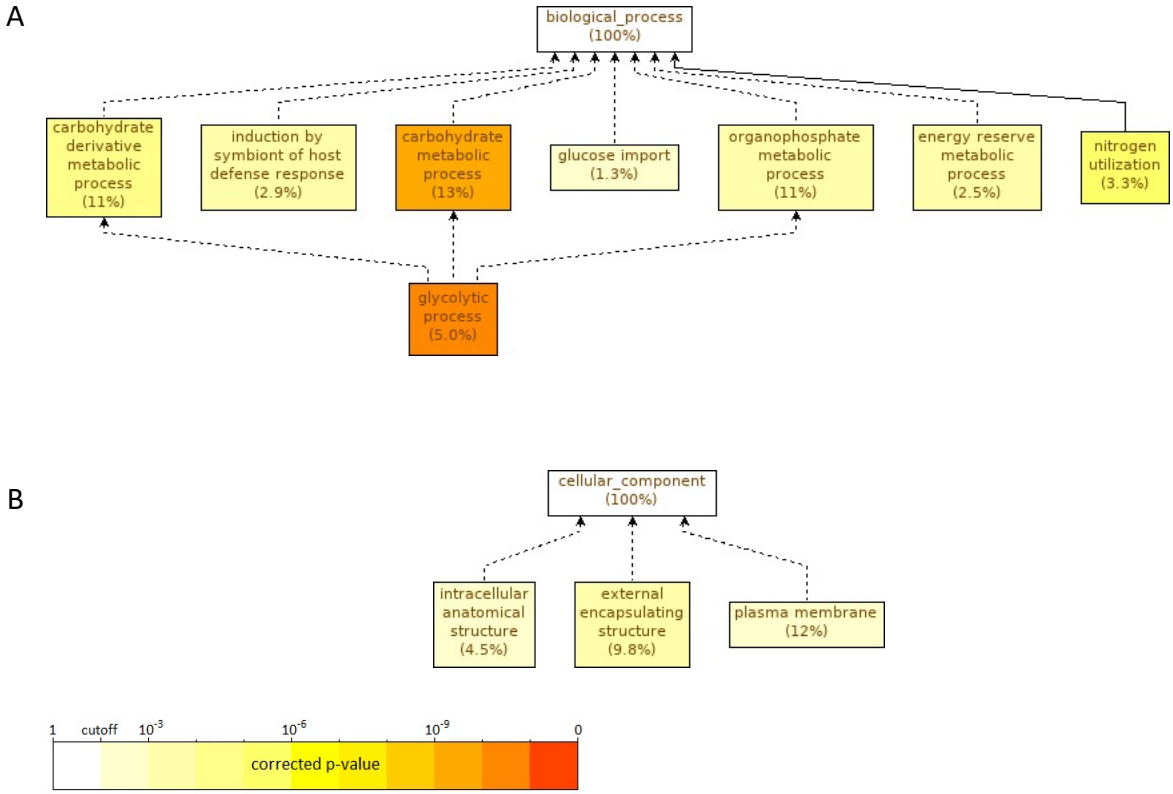

Supplementary Figure 14: GO enrichment analysis of downregulated differentially expressed genes of 5-Aza treated (PA2) versus untreated (PA3) yeast (pre-)culture.(A) Biological process (BP). (B) Cellular component (CC). Analysis was conducted with GOEnrichment. P value <0.0

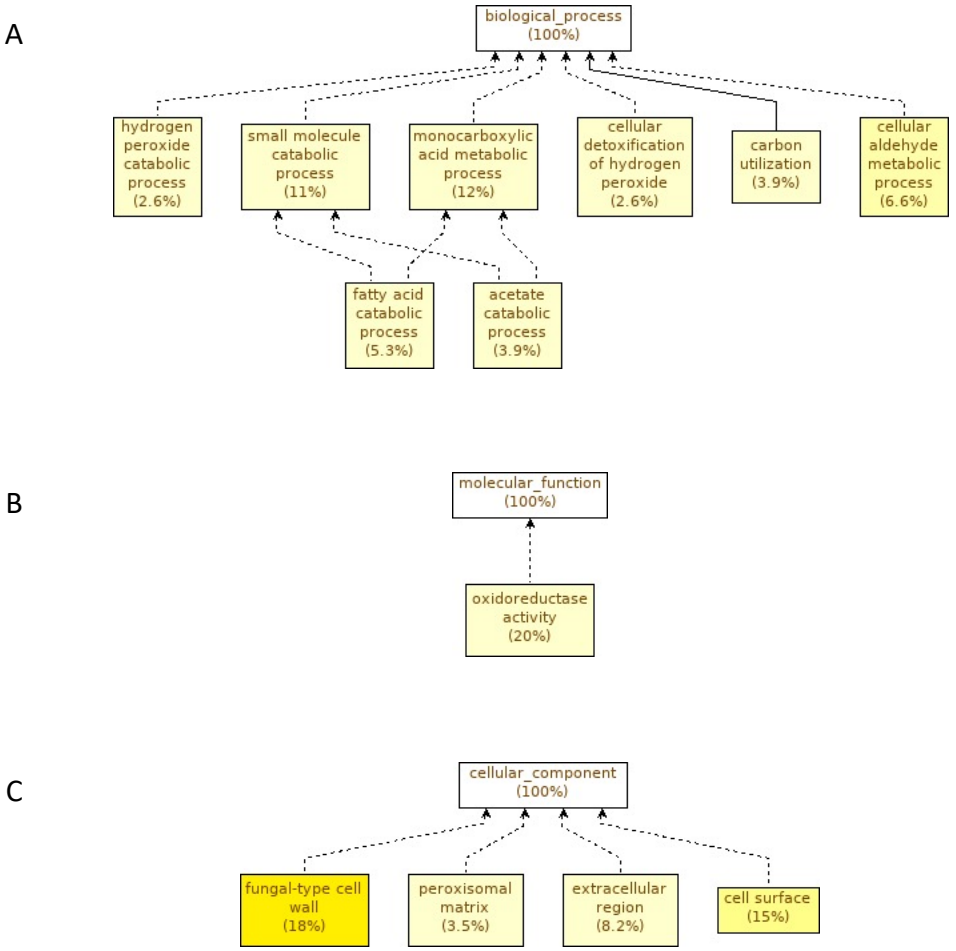

Supplementary Figure 15: GO enrichment analysis of upregulated differentially expressed genes (p adjusted value <0.01 and log2FC >1.1) of 5-Aza treated [100 µM] (PA5) versus untreated (PA7) yeast cultures. (A) Biological process. (B) Molecular function. (C) Cellular component. Analysis was conducted with GOEnrichment (p value <0.05).

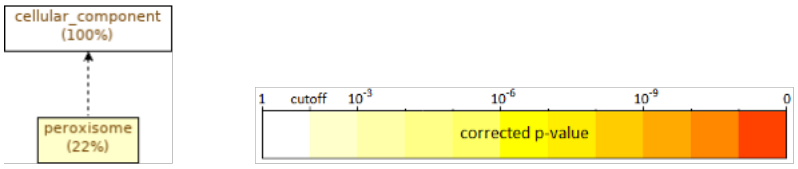

Supplementary Figure 16: GO enrichment analysis of upregulated differentially expressed genes (p adjusted value <0.01 and log2FC >1.1) of 5-Aza treated [100 µM] (PA4) versus untreated (PA6) hyphae cultures. (A) Biological process. (B) Molecular function. (C) Cellular component. Analysis was conducted with GOEnrichment (p value <0.05)